

CAIO CÉSAR BARBOSA BOMFIM

**Estudo das células mieloides supressoras e das
vias de indução da expressão do gene *Irg1* na
tuberculose**

Tese apresentada ao Programa de Pós-Graduação em Imunologia do Instituto de Ciências Biomédicas da Universidade de São Paulo, para obtenção do Título de Doutor em Ciências.

São Paulo
2020

CAIO CÉSAR BARBOSA BOMFIM

**Estudo das células mieloides supressoras e das
vias de indução da expressão do gene *Irg1* na
tuberculose**

Tese apresentada ao Programa de Pós-Graduação em Imunologia do Instituto de Ciências Biomédicas da Universidade de São Paulo, para obtenção do Título de Doutor em Ciências.

Área de concentração: Imunologia

Orientadora: Prof^a. Dr^a. Maria Regina D'Império Lima

Versão original

São Paulo
2020

CATALOGAÇÃO NA PUBLICAÇÃO (CIP)
Serviço de Biblioteca e informação Biomédica
do Instituto de Ciências Biomédicas da Universidade de São Paulo

Ficha Catalográfica elaborada pelo(a) autor(a)

Bomfim, Caio César Barbosa

Estudo das células mieloides supressoras e das
vias de indução da expressão do gene Irg1 na
tuberculose / Caio César Barbosa Bomfim;
orientadora Maria Regina D'Império Lima. -- São
Paulo, 2020.

190 p.

Tese (Doutorado) -- Universidade de São Paulo,
Instituto de Ciências Biomédicas.

1. Tuberculose. 2. Resposta imune. 3. Célula
Mieloide Supressora. 4. Irg1. 5. Itaconato. I.
D'Império Lima, Maria Regina , orientador. II.
Título.

UNIVERSIDADE DE SÃO PAULO
INSTITUTO DE CIÊNCIAS BIOMÉDICAS

Candidato(a): Caio César Barbosa Bomfim

Título da Tese: Estudo das células mieloides supressoras e das vias de indução da expressão do gene *Irg1* na tuberculose

Orientador(a): Prof^a. Dr^a. Maria Regina D'Império Lima

A Comissão Julgadora dos trabalhos de Defesa da Tese de Doutorado em sessão pública realizada a//, considerou o(a) candidato(a):

Aprovado(a)

Reprovado(a)

Examinador(a): Assinatura:

Nome:

Instituição:

Examinador(a): Assinatura:

Nome:

Instituição:

Examinador(a): Assinatura:

Nome:

Instituição:

Presidente(a): Assinatura:

Nome:

Instituição:



COMISSÃO DE ÉTICA NO USO DE ANIMAIS
INSTITUTO DE CIÊNCIAS BIOMÉDICAS
UNIVERSIDADE DE SÃO PAULO

Cidade Universitária "Armando de Salles Oliveira", Butantã, São Paulo, SP - Av. Professor Lineu Prestes, 2415 - ICB III - 05508 000
CEUA-ICB/USP - Telefone (11) 3091-7733 - e-mail: cep@icb.usp.br

CERTIFICADO

Certificamos que o projeto intitulado "*Mecanismos de modulação da ativação de células mielóides por cepas micobacterianas hipervirulentas*", registrado sob o protocolo nº **31/2016**, que envolve a produção, manutenção e/ou utilização de animais pertencentes ao filo Chordata, subfilo Vertebrata (exceto o homem), para fins de *Pesquisa Científica*, encontra-se de acordo com os preceitos da Lei nº 11.794, de 8 de outubro de 2008, do Decreto nº 6.899, de 15 de julho de 2009, e com as normas editadas pelo Conselho Nacional de Controle e Experimentação Animal (CONCEA). Ante esta conformidade, o referido projeto foi avaliado e aprovado em pela COMISSÃO DE ÉTICA NO USO DE ANIMAIS do Instituto de Ciências Biomédicas da Universidade de São Paulo (CEUA-ICB/USP), outorgando esta licença de uso de animais com validade de **4 ano(s)** a partir da data de aprovação.

- Investigador Principal: **Dr.(a.) Maria Regina D'Imperio Lima**

- Departamento: *Imunologia*

- Membros da Equipe: *Caio César Barbosa Bomfim (Pós-graduando), Rosana Ferreira Silva Moreira (Pós-graduando), Eduardo Pinheiro Amaral (Pós-doutorando)*

Ao final do período outorgado por esta licença, o pesquisador responsável deverá encaminhar a esta comissão, até o último dia de validade da atual proposta, *relatório final* de acordo com a Resolução Normativa CONCEA nº 30/2016 - Diretriz Brasileira para o Cuidado e a Utilização de Animais em Atividades de Ensino ou de Pesquisa Científica (DBCA), conforme modelo constante no endereço eletrônico http://www3.icb.usp.br/corpoeditorial/index.php?option=com_content&view=article&id=702. Havendo interesse na renovação do projeto, a solicitação deverá ser protocolada pela Secretaria da CEUA-ICB/USP até o último dia de validade da atual proposta. Após esta data uma nova proposta deverá ser encaminhada.

CERTIFICATE

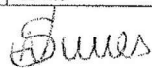
We hereby certify that the project entitled "*Modulation mechanisms of myeloid cells activation by hypervirulent mycobacterium strains*", protocol nº **31/2016**, which involves the production, maintenance and/or use of animals belonging to the phylum Chordata, subphylum Vertebrata (except human), for *Scientific Research Purposes*, is in accordance with the provisions of the Law nº 11.794 passed on October 8th, 2008, Decree nº 6899 passed on July 15th, 2009, and the rules issued by the National Council for Control and Animal Experimentation (CONCEA). According to this legislation, the project was evaluated and approved on **12:00:00 AM** by the ETHICS COMMITTEE ON ANIMAL USE, Institute of Biomedical Sciences, University of Sao Paulo (CEUA-ICB/USP), and the license for animal use is valid for **4 year(s)** from the date of approval.

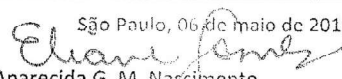
- Principal Investigator: **Dr.(a.) Maria Regina D'Imperio Lima**

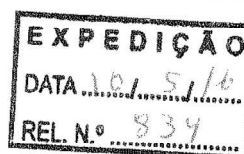
- Team members: *Caio César Barbosa Bomfim (Graduate Student), Rosana Ferreira Silva Moreira (Graduate Student), Eduardo Pinheiro Amaral (Postdoctoral Researcher)*

At the end of the period granted by this license, the Principal investigator must submit a final report of the project to this committee, according to the Rule nº 30 and the Diretriz Brasileira para o Cuidado e a Utilização de Animais em Atividades de Ensino ou de Pesquisa Científica (DBCA) issued by the CONCEA. If a renewal of the project is intended, the request must be submitted to the CEUA-ICB/USP secretary before the expiration of the current proposal. After this date, a new proposal must be prepared.

Espécie/Species	Linhagem/Strain	Sexo/Gender	Idade-Peso/ Age-Weight	Total
<i>Mus musculus</i>	C57BL/6	Macho/male	6 semanas/weeks	1200
	CD45.1	Macho/male	6 semanas/weeks	200
	C57BL/6 GFP	Macho/male	6 semanas/weeks	120
	P2X7RKO	Macho/male	6 semanas/weeks	120
	C57BL/6 NUDE	Macho/male	6 semanas/weeks	120
	CD4KO	Macho/male	6 semanas/weeks	120


Prof. Dr. Anderson de Sá Nunes
Coordenador CEUA-ICB/USP

São Paulo, 06 de maio de 2016.

Eliane Aparecida G. M. Nascimento
Secretária CEUA-ICB/USP



Esta tese é dedicada aos meus pais, Elcio e Cícera
às minhas irmãs, Vanessa, Letícia e Larissa
e a todos os meus professores

AGRADECIMENTOS

À Deus, pelo dom da vida e por todas as lições, que embora muitas das vezes fossem árduas, porém necessárias para o meu crescimento pessoal.

Aos meus pais, por toda dedicação e empenho na minha educação e por sempre me motivarem a correr atrás dos meus sonhos. Sem vocês eu não teria chegado até aqui.

Às minhas irmãs Vanessa, Letícia e Larissa, por sempre se fazerem presentes mesmo morando tão longe e por vibrarem comigo com todas as minhas conquistas. Vocês me dão forças para ir cada dia mais longe.

À minha orientadora Prof^a. Dr^a. Maria Regina, por ter acreditado em mim e aceitado essa missão de me orientar, dando todo suporte teórico-científico que eu precisava. Você contribuiu grandemente para o meu amadurecimento profissional como cientista.

Ao meu supervisor no exterior Dr. Alan Sher, por ter aberto as portas do seu laboratório no Estados Unidos para que eu pudesse desenvolver parte do meu projeto lá. Os seus conselhos vão ficar para sempre gravados em minha memória e espero um dia ser um grande cientista e contribuir tanto para o desenvolvimento da ciência assim como você.

Ao meu amigo e também “co-orientador” Edu, por toda paciência e dedicação em me ensinar a trabalhar com TB. Parte do que conquistei até hoje na minha carreira científica eu devo a você.

A todos os amigos que fiz no decorrer do meu doutorado no laboratório de imunologia de doenças infecciosas: Érika, Rafa, Bia, Rosana, Rogério, Maria, Alê, Renan, Raissa, Henrique, Sheyla; e aos mais recentes membros do lab: Bruna, Paulo, Débora, Joaquin e Matheus; em especial à equipe de TB: Igor, Gislane e Paula por contribuírem com o meu trabalho e também por todos os momentos alegres e de distração.

Aos técnicos de laboratório Rogério, Áurea e Silvana, por sempre estarem disponíveis e prontos para ajudar no que fosse preciso.

A todos os amigos do laboratório do Alan Sher: Diego, Alice, Ranjaine, Olu, Lexi, Kerry e Takashi. Aos técnicos: Lara Mitterender, Sara Hieny, Sandy Oland, Gil e Logan, por todo companheirismo e claro, muitas risadas, vocês tornaram os meus dias mais fáceis nos Estados Unidos. Em especial a Dr^a. Dragana Jankovic, por todas as conversas, conselhos, orientações e dicas sobre o projeto e experimentos. Ao Dr. Daniel Barber e à Dr^a. Katrin Mayer-Barber e aos membros dos seus respectivos laboratórios: Sake, Keith Kauffman,

Tayler, Paul, Maíke e Ehydel Castro, pela imensa contribuição com as nossas discussões nos *lab meetings*.

Aos amigos que fiz durante todos esses anos na USP: Rodolfo, Eliana Rosa, Thaís Cristina, Flavinha, Mariel, Loreana, Kelly e Jefferson Tenório, pela paciência em ouvir todas as minhas reclamações nos momentos de ansiedade e pelos inúmeros conselhos. Vocês foram a minha família aqui em São Paulo.

À minha família norte americana: Nick, Lauren e Henry por todos os momentos felizes e pela paciência. Meu inglês melhorou muito durante a nossa convivência nesses 14 meses.

Ao professor Mario Hirata, pela colaboração e por nos fornecer toda a infraestrutura necessária de um laboratório nível 3 de biossegurança para trabalhar com tuberculose.

Ao professor Pepe, pelas suas inúmeras sugestões, o meu trabalho ficou muito melhor com as suas dicas.

Aos colaboradores externos, professor Dr. Ricardo e Dr^a. Aracele, do departamento de análises clínicas e toxicológicas, por me ajudarem com todas as avaliações dos parâmetros hematológicos.

A todos os professores do departamento de Imunologia que contribuíram com o meu aprendizado.

A todos os funcionários do Biotério de Camundongos Isogênicos do Departamento de Imunologia do ICB – USP, pela manutenção e fornecimento dos animais; e aos funcionários da secretaria: Eni, João, Jotelma e Amanda, pela imensa ajuda durante todos esses anos.

E por fim, mas não menos importante, a todos os meus parentes da família Barbosa e da família Bomfim. sei que todos vocês estiveram orando e torcendo para o meu sucesso durante todo esse tempo.

MUITO OBRIGADO !!!

Estudo realizado no Laboratório de Imunologia das Doenças Infecciosas do Departamento de Imunologia, do Instituto de Ciências Biomédicas, da Universidade de São Paulo, sob orientação da prof^a. Dr^a. Maria Regina D'Império Lima, e no Laboratório Nível 3 de Biossegurança, do Departamento de Análises Clínicas e Toxicológicas, da Faculdade de Ciências Farmacêuticas, da Universidade de São Paulo, sob responsabilidade do Prof. Dr. Mário Hirouyki Hirata. Este projeto recebeu auxílio financeiro da FAPESP (Fundação de Amparo à Pesquisa do Estado de São Paulo) projetos números 2014/22986-8 e 2017/09110-4, do CNPq (Conselho Nacional de Desenvolvimento Científico e Tecnológico) e CAPES (Coordenação de Aperfeiçoamento de Pessoal de Nível Superior).

“Na corrida dessa vida é preciso entender que você vai rastejar, que vai cair, vai sofrer e a vida vai lhe ensinar que se aprende a caminhar e só depois a correr”

Aí sim, lá na chegada, onde o fim é evidente, é que a gente percebe que foi tudo de repente, e aprende na despedida que o sentido da vida é sempre seguir em frente.

Bráulio Bessa

Resumo

A tuberculose (TB) é uma doença infecciosa causada por bactérias pertencentes ao complexo *M. tuberculosis*. A pneumonia exacerbada com áreas necróticas e infiltrados granulocíticos caracteriza algumas das formas graves de TB que acomete não apenas crianças e indivíduos imunocomprometidos, mas também pessoas infectadas com cepas de alta virulência. Embora os granulócitos contribuam na resposta do hospedeiro contra infecções bacterianas, seu papel na progressão da doença grave é ainda controverso. Além disso, um importante mecanismo envolvido na regulação do recrutamento de granulócitos na TB se dá através da expressão do gene *Irg1* e produção do itaconato. Portanto, compreender as vias moleculares que induzem a expressão do gene *Irg1* é um importante passo para entender a etiologia das formas graves de TB. Considerando esses aspectos, este estudo foi subdividido em duas partes: a) avaliar o papel das células mieloides supressoras (MDSCs) na progressão da TB grave causada pela cepa hipervirulenta MP287/03 (*Mycobacterium bovis*), em camundongos C57BL/6; e b) investigar os mecanismos moleculares pelos quais a *Mycobacterium tuberculosis* induz a expressão do gene *Irg1* em macrófagos murinos. Em relação à TB causada pelas micobactérias MP287/03, observamos uma diminuição da massa corpórea, bem como uma piora da patologia pulmonar do dia 21 ao 28 pós-infecção (p.i.). Durante este período, as células CD11b⁺GR1^{int} acumularam progressivamente na medula óssea, sangue e pulmão, sugerindo que elas são originadas na medula óssea e migram para o pulmão através da corrente sanguínea. Enquanto as células CD11b⁺GR1^{high} e CD11b⁺GR1^{int} nos controles eram respectivamente neutrófilos (Ly6G⁺Ly6C^{low}) e monócitos (Ly6G⁻Ly6C^{high}), a população CD11b⁺GR1^{int} em camundongos infectados com a cepa hipervirulenta apresentaram expressão intermediária de Ly6G e Ly6C e granulocidade semelhante à neutrófilos. Essa população também expressou marcadores de células mieloides imaturas como CD117 (c-KIT), CD124 (IL-4R α) e CD135 (Flt-3). Além disso, as células CD11b⁺GR1⁺ da medula óssea de animais infectados com a cepa hipervirulenta suprimiram a proliferação de linfócitos T CD4⁺ e CD8⁺, assim como a produção de IFN- γ . A supressão de linfócitos T *in vivo* foi evidenciada pela diminuição da produção de IFN- γ e IL-17 no pulmão do dia 28 p.i. comparado com o dia 21 p.i., enquanto que a produção de IL-10 estava aumentada. A expressão de PD-L1 em altos níveis na superfície das MDSCs parece ser um dos mecanismos envolvidos na imunossupressão. Para eliminar as MDSCs, camundongos infectados com a cepa hipervirulenta, já apresentando perda da massa corpórea, foram tratados com o anticorpo monoclonal anti-GR1. Uma redução na carga bacteriana e na inflamação pulmonar, bem como aumento na produção de IFN- γ e na sobrevivência dos animais, foi observada nos camundongos tratados com anticorpo anti-GR1. Esses resultados comprovam que as MDSCs induzem imunossupressão e, conseqüentemente, agravam a doença causada por micobactérias hipervirulentas. A cerca do mecanismo envolvido na indução da expressão do gene *Irg1* pela *M. tuberculosis*, nós observamos a participação parcial da via de sinalização do TLR2-MyD88-NF κ B. Além disso, ensaios utilizando substâncias inibidoras revelaram que a fagocitose e a acidificação do fagossomo são importantes para a resposta a micobactérias, mas não a LPS ou PAM3CSK4. Interessantemente, nós mostramos que a indução da resposta do *Irg1* causada pelas micobactérias é também dependente da molécula bacteriana ESAT-6 e das vias de sinalização do macrófago STING e interferon do tipo I (IFN-I). Baseado nesses achados nós hipotetizamos que as micobactérias induzem a expressão do gene *Irg1* através da interação de 2 vias: 1) indução de NF κ B dependente de TLR2-MyD88 presumidamente na superfície da célula do hospedeiro

e 2) um sinal amplificador crítico estimulado pela fagocitose e dependente da liberação no citosol mediada por ESAT-6 de produtos bacterianos com consequente ativação de STING e produção de IFN-I. Juntos, os dados obtidos nesse estudo contribuem para uma maior compreensão da imunopatologia da TB e abre perspectivas para o desenvolvimento de novas abordagens terapêuticas que visam atenuar a gravidade da doença.

Palavras chaves: tuberculose, MDSC, *Irg1*, Itaconato

ABSTRACT

Tuberculosis (TB) is an infectious disease caused by bacteria belonging to *M. tuberculosis complex*. Extensive pneumonia with necrotic areas and granulocytic infiltrates characterizes some of the aggressive forms of TB that affects not only children and immunocompromised individuals, but also individuals infected with high-virulence strains. Although granulocytes contribute to the early immune response against TB, their role in progression of severe disease is still controversial. In addition, an important mechanism involved in regulating the granulocyte recruitment in TB occurs through *Irg1* expression and itaconate production. Therefore, understanding the molecular mechanisms that induce *Irg1* expression is an important step to understand the etiology of severe forms of TB. Considering these aspects, this study was subdivided in two main branches: a) to assess the role of myeloid-derived suppressor cells (MDSCs) in the progression of severe TB caused by hypervirulent MP287/03 (*Mycobacterium bovis*) in C57BL/6 mice; and b) to investigate the molecular pathways by which *Mycobacterium tuberculosis* (*Mtb*) triggers *Irg1* gene expression in murine macrophages. Regarding TB caused by MP287/03 mycobacteria, a decrease in body weight, as well as a worsening of the pulmonary pathology, was observed from day 21 to 28 post-infection (p.i.). During this period, CD11b⁺GR1^{int} cells progressively accumulated in the bone marrow, blood and lungs, which suggests that they originate in the bone marrow and migrate into the lungs through blood stream. While lung CD11b⁺GR1^{high} and CD11b⁺GR1^{int} cells in controls were respectively the neutrophils (Ly6G⁺Ly6C^{low}) and monocytes (Ly6G⁻Ly6C^{high}), the CD11b⁺GR1^{int} population in MP287/03-infected mice showed intermediate Ly6G and Ly6C expression and granularity similar to neutrophils. These cells also expressed the immature myeloid cell markers CD117 (c-kit), CD124 (IL-4R α) and CD135 (Flt-3). Moreover, bone marrow CD11b⁺GR1⁺ cells from hypervirulent strain infected mice suppressed CD4⁺ and CD8⁺ T cell proliferation and IFN- γ production. T cell suppression *in vivo* was evidenced by decreased IFN- γ and IL-17 production in the lungs at day 28 p.i. compared to day 21 p.i., while IL-10 production was increased. The high levels of PD-L1 expression on MDSCs surface seem to be one of the mechanisms involved in the immunosuppression. To eliminate MDSCs, MP287/03-infected mice already showing weight loss were treated with anti-GR1 monoclonal antibodies. A reduction in the pulmonary bacterial load and inflammation, as well as increased IFN- γ production and prolonged mouse survival, was observed in anti-GR1 treated mice. These results show that MDSCs induce immunosuppression and consequently aggravate the disease caused by hypervirulent mycobacteria. Regarding the mechanism involved in the induction of *Irg1* gene expression by *M. tuberculosis*, we observed a partial role for the TLR2-MyD88-NF κ B signaling pathway. In addition, assays using inhibitory drugs revealed a major requirement for phagocytosis and endosomal acidification in the response to mycobacteria, but not to LPS or PAM3CSK4. Importantly, we found that the *Irg1* response induced by mycobacteria is also highly dependent on bacterial ESAT-6 and the macrophage signaling pathways mediated by STING and Type 1 interferon (IFN-I). Based on these findings, we hypothesize that mycobacteria induce *Irg1* expression in macrophages via two interacting triggers: 1) TLR2-MyD88 dependent NF κ B induction presumably at the host cell plasma membrane and 2) a critical amplifying signal stimulated by phagocytosis and dependent of ESAT-6-mediated release into the cytosol of bacterial products with consequent STING activation and IFN-I production. Together, the data obtained in this study contribute to a better understanding of the immunopathology of TB and opens perspectives for the

development of new therapeutic approaches that aim to mitigate the severity of the disease.

Keywords: tuberculosis, MDSC, *Irg1*, Itaconate

LISTA DE ILUSTRAÇÕES

Figura 1: Estimativa do índice de incidência da TB no ano de 2018.....	26
Figura 2: Sistema de defesa do hospedeiro contra a <i>Mtb</i>	29
Figura 3: Mecanismos de imunossupressão das MDSCs	39
Figura 4: Via de produção do Itaconato e seu papel na resposta imune	42
Figura 5: Progressão da TB e análises macroscópica e microscópica do pulmão de camundongos infectados com as cepas H37Rv e MP287/03	57
Figura 6: Células mieloides CD11b ⁺ GR1 ^{int} migram para o pulmão durante a TB grave induzida pela cepa hipervirulenta MP287/03	59
Figura 7: Células granulocíticas imaturas predominam no pulmão durante a forma grave da TB	62
Figura 8: Células CD11b ⁺ GR1 ⁺ suprimem proliferação de linfócitos T e produção de IFN- γ por mecanismo dependente de contato e expressam níveis altos de PD-L1 ..	64
Figura 9: Supressão da resposta imune coincide com acúmulo de células CD11b ⁺ GR1 ^{int} no pulmão durante a TB grave	67
Figura 10: Depleção das células GR1 ⁺ reduz gravidade da TB induzida pela cepa hipervirulenta MP287/03.....	69
Figura 11: Eliminação de células CD11b ⁺ GR1 ⁺ restaura a resposta imune	71
Figura 12: <i>Mtb</i> induz expressão do gene <i>Irg1</i> <i>in vitro</i> e <i>in vivo</i>	73
Figura 13: Sinalização via TLR2-MyD88-NF κ B contribui para expressão do gene <i>Irg1</i> durante infecção por <i>Mtb</i>	75
Figura 14: Fagocitose da <i>Mtb</i> é importante para induzir expressão do gene <i>Irg1</i>	77
Figura 15: Detecção citosólica de <i>Mtb</i> atua como segundo sinal necessário para amplificar a expressão do gene <i>Irg1</i>	80
Figura 16: Sinalização via IFN-I é crucial para aumento da expressão do gene <i>Irg1</i>	82
Figura 17: Produção do metabólito itaconato em macrófagos B6 e IFN α / β TKO infectados com <i>Mtb</i> 24h p.i	83

Figura 18: Expressão do gene <i>Irg1</i> no pulmão de camundongos infectados com as cepas MP287/03 ou H37Rv 21 e 28 dias p.i.	84
Figura 19: Ilustração esquemática que explica o papel das MDSCs no agravamento da TB	92
Figura 20: Modelo esquemático da via de sinalização ativada em macrófagos infectados com <i>Mtb</i> para indução da expressão do gene <i>Irg1</i>	96

LISTA DE TABELAS

Tabela 1: Sequência de nucleotídeos dos <i>primers</i> utilizados	51
---	----

LISTA DE ABREVIATURAS E SIGLAS

Acod1	do inglês, <i>Aconitate decarboxylase 1</i>
ActD	Actinomocina D
ADAM17	do inglês, <i>ADAM metallopeptidase domain 1</i>
ADC	Albumina, dextrose e catalase
AIDS	Síndrome da imunodeficiência adquirida
AM	Macrófago alveolar
AMP	Monofosfato de adenosina
ARG	arginase
ATP	Trifosfato de adenosina
AT-I	Célula epitelial alveolar do tipo I
AT-II	Célula epitelial alveolar do tipo II
BAAR	Bacilo álcool-ácido resistente
BCG	Bacilo de Calmette-Guérin
BCR	Receptor de célula B
BMDM	Macrófago derivado da medula óssea
CAC	Ciclo do ácido cítrico
CBA	do inglês, <i>Cytometric bead array</i>
CARD	do inglês, <i>Caspase activating and recruitment domain</i>
CD	do inglês, <i>Cluster of differentiation</i>
cDNA	DNA complementar
CFU	Unidades formadoras de colônia
cGAS	Sintase cíclica de GMP-AMP
CHX	Cicloheximida
CMP	Progenitores mielóides comum
CpG	DNA metilado
DC	Célula dendrítica
DNA	Ácido desoxirribonucleico
DO	Densidade ótica
ELISA	do inglês, <i>enzyme-linked immunosorbent assay</i>
ESAT-6	do inglês, <i>Early-secreted target antigen</i>
ESX-1	do inglês, <i>Esat-6 secretion system 1</i>
FasL	do inglês, <i>TNF superfamily member 6 ligand</i>

GL	Gotas de lipídeo
G-MDSC	Célula mieloide supressora granulocítica
HE	Hematoxilina/eosina
HIV	Vírus da imunodeficiência humana
ICL	Isocitratoliase
IDO	Indoleamine 2,3-dioxygenase
IFN	Interferon
IFN α/β R	Receptor de Interferon do tipo I
IFN-I	Interferon do tipo I
Ig	imunoglobulina
IL	Interleucina
ILC	do inglês, <i>Innate lymphoid cells</i>
iNOS	Óxido nítrico sintase induzível
IRF	Fator regulador de interferon
Irg-1	Gene imunorresponsivo 1
ISG	Genes induzidos por interferons
LPS	Lipopolissacarídeo
<i>Mbv</i>	<i>Mycobacterium bovis</i>
MDSC	Célula mieloide supressora
MHC	Complexo principal de histocompatibilidade
M-MDSC	Célula mieloide supressora monocítica
MOI	do inglês, <i>multiplicity of infection</i>
mRNA	RNA mensageiro
<i>Mtb</i>	<i>Mycobacterium tuberculosis</i>
MX2	do inglês, <i>Myxovirus resistance 2</i>
MycB	do inglês, <i>Mycalolide B</i>
MyD88	do inglês, <i>Myeloid differentiation primary response gene 88</i>
NF κ B	do inglês, <i>Nuclear Factor κB</i>
NK	do inglês, <i>Natural killer cell</i>
NO	Óxido nítrico
NOX2	NDPH oxidase 2
OADC	Oleato, albumina, dextrose e catalase
OAS1	do inglês, 2'5'-oligoadenylato synthetase 1
OMS	Organização mundial da saúde

PAMP	Padrões moleculares associados à patógenos
PBS	Solução fosfatada tamponada
PCR	Reação em cadeia da polimerase
PD-L1	do inglês, <i>Programmed death-ligand 1</i>
pH	Potencial hidrogeniônico
Poly IC	Ácido polinosínico-policitidílico
PPT	Tuberculose primária progressiva
PRR	Receptor de reconhecimento de padrões
RD1	do inglês, <i>Region of difference -1</i>
RNA	Ácido ribonucleico
ROS	Espécies reativas de oxigênio
SDH	Succinato desidrogenase
SPF	Livre de patógenos específicos
SPLC	Esplenócitos
STING	Estimulador de genes de interferon
TB	Tuberculose
TCR	Receptor de célula T
TGF- β	Fator de transformação do crescimento beta
Th	Linfócito T auxiliar
TLR	Receptor do tipo toll
TNF- α	Fator de necrose tumoral
TR	Trato respiratório
Treg	Linfócito T regulador
TRIF	do inglês, <i>TIR-domain-containing adapter-inducing interferon-β</i>
tSNE	do inglês, <i>t-distributed stochastic neighbor embedding</i>
ZN	Coloração de Ziehl-Neelsen

α	alpha
β	beta
γ	gamma
κ	kappa
ζ	zeta

SUMÁRIO

1 INTRODUÇÃO:	23
1.1 Tuberculose	24
1.2 Epidemiologia	25
1.3 Aspectos imunológicos na TB pulmonar	27
1.3.1 Invasão, reconhecimento e mecanismos da imunidade inata	27
1.3.2 Mecanismos da imunidade adaptativa	32
1.4 TB grave e modelo murino como ferramenta para estudo	33
1.5 Células mieloides supressoras (MDSCs)	36
1.6 Irg1 e Itaconato	39
2 OBJETIVOS	43
2.1 Geral	44
2.2 Específicos	44
3 METODOLOGIA	45
3.1 Micobactérias	46
3.2 Animais	46
3.3 Infecção dos animais	47
3.4 Análises macroscópicas e microscópicas dos pulmões	47
3.5 Obtenção de células do pulmão	48
3.6 Obtenção de células do sangue	48
3.7 Obtenção de células da medula óssea	48
3.8 Análise fenotípica de células por citometria de fluxo	49
3.9 Avaliação da produção de citocinas por Cytometric Bead Array (CBA)	49
3.10 Isolamento da população CD11b⁺GR1⁺	49
3.11 Ensaio funcional de inibição da proliferação de linfócitos T	50
3.12 Ensaio funcional de inibição da produção de IFN-γ por ELISA	50
3.13 Extração de RNA do tecido pulmonar e avaliação da expressão gênica por qRT-PCR	50

3.14	Eliminação <i>in vivo</i> de células GR1 ⁺	51
3.15	Extração da medula óssea, diferenciação de macrófagos e infecção <i>in vitro</i>	52
3.16	Diferenciação de macrófagos humanos	52
3.17	Quantificação do Itaconato	53
3.18	Análise estatística	53
4	RESULTADOS	54
	Capítulo 1 – Participação das MDSCs no agravamento da TB	55
4.1	Células mieloides CD11b ⁺ GR1 ^{int} migram para o pulmão durante a TB grave induzida pela cepa hipervirulenta MP287/03.....	55
4.2	População heterogênea de células granulocíticas imaturas CD11b ⁺ GR1 ^{int} é predominante no pulmão durante a forma grave de TB	60
4.3	Células CD11b ⁺ GR1 ⁺ de camundongos infectados com a cepa MP287/03 suprimem a proliferação de células T CD4 ⁺ através da interação PD1/PD-L1	63
4.4	Perfil imunorregulado no pulmão de camundongos com TB grave coincide com o vasto aumento da população CD11b ⁺ GR1 ^{int}	65
4.5	Eliminação de células CD11b ⁺ GR1 ⁺ reduz a gravidade da TB induzida pela cepa MP287/03	68
4.6	Tratamento com anticorpo anti-GR1 restaura a resposta imune em camundongos com TB grave	70
	Capítulo 2 – Mecanismo molecular de indução do gene <i>Irg1</i> durante infecção por <i>Mycobacterium tuberculosis</i> e geração de itaconato	72
4.7	<i>Mtb</i> induz expressão de <i>Irg1</i> <i>in vitro</i> e <i>in vivo</i>	72
4.8	Indução da expressão do gene <i>Irg1</i> é parcialmente dependente da via de sinalização TLR2-MyD88-NFκB	74
4.9	Fagocitose de <i>Mtb</i> contribui para indução da expressão do gene <i>Irg1</i>	76
4.10	Acidificação do fagossomo e detecção citosólica de <i>Mtb</i> são etapas importantes para expressão do gene <i>Irg1</i>	78
4.11	Sinalização ativada por IFN-I é crucial para elevação da expressão do gene <i>Irg1</i>	81
5	DISCUSSÃO:	85

6 CONCLUSÃO	97
REFERÊNCIAS	99
APÊNDICE A - Estratégia de <i>gates</i> utilizada para análise da população de células mieloides e linfoides	115
APÊNDICE B - Presença de monócitos imaturos no pulmão de camundongos 28 dias p.i. com a cepa MP287/03.....	117
APÊNDICE C - Frequência de monócitos (maduros e imaturos) e linfócitos no sangue de camundongos infectados tratados com anticorpos anti-GR1 ou com controle isotópico	119
APÊNDICE D - Viabilidade celular de BMDM tratados com os inibidores MycB, dynasore ou cultivados à 4°C	121
APÊNDICE E - P2X7 receptor in bone marrow-derived cells aggravates tuberculosis caused by hypervirulent <i>Mycobacterium bovis</i> . <i>Frontiers in Immunology</i> , 2017.....	123
APÊNDICE F - Inhibiting Adenosine Receptor Signaling Promotes Accumulation of Effector CD4+ T Cells in the Lung Parenchyma During Severe Tuberculosis. <i>The Journal of Infectious Diseases</i> , 2019.....	134
APÊNDICE G - Human CD40 ligand deficiency dysregulates the macrophage transcriptome causing functional defects that are improved by exogenous IFN- γ . <i>Journal of Allergy and Clinical Immunology</i> , 2017.....	146
APÊNDICE H - Interferon-gamma reduces the proliferation of <i>M. tuberculosis</i> within macrophages from a patient with a novel hypomorphic NEMO mutation. <i>Pediatric Blood & Cancer</i> . 2016.....	167
APÊNDICE I – Synthesis, cytotoxic activity on leukemia cell lines and quantitative structure-activity relationships (qsar) studies of morita-baylis-hillman adducts. <i>Medicinal Chemistry</i> , 2016	172
APÊNDICE J - Effects of curine in HL-60 leukemic cells: cell cycle arrest and apoptosis induction. <i>Journal of Natural Medicines</i> , 2015.....	184

1 Introdução

1.1 Tuberculose

A Tuberculose (TB) é uma doença infectocontagiosa que afeta principalmente o pulmão, porém outros órgãos e sistemas, como o esqueleto, trato geniturinário e sistema nervoso central também podem ser afetados (KULCHAVENYA, 2014; WHO, 2019). Do ponto de vista de saúde pública, a forma pulmonar é a mais relevante, pois além de representar cerca de 85% de todos os casos, é a principal forma relacionada com a transmissão da doença (KAUFMANN; DORHOI, 2013; WHO, 2019).

Descoberta no século XIX como o agente etiológico da TB pelo cientista Robert Kock, a *Mycobacterium tuberculosis* (*Mtb*) foi também denominada de bacilo de Kock. Atualmente, sabe-se que a TB também pode ser causada por algumas diferentes espécies do gênero *Mycobacterium*, como *Mycobacterium bovis*, *Mycobacterium africanum*, *Mycobacterium canettii* entre outras, porém a *Mtb* é a principal responsável pelos casos reportados em humanos (COSMA; SHERMAN; RAMAKRISHNAN, 2003).

A infecção ocorre tipicamente através da inalação de bactérias expelidas na fala, tosse ou espirro de um indivíduo com a forma pulmonar ativa da TB (RILEY; MILLS; NYKA; WEINSTOCK *et al.*, 1995). Os principais sintomas da doença são: tosse, febre, fraqueza, sudorese noturna e presença de sangue no escarro (BRANDLI, 1998). O diagnóstico clínico é realizado através da observação de sinais e sintomas típicos da doença, anormalidades da radiografia do tórax e/ou histologia sugestivas, e identificação da presença do bacilo no escarro por exame microscópico direto (baciloscopia direta) (BRASIL, 2011; WHO, 2019). Com o diagnóstico e o tratamento oportunos com antibióticos de primeira linha por 6 meses, a maioria das pessoas que desenvolvem TB pode ser curada e a transmissão contínua de infecção reduzida (WHO, 2019). Porém, o surgimento de cepas resistentes aos antibióticos bem como de alta virulência tem sido uma das principais preocupações da saúde pública.

Logo após a infecção com o bacilo, o hospedeiro pode responder de três formas distintas: 1) Cura - o indivíduo consegue eliminar a bactéria. 2) TB latente - ocorre a infecção primária mas o indivíduo permanece com o bacilo em estágio quiescente por longos períodos, sem apresentar dano e sem risco de transmissão. Esse bacilo pode então ser reativado anos mais tarde e promover a doença ativa. 3) Tuberculose primária progressiva (PPT) - o indivíduo progride rapidamente para a forma ativa da doença (KAUFMANN; DORHOI, 2013; O'GARRA; REDFORD; MCNAB; BLOOM *et al.*, 2013).

Os fatores determinantes para o desenvolvimento da doença são resultantes da interação entre ambiente, hospedeiro e patógeno. Algumas condições de risco também são conhecidas como a coinfeção com o HIV (*Human Immunodeficiency virus*), imunodeficiência, diabetes mellitus, mal nutrição e pobreza em geral (YOUNG; PERKINS; DUNCAN; BARRY, 2008). Além disso, a vacina BCG (bacilo de Calmette-Guérin), que é usada na profilaxia da TB, confere proteção contra a forma disseminada da doença em crianças mas a sua eficácia contra a forma pulmonar em adultos é contestada (WILKIE; MCSHANE, 2015).

1.2 Epidemiologia

Responsável por assolar a humanidade há milênios e levar à morte um grande número de pessoas, a TB permanece ainda hoje como um sério problema de saúde pública apesar da existência de medidas profiláticas e terapêuticas. É estimado que aproximadamente 1,7 bilhões de pessoas, ou seja, quase um quarto da população mundial, estejam infectadas com a micobactéria mas permanecem assintomáticas (TB latente) (HOUBEN; DODD, 2016; WHO, 2019). Dos indivíduos infectados, calcula-se que 5-15% irão desenvolver a forma ativa da doença ao longo de suas vidas (WHO, 2019).

Em 2018, houve cerca de 7 milhões de novos casos de TB notificados para a Organização Mundial da Saúde (OMS). A incidência vem aumentando progressivamente desde 2013, quando foram notificados 5,7 milhões de novos casos (WHO, 2019). Os principais países responsáveis pelo aumento das notificações globais dos casos de TB são a Índia e a Indonésia, que ocupam o primeiro e o terceiro lugares em termos de casos estimados de incidentes por ano. Na Índia, as notificações de novos casos subiram de 1,2 milhões para 2 milhões entre 2013 e 2018 (aumento de 60%), enquanto que na Indonésia houve um aumento de 331.703 em 2015 para 563.879 em 2018 (aumento de 70%) (WHO, 2019).

Apesar do aumento nos casos notificados, a incidência global de TB em 2018 ainda representa apenas 70% do número estimado que é de 10 milhões de novos casos nesse ano. Dez países são responsáveis por 80% do déficit global de 3 milhões de casos notificados. Índia, Indonésia, Nigéria e Filipinas lideram esse ranking de não notificação com 25%, 12%, 10% e 8%, respectivamente. As lacunas entre o número estimado de novos casos e o número realmente relatado devem-se à subnotificação

de casos detectados e subdiagnosticados, seja porque as pessoas não têm acesso à assistência médica ou porque não são diagnosticadas quando o fazem. A Figura 1 mostra a taxa de incidência estimada de TB em 2018 (WHO, 2019).

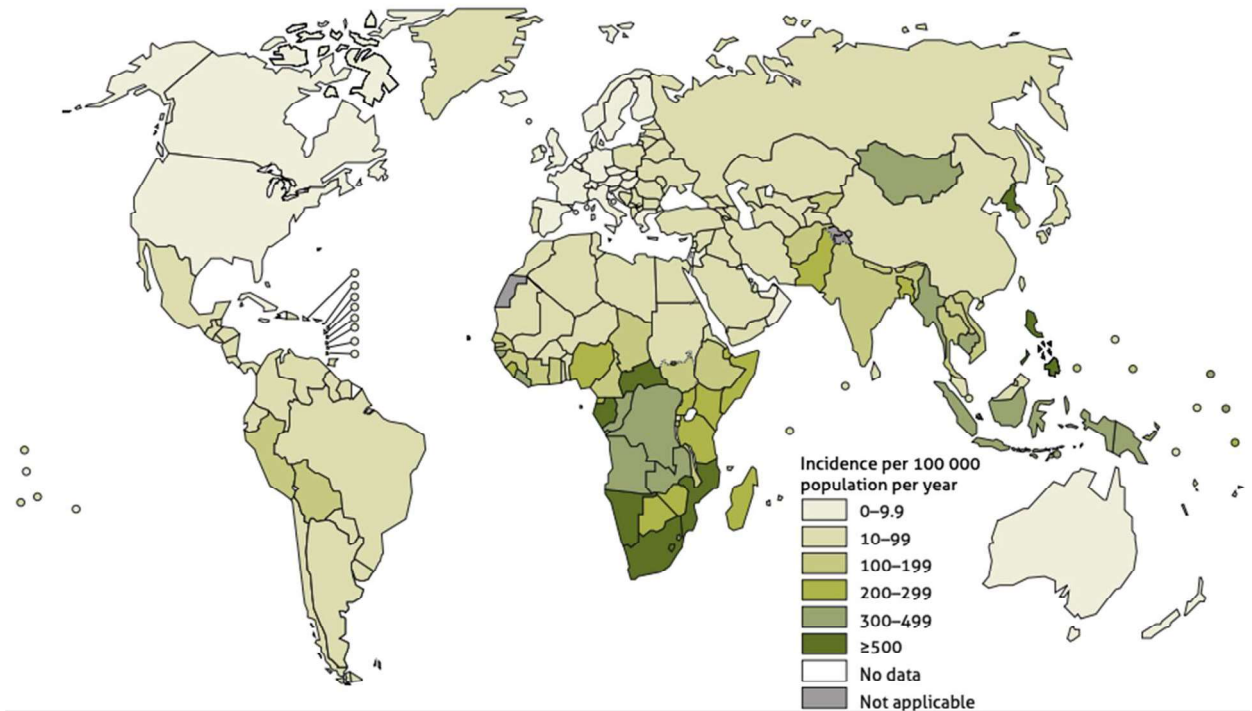


Figura 1: Estimativa do índice de incidência da TB no ano de 2018.

Fonte: WHO, 2019.

Ainda segundo a OMS, a TB está entre as dez principais causas de morte no mundo, e é a primeira causa de óbito entre as doenças infecciosas induzidas por um único agente etiológico, ficando acima até mesmo de HIV/AIDS. Só em 2018, a TB causou a morte de aproximadamente 1,2 milhões de pessoas HIV negativas, e um adicional de 251.000 óbitos de pacientes co-infectados com HIV (WHO, 2019). Além disso, a TB é a principal causa infecciosa de morte entre os pacientes infectados com HIV.

Em relação aos casos de TB resistentes aos antibióticos, foram relatados em 2018 aproximadamente 500.000 novos casos de TB resistente à rifampicina (TB-RR), sendo que cerca de 78% deles apresentaram resistência a múltiplas drogas (MDR). Nesse caso, as micobactérias eram resistentes às drogas rifampicina e isoniazida, os dois mais potentes fármacos anti-TB. Globalmente, 3,4% dos novos casos e 18% dos casos já tratados previamente eram TB-RR ou MDR (WHO, 2019). O tratamento das

pessoas com TB-RR ou TB-MDR é longo e requer o uso de antibióticos injetáveis mais tóxicos e muito mais caros como a amicacina, canamicina e capreomicina (RABAHI; DA SILVA JÚNIOR; FERREIRA; TANNUS-SILVA *et al.*, 2017). Mesmo assim, a taxa de sucesso após o tratamento da TB-MDR não excede 56% (WHO, 2019).

O Brasil é um dos 20 países com maior número absoluto de casos de TB. Todas essas nações juntas são responsáveis por 84% do total reportado no mundo (WHO, 2019). A incidência no país foi de aproximadamente 34,8 casos/100.000 habitantes em 2018, e o índice de mortalidade de 2,2 casos/100.000 habitantes (BRASIL, 2019). Além disso, houve a notificação de 72.788 novos casos apenas no ano de 2018. Vale ressaltar ainda que incidência da doença no país é bastante heterogênea entre as regiões, variando de 20 casos/100.000 habitantes no centro-oeste a 42,7 casos/100.000 no norte (BRASIL, 2019).

Esses dados indicam que apesar das políticas públicas de saúde adotadas para combater a TB, ela ainda permanece como uma das mazelas que assolam o País. Além disso, levando em consideração o contexto global em que se observa uma alta prevalência da TB em todo o mundo e o surgimento de casos cada vez mais resistentes a medicamentos com uma baixa taxa de cura de apenas 56% (WHO, 2019), nota-se que são urgentemente necessárias vacinas mais eficazes, diagnósticos rápidos e novas terapias. A manipulação da resposta imune do hospedeiro contra a *Mtb* pode ser uma abordagem racional para o tratamento da TB, uma vez que, grande parte da população está infectada com o bacilo, mas apenas uma pequena parcela sucumbe à doença (CHAI; LU; LIU, 2019).

1.3 Aspectos imunológicos na TB pulmonar

1.3.1 Invasão, reconhecimento e mecanismos da imunidade inata

Uma vez inaladas, as micobactérias encontram uma barreira física formada pela presença de células epiteliais firmemente aderidas ao longo da superfície aérea que dificulta a sua invasão. O epitélio do trato respiratório (TR), incluindo traqueia, brônquios e bronquíolos, é formado por células ciliadas, células claras, células caliciformes, células neuroendócrinas e células basais regenerativas (Figura 2A) (CHAI; LU; LIU, 2019). A primeira linha de defesa do hospedeiro que atua contra a *Mtb* é composta pelo muco presente no TR secretado pelas células caliciformes, que é rico em moléculas com potencial antimicrobianos como defensinas,

imunoglobulinas, lisozimas e várias citocinas (NICHOLAS; SKIPP; MOULD; RENNARD *et al.*, 2006). De fato, alguns estudos têm mostrado que camundongos deficientes em IgA são mais susceptíveis às infecções do TR por micobactérias do que os imuno-competentes, e que as defensinas podem causar rupturas no envelope micobacteriano (ALMATAR; MAKKY; YAKICI; VAR *et al.*, 2018; TJARNLUND; RODRIGUEZ; CARDONA; GUIRADO *et al.*, 2006). A presença de mucinas glicosiladas também contribui indiretamente para a defesa do hospedeiro, pois essas moléculas são essenciais para acomodar microrganismos comensais na camada mais externa do muco que competem com os microrganismos invasores ajudando na eliminação de patógenos (WHITSETT; ALENGHAT, 2015). Além disso, as células ciliadas, através dos seus movimentos rítmicos, auxiliam na depuração eficaz do TR que permite expulsar até 90% das partículas e microrganismos estranhos inalados (ROY; LIVRAGHI-BUTRICO; FLETCHER; MCELWEE *et al.*, 2014).

Por outro lado, a superfície do alvéolo é formada predominantemente por células epiteliais alveolares do tipo 1 (AT1), responsáveis por realizar as trocas gasosas, e do tipo 2 (AT2), que atuam como progenitoras das AT1 (Figura 2B) (CRAPO; BARRY; GEHR; BACHOFEN *et al.*, 1982; GHOSH; GORANTLA; MAKENA; LUELLEN *et al.*, 2013). Ambas as células AT1 e AT2 possuem receptores de reconhecimento de padrões (PRRs), que quando ativados induzem a secreção de várias citocinas, promovem o recrutamento de neutrófilos e linfócitos para o sítio infeccioso, e potencializam os mecanismos microbicidas intracelulares dos macrófagos (NOUAILLES; DORHOI; KOCH; ZERRAHN *et al.*, 2014; REUSCHL; EDWARDS; PARKER; CONNELL *et al.*, 2017). Quando alcançam os alvéolos pulmonares, além das células AT1 e AT2, os bacilos são também reconhecidos por macrófagos alveolares (AM) e células dendríticas (DCs) residentes do pulmão que estão presentes em menor proporção (FENNELLY; JONES-LOPEZ; AYAKAKA; KIM *et al.*, 2012). Vários PRRs são importantes para esse processo inicial de identificação da *Mtb*, como os TLR (*Toll-like receptor*)2, TLR4 e o TLR9, além dos receptores de manose, mincle e dectina 1 e 2 (BAFICA; SCANGA; FENG; LEIFER *et al.*, 2005; HUYNH; JOSHI; BROWN, 2011; SCHOENEN; BODENDORFER; HITCHENS; MANZANERO *et al.*, 2010; WAGENER; HOVING; NDLOVU; MARAKALALA, 2018). Por outro lado, diferentes padrões moleculares associados aos patógenos (PAMPs), que encontram-se presentes na superfície da *Mtb*, tais como peptidoglicano, lipoarabinomanana, ácido lipoteicóico, trehalose, dentre outros, podem ser

reconhecidos pelos PRRs levando à ativação de cascatas de sinalizações e à produção de citocinas pró inflamatórias (CERVANTES, 2017; WAGENER; HOVING; NDLOVU; MARAKALALA, 2018).

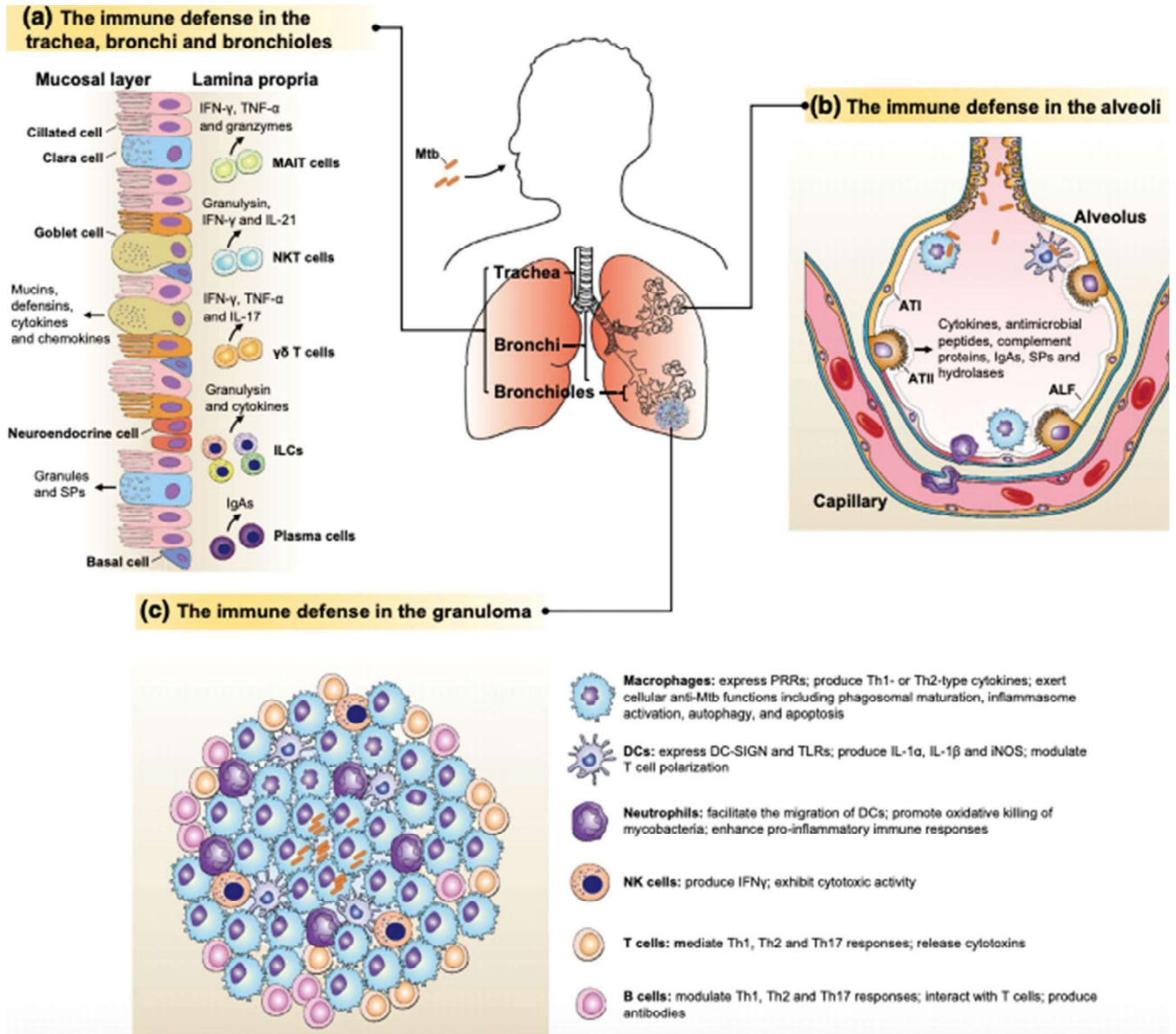


Figura 2: Sistema de defesa do hospedeiro contra a *Mtb*.

Fonte: CHAI; LU; LIU, 2019

Uma das principais vias de sinalização celular estimulada pela *Mtb* é dependente de MyD88, que atua como molécula adaptadora dos receptores TLR2, TLR4 e TLR9. Uma vez estimulado, o MyD88 irá ativar o fator de transcrição nuclear NFκB e consequentemente induzir a expressão dos genes pro-inflamatórios TNF-α, IL-1, IL6 entre outros. Além disso, a ativação dos TLRs também estimula o aumento da expressão dos receptores de complemento, scavengers, MARCO e muitos outros

genes que regulam a fagocitose (CERVANTES, 2017). Paralelamente a ativação da cascata de sinalização dependente de MyD88, o estímulo do TLR4 pela *Mtb* também induz a ativação da via TRIF (TIR-domain-containing adapter-inducing interferon- β), que por sua vez ativa IRF3 e promove a secreção de IFN- β (TAKEDA; AKIRA, 2005). Ambos IRF3 e IFN- β possuem um papel crucial na patogênese da TB (STANLEY; JOHNDROW; MANZANILLO; COX, 2007).

Após o reconhecimento inicial na superfície do alvéolo, os bacilos são então fagocitados pelos AMs e mantidos no interior de vesículas, chamadas de fagossomos, que logo são endereçadas para a fusão com os lisossomos, num evento chamado de maturação fagossomal (PAUWELS; TROST; BEYAERT; HOFFMANN, 2017). Durante esse processo ocorre uma redução gradual do pH no interior da vesícula, que é de suma importância para a indução de morte e digestão do patógeno. Esta etapa é essencial para uma ótima resposta à bactéria, pois o ambiente ácido no interior do fagossomo ativa as enzimas do hospedeiro que irão processar os antígenos e, conseqüentemente, os receptores TLRs endossomais irão reconhecê-los com maior facilidade (IP; SOKOLOVSKA; CHARRIERE; BOYER *et al.*, 2010). Por outro lado, as micobactérias patogênicas conseguem inibir o endereçamento lisossomal do fagossomo através da produção de PknG, uma proteína solúvel que é semelhante à proteína quinase de eucariotos (SCHERR; MULLER; PERISA; COMBALUZIER *et al.*, 2009; ZHAI; WU; ZHANG; FU *et al.*, 2019). Esta molécula é translocada do fagossomo para o citosol onde induz a fosforilação de várias moléculas do hospedeiro, evitando assim a fusão do fagossomo com lisossomo (SAJID; ARORA; SINGHAL; KALIA *et al.*, 2015). Dessa forma, a acidificação do fagossomo é prejudicada e outros mecanismos microbicidas resultantes da fusão fagossomo-lisossomo não ocorrem, tornando o vacúolo fagocítico um ambiente adequado para a sobrevivência da bactéria (CLEMENS; HORWITZ, 1995; MUELLER; PIETERS, 2006).

Os neutrófilos são as primeiras células recrutadas da corrente sanguínea para o sítio infeccioso e iniciam o processo de fagocitose e eliminação do bacilo (BRU; CARDONA, 2010). Diversos fatores bactericidas são produzidos por essas células durante a infecção, como peptídeos antimicrobianos, espécies reativas de oxigênio (ROS) e diferentes enzimas hidrolíticas (AMULIC; CAZALET; HAYES; METZLER *et al.*, 2012). Entretanto, embora os neutrófilos tenham atividade importante na resposta do hospedeiro contra infecções bacterianas, o seu papel na TB ainda é muito controverso (DALLENGA; SCHAIBLE, 2016; ERUSLANOV; LYADOVA;

KONDRATIEVA; MAJOROV *et al.*, 2005; LOWE; REDFORD; WILKINSON; O'GARRA *et al.*, 2012). O acúmulo excessivo dessas células no pulmão é prejudicial, e está associado com a lesão tecidual durante a TB grave (DALLENGA; SCHAIBLE, 2016; LOWE; REDFORD; WILKINSON; O'GARRA *et al.*, 2012). Ademais, vários estudos já revelaram que algumas cepas virulentas de *Mtb* também conseguem sobreviver no interior de neutrófilos, alterando algumas funções dessas células e favorecendo a sua subsistência (BLOMGRAN; DESVIGNES; BRIKEN; ERNST, 2012). A inibição da apoptose, por exemplo, é uma das vias utilizadas por esses patógenos, pois além de impedir a sua eliminação durante esse tipo de morte celular também promove atraso da ativação de linfócitos T, que são essenciais na resposta imune contra *Mtb* (BLOMGRAN; DESVIGNES; BRIKEN; ERNST, 2012). Esse atraso ocorre porque a ingestão de antígenos micobacterianos a partir de corpos apoptóticos de neutrófilos torna as DCs mais eficientes em induzir a ativação de linfócitos T e, portanto, a inibição da apoptose afeta esse processo (BLOMGRAN; DESVIGNES; BRIKEN; ERNST, 2012; BLOMGRAN; ERNST, 2011). A indução da necrose, morte celular com ruptura da membrana plasmática, é outra via utilizada pelas cepas virulentas de *Mtb* que contribui para sua sobrevivência, pois resulta na liberação no meio extracelular de bacilos viáveis, os quais irão infectar novas células dando continuidade ao ciclo infeccioso (FRANCIS; BUTLER; STEWART, 2014).

Como parte do sistema imune inato, as DCs também reconhecem a *Mtb* através de diferentes TLRs. Após a ativação, as DCs apresentam os componentes processados do patógeno aos linfócitos T nos linfonodos, fazendo a conexão entre a resposta imune inata e adaptativa. Porém, as micobactérias virulentas também são capazes de atrasar o início da resposta imune adaptativa por afetar diretamente na migração de DCs para o linfonodo mediastinal, órgão responsável por drenar os pulmões, e inibir a apresentação de antígenos via MHC-II (*major histocompatibility complex-II*) (ROBERTS; ROBINSON, 2014; WOLF; LINAS; TREVEJO-NUNEZ; KINCAID *et al.*, 2007). Esse retardo do início da ativação da resposta imune adaptativa favorece a disseminação da bactéria, pois garante o tempo necessário para o bacilo alcançar a massa crítica infectante suficiente para consolidar a infecção.

As ILCs (*innate lymphoid cells*) consistem numa população de linfócitos inatos encontrados na superfície de mucosas, tanto do pulmão como do intestino, que foram descobertas há pouco tempo e têm sido amplamente estudadas em diferentes contextos, inclusive na TB (VACCA; CHIOSSONE; MINGARI; MORETTA, 2019).

Diferentemente dos linfócitos T e B, as ILCs não possuem receptores específicos de antígenos como os TCR e BCR, e portanto não são restritas pela apresentação via MHC, porém elas possuem algumas funções semelhantes aos linfócitos da resposta imune adaptativa (VACCA; CHIOSSONE; MINGARI; MORETTA, 2019). De acordo com os seus diferentes fatores de transcrição e funções efetoras elas podem ser classificadas em 5 subgrupos: NK (Natural killer) cells, ILC1, ILC2, ILC3, LTi (lymphoid tissue inducer) (VIVIER; ARTIS; COLONNA; DIEFENBACH *et al.*, 2018; ZITTI; BRYCESON, 2018). Vários estudos já mostraram o papel protetor contra a *Mtb* do IFN- γ produzido pelas células NK no pulmão (FENG; KAVIRATNE; ROTHFUCHS; CHEEVER *et al.*, 2006; KUPZ; ZEDLER; STABER; PERDOMO *et al.*, 2016; LAI; CHANG; LIN; WU *et al.*, 2018). Em um estudo *in vitro*, Esin e colaboradores também mostraram que as células NK atuam diretamente na superfície do bacilo executando sua atividade citotóxica (ESIN; BATONI; COUNOUPAS; STRINGARO *et al.*, 2008). Além disso, a expansão de ILC3 induzida por IL-23 pode induzir a produção de IL-17 e IL22, que desempenham um papel importante na imunidade contra a *Mtb* (ARDAIN; DOMINGO-GONZALEZ; DAS; KAZER *et al.*, 2019).

1.3.2 Mecanismos da imunidade adaptativa

A resposta imune protetora contra a *Mtb* é também dependente de linfócitos T, uma vez que camundongos deficientes em células T CD4⁺ ou MHC-II são incapazes de controlar a proliferação bacteriana, e dessa forma sucumbem à doença. Além disso, pacientes com AIDS, cujo número total de linfócitos T CD4⁺ é reduzido, também têm maior susceptibilidade a desenvolver TB (HAVLIR; BARNES, 1999; O'GARRA; REDFORD; MCNAB; BLOOM *et al.*, 2013). Logo após a ativação, os linfócitos T migram para o sítio infeccioso por volta do 15^o- 18^o dia pós infecção, aonde então irão exercer a sua função protetora ativando os macrófagos infectados (REILEY; CALAYAG; WITTMER; HUNTINGTON *et al.*, 2008). A polarização de linfócitos CD4⁺ para o perfil Th1, que produzem IFN- γ e ativam classicamente os macrófagos para o perfil M1, é extremamente importante para a eliminação da *Mtb*. Alguns estudos mostraram que camundongos são incapazes de controlar uma infecção com baixas doses de *Mtb* na ausência de IFN- γ (COOPER; DALTON; STEWART; GRIFFIN *et al.*, 1993; FLYNN; CHAN; TRIEBOLD; DALTON *et al.*, 1993).

Outra subpopulação de linfócitos T que também é induzida durante a infecção por *Mtb* é a Th17, que se caracteriza pela produção de IL-17. O seu papel na TB não é completamente conhecido e ainda hoje é bastante questionável. Vários trabalhos já mostraram o efeito protetor dos linfócitos Th17 na TB, que se deve principalmente ao efeito da citocina IL-17 em induzir o recrutamento de neutrófilos (PERREAU; ROZOT; WELLES; BELLUTI-ENDERS *et al.*, 2013; PREZZEMOLO; GUGGINO; LA MANNA; DI LIBERTO *et al.*, 2014). Além disso, as células Th17 também são capazes de induzir o recrutamento de monócitos e linfócitos Th1 para o sítio de formação do granuloma (JURADO; PASQUINELLI; ALVAREZ; PENA *et al.*, 2012; PREZZEMOLO; GUGGINO; LA MANNA; DI LIBERTO *et al.*, 2014). Por outro lado, alguns estudos mostraram que a estimulação contínua das células Th17 promove uma inflamação exacerbada mediada por neutrófilos e monócitos que migram em grandes quantidades para sítio infeccioso e causam lesão tecidual (PREZZEMOLO; GUGGINO; LA MANNA; DI LIBERTO *et al.*, 2014).

Os linfócitos T CD8⁺ também são indispensáveis no combate a TB. Esses linfócitos podem eliminar o patógeno diretamente, através da liberação de granulosa, e também indiretamente, por induzir a lise de macrófagos e DCs infectadas (STENGER; HANSON; TEITELBAUM; DEWAN *et al.*, 1998).

Os bacilos sobreviventes continuam se multiplicando no interior dos fagócitos e, na maioria dos casos, são contidos no interior do granuloma (Figura 2C). Essa estrutura é um agregado organizado de células imunes que se forma em resposta à um estímulo persistente e contém a disseminação do agente infeccioso (RAMAKRISHNAN, 2012). O equilíbrio entre a micobactéria e a resposta imune do hospedeiro ocasiona a infecção latente, e o indivíduo apresenta-se assintomático e sem evidências clínicas da doença, porém mantendo o bacilo na forma quiescente (O'GARRA; REDFORD; MCNAB; BLOOM *et al.*, 2013). A quebra desse equilíbrio resulta na reativação do bacilo e desenvolvimento da doença.

1.4 TB grave e modelo murino como ferramenta para estudo

Os casos de TB grave são caracterizados pela rápida expansão do infiltrado granulomatoso que resulta em pneumonia tuberculosa, e eventualmente disseminação bacilar hematogênica. Uma das principais características da forma grave da doença é a presença de granulomas que possuem centro necrótico caseoso

com presença de bacilos no meio extracelular e *debri* celular (DORHOI; REECE; KAUFMANN, 2011). Os fatores que determinam a transição da infecção bacteriana para a TB ativa com rápida progressão da doença ainda não são completamente compreendidos. Porém, algumas características do hospedeiro (predisposição genética, imunodeficiência e mal nutrição) e da bactéria (alta virulência ou alta dose infectante) podem contribuir para esse processo (CAWS; THWAITES; DUNSTAN; HAWN *et al.*, 2008). A virulência das micobactérias pode ser caracterizada *in vitro* por vários modelos de infecção de macrófagos ou *in vivo* através da infecção de animais (PROZOROV; FEDOROVA; BEKKER; DANILENKO, 2014). *In vitro*, as diferenças na virulência têm sido definidas pelo crescimento bacteriano intracelular e indução da morte das células hospedeiras, enquanto que *in vivo* são estabelecidas com base na proliferação bacteriana nos órgãos, alterações histopatológicas e curva de sobrevivência dos animais infectados (DORMANS; BURGER; AGUILAR; HERNANDEZ-PANDO *et al.*, 2004; SOHN; LEE; KIM; SHIN *et al.*, 2009). Micobactérias de alta virulência proliferam mais rápido, causam mais dano no tecido pulmonar e alta taxa de mortalidade, e são transmitidas com maior facilidade do que as cepas atenuadas ou de baixa virulência (DORMANS; BURGER; AGUILAR; HERNANDEZ-PANDO *et al.*, 2004; MANCA; TSENOVA; BERGTOLD; FREEMAN *et al.*, 2001; MARQUINA-CASTILLO; GARCIA-GARCIA; PONCE-DE-LEON; JIMENEZ-CORONA *et al.*, 2009; THEUS; EISENACH; FOMUKONG; SILVER *et al.*, 2007). Esses fenótipos podem ser resultados de uma redução e/ou atraso na ativação da resposta pró-inflamatória do hospedeiro causados pelas cepas de alta virulência (MANCA; TSENOVA; BERGTOLD; FREEMAN *et al.*, 2001; THEUS; EISENACH; FOMUKONG; SILVER *et al.*, 2007).

O modelo animal para estudo da TB tem fornecido muita informação acerca da patogênese e resposta imune do hospedeiro (ORME, 2011). Entretanto, uma limitação da maioria dos modelos amplamente utilizados, como camundongos, é o fato de não apresentarem necrose pulmonar, uma das principais características da TB grave. A necrose tecidual é atípica até mesmo quando infectados com cepas virulentas de *Mtb*, como a cepa referência H37Rv (DORHOI; KAUFMANN, 2016; DORHOI; REECE; KAUFMANN, 2011). Os pesquisadores normalmente utilizam camundongos deficientes em moléculas imunologicamente importantes, como IFN- γ , iNOS, receptor de células T (TCR) $\alpha\beta$ e receptor de TNF- α , para que ocorra lesões teciduais necróticas induzidas pela micobactéria (GIL; GUIRADO; GORDILLO; DIAZ *et al.*,

2006). Além disso, infecções com elevadíssimas doses do bacilo, ou ainda infecções com baixas doses seguida pela administração de LPS (lipopolissacarídeo) ou Poly IC (polinosínico-policitidílico), também são usadas para induzir necrose pulmonar (ANTONELLI; GIGLIOTTI ROTHFUCHS; GONCALVES; ROFFE *et al.*, 2010; CARDONA; LLATJOS; GORDILLO; DIAZ *et al.*, 2001). Entretanto, embora essas medidas promovam uma TB com dano tecidual, elas são condições artificiais que não reproduzem o que de fato acontece durante e após a infecção natural. Várias outras alternativas de modelos experimentais de infecção utilizando diferentes espécies de animais, como coelhos, cobaias (porquinho-da-índia) e primatas não humanos também têm sido empregadas para estudar a patogênese da TB (REILING; HOMOLKA; KOHL; STEINHAUSER *et al.*, 2018). O curso da doença em modelos experimentais de primatas não humanos é o que possui maior similaridade com o curso em humanos (PENA; HO, 2015). Entretanto, o uso desses animais é limitado devido a razões éticas e ao alto custo de manutenção.

O nosso laboratório mostrou recentemente que o isolado clínico hipervirulento MP287/03 de *M. bovis* é capaz de induzir a forma grave de TB em camundongos mesmo com baixas doses infectantes. Nesse caso, a doença é caracterizada por intenso infiltrado inflamatório, ampla área de necrose tecidual, disseminação bacilar para outros órgãos e morte prematura dos animais (AMARAL; RIBEIRO; LANES; ALMEIDA *et al.*, 2014). Dessa forma, a infecção com a cepa MP287/03 apresenta características de desenvolvimento da doença similares às observadas na evolução da PPT em humanos. Além disso, estudos prévios em nosso laboratório também revelaram a presença de uma população distinta de células no pulmão desses animais infectados com a cepa MP287/03, que possuía características semelhantes às das MDSCs (*myeloide derived supressor cells*). Recentemente, alguns trabalhos também têm revelado a presença de MDSCs em diferentes modelos de TB (KNAUL; JORG; OBERBECK-MUELLER; HEINEMANN *et al.*, 2014; OBREGON-HENAO; HENAO-TAMAYO; ORME; ORDWAY, 2013; TSIGANOV; VERBINA; RADAIEVA; SOSUNOV *et al.*, 2014). Porém, devido às dificuldades de se ter um modelo de TB que reproduza as lesões teciduais da infecção natural, pouco ainda é conhecido acerca do real papel dessas células na TB grave. Portanto, decidimos avaliar em nosso modelo de infecção com a cepa MP287/03 em camundongos C57BL/6, que representa de forma mais fidedigna o que acontece nas formas agressivas de TB em humanos, o papel das MDSCs no agravamento da doença. A compreensão desses mecanismos envolvidos

na severidade da TB é extremamente importante, pois podem abrir alternativas para o desenvolvimento de novas abordagens terapêuticas que visam atenuar as formas graves da doença.

1.5 Células mieloides supressoras (MDSCs)

As MDSCs são uma população heterogênea de células que possuem em comum o fato de serem derivadas da linhagem mieloide, ainda estarem no estágio imaturo e possuírem função imunossupressora (GABRILOVICH; BRONTE; CHEN; COLOMBO *et al.*, 2007). Nos organismos saudáveis as células mieloides imaturas são geradas na medula óssea e rapidamente se diferenciam em granulócitos maduros, macrófagos e DCs. Porém, em algumas situações patológicas como câncer, sepse, inflamações crônicas, autoimunidade e também em várias doenças infecciosas, ocorre um bloqueio parcial na diferenciação das células mieloides imaturas, que resulta na expansão dessa população e na migração dessas células ainda em seu estágio imaturo para o órgão afetado (GABRILOVICH, 2017; GABRILOVICH; NAGARAJ, 2009).

Essa população de células mieloides foi definida inicialmente como células com fenótipo GR1⁺CD11b⁺ que possuem atividade imunossupressora *in vitro* (YOUN; GABRILOVICH, 2010). Posteriormente, devido a existência de diferenças entre as MDSCs, estas foram então subdivididas fenotipicamente e morfologicamente em dois subgrupos: as granulocíticas (G-MDSC) e as monocíticas (M-MDSC) (GABRILOVICH, 2017). As G-MDSCs se assemelham aos neutrófilos e apresentam o fenótipo CD11b⁺GR1^{high}Ly6G⁺Ly6C^{low}, enquanto as M-MDSCs são semelhantes aos monócitos e possuem o fenótipo CD11b⁺GR1^{int}Ly6G⁻Ly6C^{high} (MOVAHEDI; GUILLIAMS; VAN DEN BOSSCHE; VAN DEN BERGH *et al.*, 2008; YOUN; NAGARAJ; COLLAZO; GABRILOVICH, 2008). Entretanto, apenas critérios fenotípicos não são suficientes para identificar as MDSCs. Algumas outras metodologias, como por exemplo os ensaios funcionais de supressão de linfócitos T *in vitro* e expressão gênica, são necessárias para ajudar a diferenciar essas células imaturas dos neutrófilos e monócitos maduros (GABRILOVICH, 2017).

Diferentes vias de imunossupressão são utilizadas pelas subpopulações de MDSCs como: indução de células imunossupressoras, comprometimento do tráfego de linfócitos, produção de radicais livres, depleção metabólica, produção de adenosina

e expressão de moléculas reguladoras. Parte desses mecanismos estão representados na figura 3 e descritos mais detalhadamente a seguir:

- Indução da geração de células Tregs e polarização de macrófagos para o subtipo M2 através da produção de IL-10 (Figura 3A) (BEURY; PARKER; NYANDJO; SINHA *et al.*, 2014; HUANG; PAN; LI; SATO *et al.*, 2006; SERAFINI; MGE BROFF; NOONAN; BORRELLO, 2008).
- Altos níveis de expressão de iNOS, enzima que produz óxido nítrico (NO) a partir do metabolismo da L-arginina. O NO em nível muito alto pode causar a anergia de linfócitos T. Além disso, essa molécula também compromete a migração de linfócitos por induzir a redução da expressão de moléculas de adesão como a ligante de P-selectina (CD162) e CD44 (Figura 3B) (BINGISSER; TILBROOK; HOLT; KEES, 1998; FLEMING; HU; WEBER; NAGIBIN *et al.*, 2018; SATO; OZAKI; OH; MEGURO *et al.*, 2007).
- Expressão elevada de ADAM17 (*ADAM metallopeptidase domain 17*), enzima que cliva o CD62L (L-selectina). A redução no nível de CD62L diminui o tráfego de linfócitos T *naive* para o linfonodo, local onde eles reconheceriam os antígenos e seriam ativados (Figura 3B) (HANSON; CLEMENTS; SINHA; ILKOVITCH *et al.*, 2009).
- Produção exacerbada de ROS. Algumas populações de MDSCs expressam NOX2 (NADPH oxidase 2), que é responsável por produzir radicais livres como ROS. Quando presente em alta concentração, o ROS é capaz de induzir apoptose de linfócitos T (KUMAR; PATEL; TCYGANOV; GABRILOVICH, 2016; OSTRAND-ROSENBERG; SINHA, 2009). Ainda mais, a reação do ROS com o NO forma o peroxinitrito, o qual causa nitrosilação do TCR resultando na anergia de linfócitos T (Figura 3C) (HARDY; WICK; WEBB, 2008).
- Alta expressão de Arg-1 (arginase) é um dos principais fatores responsáveis pelo efeito imunossupressor das MDSCs. Essa enzima converte a L-arginina em L-ornitina e ureia. O aumento da captura de L-arginina através do transportador CAT2B, expresso nas MDSCs, causa a depleção desse aminoácido disponível no meio (Figura 3D). Por sua vez, a carência de L-arginina causa um atraso no ciclo celular dos linfócitos T na fase G₀-G₁ (RODRIGUEZ; QUICENO; OCHOA, 2007). Além disso, a escassez de L-

- arginina torna as células T anérgicas devido à redução da expressão da cadeia ζ do TCR (BANIYASH, 2004; FLEMING; HU; WEBER; NAGIBIN *et al.*, 2018).
- Depleção de cisteína. Embora as MDSCs não expressem ASC (transportador de Alanina-Serina-Cisteína), elas apresentam alto nível de SLC7A11, um transportador de cistina (Figura 3D). A cistina é utilizada como precursor para produção de cisteína pelos macrófagos e DCs. O sequestro de cistina realizado pelas MDSCs através da SLC7A11 resulta na redução da conversão e excreção de cisteína pelos macrófagos e DCs. Consequentemente, a escassez de cisteína inibe a síntese de proteínas, a produção de glutatona e prejudica a proliferação de células T (SRIVASTAVA; SINHA; CLEMENTS; RODRIGUEZ *et al.*, 2010).
 - Expressão elevada de IDO (indoleamine 2,3-dioxygenase), enzima que degrada triptofano em N-formil-quinurenina. A escassez de triptofano além de promover parada no ciclo celular de linfócitos T e anergia, também induz a polarização de linfócitos T CD4⁺ para um perfil regulador (Treg) (MUNN; SHARMA; BABAN; HARDING *et al.*, 2005; PLATTEN; WICK; VAN DEN EYNDE, 2012). Somado a isto, a quinurenina, produto da ação da IDO, inibe a proliferação e a sobrevivência de linfócitos T efetores além de também induzir a polarização para linfócitos Treg (FRUMENTO; ROTONDO; TONETTI; DAMONTE *et al.*, 2002; MEZRICH; FECHNER; ZHANG; JOHNSON *et al.*, 2010).
 - Expressão elevada das ectonucleotidases CD39 e CD73. Essas moléculas estão envolvidas na conversão de ATP em AMP e AMP em adenosina, respectivamente (LI; WANG; CHEN; LI *et al.*, 2017). A adenosina, por sua vez, inibe o *priming* de células T virgens por inibir a cascata de sinalização de ativação. Além disso, a adenosina também reduz a expressão de moléculas efetoras nos linfócitos T já ativados, como CD95L (FAS-L), perforinas, IFN- γ e TNF- α (LINDEN; CEKIC, 2012).
 - Alta expressão de moléculas reguladoras como PDL-1 e FAS-L, as quais interagem com seus respectivos receptores na superfície de linfócitos T e causam anergia e apoptose (LU; REDD; LEE; SAVAGE *et al.*, 2016; ZHU; POWIS DE TENBOSSCHE; CANE; COLAU *et al.*, 2017).

- Secreção de citocinas anti-inflamatórias como TGF- β e IL-10. Essas citocinas reduzem a atividade de linfócitos T efetores além de induzir o recrutamento de células Treg e afetar negativamente a maturação de células NK (FLEMING; HU; WEBER; NAGIBIN *et al.*, 2018; SINHA; CLEMENTS; BUNT; ALBELDA *et al.*, 2007; UMEMURA; SAIO; SUWA; KITOH *et al.*, 2008).

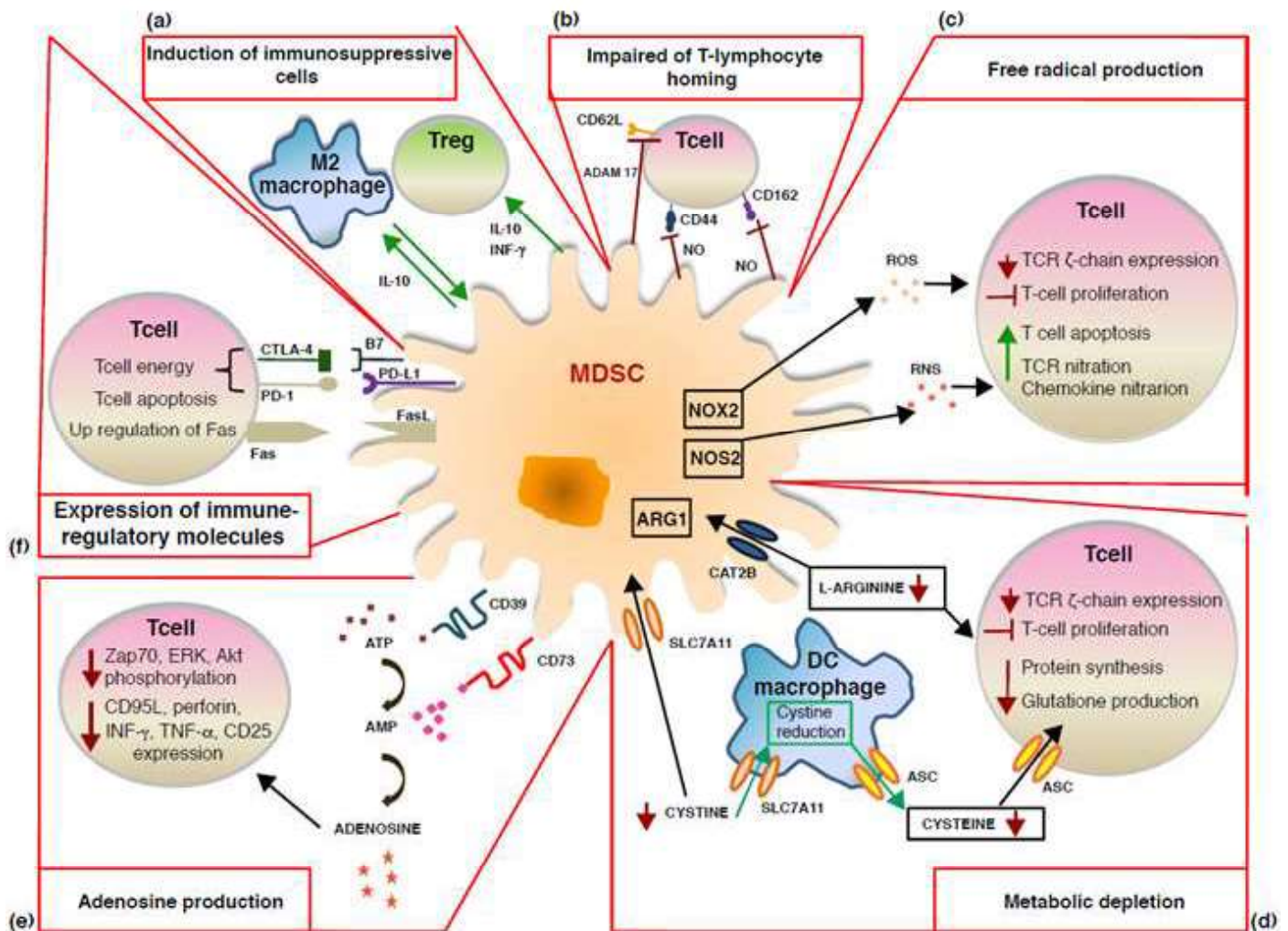


Figura 3: Mecanismos de imunossupressão das MDSCs.

Fonte: PRINCIPI; RAFFAGHELLO, 2019

1.6 Irg1 e Itaconato

Ao longo de milênios de evolução a *Mtb* desenvolveu múltiplas estratégias para impedir com sucesso a sua eliminação pelas células do sistema imune e promover a sua disseminação e sobrevivência no hospedeiro. Sabe-se que para crescer dentro do fagossomo, o qual é um ambiente escasso de substratos para realizar a glicólise,

a *Mtb* altera o seu perfil metabólico para conseguir obter energia (DUNN; RAMIREZ-TRUJILLO; HERNANDEZ-LUCAS, 2009). A ICL (isocitratoliasa) é uma enzima essencial para a via do glioxilato, que é uma variação do ciclo do ácido cítrico presente somente em plantas e microrganismos. Essa via metabólica facilita o uso de lipídeos e colesterol do hospedeiro como fonte de carbono para geração de ATP (LORENZ; FINK, 2002). A *Mtb* tem pelo menos duas enzimas ICLs (ICL1 e ICL2) que são responsáveis por fazer essa mudança para a via do glioxilato (DUNN; RAMIREZ-TRUJILLO; HERNANDEZ-LUCAS, 2009; HONER ZU BENTRUP; MICZAK; SWENSON; RUSSELL, 1999).

Por outro lado, o *Irg1* (gene imunorresponsivo) é uma enzima mitocondrial codificado pelo gene *Irg1*, também conhecido como *Acod1* (*Aconitate decarboxylase 1*), induzida por estímulos inflamatórios. Essa enzima é responsável por produzir o metabólito itaconato através da descarboxilação do cis-aconitato, um intermediário do ciclo do ácido cítrico (CAC) (Figura 4). Vários trabalhos já haviam mostrado há quase meio século atrás o efeito bactericida do itaconato, entretanto essa molécula não tinha ganhado notoriedade até descobrirem que ela poderia ser gerada de forma natural nas células de mamíferos (LUAN; MEDZHITOV, 2016; MCFADDEN; PUROHIT, 1977; SHIN; YANG; JEON; YOON *et al.*, 2011; WILLIAMS; ROCHE; MCFADDEN, 1971). A atividade bactericida desse metabólito foi mostrada em bactérias de diferentes espécies como *Salmonella enterica*, *Acinetobacter baumannii*, MRSA (*Staphylococcus aureus* resistente à metilicilina), *Legionella pneumophila* (MICHELUCCI; CORDES; GHELFI; PAILOT *et al.*, 2013; NAUJOKS; TABELING; DILL; HOFFMANN *et al.*, 2016). Michelucci e colaboradores mostraram que esse metabólito também inibe a proliferação de *Mtb* em meio de cultura líquido (MICHELUCCI; CORDES; GHELFI; PAILOT *et al.*, 2013). O mecanismo proposto para esse efeito bacteriostático do itaconato é a inibição da enzima ICL, que é necessária para a persistência da micobactéria no macrófago.

Além disso, o itaconato também tem um papel importante na regulação do metabolismo das células imunes e da resposta inflamatória. A reprogramação metabólica da população de células imunes pode influenciar drasticamente a resposta imunológica e modular as propriedades antimicrobianas das células infectadas do hospedeiro, demonstrando que os metabólitos estão fortemente ligados às funções efetoras (HOFFMANN; MACHELART; BELHAOUANE; DEBOOSERE *et al.*, 2019). Em 2016, Lampropoulou e colaboradores mostraram que o itaconato modula o

metabolismo do macrófago através da inibição da oxidação do succinato pela enzima succinato desidrogenase (SDH) (LAMPROPOULOU; SERGUSHICHEV; BAMBOUSKOVA; NAIR *et al.*, 2016). A SDH é uma enzima do CAC e também um importante componente do complexo II da cadeia transportadora de elétrons (Figura 4). Portanto, a sua inibição causa uma parada no CAC, e conseqüentemente uma redução na fosforilação oxidativa e um aumento da glicólise, que passa a ser então a principal via de produção de energia nos macrófagos estimulados (LAMPROPOULOU; SERGUSHICHEV; BAMBOUSKOVA; NAIR *et al.*, 2016). Esse estudo também mostrou que o tratamento de macrófagos com dimetil-itaconato, uma forma do itaconato não iônica permeável à membrana, inibiu a produção de IL-6, IL-12, IL-1 β e NO em macrófagos ativados com uma variedade de estímulos inflamatórios. Ainda mais, confirmando essa hipótese, macrófagos deficientes em *Irg1* apresentaram aumento significativo da resposta pró-inflamatória (LAMPROPOULOU; SERGUSHICHEV; BAMBOUSKOVA; NAIR *et al.*, 2016).

Esse efeito na regulação da resposta pró-inflamatória faz do itaconato uma importante molécula imunomoduladora na infecção pela *Mtb*, pois sabe-se que a excessiva ativação do sistema imune pode prejudicar a eliminação do bacilo além de promover lesão tecidual. De fato, trabalhos recentes mostraram que a expressão do gene *Irg1* nas células mieloides LysM⁺ é crucial para a resistência frente à infecção pela *Mtb* com significativa redução da imunopatologia pulmonar mediada pelo recrutamento excessivo de neutrófilos (HOFFMANN; MACHELART; BELHAOUANE; DEBOOSERE *et al.*, 2019; NAIR; HUYNH; LAMPROPOULOU; LOGINICHEVA *et al.*, 2018). Além disso, Hoffmann e colaboradores mostraram que os fagócitos deficientes em *Irg1* tem uma quantidade muito elevada de gotas de lipídeos (GL), as quais favorecem a proliferação do bacilo, sugerindo a forte dependência deste patógeno dos lipídeos do hospedeiro estocados em GL (HOFFMANN; MACHELART; BELHAOUANE; DEBOOSERE *et al.*, 2019).

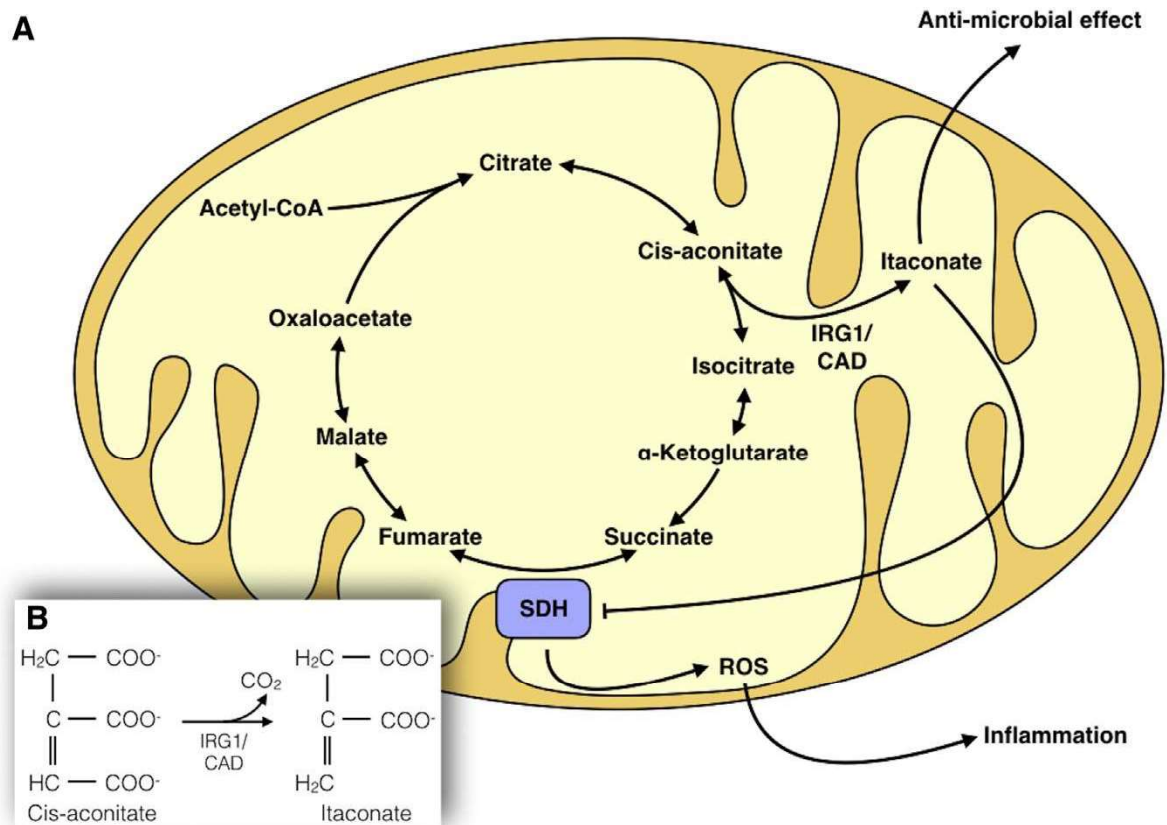


Figura 4: Via de produção do Itaconato e seu papel na resposta imune.

Fonte: LUAN; MEDZHITOV, 2016

Entretanto, uma questão importante não solucionada ainda diz respeito ao mecanismo pelo qual a *Mtb* induz a expressão do gene *Irg1*. Diante de todo exposto, decidimos avaliar nesse trabalho o papel das MDSCs na forma grave de tuberculose e possíveis vias de intervenção para redução da imunopatologia pulmonar, bem como investigar o mecanismo molecular de indução da expressão do gene *Irg1* desencadeado pela *Mtb*.

2 Objetivos

2.1 Geral

O objetivo central desse trabalho foi compreender o papel das MDSCs na TB grave utilizando um modelo murino, bem como estudar os mecanismos de indução da expressão do gene *Irg1* e produção do Itaconato.

2.2 Específicos

- **Objetivo 1:** Identificar e caracterizar o perfil fenotípico e funcional das MDSCs presentes no pulmão de camundongos com a forma grave da TB induzida por cepa hipervirulenta em camundongos imunocompetentes
- **Objetivo 2:** Verificar o mecanismo de imunossupressão utilizado pelas MDSCs na TB grave
- **Objetivo 3:** Avaliar se a eliminação das MDSCs implica na melhora da imunopatologia e no restabelecimento da ativação da resposta imune
- **Objetivo 4:** Investigar quais receptores de superfície celular envolvidos no reconhecimento da *Mycobacterium tuberculosis* e vias de sinalização estão relacionados com a indução da expressão do gene *Irg1*
- **Objetivo 5:** Averiguar a participação de sensores citosólico na indução da expressão do gene *Irg1* durante a infecção por *Mycobacterium tuberculosis* e produção do itaconato

3 Metodologia

3.1 Micobactérias

O isolado clínico hipervirulento MP287/03 (*M. bovis*) foi gentilmente cedido pelo professor Dr. José Soares Ferreira Neto da Faculdade de Medicina Veterinária e Zootecnia da USP. A cepa H37Rv (*M. tuberculosis* - ATCC), utilizada como referência de virulência na TB, foi cedida pelo Dr. Philip Stuffys da Fiocruz do Rio de Janeiro e a cepa BCG foi adquirida da ATCC.

As bactérias foram cultivadas em meio sólido Middlebrook 7H10 (Ágar) (Becton Dickinson) enriquecido com 10% de OADC (ácido oleico, albumina, dextrose e catalase – Difco Laboratories), glicerol (cepa H37Rv) ou 0,4% de piruvato sódico (cepa MP287/03) por 21 dias à 37°C. As colônias crescidas foram removidas do Ágar e suspensas em meio líquido Middlebrook 7H9 (Becton Dickinson) enriquecido com 10% de ADC (albumina, dextrose e catalase – Difco Laboratories), 0,05% de Tween 80 e com ou sem 0,04% de piruvato sódico para as cepas MP287/03 e H37Rv, respectivamente. Essas amostras foram mantidas em cultura à 37°C até alcançarem a densidade ótica (D.O.) de ~ 0,6, quando então várias alíquotas de 1 mL foram congeladas à -80°C.

3.2 Animais

Para realização do projeto foram usados camundongos da linhagem C57BL/6 livres de patógenos específicos (SPF) fornecidos pelo biotério de camundongos isogênicos do Instituto de Ciências Biomédicas (ICB) da USP. Além disso também foram usados camundongos C57BL/6, NFkBp50KO, IFN α / β RKO que foram adquiridos da Taconic Farms (Hudson, NY, EUA). Já os camundongos TLR2KO, TLR4KO e TLR9KO foram gentilmente cedidos pelo Dr. Giorgio Trinchieri, enquanto os camundongos CARD9KO, STINGKO e IFN γ RKO foram cedidos pelo Dr. Michail Lionakis, Dr^a. Mahtab Moayeri e Dr^a. Dragana Jankovic, respectivamente.

Após a infecção, os animais C57BL/6 foram mantidos em microisoladores (racks ventiladas) no biotério de experimentação do laboratório nível 3 de biossegurança (NB-3) da Faculdade de Ciências Farmacêuticas (FCF) da USP. Este projeto de pesquisa foi avaliado e aprovado pela Comissão de Ética do Uso de Animais (CEUA) do ICB (protocolo nº 31/2016) da USP.

3.3 Infecção dos Animais

Os bacilos foram descongelados e cultivados por 7 dias à 37°C em meio líquido Middlebrook 7H9 enriquecido (enriquecimento detalhado na seção 3.1) para aumentar a viabilidade bacteriana. Em seguida, as amostras foram submetidas ao banho ultrassônico e agitadas em vórtex por 1 minuto, para dispersão dos grumos bacterianos. A quantificação bacilar foi realizada no espectrofotômetro (Hitachi-model U-1100) com comprimento de onda de 600 nm.

Para o procedimento de infecção, os camundongos foram anestesiados com uma injeção intraperitoneal (i.p.) de 120 µL de uma solução contendo xilazina (15 mg/kg - Vetbrand) e ketamina (110 mg/kg – Vetbrand). Testes de reflexos foram feitos após cinco minutos da administração do anestésico para certificar se os animais estavam realmente anestesiados. Posteriormente, uma pequena incisão cirúrgica foi realizada para expor a traqueia, e então inoculou-se, via intratraqueal, 60 µL de PBS contendo ~ 100 bacilos. O corte cirúrgico foi suturado e os animais mantidos enrolados em gaze para protegê-los de hipotermia.

3.4 Análises macroscópicas e microscópicas dos pulmões

Os camundongos foram eutanasiados 21 ou 28 dias após a infecção por deslocamento cervical. Os pulmões foram então coletados, lavados com PBS (phosphate-buffered saline) estéril e pesados em balança analítica. A massa relativa do pulmão foi determinada através do quociente entre a massa do pulmão infectado e a massa do pulmão controle. Com o auxílio de uma tesoura cirúrgica os lobos do pulmão foram separados e o lobo superior direito conservado em formaldeído tamponado 10%. Foi tirada a fotografia desse lobo e, posteriormente, o mesmo foi seccionado com espessura de 4-5 µm para coloração com hematoxilina/eosina (HE), afim de visualizar as alterações teciduais, e com a técnica de Ziehl-Neelsen (ZN), para detectar a presença de bacilos álcool-ácido resistentes (BAAR). As lâminas foram examinadas com um microscópio Nikon (Japão), e as imagens capturadas com uma câmera Nikon Coolpix P995 (Japão).

3.5 Obtenção de células do pulmão

Os lobos médio e inferior direito e o pulmão esquerdo foram destinados ao processamento para posterior análise em citometria de fluxo. No processamento, esses lobos foram picotados com tesouras cirúrgicas e então suspensos em 4 mL de solução de digestão [0,5 mg/mL de Colagenase tipo IV (Sigma, USA)], durante 40 minutos sob agitação de 160 rpm à 37°C. Em seguida, as células foram dispersadas através da fricção com o êmbolo de seringa (BD), e filtradas com “cell strainer” (Corning, USA). Os eritrócitos foram então lisados com o tampão de lise ACK (Thermo Fisher Scientific, USA) por 1 minuto à temperatura ambiente. As células foram contadas em câmara de Neubauer e, posteriormente, distribuídas (10⁶ células/poço) em placas de 96 poços para marcação com anticorpos e leitura no citômetro de fluxo.

3.6 Obtenção de células do sangue

Logo após a eutanásia dos animais foi coletado o sangue, através de pulsão cardíaca, e adicionado o anticoagulante heparina. Os eritrócitos foram lisados com o tampão de lise ACK (Thermo Fisher Scientific) por 3 minutos a temperatura ambiente. As células obtidas foram colocadas em placas de 96 poços para marcação com anticorpos e leitura no citômetro de fluxo.

3.7 Obtenção de células da medula óssea

Após a eutanásia, o fêmur dos animais também foi removido e posteriormente submetidos à um *flushing* com RPMI 1640 incompleto para extração das células da medula óssea. Para dispersar os grumos de células, as mesmas foram passadas pela seringa de 10 mL com a agulha de calibre G26. As células obtidas foram então contadas em câmara de Neubauer e semeadas em placas de 96 poços na concentração de 10⁶ células/poço para marcação com anticorpos e leitura no citômetro de fluxo.

3.8 Análise fenotípica de células por citometria de fluxo

As células obtidas do pulmão, medula e sangue foram marcadas com a combinação adequada dos fluoróforos APC, APCcy7, FITC, PE, PEcy7, PercP, PB e V500, ligados aos anticorpos monoclonais anti-GR1, anti-CD11b, anti-Ly6G, anti-Ly6C, anti-CD11c, anti-CD45, anti-CCR2, anti-CD115, anti-CD135, anti-CD4, anti-CD8, anti-CD19, anti-NK1.1, anti-CD44, anti-CD69, anti-CD62L, anti-PD1, anti-PD-L1, anti-CD39, anti-CD73, anti-FASL e anti-TLR2. As amostras foram lidas por citometria de fluxo (FACSCanto, BD Biosciences, EUA) e os dados analisados com o programa FlowJo v.10.5.

3.9 Avaliação da produção de citocinas por *Cytometric Bead Array* (CBA)

As células obtidas do pulmão foram suspensas em meio RPMI 1640 completo (suplementado com 10% de SBF, 1% de L-glutamina, 1% de piruvato e 0,1% de gentamicina) e cultivadas por 48 horas à 37°C e 5% de CO₂. Em seguida, o sobrenadante foi filtrado em Spin-X e armazenado à -80°C. Os níveis de TNF- α , IFN- γ , IL-17 e IL-10 foram quantificados por CBA utilizando o *Kit Mouse Th1/Th2/Th17* seguindo as instruções do manual do fabricante (BD Biosciences, EUA). A leitura dos dados foi realizada por citometria de fluxo (FACSCanto BD Biosciences, EUA) e os resultados analisados com o programa *BD CBA Analysis Software*.

3.10 Isolamento da população CD11b⁺GR1⁺

Para enriquecer a população CD11b⁺GR1⁺, células obtidas da medula óssea do fêmur e tíbia de camundongos controles e infectados foram separadas por *sorting* magnético. Para esse procedimento, primeiramente realizamos o bloqueio do receptor FcR utilizando o *FcR Blocking Reagente* (Miltenyi Biotec) por 10 min à 4°C. Em seguida, as células foram marcadas com anticorpo anti-GR1-biotina por mais 10 min à 4°C, lavadas e então incubadas com MicroBeads streptavidina por 15 min à 4°C. As células foram novamente lavadas e então a população CD11b⁺GR1⁺ foi positivamente selecionada através de eluição em colunas magnéticas LS MACS (Miltenyi Biotec). A pureza foi superior a 90%.

3.11 Ensaio funcional de inibição da proliferação de linfócitos T

A população CD11b⁺GR1⁺ purificada da medula óssea foi plaqueada em diferentes proporções com splenócitos *naïve*, os quais foram previamente marcados com *cell tracer* de acordo com as instruções do fabricante. Esta cocultura foi suspensa em meio RPMI 1640 completo (10% de SBF, 1% de L-glutamina, 1% de piruvato e 0,1% de gentamicina), estimulada com anti-CD3 (1 µg/mL) e anti-CD28 (1 µg/mL) e incubada por 48h à 37°C e 5% de CO₂. As células foram então marcadas com anticorpos anti-CD4 e anti-CD8, fixadas e posteriormente foi realizada a avaliação da proliferação por citometria de fluxo (FACSCanto BD Biosciences, EUA). Para o experimento *transwell*, os splenócitos foram plaqueados na base e as células CD11b⁺GR1⁺ na *chamber* do *transwell*. O estímulo e os ensaios seguintes foram realizados como explicado acima.

3.12 Ensaio funcional da inibição da produção de IFN-γ por ELISA

As células CD11b⁺GR1⁺ purificadas da medula óssea foram co-cultivadas com splenócitos como explicado no item 3.11. Após 48h de cultivo o sobrenadante foi coletado, filtrado com Spin-X e armazenado à -80°C. A quantificação da produção de IFN-γ por ELISA com o Kit Mouse IFNγ-ELISA Set - (BD-OptEIA, EUA) de acordo com as instruções do fabricante.

3.13 Extração de RNA do tecido pulmonar e avaliação da expressão gênica por qRT-PCR

O lobo pós-caudal do pulmão foi removido e conservado em trizol à -20°C. Posteriormente, ele foi macerado na presença de nitrogênio líquido com o auxílio de um pistilo previamente esterilizado. O produto foi centrifugado e o sobrenadante recolhido para a extração de RNA. O processo de extração do RNA foi realizado com o Kit RNeasy® Mini (Qiagen, Germantown, USA). Todas as amostras de RNAs extraídas tiveram o resultado da relação DO₂₆₀/DO₂₈₀ entre 1,8 e 2, onde DO é a densidade óptica nos respectivos comprimentos de onda de 260 e 280nm. O RNA isolado foi então quantificado e diluído à concentração de 100 ng/µL. Em seguida, adicionou-se os reagentes para conversão em cDNA (High Capacity cDNA Reverse

Transcription Kit, Applied Biosystems Life Technologies, California, USA) e incubou-se no termociclador (PTC-100™ Programmable Thermal Controller, MJ Reserach, Inc.). O cDNA produzido foi armazenado no freezer à -80°C. À posteriori, foi realizado o PCR em tempo real para quantificar a expressão gênica utilizando o ensaio Platinum® SYBR® Green (Invitrogen Life Technologies. Os seguintes genes foram avaliados: arginase (*Arg1*), TNF- α (*Tnf*), IFN- γ (*Ifn*), IL-17 (*Il17a*), IL-10 (*Il10*), Irg1 (*Irg1*), IL12 (*Il12p35*), IFN- β (*Ifnb1*), MX2 (*Mx2*) e OAS1 (*Oas1a*). O gene endógeno utilizado foi o GAPDH e os resultados foram expressos como $2^{-\Delta\Delta CT}$. As sequências de todos o *primers* utilizados estão na tabela abaixo.

Gene	Forward Primer	Reverse Primer
<i>Gapdh</i>	5'- TGA AGC AGG CAT CTG AGG G -3'	3'- CGA AGG TGG AAG AGT GGG AG -5'
<i>Arg1</i>	5'- AAA GCT GGT CTG CTG GAA AA -3'	3'- ACA GAC CGT GGG TTC TTC AC -5'
<i>Tnf</i>	5'- CAT CTT CTC AAA ATT CGA GTG ACA A -3'	3'- TGG GAG TAG ACA AGG TAC AAC CC -5'
<i>Ifn</i>	5'- TCA AGT GGC ATA GAT GTG GAA GAA -3'	3'- TGG CTC TGC AGG ATT TTC ATG -5'
<i>Il17a</i>	5'- GCT CCA GAA GGC CCT CAG A -3'	3'- AGC TTT CCC TCC GCA TTG A -5'
<i>Il10</i>	5'- GGT TGC CAA GCC TTA TCG GA -3'	3'- ACC TGC TCC ACT GCC TTG CT -5'
<i>Irg1</i>	5'- GCG AAC GCT GCC ACT CA -3'	5'- ATC CCA GGC TTG GAA GGT C -3'
<i>Il12p35</i>	5' – ACG TCT TTG ATG ATG ACC CTG T-3'	5'-TTC TGA AGT GCT GCG TTG A-3'
<i>Ifnb1</i>	5'- GTC CGA GCA GAG ATC TTC AGG-3'	5'- ACT ACC AGT CCC AGA GTC CG -3'
<i>Mx2</i>	5'- CCA GTT CCT CTC AGT CCC AAG ATT -3'	5'- TAC TGG ATG AAG GGA ACG TGG -3'
<i>Oas1a</i>	5'- CCC TAT CTG ACA CAT TGA CGG T -3'	5'- TAT TCT ATG GTC CCC CAG CCT -3'

3.14 Eliminação *in vivo* de células GR1⁺

Para os experimentos envolvendo a eliminação de células GR1⁺, os camundongos C57BL/6 infectados com a cepa MP287/03 de *M. bovis* foram tratados com anticorpo anti-GR1 (hibridoma RB6-8C5) com dose de 200 μ g/animal via intraperitoneal a cada três dias a partir do 21° dia após infecção. Subsequentemente, para acompanhar a eficácia do tratamento, foi realizado esfregaços sanguíneos a cada 24h de cada animal e então analisados por microscopia óptica. Os animais foram sacrificados no 28° após infecção. Camundongos infectados e tratados com IgG2b-kappa foram usados como controle isotípico. Além disso, camundongos não infectados e tratados com anti-GR1 foram usados como controle experimental.

3.15 Extração da medula óssea, diferenciação de macrófagos e infecção *in vitro*

Os camundongos foram eutanaziados em câmara de gás com CO. A medula óssea foi coletada a partir do fêmur e tíbia dos animais através de punção com PBS. Para dissociação da medula foi realizado a passagem cuidadosa através de uma agulha calibre 26. Em seguida as células foram cultivadas em placas de Petri com meio DEMEM F12 (Gibco, USA) suplementado com 1 mM de piruvato de sódio, 2 mM de L-glutamina, 0,05% de gentamicina, 10% de soro bovino fetal e 20% de sobrenadante de L929 em uma estufa à 37°C e 5% CO₂. Um volume de 10 mL adicionais desse mesmo meio, porém sem antibiótico, foi colocado após 4 dias de incubação. Os macrófagos derivados da medula óssea (BMDMs) obtidos no sétimo dia de diferenciação foram então removidos das placas de Petri, contados e plaqueados na concentração de 10⁶ células/poço em placas de 24 poços. As células foram incubadas durante a noite para uma adequada aderência à superfície da placa e então foram infectadas com *Mtb* (H37Rv) ou BCG (MOI 1:1) durante 3 horas. Após esse período, elas foram lavadas com PBS para remoção das bactérias que não foram fagocitadas e então incubadas novamente na estufa à 37°C e 5% CO₂ até o tempo desejado (3, 6, 9, 12 ou 24h).

Em alguns experimentos os BMDMs foram tratados com inibidores de fagocitose (1 µM de mycalolide B ou 40 µM de dynasore) aproximadamente 1 hora antes da infecção, ou então com inibidor de transcrição gênica (1 µg/mL de actinomicina D) ou de síntese proteica (10 µg/mL de cicloheximidina) aproximadamente 2h antes da infecção. Em outros experimentos, as BMDM foram tratadas com IFN-β (10 ng/mL) ou IFN-γ (10 U/mL) recombinantes ou com bafilomicina (1 µM) concomitantemente com a infecção. Algumas amostras foram estimuladas com LPS (10 ng/mL), PAM3CSK4 (10 ng/mL), CpG (1 µM), Trehalose (1 µg/mL) ou PolyIC (20 µg/L) ao invés de serem infectadas.

3.16 Diferenciação de macrófagos humanos

O elutriado de leucócitos humanos foi obtido a partir de doadores saudáveis e a fração de monócitos CD14⁺ purificada por coluna magnética. Os macrófagos foram gerados a partir da cultura de monócitos com meio contendo M-CSF (60 ng/mL) por 7 dias. A cada 48 horas foi adicionado meio de cultura novo enriquecido com soro humano, L-glutamina, piruvato, aminoácidos essenciais e o referido fator de crescimento M-CSF. Após o término da diferenciação os macrófagos foram então infectados com micobactérias da cepa H37Rv.

3.17 Quantificação do Itaconato

Após a diferenciação, os BMDMs foram infectados com *Mtb* (H37Rv) durante 3h e então lavados com PBS e mantidos em cultura à 37°C e 5% CO₂ por 24h. Em seguida, as células foram lisadas com solução metanol:água (80:20), filtradas em Spin-X e congeladas à -80°C. Os metabólitos itaconato e cis-acnitato das amostras foram quantificados por HPLC/MS.

3.18 Análise estatística

Os resultados foram analisados com o software Prism 7 (GraphPad Software Incorporated, EUA). As análises foram feitas utilizando os testes T de student, One-Way ANOVA ou Two-Way ANOVA seguidos por pós teste de Tukey. As diferenças entre os grupos foram consideradas significativas quando o valor de *p* foi < 0.05.

6 Conclusão

Os resultados apresentados nessa tese mostram que as G-MDSCs têm um papel relevante no agravamento do quadro da TB induzido por cepa hipervirulenta em modelos imunocompetentes, principalmente por levar à uma imunossupressão e favorecer a proliferação e disseminação bacteriana, acarretando na morte precoce. Nossos dados sugerem que a interação PD1/PD-L1 é um dos mecanismos envolvidos na imunossupressão induzida pelas G-MDSCs. A depleção dessa população causou uma expressiva melhora na imunopatologia pulmonar e foi associada com redução da carga bacteriana e aumento na sobrevivência. Além disso, também mostramos que as vias do TLR2/MyD88/NFκB bem como a do STING/IFN-I estão envolvidas na indução da expressão do gene *Irg1* e produção do itaconato, importante molécula que reduz a imunopatologia pulmonar mediada pelo recrutamento excessivo de granulócitos. Esse estudo revela novas possibilidades de abordagens terapêuticas que visam atenuar as formas graves de TB, através da intervenção em vias imunossupressoras, como depleção de MDSCs ou inibição da interação PD1/PDL1, ou ainda em vias que reduzam o recrutamento de granulócitos, como a do itaconato.

REFERÊNCIAS

AGATA, Y.; KAWASAKI, A.; NISHIMURA, H.; ISHIDA, Y. *et al.* Expression of the PD-1 antigen on the surface of stimulated mouse T and B lymphocytes. **Int Immunol**, 8, n. 5, p. 765-772, May 1996.

ALMATAR, M.; MAKKY, E. A.; YAKICI, G.; VAR, I. *et al.* Antimicrobial peptides as an alternative to anti-tuberculosis drugs. **Pharmacol Res**, 128, p. 288-305, Feb 2018.

AMARAL, E. P.; LASUNSKAIA, E. B.; D'IMPERIO-LIMA, M. R. Innate immunity in tuberculosis: how the sensing of mycobacteria and tissue damage modulates macrophage death. **Microbes Infect**, 18, n. 1, p. 11-20, Jan 2016.

AMARAL, E. P.; MACHADO DE SALLES, E.; BARBOSA BOMFIM, C. C.; SALGADO, R. M. *et al.* Inhibiting Adenosine Receptor Signaling Promotes Accumulation of Effector CD4+ T Cells in the Lung Parenchyma During Severe Tuberculosis. **J Infect Dis**, 219, n. 6, p. 964-974, Feb 23 2019.

AMARAL, E. P.; RIBEIRO, S. C.; LANES, V. R.; ALMEIDA, F. M. *et al.* Pulmonary infection with hypervirulent Mycobacteria reveals a crucial role for the P2X7 receptor in aggressive forms of tuberculosis. **PLoS Pathog**, 10, n. 7, 2014. Research Support, Non-U S Gov't.

AMULIC, B.; CAZALET, C.; HAYES, G. L.; METZLER, K. D. *et al.* Neutrophil function: from mechanisms to disease. **Annu Rev Immunol**, 30, p. 459-489, 2012.

ANTONELLI, L. R.; GIGLIOTTI ROTHFUCHS, A.; GONCALVES, R.; ROFFE, E. *et al.* Intranasal Poly-IC treatment exacerbates tuberculosis in mice through the pulmonary recruitment of a pathogen-permissive monocyte/macrophage population. **J Clin Invest**, 120, n. 5, p. 1674-1682, May 2010.

ARDAIN, A.; DOMINGO-GONZALEZ, R.; DAS, S.; KAZER, S. W. *et al.* Publisher Correction: Group 3 innate lymphoid cells mediate early protective immunity against tuberculosis. *In: Nature*. England, 2019. v. 572, p. E10.

BAFICA, A.; SCANGA, C. A.; FENG, C. G.; LEIFER, C. *et al.* TLR9 regulates Th1 responses and cooperates with TLR2 in mediating optimal resistance to Mycobacterium tuberculosis. **J Exp Med**, 202, n. 12, p. 1715-1724, Dec 19 2005.

BANIYASH, M. TCR zeta-chain downregulation: curtailing an excessive inflammatory immune response. **Nat Rev Immunol**, 4, n. 9, p. 675-687, Sep 2004.

BANKOVICH, A. J.; SHIOW, L. R.; CYSTER, J. G. CD69 suppresses sphingosine 1-phosphate receptor-1 (S1P1) function through interaction with membrane helix 4. **J Biol Chem**, 285, n. 29, p. 22328-22337, Jul 16 2010.

BEURY, D. W.; PARKER, K. H.; NYANDJO, M.; SINHA, P. *et al.* Cross-talk among myeloid-derived suppressor cells, macrophages, and tumor cells impacts the inflammatory milieu of solid tumors. **J Leukoc Biol**, 96, n. 6, p. 1109-1118, Dec 2014.

BINGISSER, R. M.; TILBROOK, P. A.; HOLT, P. G.; KEES, U. R. Macrophage-derived nitric oxide regulates T cell activation via reversible disruption of the Jak3/STAT5 signaling pathway. **J Immunol**, 160, n. 12, p. 5729-5734, Jun 15 1998.

BLOMGRAN, R.; DESVIGNES, L.; BRIKEN, V.; ERNST, J. D. Mycobacterium tuberculosis inhibits neutrophil apoptosis, leading to delayed activation of naive CD4 T cells. **Cell Host Microbe**, 11, n. 1, p. 81-90, Jan 19 2012.

BLOMGRAN, R.; ERNST, J. D. Lung neutrophils facilitate activation of naive antigen-specific CD4+ T cells during Mycobacterium tuberculosis infection. **J Immunol**, 186, n. 12, p. 7110-7119, Jun 15 2011.

BOETTCHER, S.; MANZ, M. G. Regulation of Inflammation- and Infection-Driven Hematopoiesis. **Trends Immunol**, 38, n. 5, p. 345-357, May 2017.

BRANDLI, O. The clinical presentation of tuberculosis. **Respiration**, 65, n. 2, p. 97-105, 1998.

BRASIL. Ministério da Saúde. Manual de recomendações para o controle da Tuberculose. EPIDEMIOLOGICA, D. D. V. Brasília / DF -: 284 p. 2011.

BRASIL. Ministério da Saúde: Boletim Epidemiológico. Brasil. 49: 18 p. 2019.

BRODIN, P.; MAJLESSI, L.; MARSOLLIER, L.; DE JONGE, M. I. *et al.* Dissection of ESAT-6 system 1 of Mycobacterium tuberculosis and impact on immunogenicity and virulence. **Infect Immun**, 74, n. 1, p. 88-98, Jan 2006.

BRU, A.; CARDONA, P. J. Mathematical modeling of tuberculosis bacillary counts and cellular populations in the organs of infected mice. **PLoS One**, 5, n. 9, p. e12985, Sep 23 2010.

CARDONA, P. J.; LLATJOS, R.; GORDILLO, S.; DIAZ, J. *et al.* Towards a 'human-like' model of tuberculosis: intranasal inoculation of LPS induces intragranulomatous lung necrosis in mice infected aerogenically with Mycobacterium tuberculosis. **Scand J Immunol**, 53, n. 1, p. 65-71, Jan 2001.

CAWS, M.; THWAITES, G.; DUNSTAN, S.; HAWN, T. R. *et al.* The influence of host and bacterial genotype on the development of disseminated disease with Mycobacterium tuberculosis. **PLoS Pathog**, 4, n. 3, p. e1000034, Mar 2008.

CERVANTES, J. L. MyD88 in Mycobacterium tuberculosis infection. *In: Med Microbiol Immunol*. Germany, 2017. v. 206, p. 187-193.

CERVANTES, J. L.; HAWLEY, K. L.; BENJAMIN, S. J.; WEINERMAN, B. *et al.* Phagosomal TLR signaling upon *Borrelia burgdorferi* infection. **Front Cell Infect Microbiol**, 4, p. 55, 2014.

CHAI, Q.; LU, Z.; LIU, C. H. Host defense mechanisms against *Mycobacterium tuberculosis*. **Cell Mol Life Sci**, Nov 13 2019.

CHALMIN, F.; LADOIRE, S.; MIGNOT, G.; VINCENT, J. *et al.* Membrane-associated Hsp72 from tumor-derived exosomes mediates STAT3-dependent immunosuppressive function of mouse and human myeloid-derived suppressor cells. **J Clin Invest**, 120, n. 2, p. 457-471, Feb 2010.

CHEMNITZ, J. M.; PARRY, R. V.; NICHOLS, K. E.; JUNE, C. H. *et al.* SHP-1 and SHP-2 associate with immunoreceptor tyrosine-based switch motif of programmed death 1 upon primary human T cell stimulation, but only receptor ligation prevents T cell activation. **J Immunol**, 173, n. 2, p. 945-954, Jul 15 2004.

CHENG, P.; CORZO, C. A.; LUETTEKE, N.; YU, B. *et al.* Inhibition of dendritic cell differentiation and accumulation of myeloid-derived suppressor cells in cancer is regulated by S100A9 protein. **J Exp Med**, 205, n. 10, p. 2235-2249, Sep 29 2008.

CHENG, P.; EKSIÖGLU, E. A.; CHEN, X.; KANDELL, W. *et al.* S100A9-induced overexpression of PD-1/PD-L1 contributes to ineffective hematopoiesis in myelodysplastic syndromes. **Leukemia**, 33, n. 8, p. 2034-2046, Aug 2019.

CLEMENS, D. L.; HORWITZ, M. A. Characterization of the *Mycobacterium tuberculosis* phagosome and evidence that phagosomal maturation is inhibited. **J Exp Med**, 181, n. 1, p. 257-270, 1995. In Vitro Research Support, Non-U S Gov't Research Support, U S Gov't, P H S.

COLLINS, A. C.; CAI, H.; LI, T.; FRANCO, L. H. *et al.* Cyclic GMP-AMP Synthase Is an Innate Immune DNA Sensor for *Mycobacterium tuberculosis*. **Cell Host Microbe**, 17, n. 6, p. 820-828, Jun 10 2015.

CONDAMINE, T.; GABRILOVICH, D. I. Molecular mechanisms regulating myeloid-derived suppressor cell differentiation and function. **Trends Immunol**, 32, n. 1, p. 19-25, Jan 2011.

CONDAMINE, T.; MASTIO, J.; GABRILOVICH, D. I. Transcriptional regulation of myeloid-derived suppressor cells. **J Leukoc Biol**, 98, n. 6, p. 913-922, Dec 2015.

CONRAD, W. H.; OSMAN, M. M.; SHANAHAN, J. K.; CHU, F. *et al.* Mycobacterial ESX-1 secretion system mediates host cell lysis through bacterium contact-dependent gross membrane disruptions. **Proc Natl Acad Sci U S A**, 114, n. 6, p. 1371-1376, Feb 7 2017.

COOPER, A. M.; DALTON, D. K.; STEWART, T. A.; GRIFFIN, J. P. *et al.* Disseminated tuberculosis in interferon gamma gene-disrupted mice. **J Exp Med**, 178, n. 6, p. 2243-2247, Dec 01 1993.

COSMA, C. L.; SHERMAN, D. R.; RAMAKRISHNAN, L. The secret lives of the pathogenic mycobacteria. **Annu Rev Microbiol**, 57, p. 641-676, 2003. Research Support, Non-U S Gov't Research Support, U S Gov't, P H S Review.

CRAPO, J. D.; BARRY, B. E.; GEHR, P.; BACHOFEN, M. *et al.* Cell number and cell characteristics of the normal human lung. **Am Rev Respir Dis**, 126, n. 2, p. 332-337, Aug 1982.

DALLENKA, T.; SCHAIBLE, U. E. Neutrophils in tuberculosis--first line of defence or booster of disease and targets for host-directed therapy? **Pathog Dis**, 74, n. 3, Apr 2016.

DAMUZZO, V.; PINTON, L.; DESANTIS, G.; SOLITO, S. *et al.* Complexity and challenges in defining myeloid-derived suppressor cells. **Cytometry B Clin Cytom**, 88, n. 2, p. 77-91, Mar 2015.

DE JONGE, M. I.; PEHAU-ARNAUDET, G.; FRETZ, M. M.; ROMAIN, F. *et al.* ESAT-6 from Mycobacterium tuberculosis dissociates from its putative chaperone CFP-10 under acidic conditions and exhibits membrane-lysing activity. **J Bacteriol**, 189, n. 16, p. 6028-6034, Aug 2007.

DORHOI, A.; KAUFMANN, S. H. Pathology and immune reactivity: understanding multidimensionality in pulmonary tuberculosis. **Semin Immunopathol**, 38, n. 2, p. 153-166, Mar 2016.

DORHOI, A.; REECE, S. T.; KAUFMANN, S. H. For better or for worse: the immune response against Mycobacterium tuberculosis balances pathology and protection. **Immunol Rev**, 240, n. 1, p. 235-251, 2011. Research Support, Non-U S Gov't Review.

DORMANS, J.; BURGER, M.; AGUILAR, D.; HERNANDEZ-PANDO, R. *et al.* Correlation of virulence, lung pathology, bacterial load and delayed type hypersensitivity responses after infection with different Mycobacterium tuberculosis genotypes in a BALB/c mouse model. **Clin Exp Immunol**, 137, n. 3, p. 460-468, Sep 2004.

DRABCZYK-PLUTA, M.; WERNER, T.; HOFFMANN, D.; LENG, Q. *et al.* Granulocytic myeloid-derived suppressor cells suppress virus-specific CD8(+) T cell responses during acute Friend retrovirus infection. **Retrovirology**, 14, n. 1, p. 42, Aug 23 2017.

DUNN, M. F.; RAMIREZ-TRUJILLO, J. A.; HERNANDEZ-LUCAS, I. Major roles of isocitrate lyase and malate synthase in bacterial and fungal pathogenesis. **Microbiology**, 155, n. Pt 10, p. 3166-3175, Oct 2009.

ERUSLANOV, E. B.; LYADOVA, I. V.; KONDRATIEVA, T. K.; MAJOROV, K. B. *et al.* Neutrophil responses to Mycobacterium tuberculosis infection in genetically susceptible and resistant mice. **Infect Immun**, 73, n. 3, p. 1744-1753, Mar 2005.

ESIN, S.; BATONI, G.; COUNOUPAS, C.; STRINGARO, A. *et al.* Direct binding of human NK cell natural cytotoxicity receptor NKp44 to the surfaces of mycobacteria and other bacteria. **Infect Immun**, 76, n. 4, p. 1719-1727, Apr 2008.

FENG, C. G.; KAVIRATNE, M.; ROTHFUCHS, A. G.; CHEEVER, A. *et al.* NK cell-derived IFN-gamma differentially regulates innate resistance and neutrophil response in T cell-deficient hosts infected with *Mycobacterium tuberculosis*. **J Immunol**, 177, n. 10, p. 7086-7093, Nov 15 2006.

FENNELLY, K. P.; JONES-LOPEZ, E. C.; AYAKAKA, I.; KIM, S. *et al.* Variability of infectious aerosols produced during coughing by patients with pulmonary tuberculosis. **Am J Respir Crit Care Med**, 186, n. 5, p. 450-457, Sep 1 2012.

FLEMING, T. J.; FLEMING, M. L.; MALEK, T. R. Selective expression of Ly-6G on myeloid lineage cells in mouse bone marrow. RB6-8C5 mAb to granulocyte-differentiation antigen (Gr-1) detects members of the Ly-6 family. **J Immunol**, 151, n. 5, p. 2399-2408, 1993. Research Support, U S Gov't, P H S.

FLEMING, V.; HU, X.; WEBER, R.; NAGIBIN, V. *et al.* Targeting Myeloid-Derived Suppressor Cells to Bypass Tumor-Induced Immunosuppression. **Front Immunol**, 9, p. 398, 2018.

FLYNN, J. L.; CHAN, J.; TRIEBOLD, K. J.; DALTON, D. K. *et al.* An essential role for interferon gamma in resistance to *Mycobacterium tuberculosis* infection. **J Exp Med**, 178, n. 6, p. 2249-2254, Dec 01 1993.

FRANCIS, R. J.; BUTLER, R. E.; STEWART, G. R. *Mycobacterium tuberculosis* ESAT-6 is a leukocidin causing Ca²⁺ influx, necrosis and neutrophil extracellular trap formation. **Cell Death Dis**, 5, p. e1474, Oct 16 2014.

FRUMENTO, G.; ROTONDO, R.; TONETTI, M.; DAMONTE, G. *et al.* Tryptophan-derived catabolites are responsible for inhibition of T and natural killer cell proliferation induced by indoleamine 2,3-dioxygenase. **J Exp Med**, 196, n. 4, p. 459-468, Aug 19 2002.

GABRILOVICH, D. I. Myeloid-Derived Suppressor Cells. **Cancer Immunol Res**, 5, n. 1, p. 3-8, Jan 2017.

GABRILOVICH, D. I.; BRONTE, V.; CHEN, S. H.; COLOMBO, M. P. *et al.* The terminology issue for myeloid-derived suppressor cells. **Cancer Res**, 67, n. 1, p. 425; author reply 426, Jan 01 2007.

GABRILOVICH, D. I.; NAGARAJ, S. Myeloid-derived suppressor cells as regulators of the immune system. **Nat Rev Immunol**, 9, n. 3, p. 162-174, 2009. Review.

GALLINA, G.; DOLCETTI, L.; SERAFINI, P.; DE SANTO, C. *et al.* Tumors induce a subset of inflammatory monocytes with immunosuppressive activity on CD8⁺ T cells. **J Clin Invest**, 116, n. 10, p. 2777-2790, Oct 2006.

GHOSH, M. C.; GORANTLA, V.; MAKENA, P. S.; LUELLEN, C. *et al.* Insulin-like growth factor-I stimulates differentiation of ATII cells to ATI-like cells through activation of Wnt5a. **Am J Physiol Lung Cell Mol Physiol**, 305, n. 3, p. L222-228, Aug 1 2013.

GIL, O.; GUIRADO, E.; GORDILLO, S.; DIAZ, J. *et al.* Intragranulomatous necrosis in lungs of mice infected by aerosol with Mycobacterium tuberculosis is related to bacterial load rather than to any one cytokine or T cell type. **Microbes Infect**, 8, n. 3, p. 628-636, Mar 2006.

GROSCHER, M. I.; SAYES, F.; SIMEONE, R.; MAJLESSI, L. *et al.* ESX secretion systems: mycobacterial evolution to counter host immunity. **Nat Rev Microbiol**, 14, n. 11, p. 677-691, Nov 2016.

HAMMERICH, L.; TACKE, F. Emerging roles of myeloid derived suppressor cells in hepatic inflammation and fibrosis. **World J Gastrointest Pathophysiol**, 6, n. 3, p. 43-50, Aug 15 2015.

HAMMERICH, L.; WARZECHA, K. T.; STEFKOVA, M.; BARTNECK, M. *et al.* Cyclic adenosine monophosphate-responsive element modulator alpha overexpression impairs function of hepatic myeloid-derived suppressor cells and aggravates immune-mediated hepatitis in mice. **Hepatology**, 61, n. 3, p. 990-1002, Mar 2015.

HANSON, E. M.; CLEMENTS, V. K.; SINHA, P.; ILKOVITCH, D. *et al.* Myeloid-derived suppressor cells down-regulate L-selectin expression on CD4+ and CD8+ T cells. **J Immunol**, 183, n. 2, p. 937-944, Jul 15 2009.

HARDY, L. L.; WICK, D. A.; WEBB, J. R. Conversion of tyrosine to the inflammation-associated analog 3'-nitrotyrosine at either TCR- or MHC-contact positions can profoundly affect recognition of the MHC class I-restricted epitope of lymphocytic choriomeningitis virus glycoprotein 33 by CD8 T cells. **J Immunol**, 180, n. 9, p. 5956-5962, May 1 2008.

HAVLIR, D. V.; BARNES, P. F. Tuberculosis in patients with human immunodeficiency virus infection. **N Engl J Med**, 340, n. 5, p. 367-373, Feb 04 1999.

HEGDE, V. L.; NAGARKATTI, P. S.; NAGARKATTI, M. Role of myeloid-derived suppressor cells in amelioration of experimental autoimmune hepatitis following activation of TRPV1 receptors by cannabidiol. **PLoS One**, 6, n. 4, p. e18281, Apr 01 2011.

HEIM, C. E.; VIDLAK, D.; SCHERR, T. D.; KOZEL, J. A. *et al.* Myeloid-derived suppressor cells contribute to Staphylococcus aureus orthopedic biofilm infection. **J Immunol**, 192, n. 8, p. 3778-3792, Apr 15 2014.

HESTDAL, K.; RUSCETTI, F. W.; IHLE, J. N.; JACOBSEN, S. E. *et al.* Characterization and regulation of RB6-8C5 antigen expression on murine bone marrow cells. **J Immunol**, 147, n. 1, p. 22-28, Jul 01 1991.

HEUVERS, M. E.; MUSKENS, F.; BEZEMER, K.; LAMBERS, M. *et al.* Arginase-1 mRNA expression correlates with myeloid-derived suppressor cell levels in peripheral blood of NSCLC patients. **Lung Cancer**, 81, n. 3, p. 468-474, Sep 2013.

HOFFMANN, E.; MACHELART, A.; BELHAOUANE, I.; DEBOOSERE, N. *et al.* IRG1 controls immunometabolic host response and restricts intracellular *Mycobacterium tuberculosis* infection. **bioRxiv**, p. 761551, 2019.

HONER ZU BENTRUP, K.; MICZAK, A.; SWENSON, D. L.; RUSSELL, D. G. Characterization of activity and expression of isocitrate lyase in *Mycobacterium avium* and *Mycobacterium tuberculosis*. **J Bacteriol**, 181, n. 23, p. 7161-7167, Dec 1999.

HONG, J. J.; AMANCHA, P. K.; ROGERS, K.; ANSARI, A. A. *et al.* Re-evaluation of PD-1 expression by T cells as a marker for immune exhaustion during SIV infection. **PLoS One**, 8, n. 3, p. e60186, 2013.

HOUBEN, R. M.; DODD, P. J. The Global Burden of Latent Tuberculosis Infection: A Re-estimation Using Mathematical Modelling. 13, n. 10, p. e1002152, Oct 2016.

HU, J.; LOU, D.; CAROW, B.; WINERDAL, M. E. *et al.* LPS regulates SOCS2 transcription in a type I interferon dependent autocrine-paracrine loop. **PLoS One**, 7, n. 1, p. e30166, 2012.

HUANG, B.; PAN, P. Y.; LI, Q.; SATO, A. I. *et al.* Gr-1+CD115+ immature myeloid suppressor cells mediate the development of tumor-induced T regulatory cells and T-cell anergy in tumor-bearing host. **Cancer Res**, 66, n. 2, p. 1123-1131, Jan 15 2006.

HUYNH, K. K.; JOSHI, S. A.; BROWN, E. J. A delicate dance: host response to mycobacteria. **Curr Opin Immunol**, 23, n. 4, p. 464-472, 2011. Review.

IP, W. K.; SOKOLOVSKA, A.; CHARRIERE, G. M.; BOYER, L. *et al.* Phagocytosis and phagosome acidification are required for pathogen processing and MyD88-dependent responses to *Staphylococcus aureus*. **J Immunol**, 184, n. 12, p. 7071-7081, Jun 15 2010.

JURADO, J. O.; PASQUINELLI, V.; ALVAREZ, I. B.; PENA, D. *et al.* IL-17 and IFN-gamma expression in lymphocytes from patients with active tuberculosis correlates with the severity of the disease. **J Leukoc Biol**, 91, n. 6, p. 991-1002, Jun 2012.

KAO, J.; KO, E. C.; EISENSTEIN, S.; SIKORA, A. G. *et al.* Targeting immune suppressing myeloid-derived suppressor cells in oncology. **Crit Rev Oncol Hematol**, 77, n. 1, p. 12-19, Jan 2011.

KAUFMANN, S. H.; DORHOI, A. Inflammation in tuberculosis: interactions, imbalances and interventions. **Curr Opin Immunol**, 25, n. 4, p. 441-449, Aug 2013.

KAZI, J. U.; RONNSTRAND, L. FMS-like Tyrosine Kinase 3/FLT3: From Basic Science to Clinical Implications. **Physiol Rev**, 99, n. 3, p. 1433-1466, Jul 1 2019.

KEIR, M. E.; BUTTE, M. J.; FREEMAN, G. J.; SHARPE, A. H. PD-1 and its ligands in tolerance and immunity. **Annu Rev Immunol**, 26, p. 677-704, 2008.

KNAUL, J. K.; JORG, S.; OBERBECK-MUELLER, D.; HEINEMANN, E. *et al.* Lung-residing myeloid-derived suppressors display dual functionality in murine pulmonary tuberculosis. **Am J Respir Crit Care Med**, 190, n. 9, p. 1053-1066, Nov 1 2014.

KOHANBASH, G.; MCKAVENEY, K.; SAKAKI, M.; UEDA, R. *et al.* GM-CSF promotes the immunosuppressive activity of glioma-infiltrating myeloid cells through interleukin-4 receptor-alpha. **Cancer Res**, 73, n. 21, p. 6413-6423, Nov 1 2013.

KULCHAVENYA, E. Extrapulmonary tuberculosis: are statistical reports accurate? **Ther Adv Infect Dis**, 2, n. 2, p. 61-70, Apr 2014.

KUMAR, V.; PATEL, S.; TCYGANOV, E.; GABRILOVICH, D. I. The Nature of Myeloid-Derived Suppressor Cells in the Tumor Microenvironment. **Trends Immunol**, 37, n. 3, p. 208-220, Mar 2016.

KUPZ, A.; ZEDLER, U.; STABER, M.; PERDOMO, C. *et al.* ESAT-6-dependent cytosolic pattern recognition drives noncognate tuberculosis control in vivo. **J Clin Invest**, 126, n. 6, p. 2109-2122, Jun 1 2016.

LAI, H. C.; CHANG, C. J.; LIN, C. S.; WU, T. R. *et al.* NK Cell-Derived IFN-gamma Protects against Nontuberculous Mycobacterial Lung Infection. **J Immunol**, 201, n. 5, p. 1478-1490, Sep 1 2018.

LAMPROPOULOU, V.; SERGUSHICHEV, A.; BAMBOUSKOVA, M.; NAIR, S. *et al.* Itaconate Links Inhibition of Succinate Dehydrogenase with Macrophage Metabolic Remodeling and Regulation of Inflammation. **Cell Metab**, 24, n. 1, p. 158-166, Jul 12 2016.

LANG, R. Recognition of the mycobacterial cord factor by Mincle: relevance for granuloma formation and resistance to tuberculosis. **Front Immunol**, 4, p. 5, 2013.

LEE, H. M.; YUK, J. M.; SHIN, D. M.; JO, E. K. Dectin-1 is inducible and plays an essential role for mycobacteria-induced innate immune responses in airway epithelial cells. **J Clin Immunol**, 29, n. 6, p. 795-805, Nov 2009.

LI, J.; WANG, L.; CHEN, X.; LI, L. *et al.* CD39/CD73 upregulation on myeloid-derived suppressor cells via TGF-beta-mTOR-HIF-1 signaling in patients with non-small cell lung cancer. **Oncoimmunology**, 6, n. 6, p. e1320011, 2017.

LIN, Y.; GUSTAFSON, M. P.; BULUR, P. A.; GASTINEAU, D. A. *et al.* Immunosuppressive CD14+HLA-DR(low)/- monocytes in B-cell non-Hodgkin lymphoma. **Blood**, 117, n. 3, p. 872-881, Jan 20 2011.

LINDEN, J.; CEKIC, C. Regulation of lymphocyte function by adenosine. **Arterioscler Thromb Vasc Biol**, 32, n. 9, p. 2097-2103, Sep 2012.

LIU, C. Y.; WANG, Y. M.; WANG, C. L.; FENG, P. H. *et al.* Population alterations of L-arginase- and inducible nitric oxide synthase-expressed CD11b+/CD14(-)/CD15+/CD33+ myeloid-derived

suppressor cells and CD8+ T lymphocytes in patients with advanced-stage non-small cell lung cancer. **J Cancer Res Clin Oncol**, 136, n. 1, p. 35-45, Jan 2010.

LORENZ, M. C.; FINK, G. R. Life and death in a macrophage: role of the glyoxylate cycle in virulence. **Eukaryot Cell**, 1, n. 5, p. 657-662, Oct 2002.

LOWE, D. M.; REDFORD, P. S.; WILKINSON, R. J.; O'GARRA, A. *et al.* Neutrophils in tuberculosis: friend or foe? **Trends Immunol**, 33, n. 1, p. 14-25, Jan 2012.

LU, C.; REDD, P. S.; LEE, J. R.; SAVAGE, N. *et al.* The expression profiles and regulation of PD-L1 in tumor-induced myeloid-derived suppressor cells. **Oncoimmunology**, 5, n. 12, p. e1247135, 2016.

LUAN, H. H.; MEDZHITOV, R. Food Fight: Role of Itaconate and Other Metabolites in Antimicrobial Defense. **Cell Metab**, 24, n. 3, p. 379-387, Sep 13 2016.

MACHELART, A.; SONG, O. R.; HOFFMANN, E.; BRODIN, P. Host-directed therapies offer novel opportunities for the fight against tuberculosis. **Drug Discov Today**, 22, n. 8, p. 1250-1257, Aug 2017.

MAGCWEBEBA, T.; DORHOI, A.; DU PLESSIS, N. The Emerging Role of Myeloid-Derived Suppressor Cells in Tuberculosis. **Front Immunol**, 10, p. 917, 2019.

MANCA, C.; TSENOVA, L.; BERGTOLD, A.; FREEMAN, S. *et al.* Virulence of a Mycobacterium tuberculosis clinical isolate in mice is determined by failure to induce Th1 type immunity and is associated with induction of IFN-alpha /beta. **Proc Natl Acad Sci U S A**, 98, n. 10, p. 5752-5757, May 8 2001.

MANDRUZZATO, S.; SOLITO, S.; FALISI, E.; FRANCESCATO, S. *et al.* IL4Ralpha+ myeloid-derived suppressor cell expansion in cancer patients. **J Immunol**, 182, n. 10, p. 6562-6568, May 15 2009.

MANZANILLO, P. S.; SHILOH, M. U.; PORTNOY, D. A.; COX, J. S. Mycobacterium tuberculosis activates the DNA-dependent cytosolic surveillance pathway within macrophages. **Cell Host Microbe**, 11, n. 5, p. 469-480, May 17 2012.

MARQUINA-CASTILLO, B.; GARCIA-GARCIA, L.; PONCE-DE-LEON, A.; JIMENEZ-CORONA, M. E. *et al.* Virulence, immunopathology and transmissibility of selected strains of Mycobacterium tuberculosis in a murine model. **Immunology**, 128, n. 1, p. 123-133, Sep 2009.

MCFADDEN, B. A.; PUROHIT, S. Itaconate, an isocitrate lyase-directed inhibitor in Pseudomonas indigofera. **J Bacteriol**, 131, n. 1, p. 136-144, Jul 1977.

MEZRICH, J. D.; FECHNER, J. H.; ZHANG, X.; JOHNSON, B. P. *et al.* An interaction between kynurenine and the aryl hydrocarbon receptor can generate regulatory T cells. **J Immunol**, 185, n. 6, p. 3190-3198, Sep 15 2010.

MICHELUCCI, A.; CORDES, T.; GHELFI, J.; PAILOT, A. *et al.* Immune-responsive gene 1 protein links metabolism to immunity by catalyzing itaconic acid production. **Proc Natl Acad Sci U S A**, 110, n. 19, p. 7820-7825, May 7 2013.

MILLRUD, C. R.; BERGENFELZ, C.; LEANDERSSON, K. On the origin of myeloid-derived suppressor cells. **Oncotarget**, 8, n. 2, p. 3649-3665, Jan 10 2017.

MONROE, K. M.; MCWHIRTER, S. M.; VANCE, R. E. Induction of type I interferons by bacteria. **Cell Microbiol**, 12, n. 7, p. 881-890, Jul 2010.

MOONEY, C. J.; CUNNINGHAM, A.; TSAPOGAS, P.; TOELLNER, K. M. *et al.* Selective Expression of Flt3 within the Mouse Hematopoietic Stem Cell Compartment. **Int J Mol Sci**, 18, n. 5, May 12 2017.

MOVAHEDI, K.; GUILLIAMS, M.; VAN DEN BOSSCHE, J.; VAN DEN BERGH, R. *et al.* Identification of discrete tumor-induced myeloid-derived suppressor cell subpopulations with distinct T cell-suppressive activity. **Blood**, 111, n. 8, p. 4233-4244, Apr 15 2008.

MUELLER, P.; PIETERS, J. Modulation of macrophage antimicrobial mechanisms by pathogenic mycobacteria. **Immunobiology**, 211, n. 6-8, p. 549-556, 2006. Research Support, Non-U S Gov't Review.

MUNN, D. H.; SHARMA, M. D.; BABAN, B.; HARDING, H. P. *et al.* GCN2 kinase in T cells mediates proliferative arrest and anergy induction in response to indoleamine 2,3-dioxygenase. **Immunity**, 22, n. 5, p. 633-642, May 2005.

MUTHU, K.; IYER, S.; HE, L. K.; SZILAGYI, A. *et al.* Murine hematopoietic stem cells and progenitors express adrenergic receptors. **J Neuroimmunol**, 186, n. 1-2, p. 27-36, May 2007.

NAIR, S.; HUYNH, J. P.; LAMPROPOULOU, V.; LOGINICHEVA, E. *et al.* Irg1 expression in myeloid cells prevents immunopathology during M. tuberculosis infection. **J Exp Med**, 215, n. 4, p. 1035-1045, Apr 2 2018.

NAUJOKS, J.; TABELING, C.; DILL, B. D.; HOFFMANN, C. *et al.* IFNs Modify the Proteome of Legionella-Containing Vacuoles and Restrict Infection Via IRG1-Derived Itaconic Acid. **PLoS Pathog**, 12, n. 2, p. e1005408, Feb 2016.

NICHOLAS, B.; SKIPP, P.; MOULD, R.; RENNARD, S. *et al.* Shotgun proteomic analysis of human-induced sputum. **Proteomics**, 6, n. 15, p. 4390-4401, Aug 2006.

NOMAN, M. Z.; DESANTIS, G.; JANJI, B.; HASMIM, M. *et al.* PD-L1 is a novel direct target of HIF-1alpha, and its blockade under hypoxia enhanced MDSC-mediated T cell activation. **J Exp Med**, 211, n. 5, p. 781-790, May 05 2014.

NORRIS, B. A.; UEBELHOER, L. S.; NAKAYA, H. I.; PRICE, A. A. *et al.* Chronic but not acute virus infection induces sustained expansion of myeloid suppressor cell numbers that inhibit viral-specific T cell immunity. **Immunity**, 38, n. 2, p. 309-321, Feb 21 2013.

NOUAILLES, G.; DORHOI, A.; KOCH, M.; ZERRAHN, J. *et al.* CXCL5-secreting pulmonary epithelial cells drive destructive neutrophilic inflammation in tuberculosis. **J Clin Invest**, 124, n. 3, p. 1268-1282, Mar 2014.

O'GARRA, A.; REDFORD, P. S.; MCNAB, F. W.; BLOOM, C. I. *et al.* The immune response in tuberculosis. **Annu Rev Immunol**, 31, p. 475-527, 2013.

OBERMAJER, N.; MUTHUSWAMY, R.; ODUNSI, K.; EDWARDS, R. P. *et al.* PGE(2)-induced CXCL12 production and CXCR4 expression controls the accumulation of human MDSCs in ovarian cancer environment. **Cancer Res**, 71, n. 24, p. 7463-7470, Dec 15 2011.

OBREGON-HENAO, A.; HENAO-TAMAYO, M.; ORME, I. M.; ORDWAY, D. J. Gr1(int)CD11b+ myeloid-derived suppressor cells in Mycobacterium tuberculosis infection. **PLoS One**, 8, n. 11, 2013. Research Support, American Recovery and Reinvestment Act Research Support, N I H , Extramural.

ORGANIZATION, W. H. Global Tuberculosis Report 2019. 2019.

ORME, I. M. Development of new vaccines and drugs for TB: limitations and potential strategic errors. **Future Microbiol**, 6, n. 2, p. 161-177, Feb 2011.

OSTRAND-ROSENBERG, S.; SINHA, P. Myeloid-derived suppressor cells: linking inflammation and cancer. **J Immunol**, 182, n. 8, p. 4499-4506, Apr 15 2009.

PAUWELS, A. M.; TROST, M.; BEYAERT, R.; HOFFMANN, E. Patterns, Receptors, and Signals: Regulation of Phagosome Maturation. **Trends Immunol**, 38, n. 6, p. 407-422, Jun 2017.

PENA, J. C.; HO, W. Z. Monkey models of tuberculosis: lessons learned. **Infect Immun**, 83, n. 3, p. 852-862, Mar 2015.

PENG, X.; SUN, J. Mechanism of ESAT-6 membrane interaction and its roles in pathogenesis of Mycobacterium tuberculosis. **Toxicon**, 116, p. 29-34, Jun 15 2016.

PERREAU, M.; ROZOT, V.; WELLES, H. C.; BELLUTI-ENDERS, F. *et al.* Lack of Mycobacterium tuberculosis-specific interleukin-17A-producing CD4+ T cells in active disease. **Eur J Immunol**, 43, n. 4, p. 939-948, Apr 2013.

PLATTEN, M.; WICK, W.; VAN DEN EYNDE, B. J. Tryptophan catabolism in cancer: beyond IDO and tryptophan depletion. **Cancer Res**, 72, n. 21, p. 5435-5440, Nov 1 2012.

PREZZEMOLO, T.; GUGGINO, G.; LA MANNA, M. P.; DI LIBERTO, D. *et al.* Functional Signatures of Human CD4 and CD8 T Cell Responses to Mycobacterium tuberculosis. **Front Immunol**, 5, p. 180, 2014.

PRINCIPI, E.; RAFFAGHELLO, L. The role of the P2X7 receptor in myeloid-derived suppressor cells and immunosuppression. **Curr Opin Pharmacol**, 47, p. 82-89, Aug 2019.

PROZOROV, A. A.; FEDOROVA, I. A.; BEKKER, O. B.; DANILENKO, V. N. [The virulence factors of Mycobacterium tuberculosis: genetic control, new conceptions]. **Genetika**, 50, n. 8, p. 885-908, Aug 2014.

QIN, W.; HU, L.; ZHANG, X.; JIANG, S. *et al.* The Diverse Function of PD-1/PD-L Pathway Beyond Cancer. **Front Immunol**, 10, p. 2298, 2019.

RABAHI, M. F.; DA SILVA JÚNIOR, J. L. R.; FERREIRA, A. C. G.; TANNUS-SILVA, D. G. S. *et al.* Tratamento da tuberculose. **Jornal Brasileiro de Pneumologia**, 43, n. 6, p. 472-486, 2017.

RAMAKRISHNAN, L. Revisiting the role of the granuloma in tuberculosis. **Nat Rev Immunol**, 12, n. 5, p. 352-366, 2012. Research Support, N I H , Extramural Review.

REILEY, W. W.; CALAYAG, M. D.; WITTMER, S. T.; HUNTINGTON, J. L. *et al.* ESAT-6-specific CD4 T cell responses to aerosol Mycobacterium tuberculosis infection are initiated in the mediastinal lymph nodes. **Proc Natl Acad Sci U S A**, 105, n. 31, p. 10961-10966, Aug 05 2008.

REILING, N.; HOMOLKA, S.; KOHL, T. A.; STEINHAUSER, C. *et al.* Shaping the niche in macrophages: Genetic diversity of the M. tuberculosis complex and its consequences for the infected host. **Int J Med Microbiol**, 308, n. 1, p. 118-128, Jan 2018.

REUSCHL, A. K.; EDWARDS, M. R.; PARKER, R.; CONNELL, D. W. *et al.* Innate activation of human primary epithelial cells broadens the host response to Mycobacterium tuberculosis in the airways. **PLoS Pathog**, 13, n. 9, p. e1006577, Sep 2017.

RILEY, R. L.; MILLS, C. C.; NYKA, W.; WEINSTOCK, N. *et al.* Aerial dissemination of pulmonary tuberculosis. A two-year study of contagion in a tuberculosis ward. 1959. **Am J Epidemiol**, 142, n. 1, p. 3-14, Jul 1 1995.

ROBERTS, L. L.; ROBINSON, C. M. Mycobacterium tuberculosis infection of human dendritic cells decreases integrin expression, adhesion and migration to chemokines. **Immunology**, 141, n. 1, p. 39-51, Jan 2014.

RODRIGUEZ, P. C.; QUICENO, D. G.; OCHOA, A. C. L-arginine availability regulates T-lymphocyte cell-cycle progression. **Blood**, 109, n. 4, p. 1568-1573, Feb 15 2007.

ROTH, F.; DE LA FUENTE, A. C.; VELLA, J. L.; ZOSO, A. *et al.* Aptamer-mediated blockade of IL4Ralpha triggers apoptosis of MDSCs and limits tumor progression. **Cancer Res**, 72, n. 6, p. 1373-1383, Mar 15 2012.

ROY, M. G.; LIVRAGHI-BUTRICO, A.; FLETCHER, A. A.; MCELWEE, M. M. *et al.* Muc5b is required for airway defence. **Nature**, 505, n. 7483, p. 412-416, Jan 16 2014.

SAJID, A.; ARORA, G.; SINGHAL, A.; KALIA, V. C. *et al.* Protein Phosphatases of Pathogenic Bacteria: Role in Physiology and Virulence. **Annu Rev Microbiol**, 69, p. 527-547, 2015.

SALMANINEJAD, A.; VALILOU, S. F.; SHABGAH, A. G.; ASLANI, S. *et al.* PD-1/PD-L1 pathway: Basic biology and role in cancer immunotherapy. **J Cell Physiol**, 234, n. 10, p. 16824-16837, Aug 2019.

SARRA, M.; CUPI, M. L.; BERNARDINI, R.; RONCHETTI, G. *et al.* IL-25 prevents and cures fulminant hepatitis in mice through a myeloid-derived suppressor cell-dependent mechanism. **Hepatology**, 58, n. 4, p. 1436-1450, Oct 2013.

SATO, K.; OZAKI, K.; OH, I.; MEGURO, A. *et al.* Nitric oxide plays a critical role in suppression of T-cell proliferation by mesenchymal stem cells. **Blood**, 109, n. 1, p. 228-234, Jan 1 2007.

SCHERR, N.; MULLER, P.; PERISA, D.; COMBALUZIER, B. *et al.* Survival of pathogenic mycobacteria in macrophages is mediated through autophosphorylation of protein kinase G. **J Bacteriol**, 191, n. 14, p. 4546-4554, 2009. Research Support, Non-U S Gov't.

SCHOENEN, H.; BODENDORFER, B.; HITCHENS, K.; MANZANERO, S. *et al.* Cutting edge: Mincle is essential for recognition and adjuvanticity of the mycobacterial cord factor and its synthetic analog trehalose-dibehenate. **J Immunol**, 184, n. 6, p. 2756-2760, Mar 15 2010.

SERAFINI, P.; MGE BROFF, S.; NOONAN, K.; BORRELLO, I. Myeloid-derived suppressor cells promote cross-tolerance in B-cell lymphoma by expanding regulatory T cells. **Cancer Res**, 68, n. 13, p. 5439-5449, Jul 1 2008.

SHIN, J. H.; YANG, J. Y.; JEON, B. Y.; YOON, Y. J. *et al.* (1)H NMR-based metabolomic profiling in mice infected with Mycobacterium tuberculosis. **J Proteome Res**, 10, n. 5, p. 2238-2247, May 6 2011.

SINHA, P.; CLEMENTS, V. K.; BUNT, S. K.; ALBELDA, S. M. *et al.* Cross-talk between myeloid-derived suppressor cells and macrophages subverts tumor immunity toward a type 2 response. **J Immunol**, 179, n. 2, p. 977-983, Jul 15 2007.

SINHA, P.; PARKER, K. H.; HORN, L.; OSTRAND-ROSENBERG, S. Tumor-induced myeloid-derived suppressor cell function is independent of IFN-gamma and IL-4Ralpha. **Eur J Immunol**, 42, n. 8, p. 2052-2059, Aug 2012.

SKABYTSKA, Y.; WOLBING, F.; GUNTHER, C.; KOBERLE, M. *et al.* Cutaneous innate immune sensing of Toll-like receptor 2-6 ligands suppresses T cell immunity by inducing myeloid-derived suppressor cells. **Immunity**, 41, n. 5, p. 762-775, Nov 20 2014.

SOHN, H.; LEE, K. S.; KIM, S. Y.; SHIN, D. M. *et al.* Induction of cell death in human macrophages by a highly virulent Korean Isolate of Mycobacterium tuberculosis and the virulent strain H37Rv. **Scand J Immunol**, 69, n. 1, p. 43-50, Jan 2009.

SRIVASTAVA, M. K.; SINHA, P.; CLEMENTS, V. K.; RODRIGUEZ, P. *et al.* Myeloid-derived suppressor cells inhibit T-cell activation by depleting cystine and cysteine. **Cancer Res**, 70, n. 1, p. 68-77, Jan 1 2010.

STANLEY, S. A.; JOHNDROW, J. E.; MANZANILLO, P.; COX, J. S. The Type I IFN response to infection with Mycobacterium tuberculosis requires ESX-1-mediated secretion and contributes to pathogenesis. **J Immunol**, 178, n. 5, p. 3143-3152, Mar 1 2007.

STENGER, S.; HANSON, D. A.; TEITELBAUM, R.; DEWAN, P. *et al.* An antimicrobial activity of cytolytic T cells mediated by granulysin. **Science**, 282, n. 5386, p. 121-125, Oct 02 1998.

TAKEDA, K.; AKIRA, S. Toll-like receptors in innate immunity. **Int Immunol**, 17, n. 1, p. 1-14, Jan 2005.

TALMADGE, J. E.; GABRILOVICH, D. I. History of myeloid-derived suppressor cells. **Nat Rev Cancer**, 13, n. 10, p. 739-752, Oct 2013.

TEBARTZ, C.; HORST, S. A.; SPARWASSER, T.; HUEHN, J. *et al.* A major role for myeloid-derived suppressor cells and a minor role for regulatory T cells in immunosuppression during Staphylococcus aureus infection. **J Immunol**, 194, n. 3, p. 1100-1111, Feb 01 2015.

THEUS, S.; EISENACH, K.; FOMUKONG, N.; SILVER, R. F. *et al.* Beijing family Mycobacterium tuberculosis strains differ in their intracellular growth in THP-1 macrophages. **Int J Tuberc Lung Dis**, 11, n. 10, p. 1087-1093, Oct 2007.

TJARNLUND, A.; RODRIGUEZ, A.; CARDONA, P. J.; GUIRADO, E. *et al.* Polymeric IgR knockout mice are more susceptible to mycobacterial infections in the respiratory tract than wild-type mice. **Int Immunol**, 18, n. 5, p. 807-816, May 2006.

TSIGANOV, E. N.; VERBINA, E. M.; RADAIEVA, T. V.; SOSUNOV, V. V. *et al.* Gr-1dimCD11b⁺ Immature Myeloid-Derived Suppressor Cells but Not Neutrophils Are Markers of Lethal Tuberculosis Infection in Mice. **J Immunol**, 7, p. 7, 2014. Journal article.

UMEMURA, N.; SAIO, M.; SUWA, T.; KITO, Y. *et al.* Tumor-infiltrating myeloid-derived suppressor cells are pleiotropic-inflamed monocytes/macrophages that bear M1- and M2-type characteristics. **J Leukoc Biol**, 83, n. 5, p. 1136-1144, May 2008.

VACCA, P.; CHIOSSONE, L.; MINGARI, M. C.; MORETTA, L. Heterogeneity of NK Cells and Other Innate Lymphoid Cells in Human and Murine Decidua. **Front Immunol**, 10, p. 170, 2019.

VIVIER, E.; ARTIS, D.; COLONNA, M.; DIEFENBACH, A. *et al.* Innate Lymphoid Cells: 10 Years On. **Cell**, 174, n. 5, p. 1054-1066, Aug 23 2018.

WAGENER, M.; HOVING, J. C.; NDLOVU, H.; MARAKALALA, M. J. Dectin-1-Syk-CARD9 Signaling Pathway in TB Immunity. **Front Immunol**, 9, p. 225, 2018.

WANG, L.; CHANG, E. W.; WONG, S. C.; ONG, S. M. *et al.* Increased myeloid-derived suppressor cells in gastric cancer correlate with cancer stage and plasma S100A8/A9 proinflammatory proteins. **J Immunol**, 190, n. 2, p. 794-804, Jan 15 2013.

WATSON, R. O.; BELL, S. L.; MACDUFF, D. A.; KIMMEY, J. M. *et al.* The Cytosolic Sensor cGAS Detects Mycobacterium tuberculosis DNA to Induce Type I Interferons and Activate Autophagy. **Cell Host Microbe**, 17, n. 6, p. 811-819, Jun 10 2015.

WEYAND, C. M.; BERRY, G. J.; GORONZY, J. J. The immunoinhibitory PD-1/PD-L1 pathway in inflammatory blood vessel disease. **J Leukoc Biol**, 103, n. 3, p. 565-575, Mar 2018.

WHITSETT, J. A.; ALENGHAT, T. Respiratory epithelial cells orchestrate pulmonary innate immunity. **Nat Immunol**, 16, n. 1, p. 27-35, Jan 2015.

WILKIE, M. E.; MCSHANE, H. TB vaccine development: where are we and why is it so difficult? **Thorax**, 70, n. 3, p. 299-301, Mar 2015.

WILLIAMS, J. O.; ROCHE, T. E.; MCFADDEN, B. A. Mechanism of action of isocitrate lyase from *Pseudomonas indigofera*. **Biochemistry**, 10, n. 8, p. 1384-1390, Apr 13 1971.

WOLF, A. J.; LINAS, B.; TREVEJO-NUÑEZ, G. J.; KINCAID, E. *et al.* Mycobacterium tuberculosis infects dendritic cells with high frequency and impairs their function in vivo. **J Immunol**, 179, n. 4, p. 2509-2519, Aug 15 2007.

YOUN, J. I.; GABRILOVICH, D. I. The biology of myeloid-derived suppressor cells: the blessing and the curse of morphological and functional heterogeneity. **Eur J Immunol**, 40, n. 11, p. 2969-2975, Nov 2010.

YOUN, J. I.; NAGARAJ, S.; COLLAZO, M.; GABRILOVICH, D. I. Subsets of myeloid-derived suppressor cells in tumor-bearing mice. **J Immunol**, 181, n. 8, p. 5791-5802, Oct 15 2008.

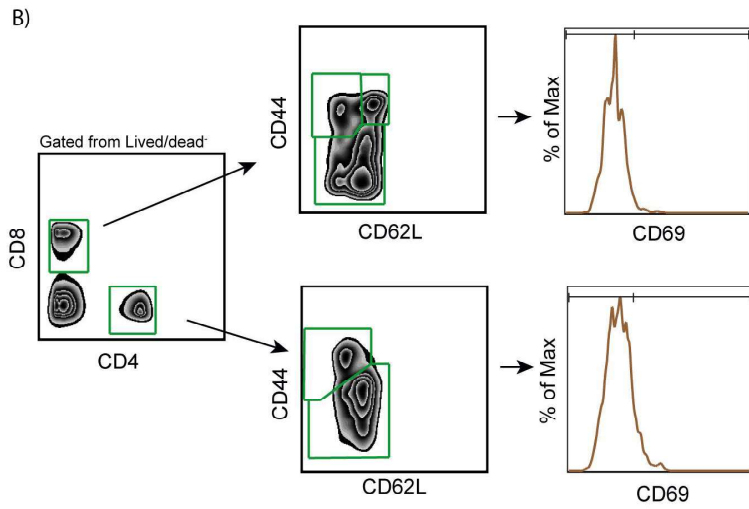
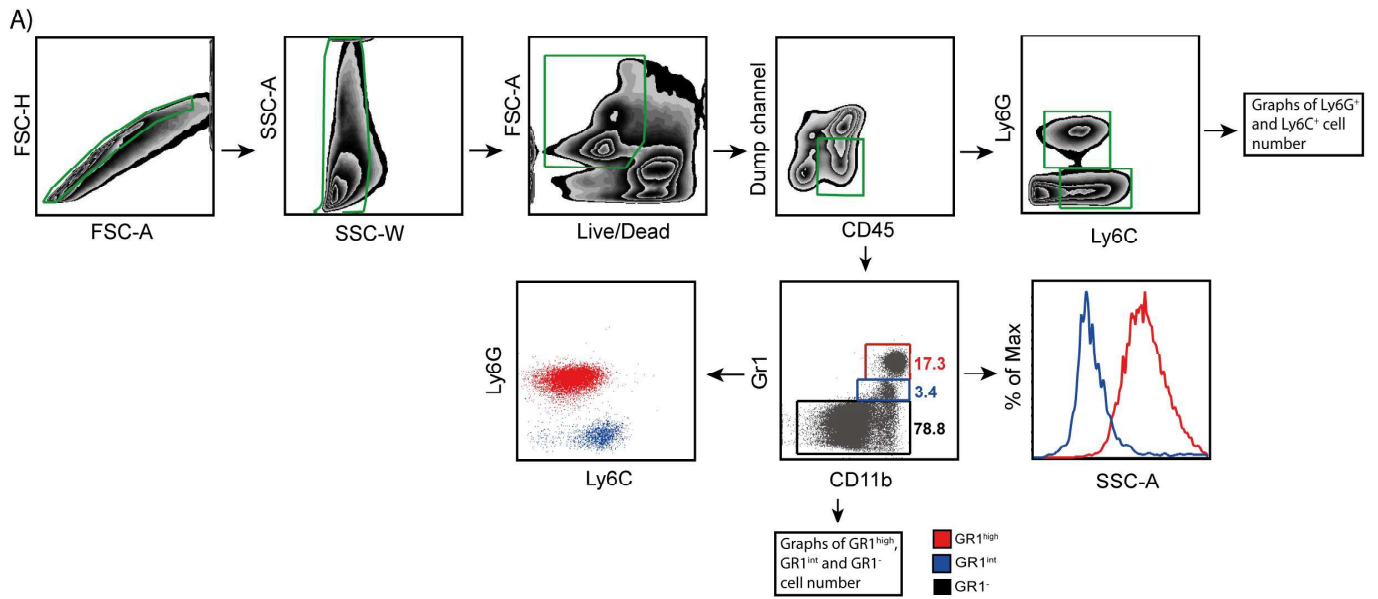
YOUNG, D. B.; PERKINS, M. D.; DUNCAN, K.; BARRY, C. E., 3RD. Confronting the scientific obstacles to global control of tuberculosis. **J Clin Invest**, 118, n. 4, p. 1255-1265, 2008. Research Support, Non-U S Gov't Review.

ZHAI, W.; WU, F.; ZHANG, Y.; FU, Y. *et al.* The Immune Escape Mechanisms of Mycobacterium Tuberculosis. **Int J Mol Sci**, 20, n. 2, Jan 15 2019.

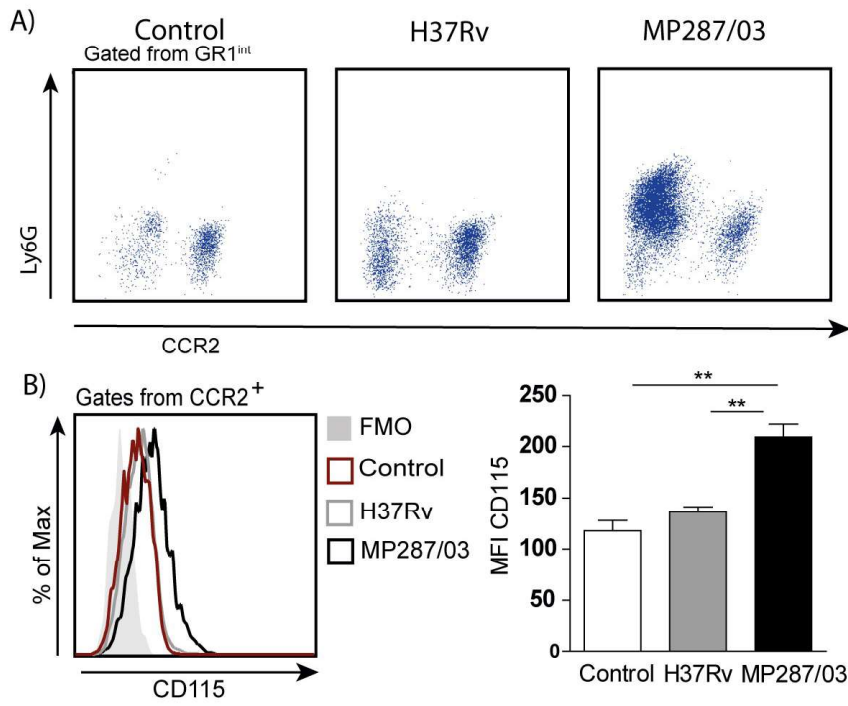
ZHU, J.; POWIS DE TENBOSSCHE, C. G.; CANE, S.; COLAU, D. *et al.* Resistance to cancer immunotherapy mediated by apoptosis of tumor-infiltrating lymphocytes. **Nat Commun**, 8, n. 1, p. 1404, Nov 10 2017.

ZITTI, B.; BRYCESON, Y. T. Natural killer cells in inflammation and autoimmunity. **Cytokine Growth Factor Rev**, 42, p. 37-46, Aug 2018.

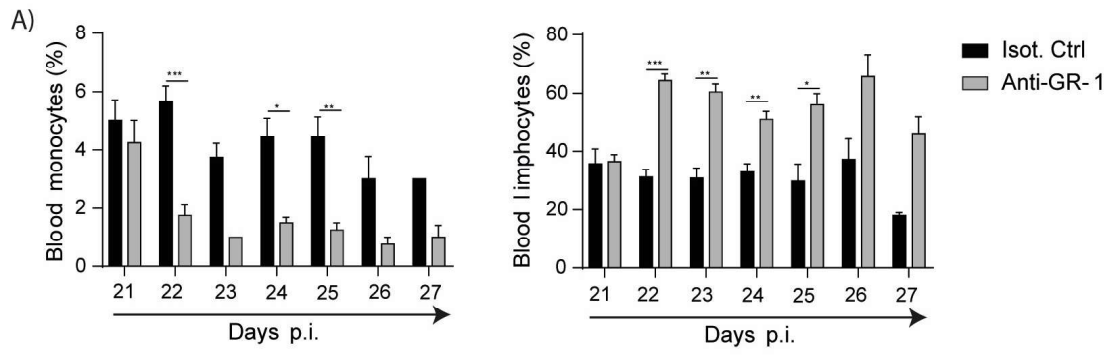
APÊNDICE A – Estratégia de *gates* utilizada para análise da população de células mieloides e linfoides



APÊNDICE B – Presença de monócitos imaturos infiltrados no pulmão de camundongos aos 28 dias p.i. com a cepa MP287/03

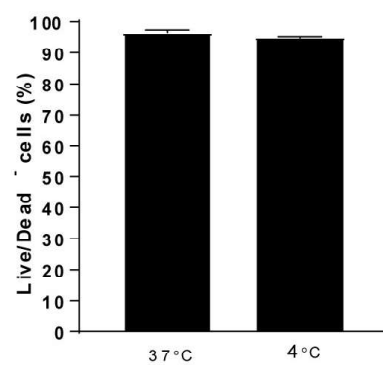
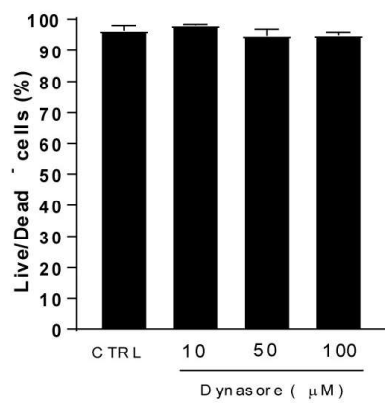
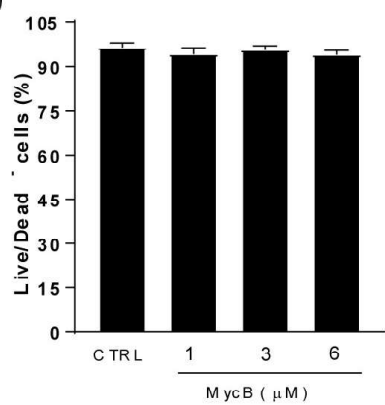


APÊNDICE C – Frequência de monócitos (maduros e imaturos) e linfócitos no sangue de camundongos infectados tratados com anticorpos anti-GR1 ou com controle isotípico



APÊNDICE D – Viabilidade celular de BMDMs tratados com os inibidores MycB, dynasore ou cultivados à 4°C

A)



APÉNDICE E – P2X7 receptor in bone marrow-derived cells aggravates tuberculosis caused by hypervirulent *Mycobacterium bovis*. **Frontiers in Immunology**, 2017



P2X7 Receptor in Bone Marrow-Derived Cells Aggravates Tuberculosis Caused by Hypervirulent *Mycobacterium bovis*

Caio César Barbosa Bomfim^{1*}, Eduardo Pinheiro Amaral^{1*}, Alexandra dos Anjos Cassado¹, Érika Machado Salles¹, Rogério Silva do Nascimento¹, Elena Lasunskaja², Mario Hiroyuki Hirata³, José Maria Álvarez¹ and Maria Regina D'Império-Lima^{1*}

OPEN ACCESS

Edited by:

Christoph Hölscher,
Forschungszentrum Borstel (LG),
Germany

Reviewed by:

Carl G. Feng,
The University of Sydney, Australia
Muazzam Jacobs,
University of Cape Town, South
Africa

*Correspondence:

Caio César Barbosa Bomfim
caiocesarbonfim@usp.br;
Eduardo Pinheiro Amaral
eduardo.amaral@nih.gov;
Maria Regina D'Império-Lima
relima@usp.br

†These authors are joint first authors
on this work.

Specialty section:

This article was submitted to
Microbial Immunology,
a section of the journal
Frontiers in Immunology

Received: 06 December 2016

Accepted: 28 March 2017

Published: 13 April 2017

Citation:

Bomfim CCB, Amaral EP,
Cassado AA, Salles ÉM,
do Nascimento RS, Lasunskaja E,
Hirata M, Álvarez JM and D'Império-
Lima MR (2017) P2X7 Receptor in
Bone Marrow-Derived Cells
Aggravates Tuberculosis Caused by
Hypervirulent *Mycobacterium bovis*.
Front. Immunol. 8:435.
doi: 10.3389/fimmu.2017.00435

¹Department of Immunology, Biomedical Science Institute, University of São Paulo (USP), São Paulo, Brazil, ²Laboratory of Biology of Recognition, State University of North Fluminense, Campos dos Goytacazes, Brazil, ³Faculty of Pharmaceutical Sciences, Department of Clinical Chemistry and Toxicology, University of São Paulo (USP), São Paulo, Brazil

Tuberculosis (TB) remains a serious public health problem despite the great scientific advances in the recent decades. We have previously shown that aggressive forms of TB caused by hypervirulent strains of *Mycobacterium tuberculosis* and *Mycobacterium bovis* are attenuated in mice lacking the P2X7 receptor, an ion channel activated by extracellular ATP. Therefore, P2X7 receptor is a potential target for therapeutic intervention. *In vitro*, hypervirulent mycobacteria cause macrophage death by a P2X7-dependent mechanism that facilitates bacillus dissemination. However, as P2X7 receptor is expressed in both bone marrow (BM)-derived cells and lung structural cells, several cellular mechanisms can operate *in vivo*. To investigate whether the presence of P2X7 receptor in BM-derived cells contributes to TB severity, we generated chimeric mice by adoptive transfer of hematopoietic cells from C57BL/6 or P2X7^{-/-} mice into CD45.1 irradiated mice. After infection with hypervirulent mycobacteria (MP287/03 strain of *M. bovis*), P2X7^{-/-}>CD45.1 mice recapitulated the TB resistance observed in P2X7^{-/-} mice. These chimeric mice showed lower lung bacterial load and attenuated pneumonia compared to C57BL/6>CD45.1 mice. Lung necrosis and bacterial dissemination to the spleen and liver were also reduced in P2X7^{-/-}>CD45.1 mice compared to C57BL/6>CD45.1 mice. Furthermore, an immature-like myeloid cell population showing a Ly6G^{int} phenotype was observed in the lungs of infected C57BL/6 and C57BL/6>CD45.1 mice, whereas P2X7^{-/-} and P2X7^{-/-}>CD45.1 mice showed a typical neutrophil (Ly6G^{hi}) population. This study clearly demonstrates that P2X7 receptor in BM-derived cells plays a critical role in the progression of severe TB.

Keywords: tuberculosis, hypervirulent mycobacteria, P2X7 receptor, bone marrow-derived cells, mouse models

INTRODUCTION

Nearly a quarter of the global population harbors bacteria of the *Mycobacterium tuberculosis* complex, resulting in an estimated 10.4 million new cases of active tuberculosis (TB) in 2015 (1, 2). Infection typically occurs when an individual inhales aerosolized droplets containing the mycobacteria (3). In the pulmonary alveoli, the mycobacteria may be ingested by alveolar

macrophages that recruit inflammatory cells (4). Surviving bacilli multiply within the macrophage and, in most cases, are trapped inside primary granulomas. The equilibrium between host defense and the mycobacteria leads to latent infection. Active TB can develop through progression of recently acquired infection (primary disease) or reactivation of latent infection. Around 10% of active TB cases are due to progressive primary TB, which is an aggressive form of the illness that affect mostly immunodeficient patients and children under 5 years (5). The rates of latent TB reactivation range from 3 to 10% per lifespan in immunocompetent patients and increase markedly in immunodeficient patients (6–8). By promoting a progressive decline in cell-mediated immunity, co-infection with human immunodeficiency virus (HIV) greatly enhances TB incidence and severity. HIV co-infection was reported in 1.2 million (11%) of the people who developed TB in 2014 (1). Therefore, TB is the leading cause of death among individuals with acquired immunodeficiency syndrome (9, 10).

Severe TB cases are distinguished by the fast increase of granulomatous infiltrates that result in tuberculous pneumonia and, eventually, in hematogenous bacillus dissemination, such as in the miliary form of the disease. A hallmark of the serious illness is the existence of pulmonary caseous granulomas in which a central necrotic lesion contains many extracellular mycobacteria (11). Intense necrotic death of macrophages seems to result from the failure of host immune response to control bacillus growth. Consequently, the respiratory function is affected by the extensive tissue injury and causes the patient death. Therefore, many efforts have been made to elucidate how macrophages die following mycobacterial infection (12). One of the main difficulties to understand the pathogenesis of severe TB was the lack of animal models that develop pulmonary necrotic granulomas, as these lesions are unusual in murine models of TB, such as infection with mycobacteria of the virulent H37Rv strain. Therefore, our research group has established murine models in which C57BL/6 mice are infected with a low dose of hypervirulent mycobacteria (13, 14). Hypervirulent Beijing 1471 *M. tuberculosis* strain and MP287/03 *Mycobacterium bovis* strain induce extensive pulmonary inflammation, necrosis, high bacillus dissemination, and mouse death (13). These experimental models were used to determine whether the recognition of damage signals modulates the disease.

During necrotic cell death, ATP is released in the extracellular environment (15–17). Extracellular ATP (eATP) is a damage signal that is recognized by many cell types through different P2 purinergic receptors. Among them, the P2X7 receptor leads to release of proinflammatory cytokines and induces cell death (18). This molecule is a ligand-gated ion channel that is activated by high eATP concentrations, a characteristic of extensive tissue injury (18, 19). P2X7 engagement causes changes in intracellular ion balance that promotes the NLRP3 inflammasome activation and secretion of active IL-1 β and IL-18, as well as cell death by pyroptosis (20). Furthermore, the stimulation of P2X7 receptor induces the opening of large pores in the plasma membrane, which allows the free flow of macromolecules. The duration and intensity of the stimulus establish whether P2X7

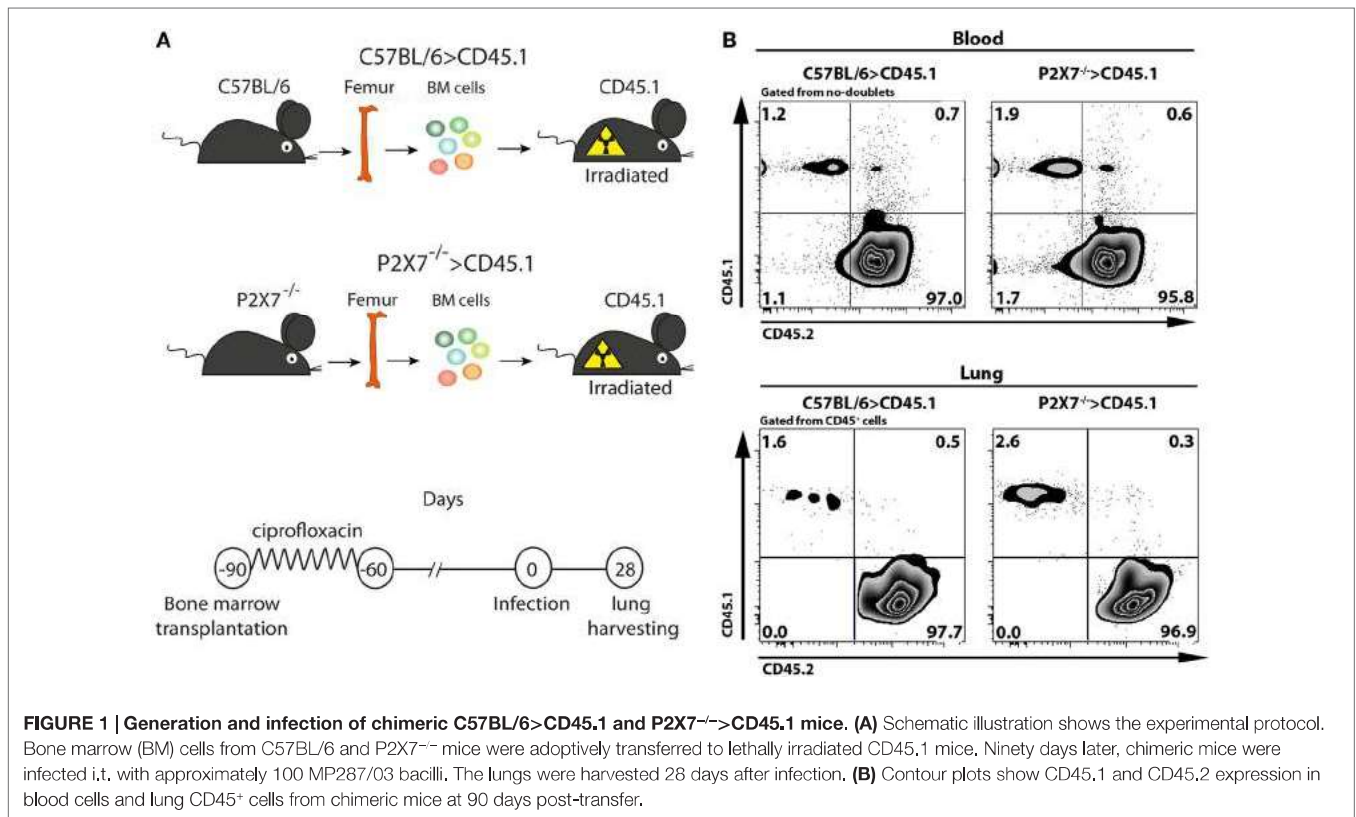
receptor activation promotes cell necrosis or apoptosis (21). By examining TB progression in mice deficient in P2X7 receptor that were infected with H37Rv, Beijing 1471, and MP287/03 bacilli, we demonstrated that the crucial role of P2X7 receptor in the aggressive forms of the disease (13). These mice showed increased resistance to infection evidenced by diminished bacterial load in the lungs, liver, and spleen. The lack of P2X7 receptor also caused reductions of inflammatory cellular infiltrate and tissue necrosis in the lung, which corroborated our hypothesis of the involvement of damage signals in the pathogenesis of severe TB.

To determine the mechanism involved in the deleterious role of P2X7 receptor in severe TB, we performed *in vitro* experiments using bone marrow (BM)-derived macrophages. We observed that eATP induces the P2X7-mediated killing of intracellular H37Rv bacilli and the P2X7-mediated release of viable hypervirulent Beijing 1471 and MP287/03 bacilli (13). Although this finding suggests that P2X7 signaling in infected macrophages facilitates the dissemination of hypervirulent mycobacteria, several other mechanisms might also operate *in vivo* because this receptor is expressed in many BM-derived cells and structural cells of the lungs, such as vascular endothelial cells, alveolar epithelial type I cells, and fibroblasts (22–25). Therefore, in the present study, we sought to investigate *in vivo* whether P2X7 receptor in BM-derived cells contributes to TB severity. Clarifying this issue may help understand the pathophysiology of aggressive forms of TB and give the theoretical background to develop new therapeutic approaches to ameliorate the outcome of the disease.

RESULTS

P2X7 Receptor in BM-Derived Cells Increases Lung Weight, Lung Relative Mass, and Cellularity in Severe TB

To determine whether P2X7 receptor in BM-derived cells is responsible for the deleterious role of this receptor in severe TB, hematopoietic cells from C57BL/6 and P2X7^{-/-} mice were transferred into irradiated CD45.1 mice (Figure 1A). After 90 days, chimeric C57BL/6>CD45.1 and P2X7^{-/-}>CD45.1 mice showed high levels of BM-derived cell reconstitution in the blood and lungs (over 95% of the CD45⁺ cells) (Figure 1B). These chimeric mice were then infected intratracheally (i.t.) with ~100 MP287/03 bacilli. We used this mycobacterial strain because it is more aggressive than Beijing 1471 strain, evidencing more clearly the effects of P2X7 receptor (13). Recapitulating the observations in infected C57BL/6 and P2X7^{-/-} mice, the lung tuberculous nodules were visually more numerous and protuberant in C57BL/6>CD45.1 mice than in P2X7^{-/-}>CD45.1 mice at 28 days post-infection (p.i.) (Figure 2A). Accordingly, lung weight, lung relative mass, and cellularity were higher in infected C57BL/6 and C57BL/6>CD45.1 mice compared to P2X7^{-/-} and P2X7^{-/-}>CD45.1 counterparts, respectively (Figures 2B–D). In addition, the number of CD45⁺ cells was also higher in C57BL/6>CD45.1 mice than in P2X7^{-/-}>CD45.1 mice (Figure 2E).



P2X7 Receptor in BM-Derived Cells Enhances Lung Pathology, Lung Bacterial Burden, and Bacterial Dissemination to the Liver and Spleen in Severe TB

Consistent with lung morphology, the histological analysis of hematoxylin–eosin (HE) stained tissue sections revealed a more severe disease in infected mice expressing the P2X7 receptor in BM-derived cells (Figure 3A). On day 28 p.i., C57BL/6 and C57BL/6>CD45.1 mice showed intense pulmonary inflammation with intra-alveolar spaces containing widespread cellular infiltrates accompanied by necrotic tissue injury. In contrast, limited cellular infiltrates and no sign of necrosis were observed in infected P2X7^{-/-} and P2X7^{-/-}>CD45.1 mice. Accordingly, the areas of alveolar space were significantly lower in infected C57BL/6 and C57BL/6>CD45.1 mice compared to infected P2X7^{-/-} and P2X7^{-/-}>CD45.1 mice (Figure 3B). In addition, Ziehl–Neelsen staining revealed the massive presence of acid-alcohol-resistant bacillus (BAARs) in the lungs of infected C57BL/6 and C57BL/6>CD45.1 mice, whereas less bacilli were observed in P2X7^{-/-} and P2X7^{-/-}>CD45.1 counterparts, respectively (Figure 3C). Compatibly, the numbers of colony-forming units (CFUs) were higher in the lungs of infected mice expressing the P2X7 receptor in BM-derived cells (Figure 4A). Moreover, infected C57BL/6 and C57BL/6>CD45.1 mice showed more bacillus dissemination to the liver and spleen than P2X7^{-/-} and P2X7^{-/-}>CD45.1 counterparts (Figure 4B). These results confirm the important role of P2X7 receptor in

BM-derived cells in defining the increased resistance of P2X7^{-/-} mice to severe TB.

P2X7 Receptor in BM-Derived Cells Leads to Enrichment of Ly6G^{int} Cells into the Lungs during Severe TB

As a hallmark of severe TB is the presence of massive neutrophil infiltrates in the lungs (26–28), we investigated whether the absence of P2X7 receptor in BM-derived cells influences the pulmonary myeloid cell populations in MP287/03-infected chimeric mice. On day 28 p.i., C57BL/6 and C57BL/6>CD45.1 mice showed higher numbers of CD11b⁺ cells compared to P2X7^{-/-} and P2X7^{-/-}>CD45.1 mice, respectively (Figures 5A,B). Furthermore, an immature-like cell population expressing intermediate levels of Ly6G predominated in infected C57BL/6 and C57BL/6>CD45.1 mice, whereas infected P2X7^{-/-} and P2X7^{-/-}>CD45.1 mice presented a typical neutrophil Ly6G^{high} population (Figures 5C–E). These data indicate that P2X7 expression in BM-derived cells contributes to TB severity, which was characterized by the predominance of immature-like myeloid cells infiltrating the lungs.

DISCUSSION

We have previously shown the deleterious role of P2X7 receptor in severe TB caused by Beijing 1471 and MP287/03 bacilli (13). *In vitro*, these hypervirulent mycobacteria induce macrophage

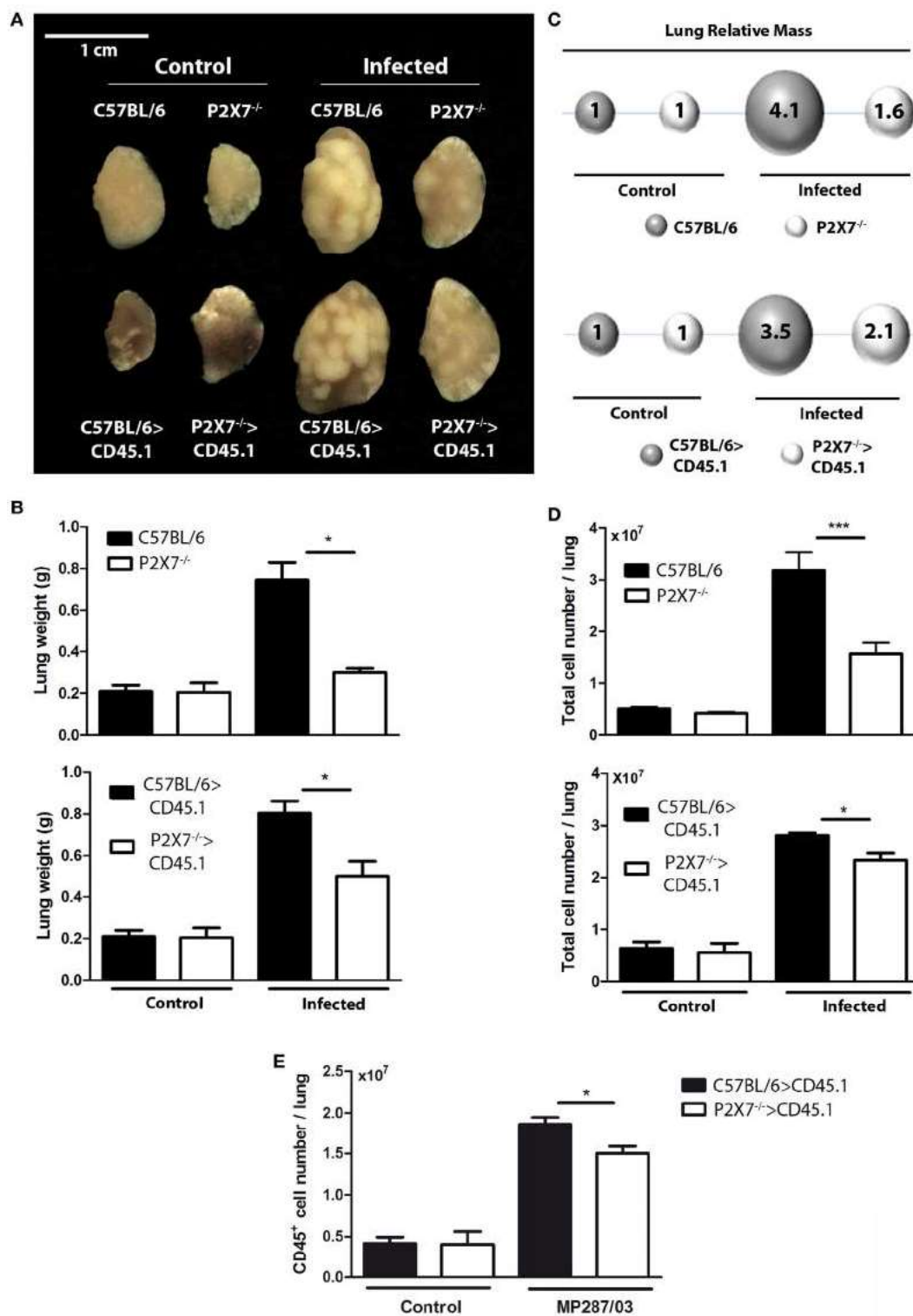
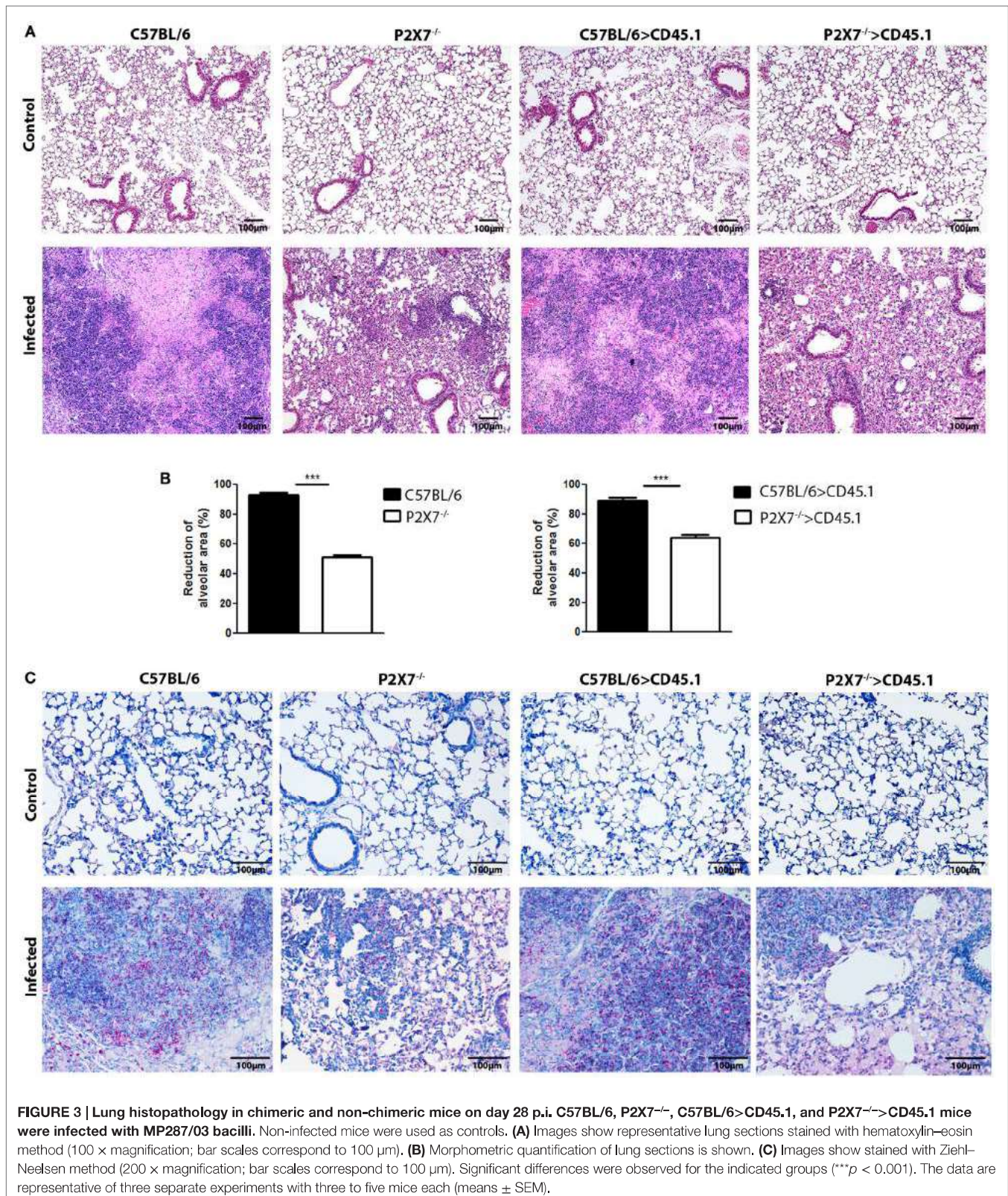
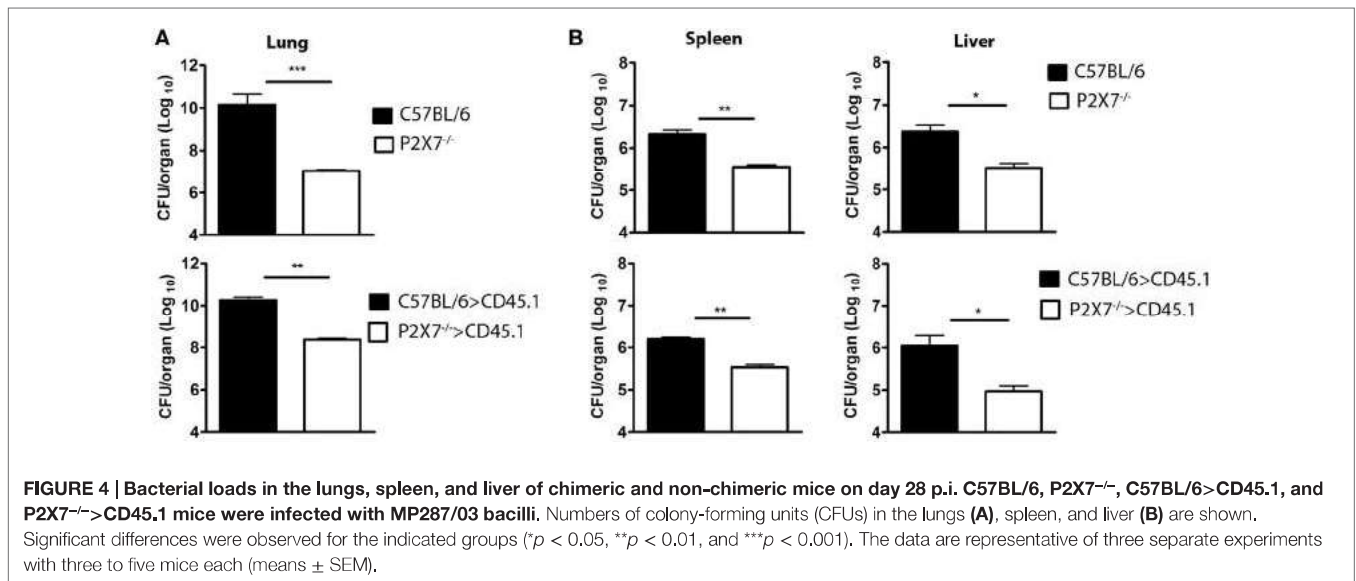


FIGURE 2 | Lung gross pathology in chimeric and non-chimeric mice on day 28 p.i., C57BL/6, P2X7^{-/-}, C57BL/6>CD45.1, and P2X7^{-/-}>CD45.1 mice were infected with MP287/03 bacilli. Non-infected mice were used as controls. **(A)** Representative images of the right lungs are shown (bar scales correspond to 1 cm). **(B)** Right lung weights and **(C)** lung relative masses (circles) were evaluated. The lung relative masses were calculated by the ratios of the mean values of the lung weights in the indicated groups and the control group. **(D)** Numbers of total cells in the lungs are shown. Significant differences were observed for the indicated groups (**p* < 0.05 and ****p* < 0.001). The data are representative of three separate experiments with three to five mice each (means ± SEM). **(E)** Numbers of CD45⁺ cells in the lungs are shown.



death by a P2X7-dependent mechanism that facilitates bacillus release. Based on these findings, we proposed that the fast intracellular multiplication of hypervirulent mycobacteria causes

widespread destruction of infected macrophages. Consequently, high amounts of eATP activate the P2X7 receptor and facilitate the development of the necrotic process by cooperating with



mycobacterial components exhibiting the membrane-lysing activity. This process leads to a vicious cycle that exacerbates pneumonia, lung damage, and bacillus dissemination.

In vivo, various cell populations can contribute to the deleterious role of P2X7 receptor in severe TB, as this receptor is expressed in many BM-derived cells (i.e., monocytes, macrophages, neutrophils, and T cells) and lung structural cells (i.e., alveolar epithelial type I cells, lung endothelial cells, and fibroblasts) (19, 22–25, 29, 30). By analyzing chimeric C57BL/6>CD45.1 and P2X7^{-/-}>CD45.1 mice infected with MP287/03 bacilli, we show here that the absence of P2X7 receptor in BM-derived cells recapitulates the TB progression observed in mice lacking this receptor. According to all parameters analyzed in this study, P2X7^{-/-}>CD45.1 mice developed a less severe TB compared to C57BL/6>CD45.1 mice. Infected mice lacking the P2X7 receptor in BM-derived cells showed lower lung bacterial load accompanied by attenuated pneumonia and no sign of lung necrosis. Bacterial dissemination to spleen and liver was also reduced in P2X7^{-/-}>CD45.1 mice compared to C57BL/6>CD45.1 mice. Furthermore, a typical Ly6G^{high} neutrophil population infiltrated the lungs of infected P2X7^{-/-}>CD45.1 mice, whereas an immature-like myeloid cell population displaying a Ly6G^{int} phenotype predominated in infected C57BL/6>CD45.1 mice.

These results are in line with our model in which P2X7 receptor of infected macrophages is decisive to aggravate the disease (11, 12). Yet, the participation of other BM-derived cell population is still an open possibility. Although neutrophils play an important role in host defense against bacterial infections, their involvement in TB is controversial (27, 28, 31). The excessive accumulation of neutrophils in the lungs is very harmful and usually associated with tissue damage during severe TB (27, 31). In addition, immature myeloid cells, mainly neutrophil precursors, are the main population infiltrating the lungs at advanced TB stages (32, 33). Myeloid cells with an immature phenotype can behave like myeloid-derived suppressor cells and make the disease worse by suppressing the immune response (32–34).

This population has a CD11b⁺GR1^{int} phenotype and expresses intermediate levels of Ly6G (32). Therefore, the accumulation of Ly6G^{int} cells in the lungs of MP287/03-infected mice could be a secondary consequence of the excessive tissue damage resulting from P2X7 signaling.

Recently, it has been shown that neutrophils express the P2X7 receptor, which once activated by ATP, leads to K⁺ efflux and, consequently, to NLRP3 inflammasome activation and IL-1 β secretion (35). However, the detrimental effect of P2X7 receptor during severe TB appears to be independent of NLRP3 inflammasome. The absence of NLRP3, ASC, and caspase-1 does not change TB progression in MP287/03-infected mice (data not shown). Moreover, differently from macrophages, P2X7 engagement does not induce neutrophil lysis (35). Therefore, it is unlikely that P2X7 receptor mediates lung injury by inducing neutrophil death. Alternatively, it has been shown that P2X7 activation induced by antibacterial protein LL-37 leads to suppression of spontaneous apoptosis in neutrophils (36). As neutrophil apoptosis limits the release of proinflammatory mediators and cytotoxic metabolites (37), it is possible that, in severe TB, prolongation of neutrophil life span mediated by P2X7 receptor could amplify the proinflammatory response and secondarily promote tissue injury.

In conclusion, this study helps to improve the knowledge concerning the critical role of P2X7 receptor in severe TB by demonstrating the importance of P2X7 receptor in BM-derived cells. This finding brings us a step forward in understanding the pathophysiology of aggressive forms of TB and reinforces the P2X7 receptor as a potential target for new therapeutic approaches to ameliorate the disease outcome.

MATERIALS AND METHODS

Mice

Specific pathogen-free C57BL/6, P2X7^{-/-} (B6.129P2-P2rx7tm1 Gab/J), and CD45.1 (B6.SJL-Ptprca Pepcb/BoyJ) male mice (The Jackson Laboratory, USA; generated by Pfizer Inc.) were bred

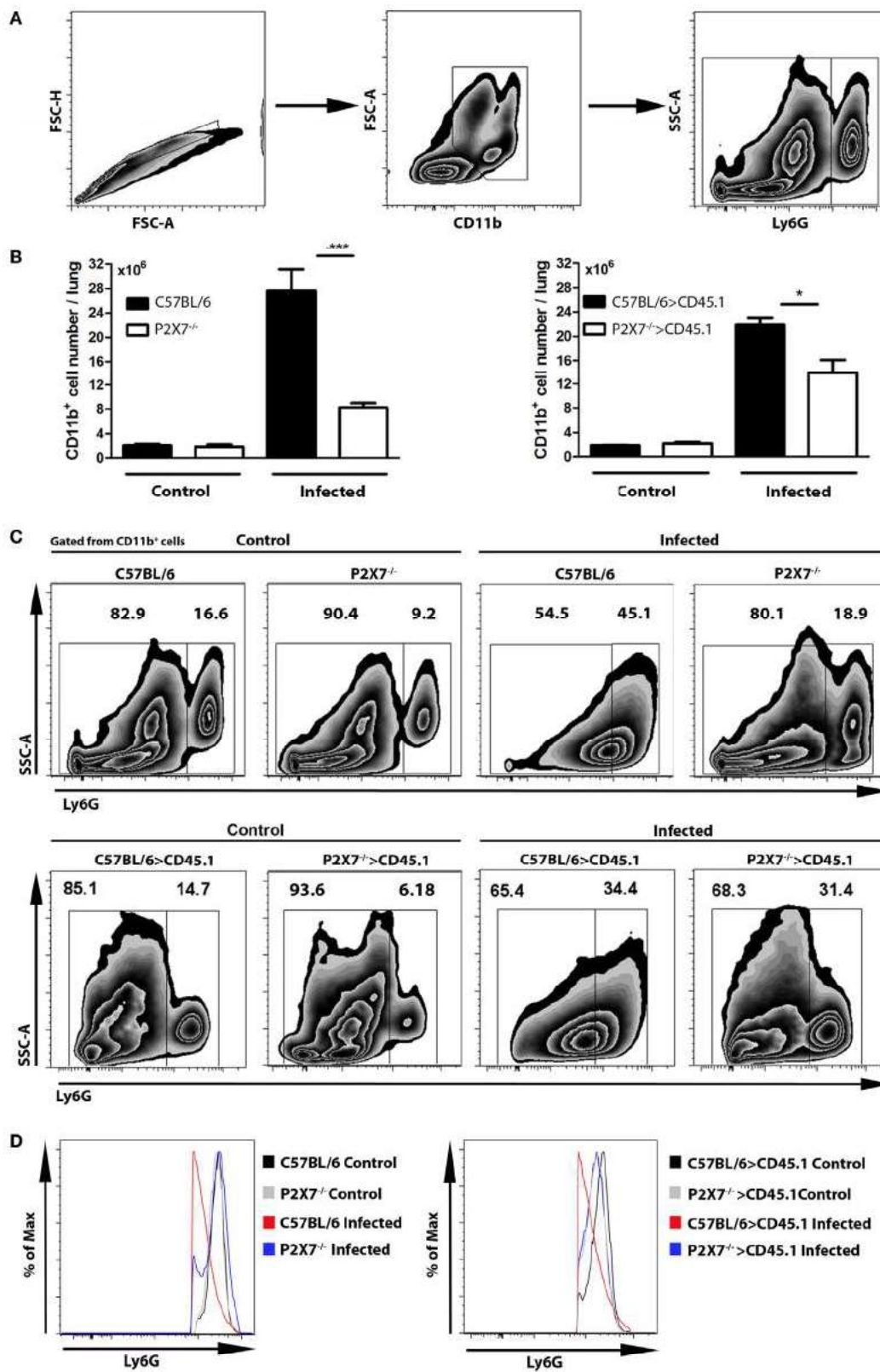


FIGURE 5 | Continued

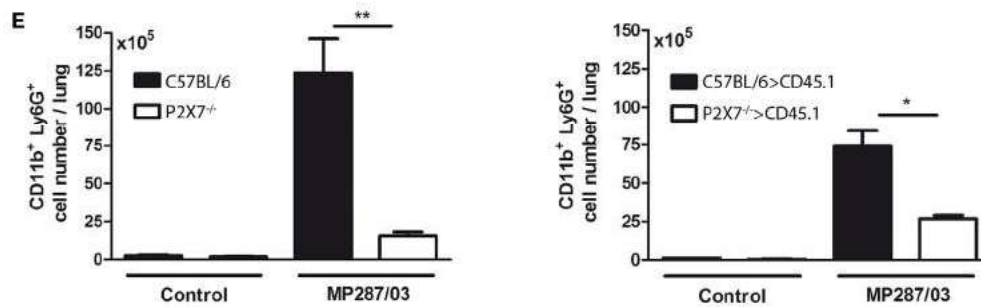


FIGURE 5 | Phenotypic profile of lung neutrophils in chimeric and non-chimeric mice on day 28 p.i. C57BL/6, P2X7^{-/-}, C57BL/6>CD45.1, and P2X7^{-/-}>CD45.1 mice were infected with MP287/03 bacilli. Non-infected mice were used as controls. (A) Contour plots show the gate strategy used to analyze lung neutrophils. (B) CD11b⁺ cell numbers in the lungs are shown. (C) Contour plots show Ly6G expression and side scatter in lung CD11b⁺ cells. (D) Expression of Ly6G molecule and (E) numbers of Ly6G⁺ cells in the lungs are shown. The cell numbers in C57BL/6 and C57BL/6>CD45.1 mice were not calculated (ND, not done), as lung CD11b⁺ cells express intermediate levels of Ly6G. Significant differences were observed for the indicated groups (* $p < 0.05$ and *** $p < 0.001$). The data are representative of three separate experiments with three to five mice each (means \pm SEM).

at the Animal Facility of the Biomedical Science Institute, USP. Six- to eight-week-old mice were infected and maintained in microisolator cages at the Biosafety Level 3 Mice Facilities at the Faculty of Pharmaceutical Sciences, USP, under controlled temperature and humidity and were fed *ad libitum*.

Mycobacteria

Dr. José Soares Ferreira Neto (Veterinary Medicine Institute, USP) provided the bovine *M. bovis* isolate (MP287/03—SB0295 spoligotyping). Mycobacteria were cultured in Middlebrook 7H9 medium (Difco, BD Biosciences, USA) with 0.4% sodium pyruvate (Sigma-Aldrich, USA), 0.05% Tween 80 (Sigma-Aldrich), and 10% ADC (albumin–dextrose–catalase; Difco). Frozen aliquots of 10^8 bacilli/ml, at -80°C , were thawed and cultured in complete medium for 7 days at 37°C . The bacilli were sonicated for 1 min, homogenized and maintained for 10 min at rest to prevent bacterial clumps, which were monitored by microscopic examination. The bacterial concentrations were determined by spectrophotometry at 600 nm.

CFU Counting

The mycobacterial burden was quantified by sequential dilutions and the culture of tissue homogenates (lung, spleen, and liver) in Middlebrook 7H10 medium (Difco) with 0.4% sodium pyruvate and 10% OADC (oleic acid–albumin–dextrose–catalase; Difco). Three weeks after incubation at 37°C , the CFU numbers were determined.

Mouse Infection

After anesthetizing mice with xylazine (Vetbrands, Brazil; 15 mg/kg) and ketamine (Vetbrands, 100 mg/kg), a volume of 60 μl of the mycobacterial suspension (~ 100 bacilli) was introduced in the trachea through a short midline incision, which was then sutured with sterile silk (38).

Lethal Irradiation and BM Reconstitution

Bone marrow cells were harvest from femur of C57BL/6 or P2X7^{-/-} mice by flushing with PBS. A single-cell preparation

was obtained by carefully cycling through a 26-gauge needle. Recipient CD45.1 mice were irradiated with a dose of 12 Gy from a ^{137}Cs source. After irradiation, 2×10^7 BM cells from C57BL/6 and P2X7^{-/-} mice in a volume of 200 μl PBS were transferred i.v. under anesthesia. The chimeric mice were housed for at least 12 weeks before infection and were fed with water containing antibiotic (0.1 mg/ml of ciprofloxacin) in the first 4 weeks after BM transplantation.

Macroscopic and Microscopic Analysis of the Lungs

Lung relative mass was calculated (infected mouse lung weight/control mouse lung weight). The superior lobes of the right lungs were fixed with 10% buffered formalin, photographed, and embedded in paraffin. Serial 4–5 μm sections were stained with HE dye to analyze the tissue alterations and by the Ziehl–Neelsen method to detected BAARs. The samples were examined with a Leica microscope (Germany), and images were captured with a Coolpix P995 Nikon camera (Japan).

Morphometric Analysis of Lung Tissue

The reduction in the percentages of pulmonary intralveolar space was determined as described elsewhere (13, 39). Eight random images of each lung HE-stained section (100 \times magnification) were analyzed using the ImageJ software (National Institutes of Health, USA).

Cell Phenotypic Analysis of Lung Infiltrates

The left lungs were dissected and digested with Collagenase type 4 (Sigma-Aldrich; 0.5 mg/ml) at 37°C for 40 min. A syringe plunger (BD Bioscience) was used to disperse the cells. Cell suspensions were then filtered with a cell strainer (Corning Inc., USA) and incubated with ACK lysing Buffer (Thermo Fisher Scientific) at room temperature for 1 min to deplete erythrocytes. Cells (1×10^6) were stained using appropriate combinations of FITC-, PercP-, Pcy7-, and APC-labeled

monoclonal antibodies to CD11b (M1/70), CD45.1 (A20), Ly6G (1A8) (BD Pharmingen, USA), and CD45.2 (104) (eBioscience). Cells were fixed with 2% paraformaldehyde and analyzed by flow cytometry (FACSCanto, BD Biosciences) using the FlowJo software.

Statistical Analysis

Data were statistically analyzed by Mann–Whitney test with the GraphPad Prism 5 software (GraphPad, USA) and were considered significantly different when $p < 0.05$ (5%).

ETHICS STATEMENT

All procedures were in accordance with the national regulations of the National Board of Health and Brazilian College of Animal Experimentation (COBEA, Brazil), with respect to their ethical guidelines for mouse experimentation and welfare. The protocol was approved by the Animal Care Committee of the Biomedical Science Institute, University of São Paulo, with permit number 153/11.

REFERENCES

1. WHO. *Global Tuberculosis Report*. Switzerland: WHO, World Health Organization (2016).
2. Houben RM, Dodd PJ. The global burden of latent tuberculosis infection: a re-estimation using mathematical modelling. *PLoS Med* (2016) 13(10):e1002152. doi:10.1371/journal.pmed.1002152
3. Riley RL, Mills CC, Nyka W, Weinstock N, Storey PB, Sultan LU, et al. Aerial dissemination of pulmonary tuberculosis. a two-year study of contagion in a tuberculosis ward. 1959. *Am J Epidemiol* (1995) 142(1):3–14. doi:10.1093/oxfordjournals.aje.a117542
4. O'Garra A, Redford PS, McNab FW, Bloom CI, Wilkinson RJ, Berry MP. The immune response in tuberculosis. *Annu Rev Immunol* (2013) 31:475–527. doi:10.1146/annurev-immunol-032712-095939
5. Cruz AT, Starke JR. Clinical manifestations of tuberculosis in children. *Paediatr Respir Rev* (2007) 8(2):107–17. doi:10.1016/j.prrv.2007.04.008
6. Ottenhoff TH, Kaufmann SH. Vaccines against tuberculosis: where are we and where do we need to go? *PLoS Pathog* (2012) 8(5):10. doi:10.1371/journal.ppat.1002607
7. Barry CE III, Boshoff HI, Dartois V, Dick T, Ehrt S, Flynn J, et al. The spectrum of latent tuberculosis: rethinking the biology and intervention strategies. *Nat Rev Microbiol* (2009) 7(12):845–55. doi:10.1038/nrmicro2236
8. Corbett EL, Watt CJ, Walker N, Maher D, Williams BG, Raviglione MC, et al. The growing burden of tuberculosis: global trends and interactions with the HIV epidemic. *Arch Intern Med* (2003) 163(9):1009–21. doi:10.1001/archinte.163.9.1009
9. Raviglione MC, Snider DE Jr, Kochi A. Global epidemiology of tuberculosis. Morbidity and mortality of a worldwide epidemic. *JAMA* (1995) 273(3):220–6. doi:10.1001/jama.273.3.220
10. Zwang J, Garenne M, Kahn K, Collinson M, Tollman SM. Trends in mortality from pulmonary tuberculosis and HIV/AIDS co-infection in rural South Africa (Agincourt). *Trans R Soc Trop Med Hyg* (2007) 101(9):893–8. doi:10.1016/j.trstmh.2007.04.023
11. Dorhoi A, Reece ST, Kaufmann SH. For better or for worse: the immune response against *Mycobacterium tuberculosis* balances pathology and protection. *Immunol Rev* (2011) 240(1):235–51. doi:10.1111/j.1600-065X.2010.00994.x
12. Amaral EP, Lasunskaja EB, D'Imperio-Lima MR. Innate immunity in tuberculosis: how the sensing of mycobacteria and tissue damage modulates macrophage death. *Microbes Infect* (2016) 18(1):11–20. doi:10.1016/j.micinf.2015.09.005

AUTHOR CONTRIBUTIONS

CCB, EA, and MD-L designed and conceived the experiments, analyzed the data, and wrote the manuscript. CCB, EA, AC, ES, and RN performed the experiment. MH, JA, and EL contributed with reagents, materials, and analysis tools.

ACKNOWLEDGMENTS

We are grateful to Maria Áurea de Alvarenga and Bernardo Paulo Albe for technical assistance.

FUNDING

This work was supported by São Paulo Research Foundation (FAPESP, Brazil) grant 2013/07140-2 and 2015/20432-8 (MD-L) and National Council for Scientific and Technological Development (CNPq, Brazil) grants 303676/2014-0 and 448765/2014-4 (MD-L). CCB received fellowships from FAPESP (2012/22587-0 and 2014/22986-8).

13. Amaral EP, Ribeiro SC, Lanes VR, Almeida FM, de Andrade MR, Bomfim CC, et al. Pulmonary infection with hypervirulent mycobacteria reveals a crucial role for the P2X7 receptor in aggressive forms of tuberculosis. *PLoS Pathog* (2014) 10(7):e1004188. doi:10.1371/journal.ppat.1004188
14. Ribeiro SC, Gomes LL, Amaral EP, Andrade MR, Almeida FM, Rezende AL, et al. *Mycobacterium tuberculosis* strains of the modern sublineage of the Beijing family are more likely to display increased virulence than strains of the ancient sublineage. *J Clin Microbiol* (2014) 52(7):2615–24. doi:10.1128/jcm.00498-14
15. Jacob F, Perez Novo C, Bachert C, Van Crombruggen K. Purinergic signaling in inflammatory cells: P2 receptor expression, functional effects, and modulation of inflammatory responses. *Purinergic Signal* (2013) 9(3):285–306. doi:10.1007/s11302-013-9357-4
16. Antonoli L, Blandizzi C, Pacher P, Hasko G. Immunity, inflammation and cancer: a leading role for adenosine. *Nat Rev Cancer* (2013) 13(12):842–57. doi:10.1038/nrc3613
17. Ferrari D, McNamee EN, Idzko M, Gambari R, Eltzschig HK. Purinergic signaling during immune cell trafficking. *Trends Immunol* (2016) 37(6):399–411. doi:10.1016/j.it.2016.04.004
18. Di Virgilio F. P2X receptors and inflammation. *Curr Med Chem* (2015) 22(7):866–77. doi:10.2174/0929867322666141210155311
19. Cekic C, Linden J. Purinergic regulation of the immune system. *Nat Rev Immunol* (2016) 16(3):177–92. doi:10.1038/nri.2016.4
20. Mariathasan S, Weiss DS, Newton K, McBride J, O'Rourke K, Roose-Girma M, et al. Cryopyrin activates the inflammasome in response to toxins and ATP. *Nature* (2006) 440(7081):228–32. doi:10.1038/nature04515
21. Di Virgilio F, Chiozzi P, Falzoni S, Ferrari D, Sanz JM, Venketaraman V, et al. Cytolytic P2X purinoceptors. *Cell Death Differ* (1998) 5(3):191–9. doi:10.1038/sj.cdd.4400341
22. Feng W, Wang L, Zheng G. Expression and function of P2 receptors in hematopoietic stem and progenitor cells. *Stem Cell Investig* (2015) 2:14. doi:10.3978/j.issn.2306-9759.2015.07.01
23. Chen Z, Jin N, Narasaraju T, Chen J, McFarland LR, Scott M, et al. Identification of two novel markers for alveolar epithelial type I and II cells. *Biochem Biophys Res Commun* (2004) 319(3):774–80. doi:10.1016/j.bbrc.2004.05.048
24. Oliveira SD, Coutinho-Silva R, Silva CL. Endothelial P2X7 receptors' expression is reduced by schistosomiasis. *Purinergic Signal* (2013) 9(1):81–9. doi:10.1007/s11302-012-9332-5
25. Moncao-Ribeiro LC, Faffe DS, Santana PT, Vieira FS, da Graca CL, Marques-da-Silva C, et al. P2X7 receptor modulates inflammatory and functional

- pulmonary changes induced by silica. *PLoS One* (2014) 9(10):e110185. doi:10.1371/journal.pone.0110185
26. Keller C, Hoffmann R, Lang R, Brandau S, Hermann C, Ehlers S. Genetically determined susceptibility to tuberculosis in mice causally involves accelerated and enhanced recruitment of granulocytes. *Infect Immun* (2006) 74(7):4295–309. doi:10.1128/iai.00057-06
 27. Lowe DM, Redford PS, Wilkinson RJ, O'Garra A, Martineau AR. Neutrophils in tuberculosis: friend or foe? *Trends Immunol* (2012) 33(1):14–25. doi:10.1016/j.it.2011.10.003
 28. Eruslanov EB, Lyadova IV, Kondratieva TK, Majorov KB, Scheglov IV, Orlova MO, et al. Neutrophil responses to *Mycobacterium tuberculosis* infection in genetically susceptible and resistant mice. *Infect Immun* (2005) 73(3):1744–53. doi:10.1128/iai.73.3.1744-1753.2005
 29. Karmakar M, Katsnelson MA, Dubyak GR, Pearlman E. Neutrophil P2X7 receptors mediate NLRP3 inflammasome-dependent IL-1beta secretion in response to ATP. *Nat Commun* (2016) 7:10555. doi:10.1038/ncomms10555
 30. Rissiek B, Haag F, Boyer O, Koch-Nolte F, Adriouch S. P2X7 on mouse T cells: one channel, many functions. *Front Immunol* (2015) 6:204. doi:10.3389/fimmu.2015.00204
 31. Dallenga T, Schaible UE. Neutrophils in tuberculosis – first line of defence or booster of disease and targets for host-directed therapy? *Pathog Dis* (2016) 74(3):ftw012. doi:10.1093/femspd/ftw012
 32. Tsiganov EN, Verbina EM, Radaeva TV, Sosunov VV, Kosmiadi GA, Nikitina IY, et al. Gr-1dimCD11b+ immature myeloid-derived suppressor cells but not neutrophils are markers of lethal tuberculosis infection in mice. *J Immunol* (2014) 192(10):4718–27. doi:10.4049/jimmunol.1301365
 33. Knaul JK, Jorg S, Oberbeck-Mueller D, Heinemann E, Scheuermann L, Brinkmann V, et al. Lung-residing myeloid-derived suppressors display dual functionality in murine pulmonary tuberculosis. *Am J Respir Crit Care Med* (2014) 190(9):1053–66. doi:10.1164/rccm.201405-0828OC
 34. Obregon-Henao A, Henao-Tamayo M, Orme IM, Ordway DJ. Gr1(int) CD11b+ myeloid-derived suppressor cells in *Mycobacterium tuberculosis* infection. *PLoS One* (2013) 8(11):e80669. doi:10.1371/journal.pone.0080669
 35. Karmakar M, Katsnelson MA, Dubyak GR. Neutrophil P2X7 receptors mediate NLRP3 inflammasome-dependent IL-1beta secretion in response to ATP. *Nat Commun* (2016) 7:10555. doi:10.1038/ncomms10555
 36. Nagaoka I, Tamura H, Hirata M. An antimicrobial cathelicidin peptide, human CAP18/LL-37, suppresses neutrophil apoptosis via the activation of formyl-peptide receptor-like 1 and P2X7. *J Immunol* (2006) 176(5):3044–52. doi:10.4049/jimmunol.176.5.3044
 37. Oberholzer C, Oberholzer A, Clare-Salzler M, Moldawer LL. Apoptosis in sepsis: a new target for therapeutic exploration. *FASEB J* (2001) 15(6):879–92. doi:10.1096/fj.00-058rev
 38. Ordway DJ, Orme IM. Animal models of mycobacteria infection. *Curr Protoc Immunol* (2011) Chapter 19:Unit 19.5. doi:10.1002/0471142735.im1905s94
 39. Neres R, Marinho CR, Goncalves LA, Catarino MB, Penha-Goncalves C. Pregnancy outcome and placenta pathology in *Plasmodium berghei* ANKA infected mice reproduce the pathogenesis of severe malaria in pregnant women. *PLoS One* (2008) 3(2):e1608. doi:10.1371/journal.pone.0001608

Conflict of Interest Statement: The authors declare that the research was conducted in the absence of any commercial or financial relationships that could be construed as a potential conflict of interest.

Copyright © 2017 Bomfim, Amaral, Cassado, Salles, do Nascimento, Lasunskaja, Hirata, Alvarez and D'Império-Lima. This is an open-access article distributed under the terms of the Creative Commons Attribution License (CC BY). The use, distribution or reproduction in other forums is permitted, provided the original author(s) or licensor are credited and that the original publication in this journal is cited, in accordance with accepted academic practice. No use, distribution or reproduction is permitted which does not comply with these terms.

APÊNDICE F – Inhibiting Adenosine Receptor Signaling Promotes Accumulation of Effector CD4⁺ T Cells in the Lung Parenchyma During Severe Tuberculosis. **The Journal of Infectious Diseases, 2019**

Inhibiting Adenosine Receptor Signaling Promotes Accumulation of Effector CD4⁺ T Cells in the Lung Parenchyma During Severe Tuberculosis

Eduardo P. Amaral,¹ Érika Machado de Salles,¹ Caio Cesar Barbosa Bomfim,¹ Rafael Moysés Salgado,¹ Fabrício M. Almeida,³ Paula Carolina de Souza,¹ José Maria Alvarez,¹ Mario H. Hirata,² Elena B. Lasunskaja,³ and Maria Regina D'Império-Lima¹

¹Department of Immunology, Biomedical Science Institute, University of São Paulo (USP), São Paulo, Brazil; ²Department of Clinical Chemistry and Toxicology, Faculty of Pharmaceutical Sciences, USP, São Paulo, Brazil; ³Laboratory of Biology of Recognition, State University of North Fluminense, Campos dos Goytacazes, Brazil

Background. Tuberculous pneumonia, necrotic granulomatous lesions, and bacterial dissemination characterize severe forms of mycobacterial infection.

Methods. To evaluate the pulmonary CD4⁺ T-cell response during severe tuberculosis, C57BL/6 mice were infected with approximately 100 bacilli of 3 hypervirulent mycobacterial isolates (*Mycobacterium tuberculosis* strain Beijing 1471 and *Mycobacterium bovis* strains B2 and MP287/03) or the H37Rv *M tuberculosis* strain as reference for mycobacterial virulence. Because high expression of both CD39 and CD73 ectonucleotidases was detected on parenchymal CD4⁺ T cells, we investigated whether CD4⁺ T-cell suppression in the context of severe disease was due to the extracellular adenosine accumulation that resulted from tissue damage.

Results. Lowest expression of CD69, which is an activation marker implicated in maintaining cells in tissues, was observed in lungs from mice displaying the most severe pulmonary pathology. Reduced interferon (IFN) γ -producing CD4⁺ T cells were also found in the lung of these mice. Intranasal administration of the adenosine receptor antagonist caffeine substantially enhanced the frequency and number of parenchymal CD4⁺ T cells as well as both CD69 expression and IFN γ production.

Conclusions. These results indicate that adenosine, which may be generated by extracellular adenosine triphosphate degradation, impairs the parenchymal CD4⁺ T-cell response and contributes to the development of severe tuberculosis.

Keywords. adenosine; caffeine; CD4⁺ T activation; immune response; severe tuberculosis.

Tuberculosis (TB) remains a major public health challenge, despite great scientific advances in recent decades. In 2016, 6.3 million new cases (up from 6.1 million in 2015) of the estimated incidence of 10.4 million cases and 1.3 million deaths were reported worldwide [1]. The absence of an efficient vaccine against TB largely contributes to this scenario [2]. Therefore, many recent studies addressed the adaptive immune response to *Mycobacterium tuberculosis* (*Mtb*) infection. Because of the critical role of T helper (Th) 1 cells in TB protection [3–5], the heterogeneity of pathogen-specific CD4⁺ T cells has been investigated using experimental mouse TB models. In the lungs of mice infected with the virulent H37Rv mycobacteria, the CX3CR1⁺KLRG1^{hi}CD4⁺ and CXCR3⁺PD-1^{hi}CD69^{hi}CD4⁺ T-cell subsets are located in the intravascular and parenchymal compartments, respectively [6]. Intravascular CD4⁺ T cells produced comparatively more interferon (IFN) γ after antigen stimulation, but parenchymal CD4⁺ T cells showed higher protective activity. The high expression of CD69 and PD-1 is a

signature of protective CD4⁺ T cells. The ability of CXCR3⁺PD-1^{hi}CD69^{hi}CD4⁺ T cells to gain access to the lung parenchyma, rather than produce high amounts of IFN γ , has been considered as a key feature of protection against TB. This finding corroborates with the evidence that CD4⁺ T cells interact directly with infected macrophages in lung tissue to control mycobacterial growth [7]. In addition, it was shown that the Th1 program orchestrates nonprotective CD4⁺ T-cell accumulation in the lung vasculature, and it is dispensable for CD4⁺ T-cell migration into the lung parenchyma [8]. Clarifying the tissue conditions that determine the protective CD4⁺ T-cell accumulation in the lung parenchyma is critical for improving immunological strategies and protecting against TB. This knowledge is particularly important for preventing severe TB, which accounts for 1.5%–2% of all TB cases and primarily affect children under 5 years of age, immunocompromised patients, and immunocompetent adults [9].

Using C57BL/6 mice infected with hypervirulent mycobacteria, we showed that the sensing of extracellular adenosine triphosphate (eATP) by purinergic P2X7 receptors promotes the development of severe TB [10]. The P2X7 receptor facilitates the necrotic death of infected macrophages and the bacterial dissemination. P2X7 expression in bone marrow-derived cells is critical for the detrimental effect of this receptor in severe TB, which implicates immunological cells in this process [11]. We

Received 12 February 2018; editorial decision 24 September 2018; accepted 5 October 2018; published online October 11, 2018.

Correspondence: Eduardo P. Amaral, PhD, Laboratory of Parasitic Diseases, National Institutes of Health, BG 33 RM 1W10A, 33 North Dr, Bethesda MD 20814 (eduardo.amaral@nih.gov).

The Journal of Infectious Diseases® 2019;219:964–74

© The Author(s) 2018. Published by Oxford University Press for the Infectious Diseases Society of America. All rights reserved. For permissions, e-mail: journals.permissions@oup.com. DOI: 10.1093/infdis/jiy586

proposed that the cell death provoked by intense intracellular multiplication of hypervirulent mycobacteria causes the release of high amounts of ATP. This process triggers a vicious cycle in which P2X7-induced macrophage necrosis and the consequent ATP release exacerbate pneumonia, lung damage, and bacterial dissemination.

Once released to extracellular milieu, ATP can be rapidly hydrolyzed by the ectonucleoside triphosphate diphosphohydrolase-1 (NTPDase1 or CD39) into adenosine monophosphate, which is converted into adenosine by CD73 ecto-5'-nucleotidase. CD39 and CD73 are expressed in a variety of tissues, including the lung [12]. Thus, the shift from a proinflammatory milieu induced by ATP to an anti-inflammatory environment driven by adenosine may contribute to disease progression during severe TB. Four G-protein-coupled P1 receptors, designed A1, A2A, A2B, and A3, mediate the immunomodulatory effects of adenosine [13]. The engagement of A2A receptors in effector T cells is partially responsible for the immune suppressive activities of regulatory T (Treg) cells, which constitutively express CD39 and CD73 on the surface [14, 15]. Adenosine inhibits the production of effector cytokines by Th1, Th2, and Th17 cells [16, 17]. Th17 cells also express ectonucleotidases and suppress the Th1-cell response via A2A signaling [18]. Suggesting that this pathway regulates the immune response to TB, an increase in blood CD25^{hi}CD39⁺CD4⁺ T-cell population is associated with a decrease in interleukin (IL)-17 production in healthy adults immunized against *Mtb* [19]. Furthermore, the eATP consumption by peripheral cells from vaccinated subjects correlates directly with the percentage of CD39⁺ Treg cells [20].

This study investigated the effects of parenchymal and intravascular CD4⁺ T-cell populations on TB severity and the role of adenosine signaling on CD4⁺ T-cell responses in the most aggressive form of TB. To assess the various spectra of TB severity, C57BL/6 mice were infected with H37Rv and Beijing 1471 *Mtb* strains and B2 and MP287/03 *Mycobacterium bovis* (*Mbv*) strains. An inverse correlation between disease severity and CD69 expression in pathogen-specific CD4⁺ T cells from lung parenchyma was observed. The activation marker CD69 is implicated in tissue retention, metabolism, and functional phenotype of effector T cells [21]. CD69 retains T cells into the tissue by blocking sphingosine 1-phosphate receptor-1 (S1P1)-regulated tissue egress [22, 23], and it is required for establishment of tissue-resident memory T cells [24, 25]. To investigate whether adenosine modulates the parenchymal CD4⁺ T-cell response to severe TB, MP287/03-infected mice received intranasal caffeine when body weight loss was noted. The inhibition of adenosine receptors with caffeine promoted the accumulation of pathogen-specific CD69⁺CD44⁺CD4⁺ T cells in the lung parenchyma, increased IFN γ production, and prolonged mouse survival. This study implicates adenosine in the suppression of

the parenchymal CD4⁺ T-cell response, which impacts the outcome of severe TB.

MATERIALS AND METHODS

Mice

Eight- to ten-week-old C57BL/6 male mice were bred under specific pathogen-free conditions at the Isogenic Mice Facility of the Biomedical Science Institute at USP, Brazil. Experimental groups were maintained in microisolator cages under controlled temperature and humidity and fed ad libitum at the Biosafety Level 3 Mice Facility. All experimental procedures were performed in accordance with national regulations of ethical guidelines for mice experimentation with permit number 0026/2009.

Mycobacteria and Mouse Infection

Dr. Eliana Roxo (Biological Institute, São Paulo, Brazil) and Dr. José Soares Ferreira Neto (Veterinary Medical Institute, University of São Paulo, São Paulo, Brazil) provided the *Mbv* strains, B2 and MP287/03 (SB0295 spoligotyping), which were isolated from buffalo and cattle, respectively. The Beijing 1471 *Mtb* strain (Beijing genotype) was isolated from a patient with pulmonary TB in Russia [26]. Dr. Philip Suffys (Fiocruz, Rio de Janeiro, Brazil) provided the H37Rv (ATCC) strain. Frozen mycobacterial aliquots at -80°C were thawed, sonicated, and cultured as described [10]. The bacillus concentration was determined using spectrophotometry at 600 nm. The bacterial suspensions (approximately 100 bacilli) were inoculated intratracheally (i.t.) in mice anesthetized with 100 mg/kg ketamine (Vetbrands, Vinhedo, Brazil) and 15 mg/kg xylazine (Vetbrands). Colony-forming units were determined after a 3-week incubation at 37°C [10].

Intravascular Staining and Drug Treatments

For intravascular staining, mice were given intravenous (i.v.) injections of 2.5 μg of a fluorophore-labeled monoclonal antibody (mAb) against CD45 (30-F11), and the lungs were harvested after 3 minutes, as described previously [27]. In some experiments, mice were treated intranasally (i.n.) with 10 mg/kg 8-(3-chlorostyryl)caffeine (Sigma-Aldrich) or 25, 115, and 400 $\mu\text{g}/\text{kg}$ 5'-(*N*-ethylcarboxamido)adenosine ([NECA] Sigma-Aldrich).

Lung Cell Preparation

Left lung lobes were digested with 100 U/mL Type IV collagenase (Sigma-Aldrich) at 37°C for 45 minutes. Cell suspensions were homogenized using a 10-mL syringe (BD Biosciences), filtered using a cell strainer (Corning), and incubated with ACK Lysing Buffer (Thermo Fisher Scientific) at room temperature for 1 minute to deplete erythrocytes.

Flow Cytometry Analysis

Lung cells (1×10^6) were stained using fluorochrome-labeled mAbs to CD4 (GK1.5), CD44 (IM7), CD69 (H1.2F3), IFN γ

(XMG-1.2), PD-1 (J43), CD39 (24DM51), and CD73 (Ty/11.8) (BD Pharmingen). I-A^bESAT-6₄₋₁₇ major histocompatibility complex tetramers were produced in the National Institute of Allergy and Infectious Diseases Tetramer Core Facility (Emory University, Atlanta, GA). For ex vivo intracellular IFN γ staining, lung cells (1×10^6) were incubated with monensin (2 μ M) for 5 hours at 37°C in 5% CO₂ atmosphere, fixed, and permeabilized with BD cytofix/cytoperm kit (BD Biosciences). Cells were analysed using a FACSCanto flow cytometer (BD Biosciences) and the FlowJo software.

Supernatant Interferon- γ Quantification

Lung cells (5×10^4) were cultured in Roswell Park Memorial Institute 1640 medium (Gibco) with 1 mM sodium pyruvate, 2 mM glutamine, 0.05% gentamicin, and 10% fetal calf serum at 37°C in 5% CO₂ atmosphere for 48 hours. The IFN γ levels in cell culture supernatants were measured using a Fluorokine kit (R&D Systems).

Statistical Analyses

Statistical analyses were performed using GraphPad Prism 5 software. Simultaneous effects of 2 factors were analysed using 2-way analysis of variance (ANOVA) test. One-way ANOVA test and Tukey's post hoc test were used to assess the effects of only 1 parameter between more than 2 groups. Mann-Whitney *U* test was performed to compare 2 groups. Survival curves were analysed with the log-rank test of the Kaplan-Meier method. Differences between groups were considered significant when $P < .05$.

RESULTS

High PD-1/CD69 Expression Ratio in Lung CD4⁺ T Cells Is Associated With Reduced Interferon- γ Production During Severe Tuberculosis

To investigate the CD4⁺ T-cell response during severe TB, C57BL/6 mice were infected i.t. with approximately 100 bacilli of the Beijing 1471, B2 and MP287/03 hypervirulent strains, or the H37Rv strain as a reference of virulent mycobacteria. We previously showed that Beijing 1471 and MP287/03 infections caused extensive cellular infiltration in the lung tissue and intra-bronchiolar space, which led to the development of pulmonary necrotic areas, bacterial dissemination, and anticipated animal death [10, 28]. On day 28 postinfection (p.i.), B2-infected mice displayed lung bacillus count approximately 100-fold higher than H37Rv-infected mice, similar to Beijing 1471-infected mice, and 100-fold lower than MP287/03-infected mice (Figure 1A). Body weight loss directly correlated with the lung bacterial load (Figure 1B). Macroscopically, in severe TB, the lungs had white nodules that were more prominent in MP287/03-infected mice (Figure 1C). Lung weight and relative mass were also greater in MP287/03-infected mice than Beijing 1471- and B2-infected mice (Figure 1C and D). These parameters were similar to the controls in H37Rv-infected mice. Large

lung necrotic areas were observed for the MP287/03 and Beijing 1471 strains (Supplementary Figure S1).

Because protective CD4⁺ T cells express high levels of CD69 and PD-1 in TB [6], these molecules were analysed in lung CD4⁺ cells of mice infected with hypervirulent mycobacteria. CD69 is implicated in T-cell activation and retention in the tissue [21–25]. PD-1 signaling suppresses T-cell inflammatory activity [29]. On day 28 p.i., most lung CD4⁺ cells in infected mice had an experienced phenotype because of the high CD44 expression, and some also expressed CD69 and PD-1 (Figure 1E). An association between CD4⁺ T-cell suppression and disease severity was demonstrated in the PD-1/CD69 mean fluorescence intensity (MFI) ratios of 0.9 (H37Rv), 1.5 (Beijing 1471), 2.3 (B2), and 3.8 (MP287/03). Consistently, the CD69⁺CD44⁺CD4⁺ cell percentage was lower in MP287/03-infected mice than in B2- and Beijing 1471-infected mice (Figure 1F and G). Considering the lung cellularity, the CD69⁺CD44⁺CD4⁺ cell population was smaller in B2- and MP287/03-infected mice compared with Beijing 1471-infected mice. CD69⁺CD44⁺CD4⁺ cells also showed higher PD-1 levels in B2- and MP287/03-infected mice (Figure 1H). In addition, these mice presented lower numbers of IFN γ -producing CD44⁺CD4⁺ cells than did Beijing 1471-infected mice (Figure 1I). Therefore, high expression of PD-1 and low expression CD69 in lung CD4⁺ cells were associated with reduced IFN γ response during severe TB.

Small Proportion of Parenchymal Pathogen-Specific CD4⁺ T Cells Expresses CD69 in MP287/03-Infected Mice

To analyze the activation pattern of parenchymal and intravascular CD4⁺ T cells in the lungs during severe TB, fluorophore-labeled anti-CD45 antibodies were inoculated i.v. 3 minutes before mouse sacrifice, as previously reported [27]. On day 28 p.i., intravascular and parenchymal CD44⁺CD4⁺ cells were clearly distinguished by CD45iv^{pos} and CD45iv^{neg} staining, respectively (Figure 2A). Intravascular CD44⁺CD4⁺ cells predominated in noninfected mice and H37Rv-infected mice, but most CD44⁺CD4⁺ cells were found in the lung parenchyma of mice infected with hypervirulent mycobacteria. As previously reported [6], pathogen-specific CD44⁺CD4⁺ T cells were primarily located in the lung vasculature of H37Rv-infected mice (Figure 2B). In contrast, these cells were predominantly found in the lung parenchyma of mice infected with hypervirulent mycobacteria. It is remarkable that despite the small pathogen-specific CD44⁺CD4⁺ cell population infiltrating the lung parenchyma of H37Rv-infected mice, approximately half of the cells expressed CD69 (Figure 2C). This proportion was approximately 30% in Beijing 1471- and B2-infected mice and 15% in MP287/03-infected mice. Mice from the latter group also presented a small population of pathogen-specific CD69⁺CD44⁺CD4⁺ cells in the lung parenchyma. Therefore, the lowest level of CD69 expression in pathogen-specific parenchymal CD4⁺ T cells was associated with weak IFN γ response and the most severe pulmonary pathology in MP287/03-infected mice.

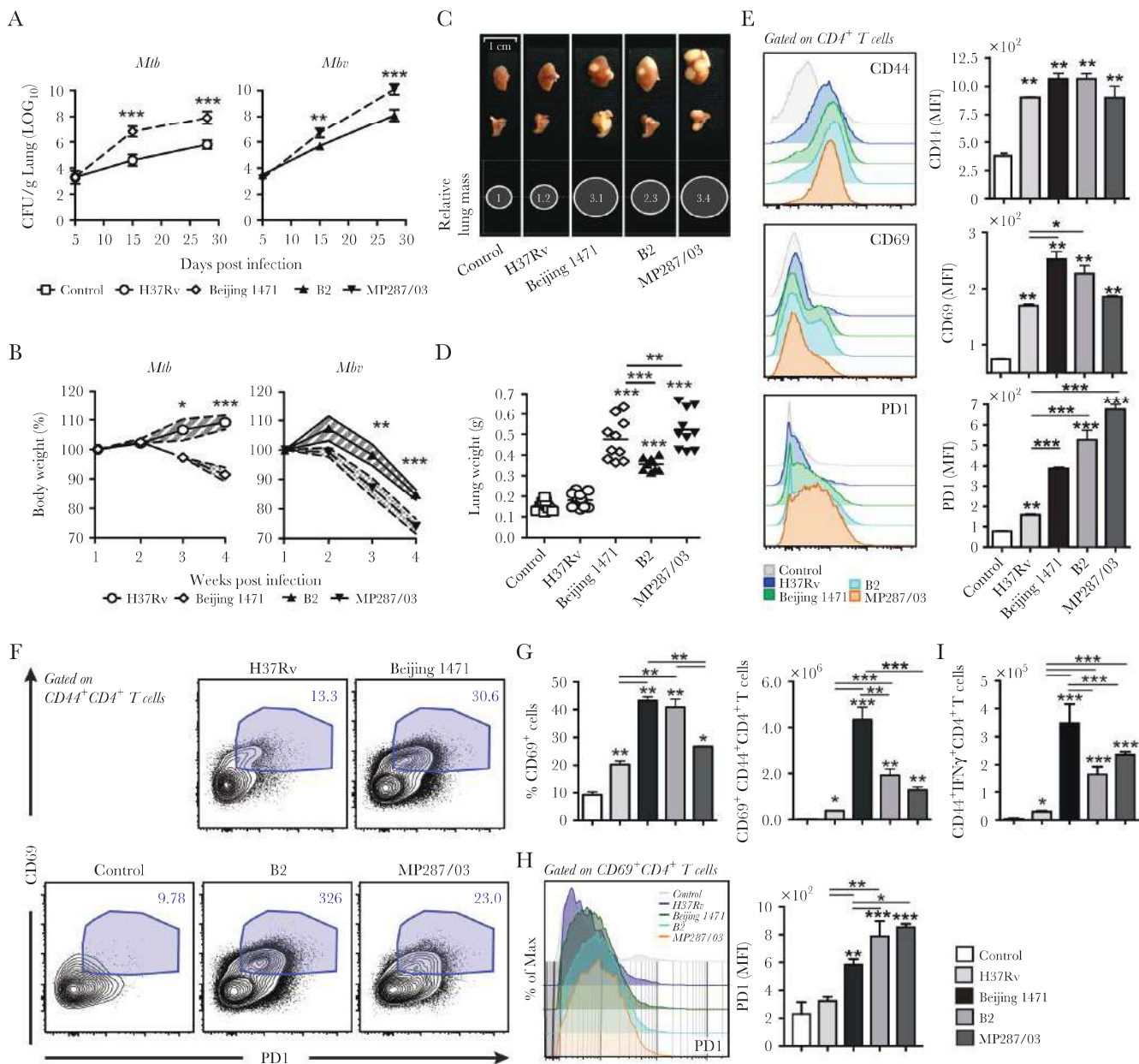


Figure 1. CD44, CD69, and PD-1 expression in lung CD4⁺ T cells during virulent and hypervirulent mycobacterial infections. C57BL/6 mice were infected intratracheally with approximately 100 bacilli of H37Rv, Beijing 1471, B2, and MP287/03 strains. Noninfected mice were used as controls. (A) At 0, 5, 15, 28, and 60 days postinfection (p.i.), the numbers of colony-forming units/gram (CFU/g) of lung tissue were determined in the left lung lobes. (B) Mouse body weights were determined weekly. (C) Representative lung macroscopic images and relative lung masses (circles) at 28 days p.i. are shown. Relative lung mass was calculated as the ratio of mean values of lung weights in indicated groups and control group. (D) Lung weights at 28 days p.i. are shown. Mean values are represented in the horizontal lines. (A–D) The data are expressed as the means \pm standard deviation (SD) ($n = 9$ –13 mice per group) from 1 of 3 independent experiments. Asterisk represents significant differences between *Mtb*- and *Mbv*-infected mice (A and B), between infected and control mice, or between indicated groups (*, $P < .05$; **, $P < .01$; and ***, $P < .001$). (E–I) Lung cells were harvested at 28 days p.i. and analyzed using flow cytometry. (E) Histograms show CD44, CD69, and PD-1 expression in CD4⁺ cells. The mean fluorescence intensity (MFI) is shown in the column bar graphs. (F) Contour plots show PD-1 and CD69 expression in CD44⁺CD4⁺ T cells. (G) Percentages of CD69⁺ cells in CD44⁺CD4⁺ cells and the numbers of CD69⁺CD44⁺CD4⁺ cells in the lungs are shown. (H) Histograms show PD-1 expression in CD69⁺CD4⁺ cells. The MFI is shown in the column bar graphs. (I) Numbers of interferon (IFN) γ -producing CD44⁺CD4⁺ cells in the lungs are shown. The data are expressed as the means \pm SD ($n = 4$ –5 mice per group) of 1 representative experiment of at least 3. Asterisk represents significant differences between infected and control mice or between indicated groups (*, $P < .05$; **, $P < .01$; and ***, $P < .001$).

Parenchymal CD4⁺ T Cells From MP287/03-Infected Mice Express High Levels of CD39 and CD73 Ectonucleotidases

We had previously proposed that the suppressive environment resulting from an excess of adenosine, as a byproduct

of ATP released by necrotic tissue, could facilitate the survival of hypervirulent mycobacteria [10]. Because adenosine is rapidly degraded, the autocrine activity of ectonucleotidases may ensure adenosine generation in the CD4⁺ T-cell

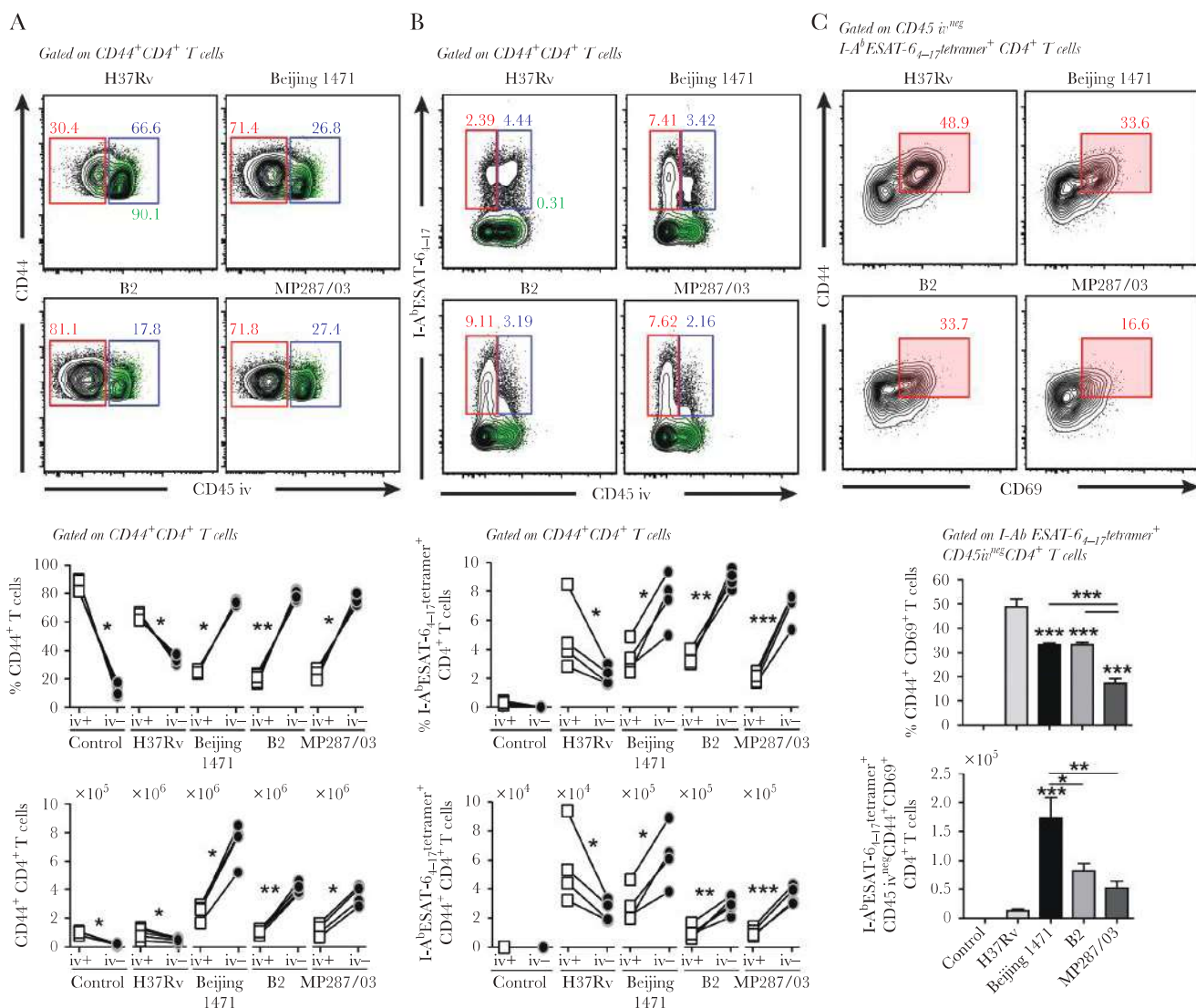


Figure 2. Intravascular and parenchymal CD4⁺ T cells in the lung during virulent and hypervirulent mycobacterial infections. C57BL/6 mice were infected intratracheally with approximately 100 bacilli of H37Rv, Beijing 1471, B2, and MP287/03 strains. Lung cells were harvested at 28 days postinfection 3 minutes after intravenous (i.v.) inoculation of fluorophore-labeled anti-CD45 monoclonal antibodies and were analyzed using flow cytometry. Noninfected mice were used as controls. (A) Contour plots show CD45_{iv}⁺ and CD44 expression in CD44⁺CD4⁺ cells. Plots from noninfected mice are shown in green. The scatter plot graphs show the percentages of CD45_{iv}⁺ and CD45_{iv}⁻ cells in CD44⁺CD4⁺ cells and the numbers of CD45_{iv}⁺ and CD45_{iv}⁻CD44⁺CD4⁺ cells in the lungs. Lines connect data from the same mouse. (B) Contour plots show CD45_{iv}⁺ and I-AbESAT-6₄₋₁₇ tetramer expression in CD44⁺CD4⁺ cells. Plots from noninfected mice are shown in green. Scatter plot graphs show the percentages of CD45_{iv}⁺ and CD45_{iv}⁻ cells in I-AbESAT-6₄₋₁₇ tetramer-specific CD44⁺CD4⁺ cells and the numbers of CD45_{iv}⁺ and CD45_{iv}⁻ I-AbESAT-6₄₋₁₇ tetramer-specific CD44⁺CD4⁺ cells in the lungs. (C) Contour plots show CD69 and CD44 expression in CD45_{iv}⁺ I-AbESAT-6₄₋₁₇ tetramer-specific CD44⁺CD4⁺ cells. The column bar graphs show the percentages of CD69⁺CD44⁺ cells in CD45_{iv}⁻ I-AbESAT-6₄₋₁₇ tetramer-specific CD4⁺ cells and the numbers of CD45_{iv}⁻ I-AbESAT-6₄₋₁₇ tetramer-specific CD69⁺CD44⁺CD4⁺ cells in the lungs. Lines connect data from the same mouse. Data are expressed as the means ± standard deviation ($n = 4$ mice per group) from 1 of 3 independent experiments. Asterisk represents significant differences between indicated groups (*, $P < .05$; **, $P < .01$; and ***, $P < .001$).

vicinity. Indeed, increased proportions of lung CD44⁺CD4⁺ cells expressing CD39 and CD73 were observed in infected mice compared with uninfected controls (Figure S2). Thus, to specifically address whether adenosine may interfere on parenchymal CD4⁺ T-cell response to severe TB, MP287/03-infected mice were herein used as a model of tissue damage. On day 28 p.i., CD39 and CD73 were expressed preferentially in CD44⁺CD4⁺ cells located in the lung parenchyma compared with those in the vasculature (Figure 3A and B). Infection

induced CD39 expression (Figure 3A), whereas CD73 was constitutively expressed at high levels in parenchymal CD44⁺CD4⁺ cells (Figure 3B). To inhibit the effects of adenosine on CD4⁺ T-cell response to infection, mice were treated from 20 to 28 days p.i. with i.n. caffeine, which is a well known antagonist of adenosine receptors (Figure 3C). Caffeine treatment did not interfere on CD39 expression but slightly decreased the CD73 levels (Figure 3D). These results suggest that eATP released from damaged lung tissue in MP287/03-infected mice may be

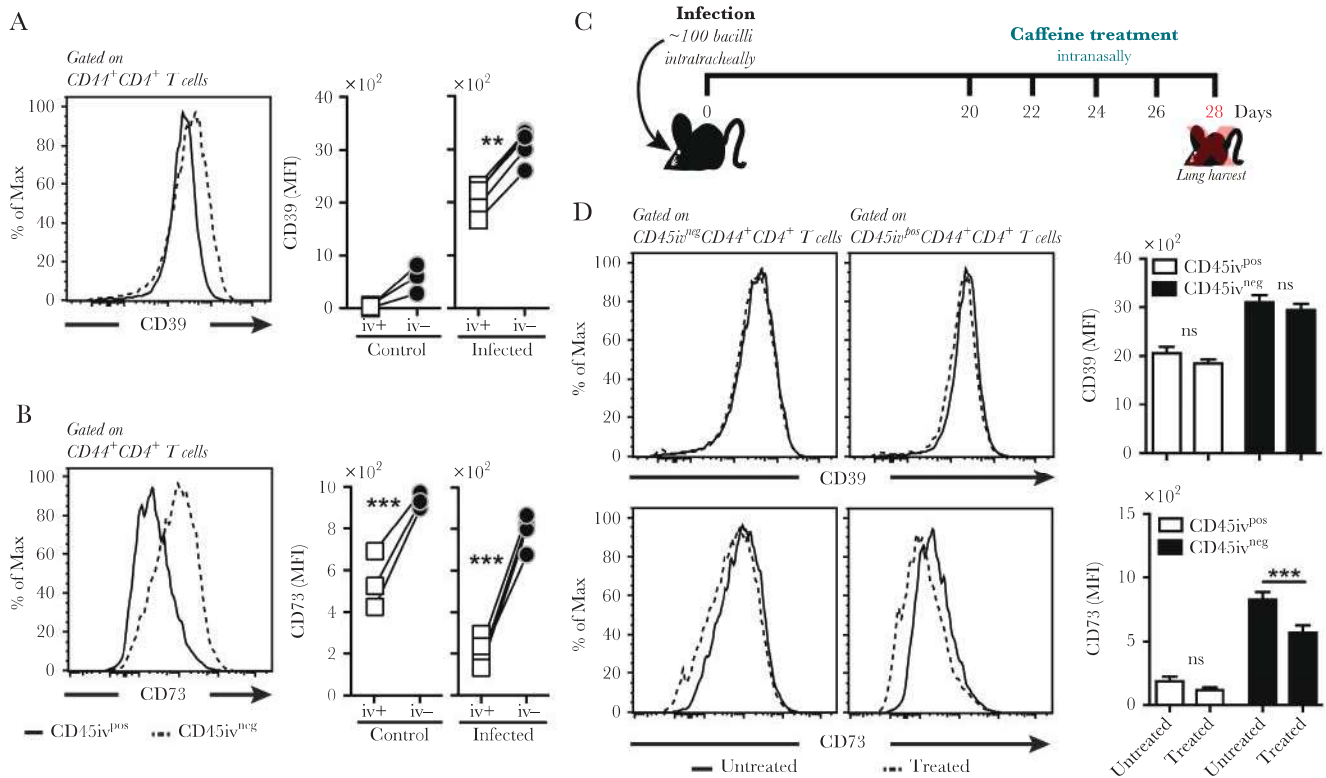


Figure 3. CD39 and CD73 expression in intravascular and parenchymal CD4⁺ T cells from the lungs of MP287/03-infected mice treated or not with caffeine. C57BL/6 mice were infected intratracheally with approximately 100 MP287/03 bacilli. Lung cells were harvested at 28 days postinfection (p.i.) 3 minutes after intravenous (i.v.) inoculation of fluorophore-labeled anti-CD45 monoclonal antibodies and analyzed using flow cytometry. Noninfected mice were used as controls. (A and B) Histograms show CD39 (A) and CD73 (B) expression in CD45^{iv+} and CD45^{iv-} cells in CD44⁺CD4⁺ cells. The mean fluorescence intensity (MFI) is shown in the scatter plot graphs. Lines connect data from the same mouse. (C) Schematic illustration of the experimental protocol for caffeine treatment is shown. Infected mice were treated with caffeine (10 mg/kg per body weight) intranasally every other day starting 20 days p.i. for 8 days. (D) Histograms show CD39 and CD73 expression in CD45^{iv+} and CD45^{iv-}CD44⁺CD4⁺ cells of caffeine-treated and untreated mice. The MFI is shown in the column bar graphs. Data are expressed as the means ± standard deviation ($n = 4-5$ mice per group) from 1 of 3 independent experiments. Asterisk represents significant differences between indicated groups (**, $P < .01$ and ***, $P < .001$). ns, nonsignificant.

degraded to adenosine in the environment surrounding parenchymal CD4⁺ T cells.

Inhibition of Adenosine Receptors Promotes Pathogen-Specific CD69⁺CD4⁺ T-Cell Accumulation in the Lung Parenchyma During Severe Tuberculosis

The next experiments evaluated how adenosine receptor signaling modulates CD4⁺ T-cell accumulation in the lung compartments of MP287/03-infected mice. On day 28 p.i., intravascular CD4⁺ cell proportion was smaller in caffeine-treated mice than in untreated controls, but no difference was observed for intravascular CD44⁺CD4⁺ cells (Figure 4A). In addition, CD69 expression in parenchymal CD4⁺ cells increased drastically after caffeine administration, which was observed in MFI levels and percentage of positive cells (Figure 4B and C). Caffeine treatment resulted in a 5-fold increase in the number of parenchymal CD44⁺CD4⁺ cells expressing CD69. A similar effect was observed for pathogen-specific CD4⁺ cells (Figure 4D). Thus, adenosine receptor signaling suppressed CD69 expression and

prevented pathogen-specific CD69⁺CD4⁺ T-cells accumulation in the lung parenchyma of MP287/03-infected mice.

To investigate whether adenosine inhibits CD4⁺ T-cell migration to the lung parenchyma in TB, H37Rv-infected mice were treated i.n. from day 20 to 28 p.i. with the nonselective adenosine receptor agonist NECA. We were surprised to find that H37Rv-infected mice treated with 400 and 115 μg/kg NECA succumbed during the 24 hour-period after drug administration (Supplementary Figure S3A), possibly due to the bronchoconstrictor effect of adenosine [30-32]. Using 25 μg/kg NECA, CD44⁺CD4⁺ cells accumulated in the lung vasculature, but no difference occurred in the lung parenchyma compared with untreated mice (Supplementary Figure S3B). Thus, low stimulation of adenosine receptors increased the intravascular CD44⁺CD4⁺ T-cell population in H37Rv-infected mice. An increase in lung bacterial burden was consistently observed in NECA-treated mice (Supplementary Figure S3C). These data show that adenosine signaling is detrimental for the host during mycobacterial infection.

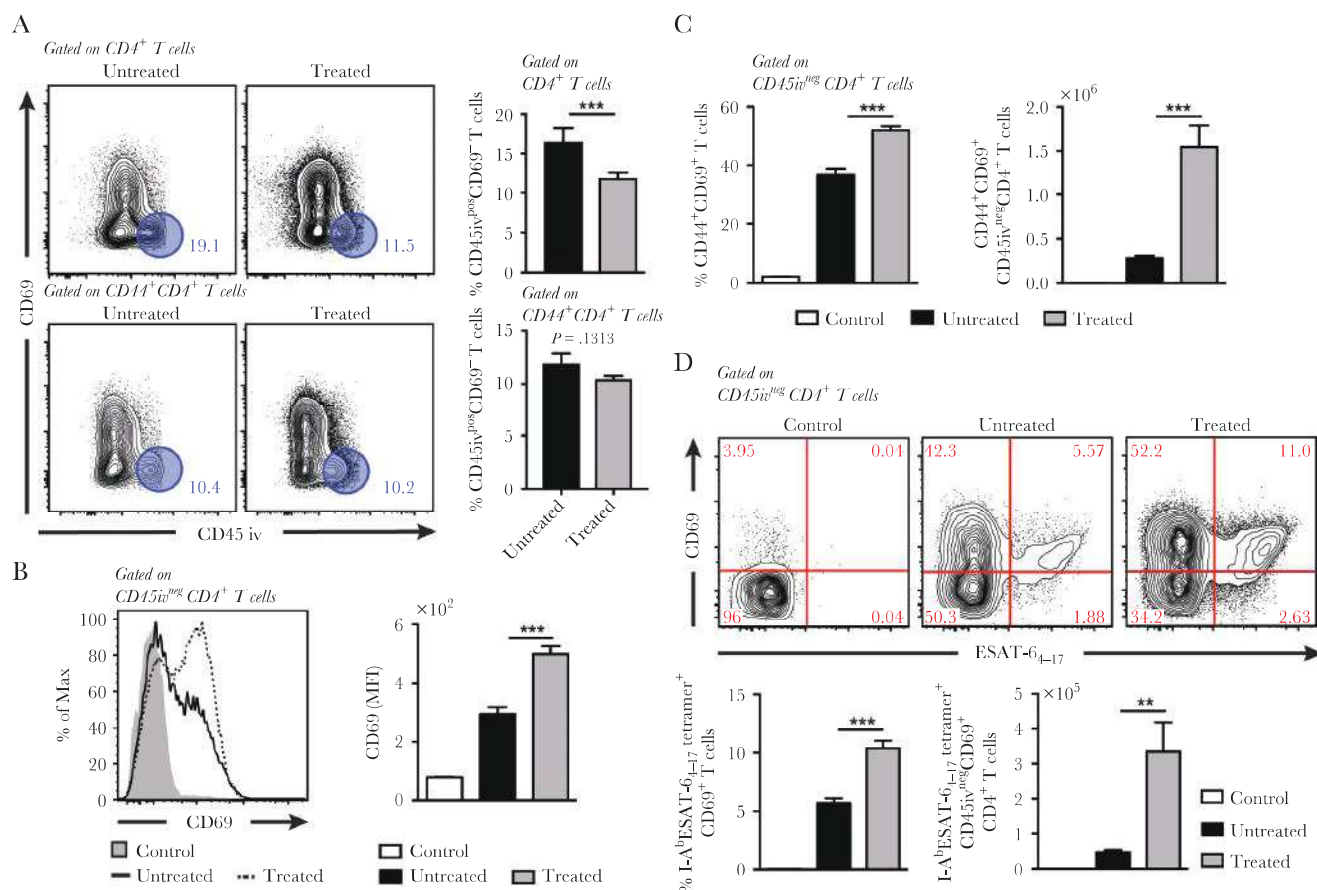


Figure 4. Effects of caffeine treatment on parenchymal CD4⁺ T-cell activation and accumulation in the lungs during MP287/03 infection. C57BL/6 mice infected intratracheally with approximately 100 MP287/03 bacilli were treated with caffeine (10 mg/kg per body weight) intranasally every other day, starting at 20 days postinfection (p.i.), as illustrated in Figure 3C. Lung cells were harvested at 28 days p.i. 3 minutes after inoculating intravenously (i.v.) fluorophore-labeled anti-CD45 monoclonal antibodies and analyzed using flow cytometry. Noninfected mice were used as controls. (A) Contour plots show CD45_{iv} and CD69 expression in CD4⁺ cells (top graph) and CD44⁺CD4⁺ cells (bottom graph). Percentages of CD45_{iv}^{pos}CD69⁺ cells in lung CD4⁺ cells and CD44⁺CD4⁺ cells are shown. (B) Histograms show CD69 expression in CD45_{iv}^{pos}CD4⁺ cells. The mean fluorescence intensity (MFI) is shown in the column bar graphs. (C) Percentages of CD69⁺CD44⁺ cells in CD45_{iv}^{pos}CD4⁺ cells and the numbers of CD45_{iv}^{pos}CD69⁺CD44⁺CD4⁺ cells in the lungs are shown. (D) Contour plots show I-AbESAT-6₄₋₁₇ tetramer and CD69 expression in CD45_{iv}^{pos}CD4⁺ cells. Percentages of I-AbESAT-6₄₋₁₇ tetramer-specific CD69⁺ cells in CD45_{iv}^{pos}CD4⁺ cells and numbers of I-AbESAT-6₄₋₁₇ tetramer-specific CD45_{iv}^{pos}CD69⁺CD4⁺ cells in the lungs are shown in the column bar graphs. Data are expressed as the means ± standard deviation ($n = 4-5$ mice per group) of 1 representative experiment of 3. Asterisk represents significant differences between infected and control mice or between indicated groups (**, $P < .01$ and ***, $P < .001$).

Caffeine Treatment Improves Interferon- γ Production by Parenchymal CD4⁺ T Cells and Prolongs Mouse Survival

Next, we investigated the effects of caffeine treatment on IFN γ production and disease progression. On day 28 p.i., a 5-fold increase in the numbers of parenchymal CD4⁺ cells producing IFN γ was observed after caffeine administration in MP287/03-infected mice (Figure 5A and B). The IFN γ levels in lung cell supernatants were drastically enhanced in caffeine-treated mice compared with untreated controls (Figure 5C). No statistical significance was observed between these groups in lung bacterial burden (Figure 5D), but long-term caffeine treatment increased mouse survival (Figure 5E and F). These data show that adenosine receptor signaling suppresses IFN γ production by parenchymal CD4⁺ T cells and contributes to TB severity.

DISCUSSION

Our study took advantage of the variability in the pathogenicity of mycobacterial strains in mice [10, 28] to unravel the molecular basis of the immunosuppression associated with severe TB. The balance between PD-1 and CD69 expression in lung CD4⁺ T cells is likely a key event that shapes the pulmonary immune response to mycobacterial infection. This was suggested by our results showing an association between the PD-1/CD69 expression ratio in lung CD4⁺ T cells with TB severity. Furthermore, the low IFN γ production by lung CD4⁺ T cells displaying high PD-1/CD69 expression ratios evidenced the immunosuppression in B2- and MP287/03-infected mice. Effector CD4⁺ T cells in the lung parenchyma exhibit the PD-1^{hi}CD69^{hi} phenotype, which may influence their interaction with infected macrophages in tissue [6, 8]. PD-1 suppresses CD4⁺ T-cell effector functions, including IFN γ production [33]. During mycobacterial infection, PD-1 expression in

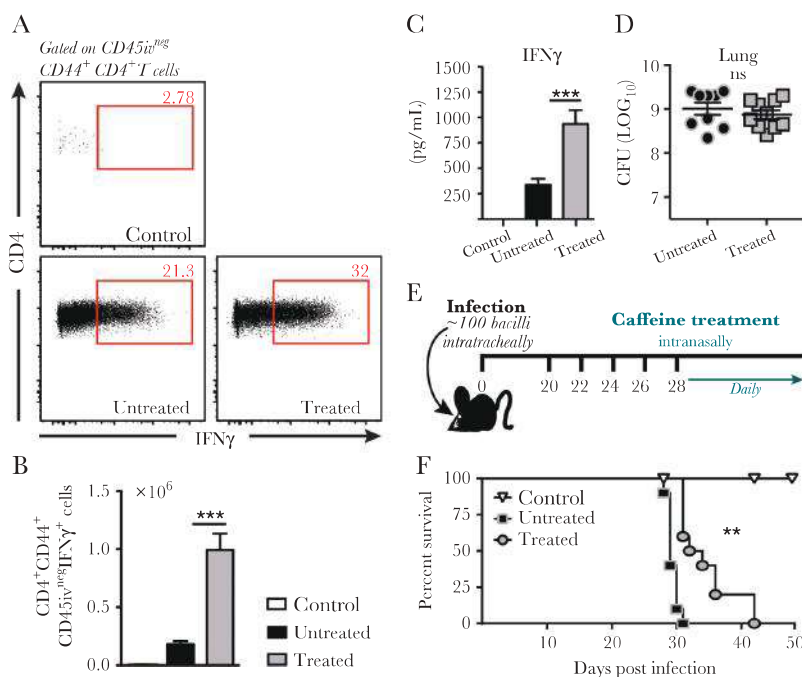


Figure 5. Effects of caffeine treatment on interferon (IFN) γ production and tuberculosis progression. (A–D) C57BL/6 mice infected intratracheally with approximately 100 MP287/03 bacilli were treated with caffeine (10 mg/kg per body weight) intranasally every other day, starting 20 days postinfection (p.i.), as illustrated in Figure 3C. Lung cells were harvested at 28 days p.i. 3 minutes after intravenous (i.v.) inoculation of fluorophore-labeled anti-CD45 monoclonal antibodies and analyzed using flow cytometry. Noninfected mice were used as controls. (A) Dot plots show intracellular interferon (IFN) γ (x-axis) and CD4 (y-axis) expression in CD45^{hi}-CD44⁺T cells. (B) Numbers of IFN γ -producing CD45^{hi}-CD44⁺T cells in the lungs are shown. (C) The IFN γ levels in lung cell supernatants from mice described in A were determined using enzyme-linked immunosorbent assay. (A–C) The data are expressed as the means \pm standard deviation (SD) ($n = 4$ –5 mice per group) from 1 of at least 2 independent experiments. (D) Lung bacterial load was determined using colony-forming unit (CFU) quantification. The data are expressed as the means \pm SD ($n = 9$ –10 mice per group, pooled from 2 independent experiments with 4–5 mice per group each). (E) Schematic illustration shows an alternative experimental protocol in which the caffeine treatment described in Figure 3C was extended by daily administration until mouse death. (F) Survival curves of mice submitted to the experimental protocol described in E are shown. The data are expressed as the means \pm SD ($n = 10$ mice per group, pooled from 2 independent experiments with 5 mice per group each). Asterisk represents significant differences between indicated groups (**, $P < .01$ and ***, $P < .001$). ns, nonsignificant.

CD4⁺ T cells inhibits the accumulation of IFN γ -producing CD4⁺ T cells in the lung parenchyma [34]. Thus, the high PD-1 expression in CD4⁺ T cells could suppress IFN γ production in B2- and MP287/03-infected mice, and the low CD69 expression could promote the egress of these cells from lung tissue.

The tissue location, population frequency, and activation state of lung CD4⁺ T cells varied considerably in mice infected with bacilli from the different strains. Most pathogen-specific CD4⁺ T cells were present in the lung parenchyma during hypervirulent mycobacterial infections, and this cell subset predominated in the lung vasculature in H37Rv-infected mice, as previously reported [6]. Of note, CD69 was expressed in approximately half of pathogen-specific CD44⁺CD4⁺ T cells located in the lung parenchyma of H37Rv-infected mice, but this proportion decreased as the disease became more aggressive in hypervirulent mycobacterial infections. MP287/03-infected mice, which exhibited a very high bacterial load and massive inflammatory lesions with necrosis in the lung, displayed low numbers of parenchymal pathogen-specific CD69⁺CD4⁺ T cells. These findings suggest that the pulmonary environment in certain forms of severe TB exhibits impairment in effector CD4⁺ T-cell accumulation in the lung parenchyma.

To explore this possibility, we examined the effects of adenosine, which is an important purine metabolite associated with inflammatory homeostasis [35], on parenchymal CD4⁺ T cells in MP287/03-infected mice. The ability of parenchymal CD4⁺ T cells to generate adenosine in their vicinity is suggested by the high CD39 and CD73 expression, as observed for other T-cell subsets [15]. In addition to T cells, these ectonucleotidases are expressed in monocytes, neutrophils, dendritic cells, and myeloid-derived suppressor cells [15, 36–40], which can promote ATP degradation in the lung tissue. The excess of ATP released from necrotic cells may be determinant to increase extracellular adenosine levels. The presence of high amounts of eATP in the lungs during severe TB is suggested by our previous studies showing the detrimental effect of the P2X7 receptor in Beijing 1471- and MP287/03-infected mice [10, 11, 41]. Caffeine administration at the time of infection where weight loss was already noted demonstrates that adenosine impaired the parenchymal accumulation of pathogen-specific CD69⁺CD4⁺ T cells and inhibited IFN γ production. Caffeine antagonizes all types of adenosine receptors but exhibits a higher affinity to A2A receptors, which are expressed on most immune cells, including T cells [35]. The absence of CD73 exacerbates the

production of proinflammatory cytokines, such as tumor necrosis factor- α , IL-6, and KC, and promotes the recruitment of neutrophils in the lung during mycobacterial infection, which is likely due to the low adenosine generation [42].

Interferon- γ secretion from CD4⁺ T cells is a key element to control mycobacteria [43, 44], but its overproduction is detrimental under some circumstances. For example, PD-1 expression in parenchymal CD4⁺ T cells is required to prevent the IFN γ overproduction that leads to host death, despite the decrease in bacterial load [34]. These data are consistent with the hypothesis that the simultaneous reduction of the damage caused by the microbe and the host immune response leads to the best host benefit [45]. Therefore, the outcome of adenosine receptor inhibition in mice with severe TB may be to prevent or promote animal death. Our data show that caffeine administration for 8 days did not affect the pulmonary bacterial load, but mice that received

additional treatment until death survived longer. Our interpretation of these results is that the protective effects of higher IFN γ production became apparent only after longer caffeine treatment. Thus, restoring the parenchymal CD4⁺ T-cell response during the late stage of severe TB benefits the host. However, we cannot exclude the possibility that caffeine treatment improves disease tolerance without affecting host resistance [46].

CONCLUSIONS

As a model to explain the suppressive role of adenosine in the parenchymal CD4⁺ T-cell response during severe TB (Figure 6), we propose that the massive destruction of macrophages by hypervirulent mycobacteria leads to the release of large amounts of ATP into the extracellular milieu. Extracellular ATP engages the P2X7 receptor and potentiates macrophage necrotic death [10] or is hydrolyzed by CD39 and CD73 into adenosine. In the lung parenchyma, CD4⁺ T

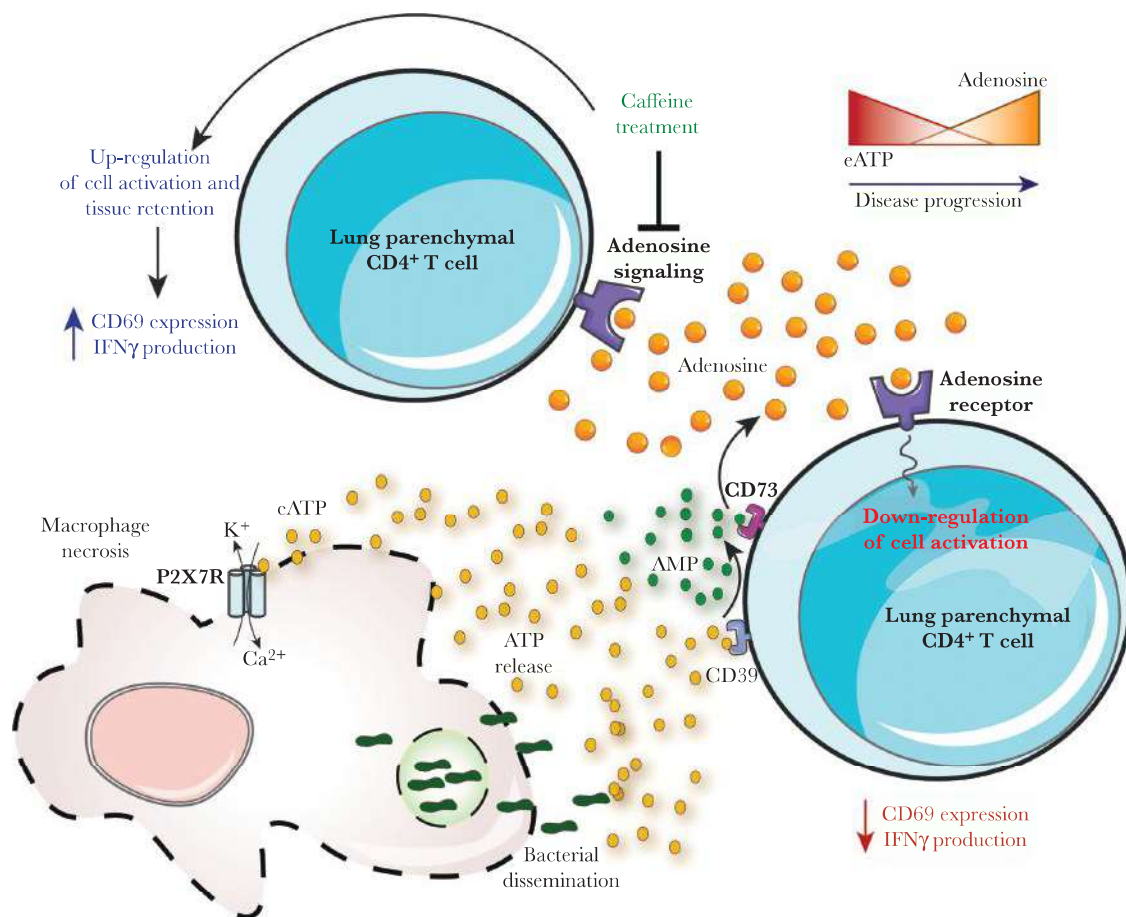


Figure 6. Schematic illustration of a hypothetical model explaining the role of adenosine in parenchymal CD4⁺ T-cell activation and accumulation in the lung during severe tuberculosis. The necrosis of infected macrophages promotes the bacterial spread and the release of large amounts of adenosine triphosphate (ATP) in the extracellular milieu. The recognition of extracellular ATP (eATP) by the P2X7 receptor contributes to the necrotic death of infected macrophages by inducing P2X7-mediated pore formation [10]. Extracellular ATP also sensitizes neighboring cells to die via P2X7-mediated necrosis or is degraded by CD39 and CD73 ectonucleotidases. In the lung parenchyma, CD4⁺ T cells express CD39 that hydrolyses ATP into adenosine diphosphate and adenosine monophosphate (AMP). The CD73 converts AMP into adenosine, which activates P1 receptors, such as the A2A receptor. Engagement of adenosine receptors leads to suppression of parenchymal CD4⁺ T-cell response, which directly impacts host resistance by facilitating mycobacterial survival. The inhibition of adenosine receptors by caffeine (A2a, A1, A3, and A2b, in order of efficiency) promotes CD69 expression. This activation is a key event for CD4⁺ T-cell activation and retention in the lung parenchyma, which allows the release of interferon (IFN) γ in close vicinity to infected macrophages, and it is crucial for host defence against mycobacteria.

cells express ectonucleotidases and contribute to increase adenosine concentrations. The engagement of P1 receptors, such as the A2A receptor, downregulates CD69 and impairs pathogen-specific CD4⁺ T-cell accumulation in the lung parenchyma and the release of IFN γ in the vicinity of infected macrophages, which is a crucial event for host defence against mycobacteria. This novel insight into TB pathogenesis, in which the sensing of damage signals by the immune system dictates the outcome of severe TB, provides a new perspective for the development of adjuvant therapies using drugs designed to inhibit P2X7 and adenosine receptors.

Notes

Author contributions. E. P. A. and M. R. D.-L. conceived and designed the experiments. E. P. A., C. C. B. B., E. M. d. S., R. M. S., and E. B. L. performed the experiments. E. P. A. and M. R. D.-L. analyzed the data. E. P. A., M. H. H., J. M. A., E. B. L., and M. R. D.-L. contributed reagents, materials, and analysis tools. E. P. A. and M. R. D.-L. wrote the paper.

Acknowledgments. We thank Drs. Eliana Roxo and José Soares Ferreira Neto for providing the B2 and MP287/03 *Mbv* strains. We also thank Mariana Franchi, Rogério S. do Nascimento, Maria Áurea de Alvarenga, and Rodrigo S. Oliveira for technical assistance.

Financial support. This work was supported by São Paulo Research Foundation (FAPESP, Brazil) grants, 2013/07140-2, 2015/20432-8 (M. R. D.-L) and 2015/191260 (E. P. A), and National Council for Scientific and Technological Development (CNPq, Brazil) grants, 303676/2014-0 and 448765/2014-4 (M. R. D.-L).

Potential conflicts of interest. All authors: No reported conflicts of interest. All authors have submitted the ICMJE Form for Disclosure of Potential Conflicts of Interest.

References

1. World Health Organization. Tuberculosis Fact Sheet. Number 104. Geneva: World Health Organization, 2017.
2. Pai M, Behr MA, Dowdy D, et al. Tuberculosis. *Nat Rev Dis Primers* 2016; 2:16076.
3. Orme IM. The kinetics of emergence and loss of mediator T lymphocytes acquired in response to infection with *Mycobacterium tuberculosis*. *J Immunol* 1987; 138:293–8.
4. Saunders BM, Frank AA, Orme IM, Cooper AM. CD4 is required for the development of a protective granulomatous response to pulmonary tuberculosis. *Cell Immunol* 2002; 216:65–72.
5. Jasenosky LD, Scriba TJ, Hanekom WA, Goldfeld AE. T cells and adaptive immunity to *Mycobacterium tuberculosis* in humans. *Immunol Rev* 2015; 264:74–87.
6. Sakai S, Kauffman KD, Schenkel JM, et al. Cutting edge: control of *Mycobacterium tuberculosis* infection by a subset of lung parenchyma-homing CD4 T cells. *J Immunol* 2014; 192:2965–9.
7. Srivastava S, Ernst JD. Cutting edge: direct recognition of infected cells by CD4 T cells is required for control of intracellular *Mycobacterium tuberculosis* in vivo. *J Immunol* 2013; 191:1016–20.
8. Sallin MA, Sakai S, Kauffman KD, Young HA, Zhu J, Barber DL. Th1 differentiation drives the accumulation of intravascular, non-protective CD4 T cells during tuberculosis. *Cell Rep* 2017; 18:3091–104.
9. Cruz AT, Starke JR. Clinical manifestations of tuberculosis in children. *Paediatr Respir Rev* 2007; 8:107–17.
10. Amaral EP, Ribeiro SC, Lanes VR, et al. Pulmonary infection with hypervirulent *Mycobacteria* reveals a crucial role for the P2X7 receptor in aggressive forms of tuberculosis. *PLoS Pathog* 2014; 10:e1004188.
11. Bomfim CCB, Amaral EP, Cassado ADA, et al. P2X7 receptor in bone marrow-derived cells aggravates tuberculosis caused by hypervirulent *Mycobacterium bovis*. *Front Immunol* 2017; 8:435.
12. Antonioli L, Pacher P, Vizi ES, Haskó G. CD39 and CD73 in immunity and inflammation. *Trends Mol Med* 2013; 19:355–67.
13. Antonioli L, Blandizzi C, Pacher P, Haskó G. Immunity, inflammation and cancer: a leading role for adenosine. *Nat Rev Cancer* 2013; 13:842–57.
14. Borsellino G, Kleinewietfeld M, Di Mitri D, et al. Expression of ectonucleotidase CD39 by Foxp3+ Treg cells: hydrolysis of extracellular ATP and immune suppression. *Blood* 2007; 110:1225–32.
15. Deaglio S, Dwyer KM, Gao W, et al. Adenosine generation catalyzed by CD39 and CD73 expressed on regulatory T cells mediates immune suppression. *J Exp Med* 2007; 204:1257–65.
16. Csóka B, Himer L, Selmečzy Z, et al. Adenosine A2A receptor activation inhibits T helper 1 and T helper 2 cell development and effector function. *FASEB J* 2008; 22:3491–9.
17. Romio M, Reinbeck B, Bongardt S, Hüls S, Burghoff S, Schrader J. Extracellular purine metabolism and signaling of CD73-derived adenosine in murine Treg and T_H17 cells. *Am J Physiol Cell Physiol* 2011; 301:C530–9.
18. Chalmin F, Mignot G, Bruchard M, et al. Stat3 and Gfi-1 transcription factors control Th17 cell immunosuppressive activity via the regulation of ectonucleotidase expression. *Immunity* 2012; 36:362–73.
19. de Cassan SC, Pathan AA, Sander CR, et al. Investigating the induction of vaccine-induced Th17 and regulatory T cells in healthy, *Mycobacterium bovis* BCG-immunized adults vaccinated with a new tuberculosis vaccine, MVA85A. *Clin Vaccine Immunol* 2010; 17:1066–73.
20. Griffiths KL, Pathan AA, Minassian AM, et al. Th1/Th17 cell induction and corresponding reduction in ATP consumption following vaccination with the novel *Mycobacterium tuberculosis* vaccine MVA85A. *PLoS One* 2011; 6:e23463.

21. Cibrián D, Sánchez-Madrid F. CD69: from activation marker to metabolic gatekeeper. *Eur J Immunol* **2017**; 47:946–53.
22. Shioh LR, Rosen DB, Brdicková N, et al. CD69 acts downstream of interferon- α/β to inhibit S1P1 and lymphocyte egress from lymphoid organs. *Nature* **2006**; 440:540–4.
23. Bankovich AJ, Shioh LR, Cyster JG. CD69 suppresses sphingosine 1-phosphate receptor-1 (S1P1) function through interaction with membrane helix 4. *J Biol Chem* **2010**; 285:22328–37.
24. Skon CN, Lee JY, Anderson KG, Masopust D, Hogquist KA, Jameson SC. Transcriptional downregulation of S1pr1 is required for the establishment of resident memory CD8⁺ T cells. *Nat Immunol* **2013**; 14:1285–93.
25. Mackay LK, Braun A, Macleod BL, et al. Cutting edge: CD69 interference with sphingosine-1-phosphate receptor function regulates peripheral T cell retention. *J Immunol* **2015**; 194:2059–63.
26. Lasunskaja E, Ribeiro SC, Manicheva O, et al. Emerging multidrug resistant *Mycobacterium tuberculosis* strains of the Beijing genotype circulating in Russia express a pattern of biological properties associated with enhanced virulence. *Microbes Infect* **2010**; 12:467–75.
27. Galkina E, Thatte J, Dabak V, Williams MB, Ley K, Braciale TJ. Preferential migration of effector CD8⁺ T cells into the interstitium of the normal lung. *J Clin Invest* **2005**; 115:3473–83.
28. Ribeiro SC, Gomes LL, Amaral EP, et al. *Mycobacterium tuberculosis* strains of the modern sublineage of the Beijing family are more likely to display increased virulence than strains of the ancient sublineage. *J Clin Microbiol* **2014**; 52:2615–24.
29. Francisco LM, Sage PT, Sharpe AH. The PD-1 pathway in tolerance and autoimmunity. *Immunol Rev* **2010**; 236:219–42.
30. Cushley MJ, Holgate ST. Adenosine-induced bronchoconstriction in asthma: role of mast cell-mediator release. *J Allergy Clin Immunol* **1985**; 75:272–8.
31. Ng WH, Polosa R, Church MK. Adenosine bronchoconstriction in asthma: investigations into its possible mechanism of action. *Br J Clin Pharmacol* **1990**; 30(Suppl 1):89S–98S.
32. Coli S, Mantovani F, Ferro J, Gonzi G, Zardini M, Ardissino D. Adenosine-induced severe bronchospasm in a patient without pulmonary disease. *Am J Emerg Med* **2012**; 30:2082 e3–5.
33. Keir ME, Butte MJ, Freeman GJ, Sharpe AH. PD-1 and its ligands in tolerance and immunity. *Annu Rev Immunol* **2008**; 26:677–704.
34. Sakai S, Kauffman KD, Sallin MA, et al. CD4 T cell-derived IFN- γ plays a minimal role in control of pulmonary *Mycobacterium tuberculosis* infection and must be actively repressed by PD-1 to prevent lethal disease. *PLoS Pathog* **2016**; 12:e1005667.
35. Cekic C, Linden J. Purinergic regulation of the immune system. *Nat Rev Immunol* **2016**; 16:177–92.
36. Bönner F, Borg N, Burghoff S, Schrader J. Resident cardiac immune cells and expression of the ectonucleotidase enzymes CD39 and CD73 after ischemic injury. *PLoS One* **2012**; 7:e34730.
37. Airas L, Jalkanen S. CD73 mediates adhesion of B cells to follicular dendritic cells. *Blood* **1996**; 88:1755–64.
38. Kansas GS, Wood GS, Tedder TF. Expression, distribution, and biochemistry of human CD39. Role in activation-associated homotypic adhesion of lymphocytes. *J Immunol* **1991**; 146:2235–44.
39. Pulte ED, Broekman MJ, Olson KE, et al. CD39/NTPDase-1 activity and expression in normal leukocytes. *Thromb Res* **2007**; 121:309–17.
40. Thomson LF, Ruedi JM, Glass A, et al. Production and characterization of monoclonal antibodies to the glycosyl phosphatidylinositol-anchored lymphocyte differentiation antigen ecto-5'-nucleotidase (CD73). *Tissue Antigens* **1990**; 35:9–19.
41. Myers AJ, Eilertson B, Fulton SA, Flynn JL, Canaday DH. The purinergic P2X7 receptor is not required for control of pulmonary *Mycobacterium tuberculosis* infection. *Infect Immun* **2005**; 73:3192–5.
42. Petit-Jentreau L, Jouvion G, Charles P, Majlessi L, Gicquel B, Tailleux L. Ecto-5'-nucleotidase (CD73) deficiency in *Mycobacterium tuberculosis*-infected mice enhances neutrophil recruitment. *Infect Immun* **2015**; 83:3666–74.
43. Cooper AM, Dalton DK, Stewart TA, Griffin JP, Russell DG, Orme IM. Disseminated tuberculosis in interferon gamma gene-disrupted mice. *J Exp Med* **1993**; 178:2243–7.
44. Flynn JL, Chan J, Triebold KJ, Dalton DK, Stewart TA, Bloom BR. An essential role for interferon gamma in resistance to *Mycobacterium tuberculosis* infection. *J Exp Med* **1993**; 178:2249–54.
45. Casadevall A, Pirofski LA. The damage-response framework of microbial pathogenesis. *Nat Rev Microbiol* **2003**; 1:17–24.
46. Medzhitov R, Schneider DS, Soares MP. Disease tolerance as a defense strategy. *Science* **2012**; 335:936–41.

APÊNDICE G – Human CD40 ligand deficiency dysregulates the macrophage transcriptome causing functional defects that are improved by exogenous IFN- γ .
Journal of Allergy and Clinical Immunology, 2017

Immune deficiencies, infection, and systemic immune disorders

Human CD40 ligand deficiency dysregulates the macrophage transcriptome causing functional defects that are improved by exogenous IFN- γ



Otavio Cabral-Marques, PhD,^{a,b} Rodrigo Nalio Ramos, PhD,^a Lena F. Schimke, MD,^{a,b} Taj Ali Khan, PhD,^{a,c} Eduardo Pinheiro Amaral, PhD,^a Caio César Barbosa Bomfim, MSc,^a Osvaldo Reis Junior, MSc,^d Tabata Takahashi França, MSc,^a Christina Arslanian, BSc,^a Joanna Darck Carola Correia Lima, MSc,^e Cristina Worm Weber, MD,^f Janaira Fernandes Ferreira, MD,^g Fabiola Scancetti Tavares, MD,^h Jing Sun, MD,ⁱ Maria Regina D'Imperio Lima, PhD,^a Marília Seelaender, PhD,^e Vera Lucia Garcia Calich, PhD,^a José Alexandre Marzagão Barbuto, MD, PhD,^{a,j} Beatriz Tavares Costa-Carvalho, MD, PhD,^k Gabriela Riemekasten, MD,^b Gisela Seminario, MD,^l Liliana Bezrodnik, MD,^l Luigi Notarangelo, MD,^m Troy R. Torgerson, MD, PhD,ⁿ Hans D. Ochs, MD,ⁿ and Antonio Condino-Neto, MD, PhD^a

São Paulo, Caxias do Sul, Fortaleza, and Brasília, Brazil; Lübeck, Germany; Kohat, Pakistan; Cincinnati, Ohio; Buenos Aires, Argentina; Boston, Mass; and Seattle, Wash

Background: CD40 ligand (CD40L) deficiency predisposes to opportunistic infections, including those caused by fungi and intracellular bacteria. Studies of CD40L-deficient patients reveal the critical role of CD40L-CD40 interaction for the function of T, B, and dendritic cells. However, the consequences of CD40L deficiency on macrophage function remain to be investigated. **Objectives:** We sought to determine the effect of CD40L absence on monocyte-derived macrophage responses. **Methods:** After observing the improvement of refractory disseminated mycobacterial infection in a CD40L-deficient patient by recombinant human IFN- γ (rhIFN- γ) adjuvant therapy, we investigated macrophage functions from CD40L-deficient patients. We analyzed the killing activity, oxidative burst, cytokine production, and *in vitro* effects of rhIFN- γ and soluble CD40 ligand (sCD40L) treatment on macrophages. In addition, the effect of CD40L absence on the macrophage transcriptome before and after rhIFN- γ treatment was studied. **Results:** Macrophages from CD40L-deficient patients exhibited defective fungicidal activity and reduced oxidative burst, both of

which improved in the presence of rhIFN- γ but not sCD40L. In contrast, rhIFN- γ and sCD40L ameliorate impaired production of inflammatory cytokines. Furthermore, rhIFN- γ reversed defective control of *Mycobacterium tuberculosis* proliferation by patients' macrophages. The absence of CD40L dysregulated the macrophage transcriptome, which was improved by rhIFN- γ . Additionally, rhIFN- γ increased expression levels of pattern recognition receptors, such as Toll-like receptors 1 and 2, dectin 1, and dendritic cell-specific intercellular adhesion molecule 3-grabbing nonintegrin in macrophages from both control subjects and patients.

Conclusion: Absence of CD40L impairs macrophage development and function. In addition, the improvement of macrophage immune responses by IFN- γ suggests this cytokine as a potential therapeutic option for patients with CD40L deficiency. (J Allergy Clin Immunol 2017;139:900-12.)

Key words: Macrophages, CD40 ligand, opportunistic infections, IFN- γ

From ^athe Department of Immunology, Institute of Biomedical Sciences, University of São Paulo; ^bthe Department of Rheumatology, University Lübeck; ^cthe Department of Microbiology, Kohat University of Science and Technology; ^dthe Central Laboratory of High Performance Technologies (LaCTAD), State University of Campinas, São Paulo; ^ethe Cancer Metabolism Research Group, Institute of Biomedical Sciences, University of São Paulo; ^fPediatric Allergy & Immunology Clinic, Caxias do Sul; ^gAlbert Sabin Hospital, Fortaleza; ^hthe Pediatric Immunology Clinic, Unit of Pediatrics, Hospital de Base do Distrito Federal Brasília, Brasília; ⁱthe University of Cincinnati College of Medicine; ^jthe Cell and Molecular Therapy Center, NETCEM, University of São Paulo; ^kthe Division of Allergy-Immunology and Rheumatology, Department of Pediatrics, Federal University of São Paulo; ^lDr Ricardo Gutierrez Children's Hospital, Immunology, Buenos Aires; ^mthe Division of Immunology, Boston Children's Hospital, Harvard Medical School, Boston; and ⁿthe Department of Pediatrics, University of Washington School of Medicine, and Seattle Children's Research Institute.

Supported by Fundação de Amparo à Pesquisa do Estado de São Paulo (grant 2012/50515-4 to O.C.-M. and grant 2012/51745-3 to A.C.-N.) and the Jeffrey Modell Foundation.

Disclosure of potential conflict of interest: C. C. Barbosa Bomfim receives payment for lectures from the São Paulo Research Foundation and travel support from São Paulo Research Foundation. M. Seelaender receives grant support from FAPESP and University Sorbonne Paris Cité-University of São Paulo and serves as a consultant from Metabolic Foods Brazil. J. A. Marzagão Barbuto receives grant support from

FAPESP and serves as a consultant for Recepta Biopharma. L. Notarangelo serves on the board for Novimmune, is an employee of Children's Hospital Pediatric Associates, receives grant support from the National Institutes of Health (NIH), and receives royalties from UpToDate. T. R. Torgerson serves as a consultant for Baxalta Biosciences, CSL Behring, and ADMA; receives grant support from Baxalta Biosciences, CSL Behring, and the NIH; and receives payments for lectures from Baxalta Biosciences, CSL Behring, Questor Pharmaceuticals, and RWJF. H. D. Ochs receives grant support from the Jeffrey Modell Foundation. The rest of the authors declare that they have no relevant conflicts of interest.

Received for publication February 6, 2016; revised June 15, 2016; accepted for publication July 12, 2016.

Available online August 20, 2016.

Corresponding author: Antonio Condino-Neto, MD, PhD, Department of Immunology—Institute of Biomedical Sciences, University of São Paulo, 1730 Lineu Prestes Ave, São Paulo, SP 05508-000, Brazil. E-mail: condino@icb.usp.br. Or: antonioccondino@gmail.com.

The CrossMark symbol notifies online readers when updates have been made to the article such as errata or minor corrections

0091-6749/\$36.00
© 2016 American Academy of Allergy, Asthma & Immunology
<http://dx.doi.org/10.1016/j.jaci.2016.07.018>

Abbreviations used

CD40L: CD40 ligand
CFU: Colony-forming units
CGD: Chronic granulomatous disease
CLR: C-type lectin receptor
DC: Dendritic cell
DEG: Differentially expressed gene
G-CSF: Granulocyte colony-stimulating factor
GO: Gene Ontology
IP-10: IFN- γ -induced protein 10
M-CSF: Macrophage colony-stimulating factor
MDM: Monocyte-derived macrophage
PMA: Phorbol 12-myristate 13-acetate
PRR: Pattern recognition receptor
rhIFN- γ : Recombinant human IFN- γ
sCD40L: Soluble CD40 ligand
TLR: Toll-like receptor

The CD40 ligand (CD40L)–CD40 interaction was initially described to play an essential role during membrane-membrane interactions between activated CD4⁺ T lymphocytes and B cells,^{1–5} as well as between CD4⁺ T cells and antigen-presenting cells.^{6,7} However, further studies showed that soluble CD40 ligand (sCD40L) produced by T cells and platelets^{8–11} can also exert an important role in immune system regulation, including myeloid progenitor cell development. Bone marrow stromal cells, hematopoietic progenitors, and myeloid progenitors express CD40. Furthermore, the CD40L–CD40 interaction has been shown to influence differentiation of these cells directly and indirectly through regulation of cell proliferation and maturation or through control of the cytokine milieu in the bone marrow, respectively.^{10,12–14}

Macrophages are essential myeloid cells, exhibiting microbicidal activity and regulating inflammatory immune responses. Thus macrophages comprise a pivotal component of the innate immune system. Macrophages express CD40 constitutively,^{15,16} but their functional capability in patients with CD40L deficiency has not been investigated.

Patients with X-linked hyper-IgM syndrome caused by mutations in the gene encoding CD40L (*CD40LG*) have a broad spectrum of opportunistic infections caused by intracellular bacteria and fungi. These infections resemble infections seen in patients with abnormal myeloid cells, such as those in patients with chronic granulomatous disease (CGD).^{17–19} Although CD40L-deficient patients can experience intermittent neutropenia, they are also susceptible to fatal opportunistic infections, even when neutrophil counts are normal or when receiving granulocyte colony-stimulating factor (G-CSF) and immunoglobulin replacement therapy.^{20,21} These observations indicate that absence of CD40L might impair macrophage function in human subjects and that new therapeutic approaches need to be investigated for optimal treatment of these patients.

Failure to produce IFN- γ has been reported in patients with CD40L deficiency.^{22–24} This cytokine primes and activates mature phagocytes. Additionally, IFN- γ affects development of progenitor cells to generate mature phagocytes capable of efficiently eliminating opportunistic pathogens.²⁵ For this reason, recombinant human IFN- γ (rhIFN- γ) has been used as an adjunctive therapy for

patients with CGD^{26,27} and patients with defects in the IL-12/IFN- γ axis to prevent and treat invasive mycobacterial or fungal infections. However, IFN- γ has not been broadly used to treat patients with adaptive primary immunodeficiency disorders.^{28–31}

Here we aimed to analyze the *in vitro* macrophage response in patients with CD40L deficiency with respect to macrophage killing activity, oxidative burst, and production of inflammatory cytokines. Furthermore, we investigated the effects of rhIFN- γ and sCD40L treatment on macrophages from CD40L-deficient patients. In addition, we assessed the effect of CD40L deficiency on the macrophage transcriptome before and after rhIFN- γ treatment.

METHODS**Case report**

An Argentinian CD40L-deficient patient included in our collaborative Latin American Society for Immunodeficiencies (LASID) studies¹⁸ was treated with adjuvant rhIFN- γ at the Dr Ricardo Gutierrez Children's Hospital. The hospital is in Argentina, where rhIFN- γ (Imukin; Boehringer Ingelheim, Ridgefield, Conn) is already approved for clinical use (Disposicion no. 1265-12). The patient was born to nonconsanguineous family and received BCG vaccine in the first month of life without complication. At 9 months of age, he was given a diagnosis of dysgammaglobulinemia (hyper-IgM syndrome), chronic neutropenia, and pneumonia caused by *Pseudomonas* species. Conventional treatment for CD40L deficiency (trimethoprim/sulfamethoxazole prophylaxis, intravenous immunoglobulin, and Granulokine) was initiated, and the patient was given a diagnosis of the mutation Q174X in *CD40LG* (details have been previously reported¹⁸). At 5 years of age, he had cervical adenomegaly caused by mycobacterial disease. The extent and severity of this mycobacterial infection were assessed by means of biopsy, which showed granulomas. Additionally, the PCR result was positive for *M tuberculosis* complex.

Conventional antituberculosis therapy with a 4-drug regimen (ethambutol, levofloxacin, isoniazid, and rifampicin) was initiated, but the patient had typhilitis requiring surgery. Abundant caseating granulomas were observed in the bowel mucous membrane, requiring colostomy for 6 months, and the patient continued to have refractory mycobacterial disease despite antituberculosis treatment. Therefore simultaneous with the conventional CD40L deficiency and antituberculosis therapy, subcutaneous rhIFN- γ (50 μ g/m² administered 3 times a week) was administered for 6 months. Under this therapeutic regimen, the patient improved clinically. After that, rhIFN- γ therapy was discontinued and isoniazid and rifampicin was continued for 1 additional year until no symptoms of mycobacterial disease were observed. Currently, the patient is 9 years old, has no stem cell donor available, and has had hepatic cryptococcosis.

Subjects

We enrolled 6 CD40L-deficient patients (age range, 3–21 years) from 6 unrelated Brazilian families. Except for the occurrence of *M tuberculosis* infection in P1, the clinical, immunologic, and genetic characteristics of these patients have been previously described¹⁸ and are summarized in Table E1 in this article's Online Repository at www.jacionline.org. For each experiment, a healthy subject (age range, 23–30 years) was included for comparison. Informed consent was obtained from the patients or their parents and from healthy control subjects. The blood was collected under institutional guidelines, and the study was performed in accordance with the Declaration of Helsinki and approved by the Ethics Committee of the Institute of Biomedical Sciences, University of São Paulo.

Generation of monocyte-derived macrophages

Human monocyte-derived macrophages (MDMs) were obtained, as previously described, with minor modifications.³² In summary, CD14⁺ monocytes were obtained from PBMCs by using the Monocyte Isolation Kit II (Miltenyi Biotec, Bergisch Gladbach, Germany), according to the manufacturer's instructions. Monocytes were cultured in RPMI 1640 containing 10% FBS at

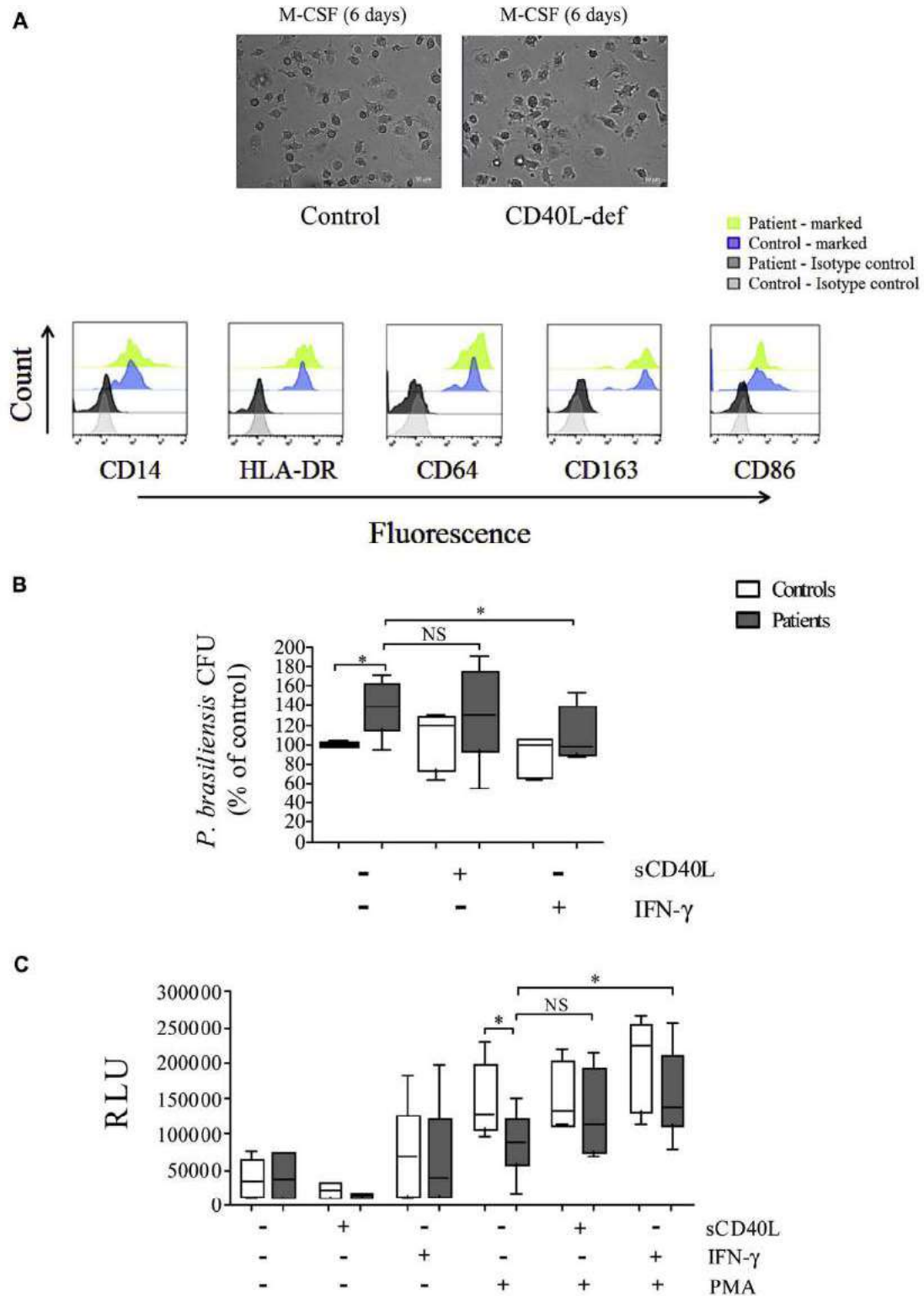


FIG 1. rhIFN- γ , but not sCD40L, improves the defective fungicidal activity and oxidative burst of MDMs from CD40L-deficient patients. **A**, Cell morphology (top) was assessed by means of phase contrast (Axio Vert.A1) after 5 days in the presence of M-CSF. Flow cytometric analysis (bottom) was used to characterize expression of CD14, HLA-DR, CD64, CD163, and CD86 on the surfaces of MDMs. **B**, After challenging MDMs with *P. brasiliensis*, fungicidal activity was assessed by determining CFU values. Before assay, MDMs were untreated (-) or treated with (+) sCD40L (500 ng/mL) or rhIFN- γ (100 U/mL) for 48 hours. CFU values (as percentages of control values) were determined in relation to the CFU number of untreated MDMs from healthy control subjects. The results in scatter plots and raw data in CFU per milliliter are shown in Fig E2. **C**, MDMs remained untreated or were cultured for 48 hours in the presence of sCD40L (500 ng/mL) or rhIFN- γ (100 U/mL); the respiratory burst of MDMs was induced by PMA (90 mmol/L). Cells were analyzed with the luminol-enhanced chemiluminescence assay, and values are expressed as relative light units (RLU). A significant difference is denoted as follows: * $P \leq .05$ (n = 6 patients and 6 control subjects), Mann-Whitney test. NS, Not significant.

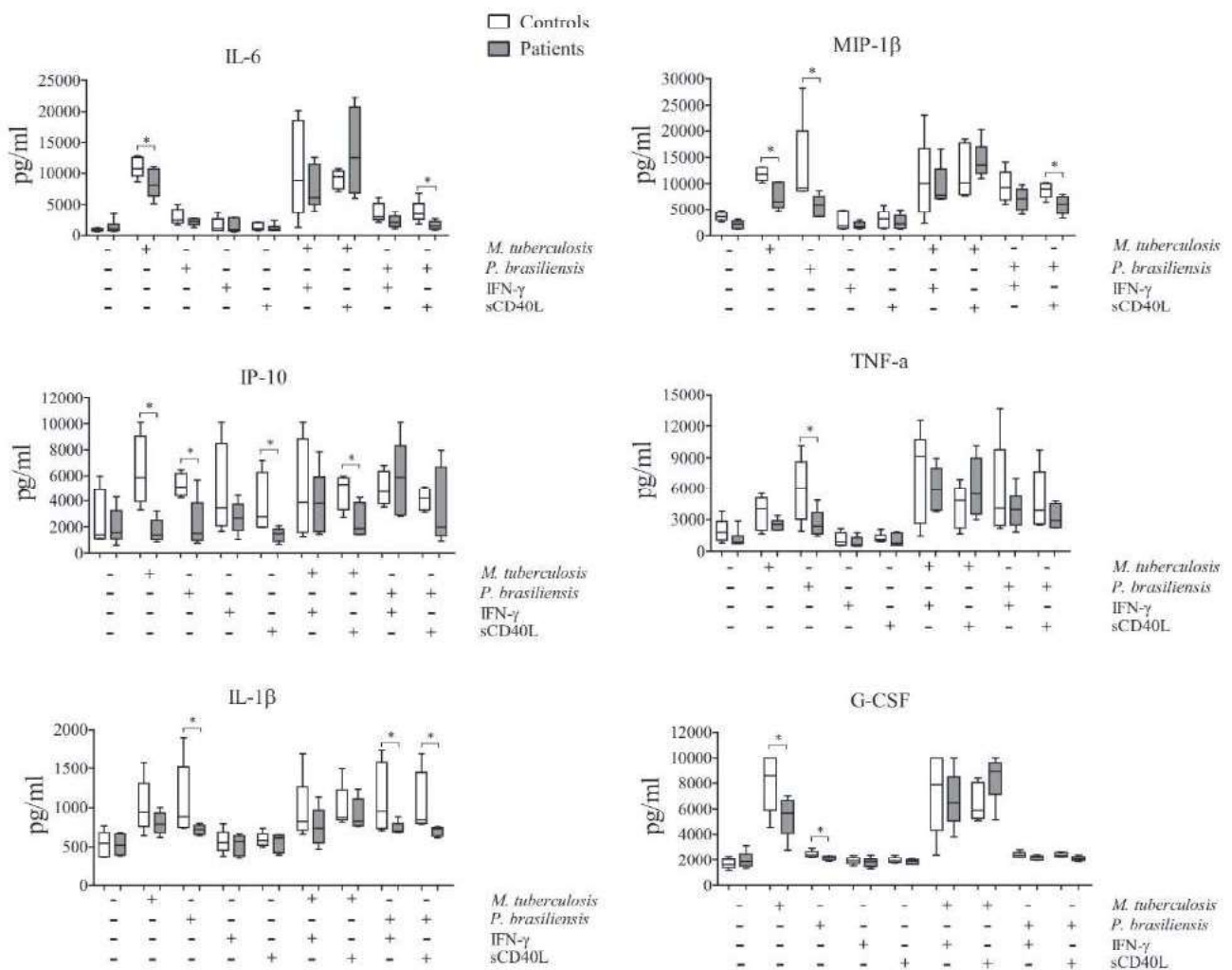


FIG 2. Impaired cytokine production by macrophages from CD40L-deficient patients. Patients' macrophages secrete abnormal levels of IL-6, TNF- α , IL-1 β , macrophage inflammatory protein 1 β [MIP-1 β], IP-10, and G-CSF in response to *M tuberculosis* and *P brasiliensis*. After 48 hours of sCD40L (500 ng/mL) or rhIFN- γ (100 U/mL) treatment, cytokine production by patients' macrophages achieved a pattern similar to that observed in healthy control subjects. Significant differences are denoted as follows: * $P \leq .05$ (n = 6 patients and 6 control subjects), Mann-Whitney test.

37°C in a humidified 5% CO₂ atmosphere for 5 days in the presence of 50 ng/mL macrophage colony-stimulating factor (M-CSF; PeproTech, Princeton, NJ). Afterward, the cells underwent phenotypic characterization, including analysis of HLA-DR, CD14, CD40, CD64, CD86, CD80, and CD163. They were also characterized for the following pattern recognition receptors (PRRs): Toll-like receptors (TLRs; TLR1, TLR2, and TLR4) and C-type lectin receptors (CLRs; dectin-1, dectin-3, mannose receptor, CD206, and dendritic cell-specific intercellular adhesion molecule 3-grabbing nonintegrin [DC-SIGN]). Phenotypic expression was analyzed by using flow cytometry (BD FACSCanto II Cytometer). The data obtained were analyzed with FlowJo software (TreeStar, Ashland, Ore). When indicated, MDMs were incubated for 2 more days in the presence of 100 U/mL rhIFN- γ (Immukine, Boehringer Ingelheim), 20 ng/mL IL-4 (PeproTech), or 500 ng/mL sCD40L (Life Technologies, Frederick, Md).

Fungicidal activity

MDMs were challenged with *Paracoccidioides brasiliensis* (Pb18, a highly virulent isolate), and the microbicidal activity was determined by counting colony-forming units (CFU), as previously described.³³ Briefly, 0.2×10^5 MDMs were cultured in 200 μ L of RPMI 1640 in 96-well flat-bottom plates and challenged with *P brasiliensis* (ratio 1:10, fungus/MDMs) for 48 hours,

Five days after seeding and challenging, *P brasiliensis* CFU were counted, and CFU values (percentage of control values) were determined in relation to the CFU numbers of untreated MDMs from healthy control subjects.

Analysis of respiratory burst by means of chemiluminescence

MDM oxidative burst was measured by using luminol-dependent chemiluminescence, as previously described.³⁴ Luminol (1 mmol/L; Sigma Laboratories, St Louis, Mo)-preloaded MDMs ($0.2 \times 10^5/300 \mu$ L) were activated with phorbol 12-myristate 13-acetate (PMA; 90 nmol/L, Sigma Laboratories), and chemiluminescence was monitored for 2 hours with a microplate luminometer reader (EG&G Berthold LB96V, Bad Wildbad, Germany). Results were expressed as relative light units.

Analysis of cytokine production

Supernatants of macrophages treated or untreated with rhIFN- γ or sCD40L were harvested 48 hours after *P brasiliensis* or *M tuberculosis* (lysate)³⁵ incubation. Cytokine levels were evaluated by using a HCYTMAG-60K-PK30 Cytokine Kit (Millipore, Bedford, Mass), and data obtained were analyzed with a Luminex instrument, according to the manufacturer's instructions.

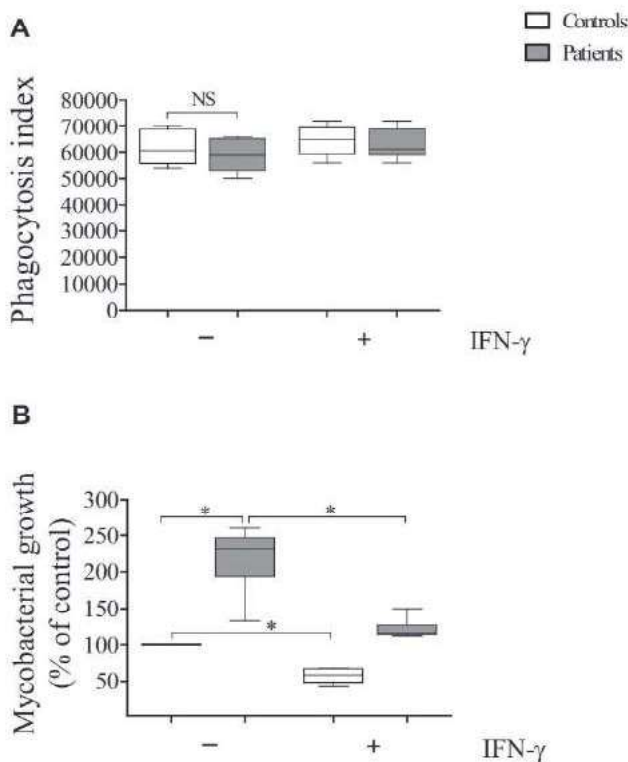


FIG 3. Defective control of the proliferation of *M tuberculosis* by MDMs from CD40L-deficient patients is improved by rhIFN- γ . **A**, Macrophages were challenged with *M tuberculosis* (H37Rv strain), and the phagocytosis index was determined on day 0 based on CFU counts. **B**, The bacterial proliferation index on day 6 was determined based on the ratio of CFU numbers on day 6 to CFU numbers on day 0. Data were normalized according to the average mycobacterial growth of untreated MDMs from healthy control subjects. Significant differences are denoted as follows: * $P \leq .05$ (n = 6 patients and 6 control subjects), Mann-Whitney test. NS, Not significant.

Phagocytosis and control of *M tuberculosis* proliferation by MDMs

Analyses of *M tuberculosis* (H37Rv strain) phagocytosis and proliferation control by MDMs were carried out, as previously described.³⁶ In brief, MDMs were challenged at a 1:1 ratio (*M tuberculosis*/MDMs) for 3 hours (day 0) and washed to remove extracellular mycobacteria. On day 0 and 6 days later, the MDMs were lysed with 0.1% saponin treatment, and the homogenates were diluted and plated in Middlebrook 7H10 medium supplemented with 10% OADC (Difco; acid/albumin/dextrose/catalase). The resultant colonies were assessed after 21 days of incubation at 37°C. *M tuberculosis* uptake (phagocytosis index) data were obtained from CFU counts performed on day 0, and the *M tuberculosis* growth index was determined based on the ratio of CFU numbers on day 6 to CFU numbers on day 0.

In addition to MDMs, to gain evidence about the role of CD40L-CD40 interaction in myeloid cell development, we analyzed the ability of the promyelocytic HL-60 cell line to control *M tuberculosis* proliferation by challenging the cells at a 1:1 ratio (*M tuberculosis*/HL-60 cells). HL-60 cells were only challenged for 3 hours because of rapid HL-60 proliferation. After this, HL-60 cells were lysed, and *M tuberculosis* proliferation was assessed based on CFU values, as performed for MDMs.

RNA sequencing and data processing

Macrophage transcriptome profiles from 3 CD40L-deficient patients and 3 healthy control subjects were analyzed, as previously described.^{32,37} Total RNA was obtained by using TRIzol (Invitrogen, Carlsbad, Calif), according to the manufacturer's instructions. RNA integrity and concentration were

assessed by using the Agilent 2100 Bioanalyser RNA Nano chip (Agilent Technologies, Santa Clara, Calif) and orthogonally validated by means of visualization of the integrity of the 28S and 18S band on an agarose gel. cDNA libraries were obtained with the Illumina CBot station and HiScanSQ using the Illumina TruSeq RNA Sample Preparation Kit (Illumina, San Diego, Calif), according to the manufacturer's instructions. Sequencing was carried out with the Illumina HiSeq 2000 paired-end 100-bp (PE 100) system.

Bioinformatic analysis

After quality assessment with FastQC (www.bioinformatics.babraham.ac.uk/projects/fastqc/), reads were aligned with the human cDNA transcriptome from Ensembl 82 by using Kallisto.³⁸ Data were further processed by using Sleuth (pachterlab.github.io/sleuth/), and the read values were expressed as transcripts per million. The transcripts with more than 5 reads in each sample for at least 47% of the sample and false discovery rate-adjusted P values (or q values) of less than .05 were considered differentially expressed genes (DEGs). Hierarchical clustering analysis was performed with Perseus (MaxQuant, v1.11, Martinsried, Germany). Gene Ontology (GO) functional enrichment analysis was performed with STRING³⁹ and DAVID^{40,41} to categorize and group DEGs based on a known functional association, as defined by the Gene Ontology Consortium.⁴² GeneMANIA/Cytoscape⁴³ was used to predict interactions between DEGs by using GO biological process and source organism *Homo sapiens* as additional parameters.

Statistical analysis

Statistical significance was assessed by using the nonparametric Mann-Whitney test. Data were expressed as medians and 25th and 75th percentiles. Statistical analyses were performed with GraphPad Prism 4.03 software (GraphPad Software, San Diego, Calif), and P values of .05 or less were considered significant.

RESULTS

MDMs from CD40L-deficient patients have defective fungicidal activity and oxidative burst that are reversed by rhIFN- γ but not sCD40L

Based on the morphologic characteristics and expression patterns of the CD14, HLA-DR, CD64, CD163, and CD86 molecules, a homogeneous population of MDMs from CD40L-deficient patients and healthy control subjects was successfully generated (Fig 1, A). When challenged with *P brasiliensis*, macrophages from patients demonstrated reduced fungicidal activity compared with those from healthy control subjects (Fig 1, B, and see Fig E1 in this article's Online Repository at www.jacionline.org). Although sCD40L treatment did not significantly increase the killing activity of macrophages from CD40L-deficient patients, rhIFN- γ improved the fungicidal activity of macrophages from patients. This finding is consistent with IFN- γ 's established beneficial therapeutic effect for patients with opportunistic infections and its well-known role as a phagocyte activator.

Considering the essential role of the oxidative burst during macrophages killing activity,⁴⁴ we evaluated the production of reactive oxygen species by PMA-activated MDMs from CD40L-deficient patients. Patients' macrophages did not trigger the oxidative burst after activation in comparison with those from healthy subjects (Fig 1, C). Although sCD40L showed a slight increase in macrophage responses, no significant enhancement was achieved. However, rhIFN- γ statistically enhanced the oxidative burst of macrophages in both patients and control subjects. After rhIFN- γ treatment, patients' MDMs displayed no significant difference compared with untreated or rhIFN- γ -treated MDMs from healthy control subjects.

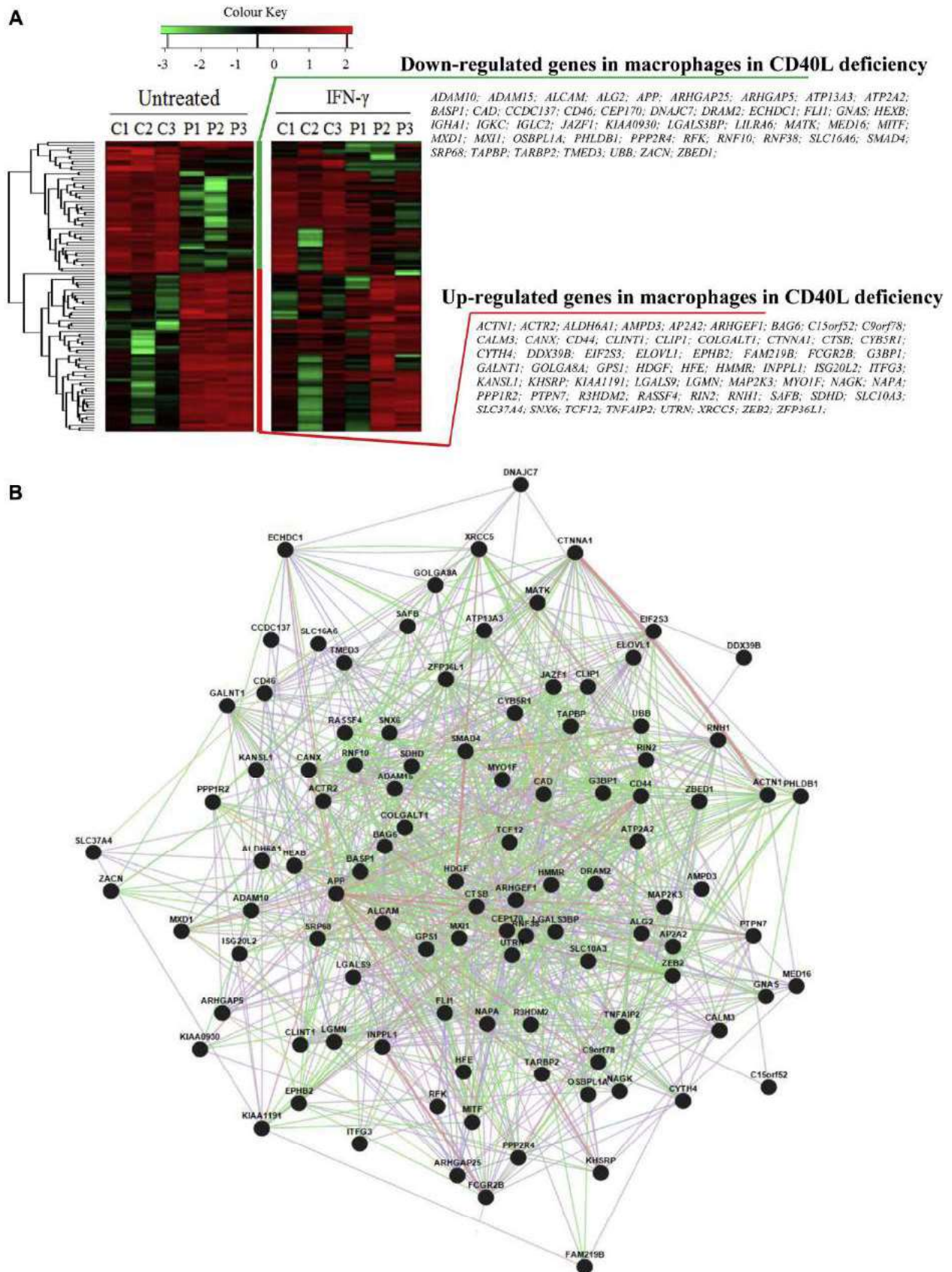


FIG 4. Hierarchical cluster analysis showing MDM gene signature in patients with CD40L deficiency and the subsequent effects of IFN- γ . **A**, RNA from MDMs was sequenced, and the transcripts per million (TPM) values are represented on a log₂ scale, where green shows low expression and red shows high expression. The results of untreated (left panel) and rIFN- γ -treated (right panel) cells are shown in the heat map. **B**, Interaction networks for the DEGs in CD40L deficiency are shown. Networks are shown as predicted by GeneMania and visualized with Cytoscape.

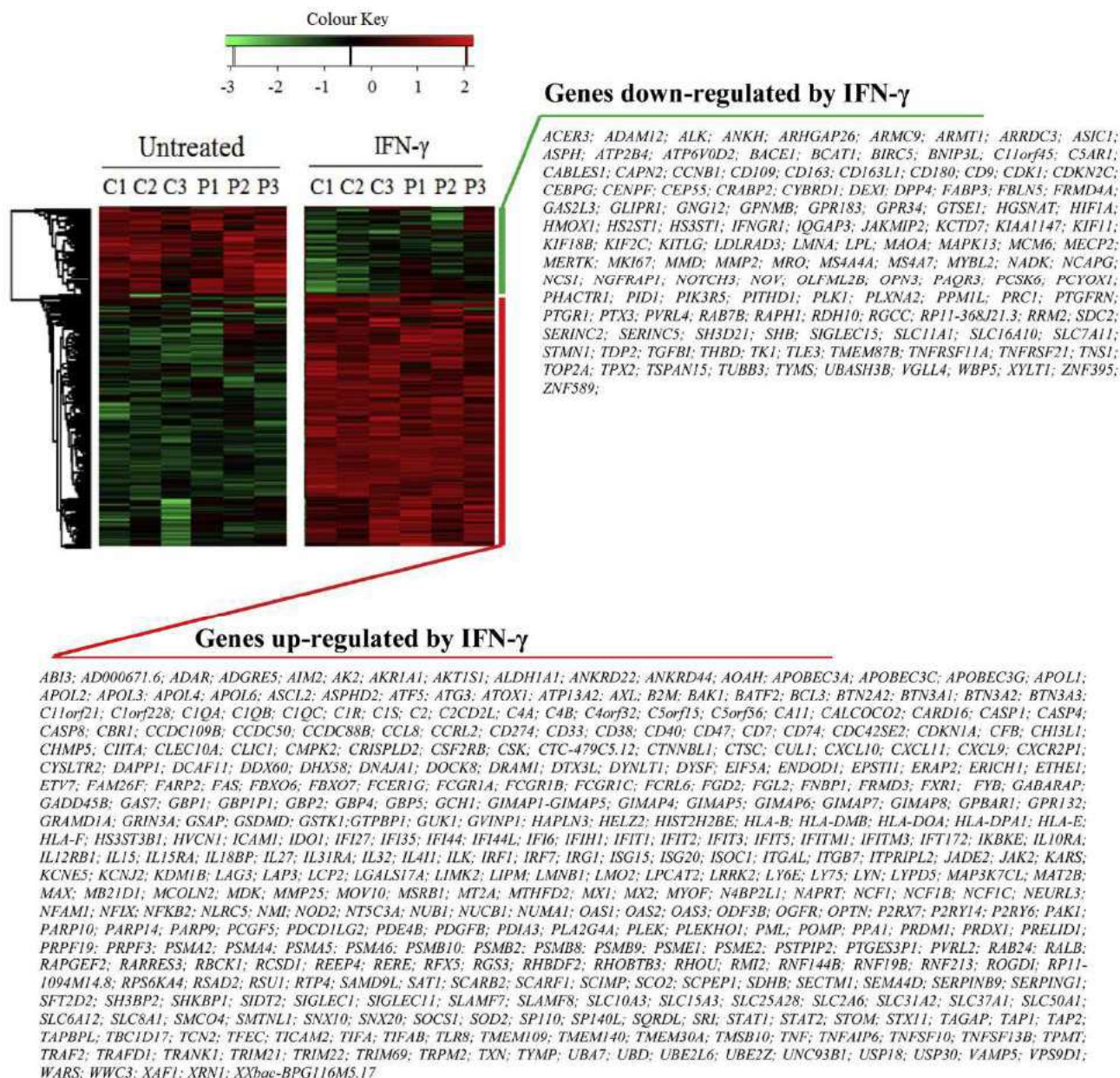


FIG 5. Heat map of genes not dysregulated in patients with CD40L deficiency but affected by rhIFN- γ treatment. Results for untreated and rhIFN- γ -treated cells are shown in the heat map. RNA from MDMs were sequenced, and the transcripts per million (TPM) values are represented on a log₂ scale, where green shows low expression and red shows high expression. Genes significantly upregulated or downregulated are listed.

Defective production of inflammatory cytokines by macrophages from CD40L-deficient patients is reversed by rhIFN- γ and sCD40L

In addition to responding to invading pathogens by inducing microbicidal activity, macrophages produce inflammatory cytokines in response to CD40L-CD40 interaction.⁴² Therefore we analyzed inflammatory cytokines released by MDMs from patients or control subjects treated or untreated with rhIFN- γ or sCD40L in response to *P brasiliensis*. In addition, considering the increased susceptibility to mycobacterial diseases reported in patients with CD40L deficiency,^{18,20,45} we also challenged the macrophages with *M tuberculosis*. After 48 hours of culture in the presence of *P brasiliensis* or *M tuberculosis*, macrophages

from CD40L-deficient patients had significantly impaired production of IL-6, TNF- α , IL-1 β , macrophage inflammatory protein 1 β , IFN- γ -induced protein 10 (IP-10), and granulocyte-colony stimulating factor (G-CSF) compared with those of healthy control subjects (Fig 2). With few exceptions, the impaired cytokine production in CD40L-deficient patients was significantly improved by both rhIFN- γ and sCD40L.

Impaired control of *M tuberculosis* proliferation by macrophages from CD40L-deficient patients is reversed by rhIFN- γ

Considering the essential role of IFN- γ in the response to mycobacteria⁴⁶ and the increased susceptibility to mycobacteria

TABLE I. Biological process dysregulated in patients with CD40L deficiency

GO term	GO category	Dysregulated genes in patients with CD40L deficiency	Genes not affected by the CD40L deficiency but modulated by rhIFN- γ treatment
GO:0002376	Immune system process	<i>ACTR2, ADAM10, ADAM15, AP2A2, APP, BAG6, CANX, CD44, CD46, CTSB, FCGR2B, FLI1, IGLL5, INPPL1, LGMN, LILRA6, MAP2K3, MATK, MITF, MYO1F, OSBPL1A, PPP2R4, TCF12, UBB, ZFP36L1</i>	<i>AOAH, APOBEC3G, APOL1, APOL2, APOL3, BCL3, BNIP3L, C1QA, C1QB, C1QC, CIR, C1S, C2, C4A, C4B, CSAR1, CALCOCO2, CCL8, CD163, CD180, CD40, CD74, CEBPG, CFB, CIITA, CLIC1, CXCL10, CXCL11, CXCL9, DHX58, FCGR1A, FCGR1C, GCH1, HIF1A, HIST2H2BE, HLA-B, HMOX1, IDO1, IFIH1, IL15, IL27, IL31RA, IL32, IRF7, ITGAL, LY75, LYN, MMP25, MX1, MX2, NCF1, NCF1C, NFAM1, NMI, NOD2, P2RX7, PRDX1, PTX3, RSAD2, SERPING1, SIGLEC1, SLAMF7, SLC11A1, TAP1, TAP2, TICAM2, TLR8, TNF, TNFAIP6</i>
GO:0048002	Antigen processing and presentation of peptide antigen	<i>AP2A2, CANX, HFE, IGLL5, LGMN, OSBPL1A, UBB</i>	<i>B2M, CD74, ERAP2, FCER1G, HLA-B, HLA-DMB, HLA-DOA, HLA-DPA1, HLA-E, HLA-F, ICAM1, PSMB8, PSMB9, PSME1, SLC11A1, TAP2, TAPBP</i>
GO:0045087	Innate immune response	<i>ACTR2, ADAM15, APP, CD44, CD46, CTSB, IGLL5, LGMN, MAP2K3, MATK, UBB, XRCC5</i>	<i>APOBEC3G, APOL1, C1QA, C1QB, C1QC, CIR, C1S, C2, C4A, C4B, CALCOCO2, CD180, CEBPG, CFB, CIITA, DHX58, FCGR1A, FCGR1C, GCH1, IFIH1, IL27, NCF1, NCF1C, NOD2, PRDX1, SERPING1, SLAMF7, SLC11A1, TICAM2, TLR8</i>
GO:0080134	Regulation of response to stress	<i>AP2A2, CD44, CD46, CTSB, DDX39B, DNAJC7, LGMN, MAP2K, MYO1F, TARBP2, UBB, XRCC5, ZEB2</i>	—
GO:0007259	JAK-STAT cascade	—	<i>IL31RA, JAK2, NMI, SOCS1, STAT1, STAT2</i>
GO:0055114	Oxidation reduction process	<i>ALDH6A1, CYB5R1, GNAS, KIAA1191, PPP1R2, UBB</i>	
GO:0006897	Endocytosis	<i>ACTR2, AP2A2, APP, CLINT1, IGLL5, INPPL1, RIN2, SNX6</i>	<i>CDC42SE2, CLEC10A, FCER1G, FCGR1A, FCGR1C, FNBP1, LY75, MERTK, P2RX7, PTX3, SCARF1, SLC11A1</i>
GO:0030335	Positive regulation of cell migration	<i>ADAM10, ARHGAP5, MYO1F</i>	<i>CXCL10, HIF1A, ICAM1, ILK, JAK2, PDGFB</i>
GO:0007264	Small GTPase-mediated signal transduction	<i>ACTR2, ARHGAP25, ARHGEF1, CLIP1, CTNNA1, G3BP1, PPP2R4, RIN2</i>	<i>FARP2, HMOX1, IQGAP3, LRRK2, MAPK13, RAB24, RAB7B, RALB, RAPGEF2, RHOA, RSU1</i>
GO:0016192	Vesicle-mediated transport	<i>ACTN1, ACTR2, APP, CLINT1, IGLL, INPPL1, MYO1F, OSBPL1A, RIN2, SNX6, TAPBP</i>	<i>CCL8, CDC42SE2, CHMP5, CLEC10A, FCER1G, FCGR1A, FCGR1C, FNBP1, LY75, LYN, MERTK, OPTN, P2RX7, PLEK, PTX3, RHOBTB3, SCARF1, SLC11A1, STX11, VAMP5</i>
GO:0007599	Hemostasis	<i>ACTN1, APP, ATP2A2, CD44, FLI1, GNAS, PPP2R4</i>	<i>CD40, CD9, FBLN5, PLEK, SERPING1, THBD</i>
GO:0010628	Positive regulation of gene expression	<i>APP, DDX39B, FLI1, HEXB, MAP2K3, MED16, SAFB, UBB</i>	<i>BCL3, CIITA, HIF1A, IL31RA, IRF1, PRDM1, SLC11A1, TNF, TNFSF13B</i>
GO:0045892	Negative regulation of transcription, DNA templated	<i>BASP1, HDGF, JAZF1, MITF, MXD1, MXI1, SMAD4, SNX6, UBB, XRCC5</i>	<i>CIITA, IRF7, MECP2, PRDM1, RFX5, TNF</i>
GO:0030154	Cell differentiation	<i>ACTR2, ADAM10, ADAM15, ALDH6A1, AP2A2, APP, ARHGEF1, BAG6, BASP1, CD74, CTSB, EPHB2, FLI1, GIMAP5, HEXB, HIF1A, ILK, JAK2, KITLG, LPL, LYN, MATK, NAPA, PRPF19, SEMA4D, SMAD4, TCF12, TNFAIP2, UBB, XRCC5, ZEB2, ZFP36L1</i>	<i>CD46, CD74, CTNNA1, EPHB2, GIMAP5, GNAS, HIF1A, ILK, JAK2, KITLG, LPL, LYN, PRPF19, SEMA4D, TCF12, XRCC5</i>
GO:0002521	Leukocyte differentiation	<i>ZFP36L1</i>	<i>BAK1, BCL3, CASP8, CD74, CEBPG, FASL, GIMAP5, GPR183, IL15, IL31RA, IRF1, NFAM1, TNF</i>
GO:0030099	Myeloid cell differentiation	<i>FLI1, GNAS, MITF</i>	<i>CASP8, CEBPG, GIMAP5, IL31RA, JAK2, LYN, PML, TNF</i>

(Continued)

TABLE I. (Continued)

GO term	GO category	Dysregulated genes in patients with CD40L deficiency	Genes not affected by the CD40L deficiency but modulated by rhIFN- γ treatment
GO:0010608	Posttranscriptional regulation of gene expression	<i>APP</i>	<i>BCL3, EIF5A, FBXO7, MOV10, PML, SLC11A1, TNF</i>
GO:0006417	Regulation of translation	<i>APP, TARBP2, ZFP36L1</i>	<i>BCL3, EIF5A, PML, TNF</i>
GO:0031401	Positive regulation of protein modification process	<i>CD44, HDGF, HFE, PPP2R4, UBB, ZEB2</i>	<i>CCNB1, CDK1, CUL1, IL31RA, JAK2, KITLG, LRRK2, LYN, NOD2, P2RX7, PLK1, PML, PSMA2, PSMA4, PSMA5, PSME2, PSMA6, PSMB10, PSMB2, PSMB8, PSMB9, PSME1, TNF</i>
GO:0045859	Regulation of protein kinase activity	<i>APP, GPS1, HDGF, SNX6, TARBP2, UBB, ZEB2</i>	<i>AKT1S1, C5AR1, CD74, CDKN1A, CDKN2C, GADD45B, ILK, JAK2, KITLG, P2RX7, PAK1, PDGFB, RGS3, SLC11A1, TNF, TRAF2</i>

in patients with CD40L deficiency,^{18,20,45} we asked whether macrophages from CD40L-deficient patients have normal capacity to control the growth of *M tuberculosis*. Macrophages from CD40L-deficient patients phagocytosed *M tuberculosis* normally compared with macrophages from healthy control subjects (Fig 3, A) but did not control the intracellular proliferation of *M tuberculosis*. Most importantly, in accordance with the observation that refractory mycobacterial disease improves with rhIFN- γ treatment (case report), rhIFN- γ significantly increased the control of *M tuberculosis* proliferation *in vitro* by macrophages from patients and healthy control subjects (Fig 3, B).

rhIFN- γ improves dysregulation of the macrophage transcriptome in patients with CD40L deficiency

Based on the multiple macrophage functional defects observed in CD40L-deficient patients, we hypothesized that macrophages from CD40L-deficient patients have systemic dysregulation at the gene expression level. Therefore we analyzed the transcriptome of MDMs from CD40L-deficient patients using RNA sequencing and evaluated the effect of rhIFN- γ on gene expression. Because it was not possible to collect enough macrophages to stimulate them with both rhIFN- γ and sCD40L, we focused on the effect of rhIFN- γ because it had the most potential as a new therapeutic option for patients with CD40L deficiency. We based this decision on the previously observed success of rhIFN- γ therapy for certain infections,²⁸⁻³¹ its approval by the US Food and Drug Administration, and its feasibility for clinical use.

We obtained sufficient numbers of MDMs from 3 patients (P1, P2, and P3). Before rhIFN- γ treatment, we identified a total of 109 dysregulated genes (DEGs; 48 downregulated and 61 upregulated genes) when macrophages from CD40L-deficient patients were compared with those from healthy control subjects (Fig 4, A, left panel). The functional association network of the DEGs in patients with CD40L deficiency is demonstrated in Fig 4, B. Dysregulation of the macrophage transcriptome in patients with CD40L deficiency was not due to M-CSF-induced CD40L effects during MDM generation because M-CSF was unable to induce CD40L expression on MDMs (see Fig E2 in this article's Online Repository at www.jacionline.org). Furthermore, no CD40L transcript was undetectable by using RNA sequencing. On the other hand, sCD40L increased the capacity of the promyelocytic HL-60 cells to control *M tuberculosis* proliferation (see Fig E3 in this article's Online Repository at www.jacionline.org), indicating a role of

CD40L-CD40 interaction on myeloid cell development. A detailed investigation about the effect of the CD40L-CD40 interaction on promyelocytic HL-60 cells will be published elsewhere (manuscript in preparation).

It is noteworthy that rhIFN- γ restored the gene expression profile of the majority of DEGs in patients' macrophages. After rhIFN- γ treatment, only 11 of 109 genes remained differentially expressed in comparison with results seen in healthy control subjects (Fig 4, A, right panel). In addition to improving the expression of 109 DEGs, rhIFN- γ influenced the expression of 526 additional genes (133 downregulated and 393 upregulated genes) compared with that seen in healthy control subjects (Fig 5). The subsets of 109 DEGs and the additional 526 genes that were affected by the rhIFN- γ treatment are shown within GO categories (Table I). The main subsets of genes are directly involved with the immune system (GO0002376), including the inflammatory response (GO0006954) and wound response (GO0009611). Moreover, genes responsible for regulation of transcription (GO:0010628 and GO:0045892) and cell differentiation (GO:0030154, GO:0000904, GO:0045597, GO:0002521, and GO:0030099) were also affected.

rhIFN- γ increases TLR and CLR expression levels

Production of proinflammatory cytokines, oxidative burst, and effective microbicidal activity are essential functions of M1 macrophages, which contrast with M2 macrophages (called alternatively activated macrophages).^{47,48} Despite the functional defects we observed, no phenotypic alteration was identified on macrophages from CD40L-deficient patients. The normal expression of CD86, CD163, and CD206 molecules is shown in Fig E4 in this article's Online Repository at www.jacionline.org, all of which are markers that have been used to distinguish M1/M2 subpopulations.⁴⁹⁻⁵¹ Moreover, macrophages from patients with CD40L deficiency expressed TLRs and CLRs normally (Fig 6). Remarkably, rhIFN- γ significantly increased expression of TLR1, TLR2, dectin-1, and CD209 molecules in macrophages from patients and healthy control subjects.

DISCUSSION

Here we show that human CD40L deficiency impairs innate immune responses by affecting macrophage differentiation and function. Macrophage defects associated with impaired dendritic

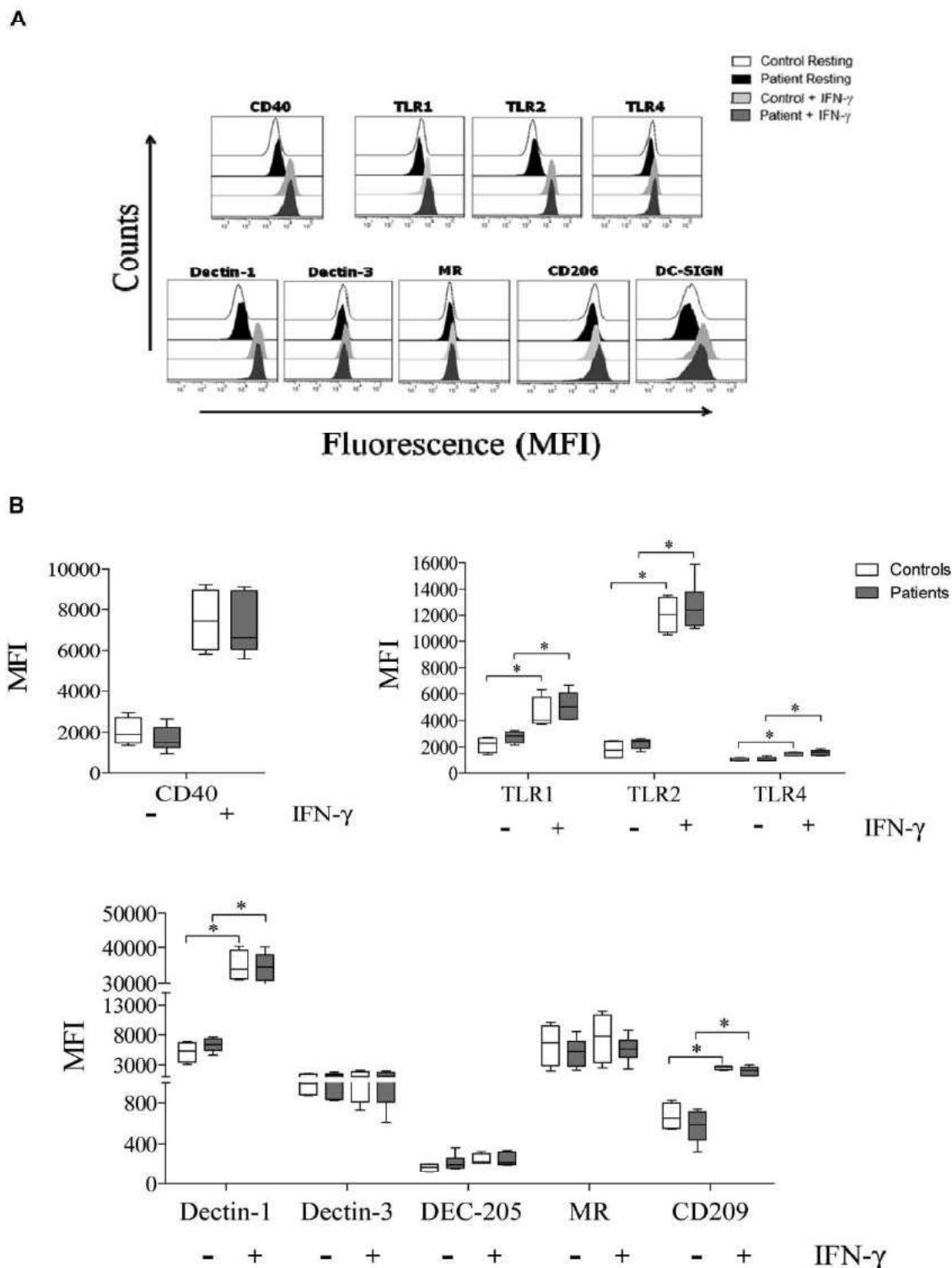


FIG 6. Effect of rhIFN- γ on expression of CD40, TLRs, and CLR by macrophages. Representative histograms (A) and graphics (B) showing CD40, TLR (TLR1, TLR2, and TLR4), and CLR (dectin-1, dectin-3, mannose receptor or MR, DEC-205, and CD209) expression, as analyzed by means of cytometry. MDMs were analyzed after 5 days in the presence of M-CFS, followed by 2 additional days in the presence or absence of rhIFN- γ . No significant differences in MDMs from patients versus healthy subjects were observed. * $P \leq .05$ ($n = 6$ patients and 6 control subjects), Mann-Whitney test. NS, Not significant; MFI, Mean fluorescence intensity.

cell (DC) response in patients with CD40L²² and CD40⁵² deficiencies point to an essential role of the CD40L-CD40 interaction during differentiation of myeloid cells. This fact clarifies a new

immunopathologic mechanism underlying the increased susceptibility of CD40L-deficient patients to opportunistic infections, which might explain the increased rate of deaths observed in

patient with CD40L deficiency despite the current treatment armamentarium.^{18,20} The possibility that the differences observed between CD40L-deficient patients and young adult control subjects are age related is unlikely. It is well known that innate immune cells, such as macrophages, from neonates and infants less than 2 years of age have inherent defects; however, older children display immune responses comparable with those of adults.⁵³⁻⁵⁹ In our diagnostic laboratory we have routinely observed that infants in the first years of life with undefined primary immunodeficiency disorders, in whom the diagnosis of CGD has been ruled out by demonstrating normal NADPH activity, have normal phagocyte responses compared with those in healthy control subjects (data not shown).

Macrophages have to undergo maturation to a stage that allows normal clearance of invading pathogens through different mechanisms, including generation of a fully potent oxidative burst. The importance of this pathway is illustrated by CGD, which is caused by defects affecting components of the phagocyte NADPH oxidase complex that are crucial in oxidative burst. Patients with CGD face life-threatening infections, even when oxidative burst is only slightly reduced or partially inhibited.^{17,60,61} Therefore the partially defective oxidative burst observed in macrophages from CD40L-deficient patients might contribute to the abnormal microbicidal activity that we demonstrated in our experiments and might be a risk factor for the increased susceptibility to opportunistic fungal and intracellular bacterial infections. However, it seems unlikely that defective fungicidal activity in macrophages from CD40L-deficient patients is solely due to reduced reactive oxygen species production because additional nonoxidative killing mechanisms might also be affected.

The impaired microbicidal activity, oxidative burst, and defective production of cytokines (eg, IL-6, TNF- α , IL-1 β , macrophage inflammatory protein 1 β , IP-10, and G-CSF) by patients' macrophages suggest that the absence of CD40L not only impairs effector function of macrophages but also initiation of inflammatory responses. These results are in accordance with the proinflammatory role of CD40L-CD40 interaction on activation of macrophages from healthy subjects.^{9,42} The multiple defects identified in macrophages from patients with CD40L deficiency indicate that more than 1 aspect of the macrophage immune response can be affected in these subjects. In accordance with the numerous functional defects displayed by patients' macrophages, we also observed a dysregulated gene expression signature, which was improved in the presence of rhIFN- γ . Considering the high number of DEGs in macrophages from CD40L-deficient patients, multiple other functions of these cells remain to be investigated further.

Contradictory results regarding IFN- γ production by CD40L-deficient T cells have been reported. However, such incongruences might be explained by the fact that PBMCs/T cells from CD40L-deficient patients are intrinsically capable of producing IL-12 and IFN- γ but do not respond to certain stimuli. We found that PBMCs from CD40L-deficient patients normally produce IL-12 in response to IFN- γ and release IFN- γ in response to IL-12 stimulation (see Fig E5 in this article's Online Repository at www.jacionline.org). These findings contrast with our previous observation of a significantly impaired IL-12/IFN- γ axis²² in DC/T-cell cocultures stimulated by *Candida albicans* or *P. brasiliensis*. Both Jain et al²³ and Subauste et al²⁴ described impaired IFN- γ production by PBMCs from CD40L-deficient patients after anti-CD3 stimulation and *Toxoplasma gondii*

exposure, respectively. In contrast, Uronen and Callard⁶² reported normal IFN- γ release by T cells from CD40L-deficient patients in response to PMA plus ionomycin. In turn, Felipe-Santos et al⁶³ observed decreased production of IL-12 and IFN- γ in response to PHA; however, normal generation of IL-12 by LPS and IFN- γ by PMA/ionomycin was seen in PBMCs from CD40L-deficient patients compared with generation in healthy control subjects.

The treatment of opportunistic infections in CD40L-deficient patients with rhIFN- γ might reduce the high mortality rate associated with CD40L deficiency, despite currently available treatment options.^{18,19,64,65} This possibility has been illustrated by the response of one of our CD40L-deficient patients who, despite all the treatment available, had refractory disseminated mycobacterial infection that was improved after rhIFN- γ adjuvant therapy. Taken together, our data point to rhIFN- γ as a possible adjunct immunotherapy, in combination with conventional therapy, for cases of disseminated opportunistic infections in CD40L-deficient patients. Furthermore, this cytokine is already available and licensed for clinical use.^{27,52,54}

Another mechanism by which rhIFN- γ might potentiate macrophage immune responses of macrophages from CD40L-deficient patients is by increasing the expression of TLRs and CLRs, both of which are essential for immune responses against different pathogens.⁶⁶ rhIFN- γ treatment of macrophages from both patients and control subjects caused significantly increased expression of TLR1, TLR2, dectin-1, and CD209. The potential of IFN- γ influencing PRR expression might explain how rhIFN- γ can restore microbicidal activity in macrophages from CD40L-deficient patients. However, we did not observe significant changes in TLR1, TLR2, dectin-1, and CD209 mRNA expression after *in vitro* rhIFN- γ treatment in our transcriptome analysis (data not shown). Whether IFN- γ regulates the protein expression of these PRRs by modulating mRNA expression at a different time point than those we assessed or whether it acts at a posttranscriptional level requires further investigation.

In conclusion, our data demonstrated that in the absence of the CD40L-CD40 interaction, macrophages from CD40L-deficient patients exhibit impaired function and differentiation because of dysregulation of gene expression that might contribute to their susceptibility to opportunistic infections. Furthermore, rhIFN- γ might represent a new therapeutic option for patients with CD40L deficiency by restoring certain functions to macrophages.

We thank all the patients and their families for participation in this study. We also thank Dr Eunice Duarte from the Lab Alfa LTDA and Lusinete Tavares from the Federal University of São Paulo for blood sample collection.

Clinical implications: The absence of CD40L impairs macrophage differentiation and function, and its lack contributes to increased susceptibility of CD40L-deficient patients to life-threatening infections. Furthermore, rhIFN- γ improves the function of macrophages from CD40L-deficient patients, indicating this cytokine as a potential new adjuvant therapy.

REFERENCES

1. Aruffo A, Farrington M, Hollenbaugh D, Li X, Milatovich A, Nonoyama S, et al. The CD40 ligand, gp39, is defective in activated T cells from patients with X-linked hyper-IgM syndrome. *Cell* 1993;72:291-300.

2. Allen RC, Armitage RJ, Conley ME, Rosenblatt H, Jenkins NA, Copeland NG, et al. CD40 ligand gene defects responsible for X-linked hyper-IgM syndrome. *Science* 1993;259:990-3.
3. DiSanto JP, Bonnefoy JY, Gauchat JF, Fischer A, de Saint Basile G. CD40 ligand mutations in x-linked immunodeficiency with hyper-IgM. *Nature* 1993;361:541-3.
4. Fuleihan R, Ramesh N, Loh R, Jabara H, Rosen RS, Chatila T, et al. Defective expression of the CD40 ligand in X chromosome-linked immunoglobulin deficiency with normal or elevated IgM. *Proc Natl Acad Sci U S A* 1993;90:2170-3.
5. Korthäuer U, Graf D, Mages HW, Brière F, Padayachee M, Malcolm S, et al. Defective expression of T-cell CD40 ligand causes X-linked immunodeficiency with hyper-IgM. *Nature* 1993;361:539-41.
6. Kim HS, Zhang X, Choi YS. Activation and proliferation of follicular dendritic cell-like cells by activated T lymphocytes. *J Immunol* 1994;153:2951-61.
7. Caux C, Massacrier C, Vanbervliet B, Dubois B, Van Kooten C, Durand L, et al. Activation of human dendritic cells through CD40 cross-linking. *J Exp Med* 1994;180:1263-72.
8. Heeschen C, Dimmeler S, Hamm CW, van den Brand MJ, Boersma E, Zeiher AM, et al. Soluble CD40 ligand in acute coronary syndromes. *N Engl J Med* 2003;348:1104-11.
9. Henn V, Stupsky JK, Grate M, Anagnostopoulos I, Forster K, Müller-Berghaus G, et al. CD40 ligand on activated platelets triggers an inflammatory reaction of endothelial cells. *Nature* 1998;391:591-4.
10. Mavroudi I, Papadaki H. The role of CD40/CD40 ligand interactions in bone marrow granulopoiesis. *Sci World J* 2011;11:2011-9.
11. Mazzei GJ, Edgerton MD, Losberger C, Lecoanet-Henchoz S, Graber P, Durandy A, et al. Recombinant soluble trimeric CD40 ligand is biologically active. *J Biol Chem* 1995;270:7025-8.
12. Saeland S, Duvert V, Caux C, Pandrau D, Favre C, Vallé A, et al. Distribution of surface-membrane molecules on bone marrow and cord blood CD34+ hematopoietic cells. *Exp Hematol* 1992;20:24-33.
13. Solaniilla A, Dechanet J, El Andaloussi A, Dupouy M, Godard F, Chabrol J, et al. CD40-ligand stimulates myelopoiesis by regulating flt3-ligand and thrombopoietin production in bone marrow stromal cells. *Blood* 2000;95:3758-64.
14. Flores-Romo L, Björck P, Duvert V, van Kooten C, Saeland S, Banchereau J. CD40 ligation on human cord blood CD34+ hematopoietic progenitors induces their proliferation and differentiation into functional dendritic cells. *J Exp Med* 1997;185:341-9.
15. Malik N, Greenfield BW, Wahl AF, Kiener PA. Activation of human monocytes through CD40 induces matrix metalloproteinases. *J Immunol* 1996;156:3952-60.
16. Geissmann F, Manz MG, Jung S, Sieweke MH, Merad M, Ley K. Development of monocytes, macrophages, and dendritic cells. *Science* 2010;327:656-61.
17. Kuhns DB, Alvord WG, Heller T, Feld JJ, Pike KM, Marciano BE, et al. Residual NADPH oxidase and survival in chronic granulomatous disease. *N Engl J Med* 2010;363:2600-10.
18. Cabral-Marques O, Klaver S, Schimke LF, Ascendino ÉH, Khan TA, Pereira PVS, et al. First report of the hyper-IgM syndrome registry of the Latin American Society for Immunodeficiencies: novel mutations, unique infections, and outcomes. *J Clin Immunol* 2014;34:146-56.
19. de Oliveira-Junior EB, Zurro NB, Prando C, Cabral-Marques O, Pereira PV, Schimke L-F, et al. Clinical and genotypic spectrum of chronic granulomatous disease in 71 Latin American patients: first report from the LASID registry. *Pediatr Blood Cancer* 2015;62:2101-7.
20. Levy J, Espanol-Boren T, Thomas C, Fischer A, Tovo P, Bordignon P, et al. Clinical spectrum of X-linked hyper-IgM syndrome. *J Pediatr* 1997;131:47-54.
21. Cabral-Marques O, Schimke L-F, Pereira PV, Falcai A, de Oliveira JB, Hackett MJ, et al. Expanding the clinical and genetic spectrum of human CD40L deficiency: the occurrence of paracoccidioidomycosis and other unusual infections in Brazilian patients. *J Clin Immunol* 2012;32:212-20.
22. Cabral-Marques O, Arslanian C, Ramos RN, Morato M, Schimke L, Soeiro Pereira PV, et al. Dendritic cells from X-linked hyper-IgM patients present impaired responses to *Candida albicans* and *Paracoccidioides brasiliensis*. *J Allergy Clin Immunol* 2012;129:778-86.
23. Jain A, Atkinson TP, Lipsky PE, Slater JE, Nelson DL, Strober W. Defects of T-cell effector function and post-thymic maturation in X-linked hyper-IgM syndrome. *J Clin Invest* 1999;103:1151-8.
24. Subauste CS, Wessendarp M, Sorensen RU, Leiva LE. CD40-CD40 ligand interaction is central to cell-mediated immunity against *Toxoplasma gondii*: patients with hyper IgM syndrome have a defective type I immune response that can be restored by soluble CD40 ligand trimer. *J Immunol* 1999;162:6690-700.
25. Ezekowitz RA, Sieff CA, Dinauer MC, Nathan DG, Orkin SH, Newburger PE. Restoration of phagocyte function by interferon-gamma in X-linked chronic granulomatous disease occurs at the level of a progenitor cell. *Blood* 1990;76:2443-8.
26. Bemiller LS, Roberts DH, Starko KM, Curnutte JT. Safety and effectiveness of long-term interferon gamma therapy in patients with chronic granulomatous disease. *Blood Cells Mol Dis* 1995;21:239-47.
27. Marciano BE, Wesley R, De Carlo ES, Anderson VL, Barnhart LA, Darnell D, et al. Long-term interferon-gamma therapy for patients with chronic granulomatous disease. *Clin Infect Dis* 2004;39:692-9.
28. Gao XF, Yang ZW, Li J. Adjunctive therapy with interferon-gamma for the treatment of pulmonary tuberculosis: a systematic review. *Int J Infect Dis* 2011;15:e594-600.
29. Abzug MJ, Walsh TJ. Interferon-gamma and colony-stimulating factors as adjuvant therapy for refractory fungal infections in children. *Pediatr Infect Dis J* 2004;23:769-73.
30. Kelleher P, Goodsall A, Mulgirigama A, Kunst H, Henderson DC, Wilson R, et al. Interferon-gamma therapy in two patients with progressive chronic pulmonary aspergillosis. *Eur Respir J* 2006;27:1307-10.
31. Al-Muhsen S, Casanova JL. The genetic heterogeneity of mendelian susceptibility to mycobacterial diseases. *J Allergy Clin Immunol* 2008;122:1043-51.
32. Beyer M, Mallmann MR, Xue J, Staratschek-Jox A, Vorholt D, Krebs W, et al. High-resolution transcriptome of human macrophages. *PLoS One* 2012;7:e45466.
33. Pina A, Saldiva PH, Restrepo LE, Calich VL. Neutrophil role in pulmonary paracoccidioidomycosis depends on the resistance pattern of hosts. *J Leukoc Biol* 2006;79:1202-13.
34. Soeiro-Pereira PV, Falcai A, Kubo CA, Oliveira-Júnior EB, Marques OC, Antunes E, et al. BAY 41-2272, a soluble guanylate cyclase agonist, activates human mononuclear phagocytes. *Br J Pharmacol* 2012;166:1617-30.
35. Verreck FA, de Boer T, Langenberg DM, Hoeve MA, Kramer M, Vaisberg E, et al. Human IL-23-producing type 1 macrophages promote but IL-10-producing type 2 macrophages subvert immunity to (myco)bacteria. *Proc Natl Acad Sci U S A* 2004;101:4560-5.
36. Amaral EP, Ribeiro SCM, Lanes VR, Almeida FM, de Andrade MR, Bomfim CC, et al. Pulmonary infection with hypervirulent *Mycobacteria* reveals a crucial role for the P2X7 receptor in aggressive forms of tuberculosis. *PLoS Pathog* 2014;10:e1004188.
37. Dong C, Zhao G, Zhong M, Yue Y, Wu L, Xiong S. RNA sequencing and transcriptomal analysis of human monocyte to macrophage differentiation. *Gen* 2013;5:19279-87.
38. Hensman J, Papastamoulis P, Glaus P, Honkela A, Rattray M. Fast and accurate approximate inference of transcript expression from RNA-seq data. *Bioinformatics* 2015;31:3881-9.
39. Szklarczyk D, Franceschini A, Wyder S, Forslund K, Heller D, Huerta-Cepas J, et al. STRING v10: protein-protein interaction networks, integrated over the tree of life. *Nucleic Acids Res* 2015;43:D447-52.
40. Huang DW, Sherman BT, Lempicki RA. Bioinformatics enrichment tools: paths toward the comprehensive functional analysis of large gene lists. *Nucleic Acids Res* 2009;37:1-13.
41. Huang da DW, Lempicki RA, Sherman BT. Systematic and integrative analysis of large gene lists using DAVID bioinformatics resources. *Nat Protoc* 2009;4:44-57.
42. Ashburner M, Ball CA, Blake JA, Botstein D, Butler H, Cherry JM, et al. Gene ontology: tool for the unification of biology. The Gene Ontology Consortium. *Nat Genet* 2000;25:25-9.
43. Warde-Farley D, Donaldson SL, Comes O, Zuberi K, Badrawi R, Chao P, et al. The GeneMANIA prediction server: biological network integration for gene prioritization and predicting gene function. *Nucleic Acids Res* 2010;38:W214-20.
44. Bustamante J, Arias AA, Vogt G, Picard C, Galicia LB, Prando C, et al. Germline CYBB mutations that selectively affect macrophages in kindreds with X-linked predisposition to tuberculous mycobacterial disease. *Nat Immunol* 2011;12:213-21.
45. Wang LL, Zhou W, Zhao W, Tian ZQ, Wang WF, Wang XF, et al. Clinical features and genetic analysis of 20 Chinese patients with X-linked hyper-IgM syndrome. *J Immunol Res* 2014;2014:683160.
46. Bustamante J, Boisson-Dupuis S, Abel L, Casanova J-L. Mendelian susceptibility to mycobacterial disease: genetic, immunological, and clinical features of inborn errors of IFN- γ immunity. *Semin Immunol* 2014;26:454-70.
47. Covarrubias A, Byles V, Hornig T. ROS sets the stage for macrophage differentiation. *Cell Res* 2013;23:984-5.
48. Pollard JW. Trophic macrophages in development and disease. *Nat Rev Immunol* 2009;9:259-70.
49. Weber M, Moebius P, Büttner-Herold M, Amann K, Preidl R, Neukam FW, et al. Macrophage polarisation changes within the time between diagnostic biopsy and tumour resection in oral squamous cell carcinomas—an immunohistochemical study. *Br J Cancer* 2015;113:510-9.
50. Biswas SK, Mantovani A. Macrophage plasticity and interaction with lymphocyte subsets: cancer as a paradigm. *Nat Immunol* 2010;11:889-96.

51. Röszer T. Understanding the mysterious M2 macrophage through activation markers and effector mechanisms. *Mediators Inflamm* 2015;2015:816460.
52. Fontana S, Moratto D, Mangal S, De Francesco M, Vermi W, Ferrari S, et al. Functional defects of dendritic cells in patients with CD40 deficiency. *Blood* 2003;102:4099-106.
53. De Kleer I, Willems F, Lambrecht B, Goriely S. Ontogeny of myeloid cells. *Front Immunol* 2014;5:423.
54. Maródi L, Káposzta R, Campbell DE, Polin RA, Csongor J, Johnston RB Jr. Candidacidal mechanisms in the human neonate. Impaired IFN-gamma activation of macrophages in newborn infants. *J Immunol* 1994;153:5643-9.
55. Lu CY, Calamai EG, Unanue ER. A defect in the antigen-presenting function of macrophages from neonatal mice. *Nature* 1979;282:327-9.
56. Weston WL, Carson BS, Barkin RM, Slater GD, Dustin RD, Hecht SK. Monocyte-macrophage function in the newborn. *Am J Dis Child* 1977;131:1241-2.
57. Maródi L. Neonatal innate immunity to infectious agents. *Infect Immun* 2006;74:1999-2006.
58. Wilson CB, Lewis DB. Basis and implications of selectively diminished cytokine production in neonatal susceptibility to infection. *Rev Infect Dis* 1990;12(suppl 4):S410-20.
59. Marodi L. Down-regulation of Th1 responses in human neonates. *Clin Exp Immunol* 2002;128:1-2.
60. Borregaard N, Cross AR, Herlin T, Jones OT, Segal AW, Valerius NH. A variant form of X-linked chronic granulomatous disease with normal nitroblue tetrazolium slide test and cytochrome b. *Eur J Clin Invest* 1983;13:243-8.
61. Roesler J, Segerer F, Morbach H, Kleinert S, Thieme S, Rösch-Wolff A, et al. P67-phox (NCF2) lacking exons 11 and 12 is functionally active and leads to an extremely late diagnosis of chronic granulomatous disease (CGD). *PLoS One* 2012;7:e34296.
62. Uronen H, Callard RE. Absence of CD40-CD40 ligand interactions in X-linked hyper-IgM syndrome does not affect differentiation of T helper cell subsets. *Clin Exp Immunol* 2000;121:346-52.
63. Filipe-Santos O, Bustamante J, Haverkamp MH, Vinolo E, Ku C-L, Puel A, et al. X-linked susceptibility to mycobacteria is caused by mutations in NEMO impairing CD40-dependent IL-12 production. *J Exp Med* 2006;203:1745-59.
64. Seminario AG, Diaz Ballve D, Comas D, Gomez Raccio A, Di Giovanni D, Bezrodnik L. Disseminated mycobacterial infection in a patient with CD40L deficiency. *J Clin Immunol* 2013;33:S108.
65. Winkelstein JA, Marino MC, Ochs H, Fuleihan R, Scholl PR, Geha R, et al. The X-linked hyper-IgM syndrome: clinical and immunologic features of 79 patients. *Medicine (Baltimore)* 2003;82:373-84.
66. Geijtenbeek TBH, Gringhuis SI. Signalling through C-type lectin receptors: shaping immune responses. *Nat Rev Immunol* 2009;9:465-79.

REFERENCES

- E1. Den Dunnen JT, Antonarakis SE. Mutation nomenclature extensions and suggestions to describe complex mutations: a discussion. *Hum Mutat* 2000;15:7-12.
- E2. Taschner PE, den Dunnen JT. Describing structural changes by extending HGVS sequence variation nomenclature. *Hum Mutat* 2011;32:507-11.

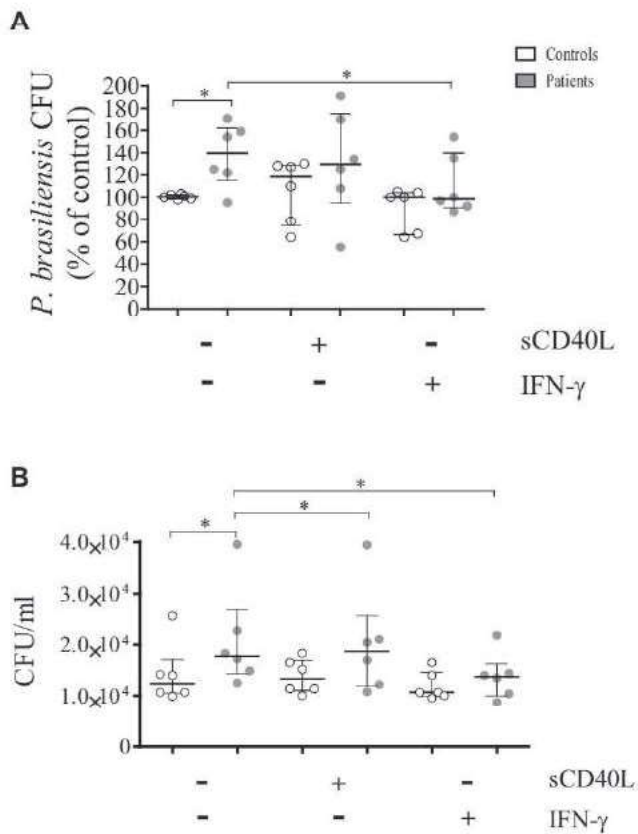


FIG E1. rhIFN- γ , but not sCD40L, improves the defective fungicidal activity seen in CD40L-deficient patients. **A.** After challenging MDMs with *P. brasiliensis*, fungicidal activity was assessed by determining CFU values. Before assay, MDMs were either untreated (-) or treated with (+) sCD40L (500 ng/mL) or rhIFN- γ (100 U/mL) for 48 hours. CFU values (percentage of control values) were determined in relation to the CFU number of untreated MDMs from healthy control subjects. **B.** Raw data in CFU/mL are also shown. Significant differences are denoted as follows: * $P \leq .05$ ($n = 6$ patients and 6 control subjects), Mann-Whitney test.

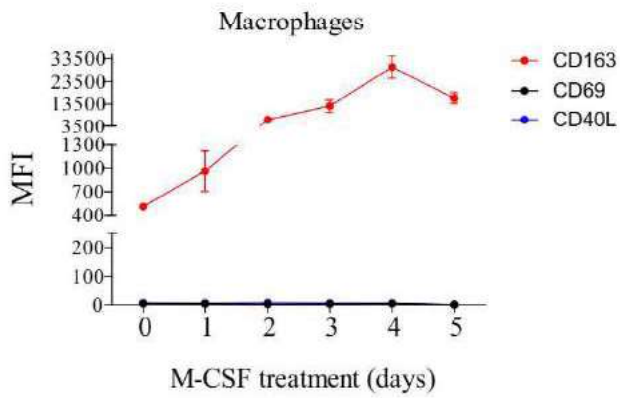


FIG E2. M-CSF does not induce CD40L expression on monocytes/macrophages. Expression of CD40L, CD69, and CD163 on MDMs was analyzed by means of flow cytometry on each day of macrophage differentiation. No expression of CD40L and CD69 on MDMs was observed. On the other hand, CD163 expression was increased in the presence of M-CSF. *MFI*, Mean fluorescence intensity.

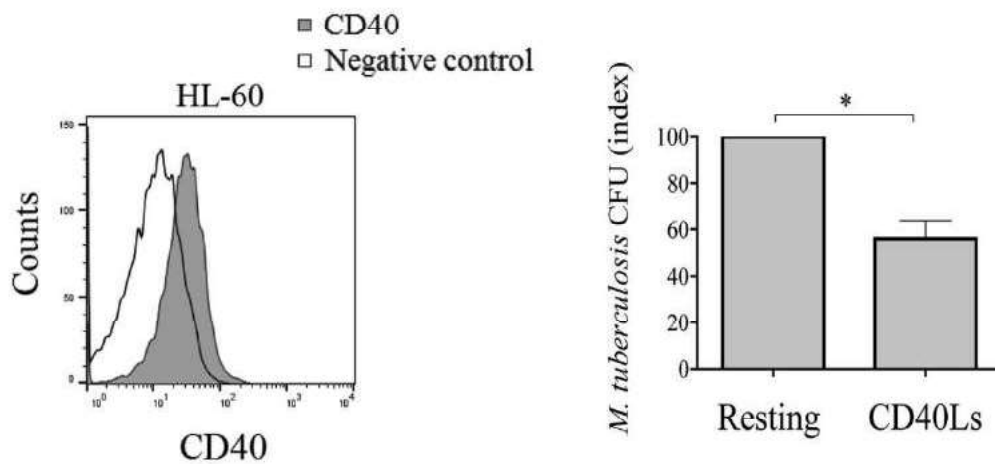


FIG E3. sCD40L increases the capacity of the promyelocytic HL-60 cells to control *M tuberculosis* proliferation. Promyelocytic HL-60 cells, which express CD40 (left panel), were cultivated in the absence presence of sCD40L (500 ng/mL), and their ability to control *M tuberculosis* proliferation was analyzed by CFU (right panel). * $P < .05$ ($n = 6$ patients and 6 control subjects), Mann-Whitney test. NS, Not significant.

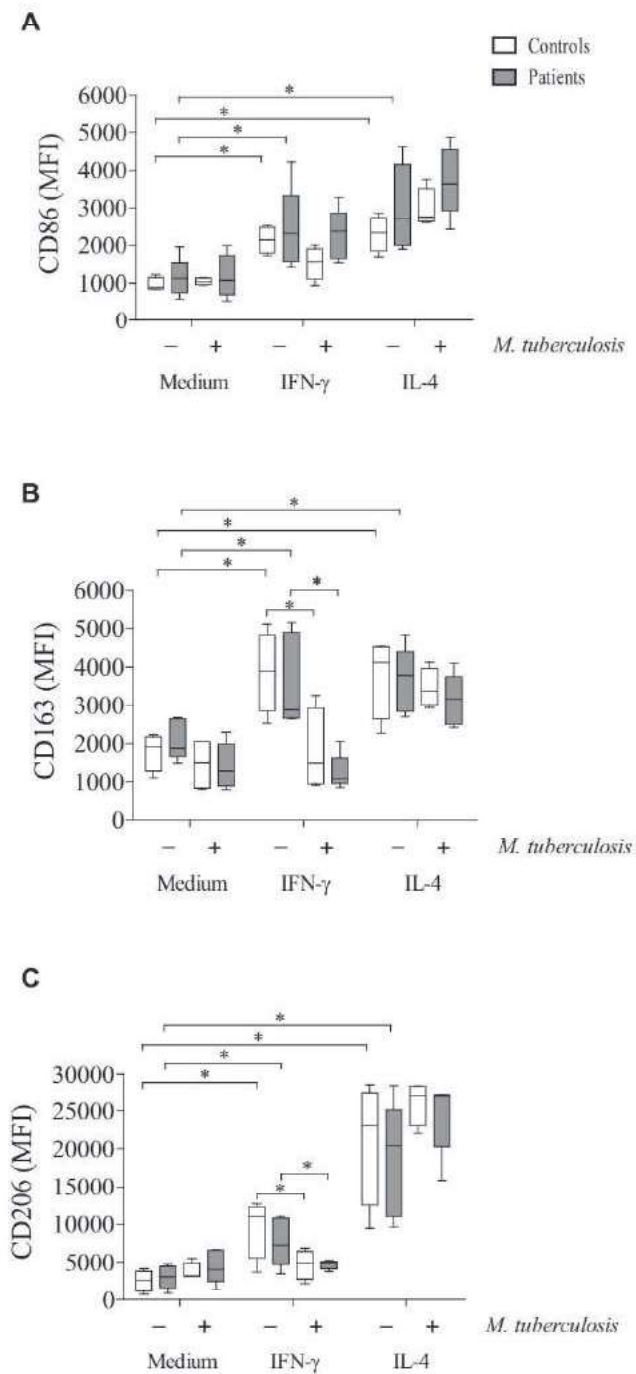


FIG E4. Normal expression of CD86, CD206, and CD163 on macrophages from CD40L-deficient patients. MDMs were cultured in the presence of IL-4 or IFN- γ alone or in concert with *M tuberculosis*. Expression of CD86 (A), CD163 (B), and CD206 (C) was analyzed by using flow cytometry, and data were represented as mean fluorescence intensity (MFI). * $P < .05$ (n = 6 patients and 6 control subjects), Mann-Whitney test. NS, Not significant.

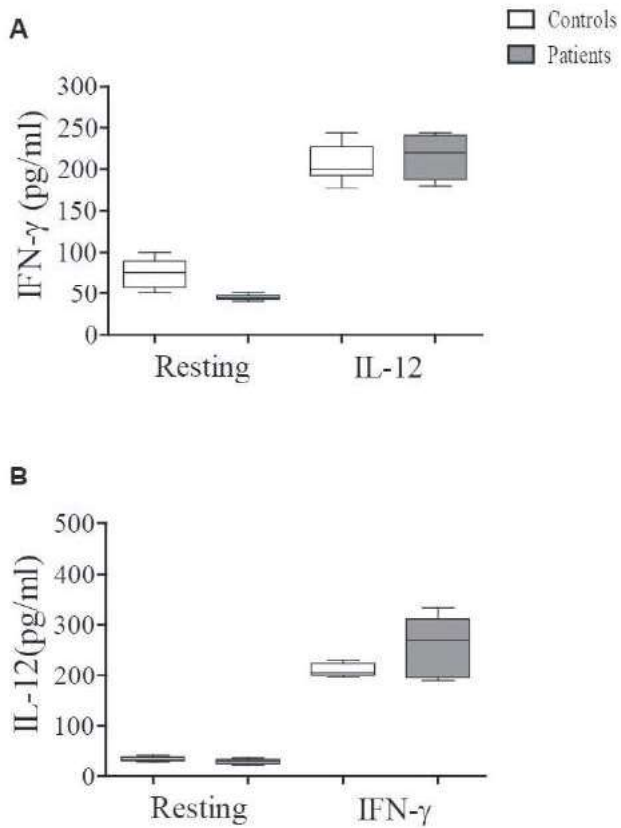


FIG E5. The IFN- γ /IL-12 axis is normally activated by rhIFN- γ and rhIL-12. **A**, PBMCs were activated for 48 hours in the presence of rhIFN- γ (100 U/mL) to induce IL-12 production. **B**, Cells were stimulated with rhIL-12 (10 ng/mL) for 48 hours to analyze IFN- γ production. Supernatants were harvested and analyzed by means of ELISA.

TABLE E1. Isolated pathogens and mutations of CD40L-deficient patients

Patient no.	Birth year	Patient's age at study date (y)	Isolated pathogens			Infections with unidentified pathogens	cDNA mutation*	Predicted effect on protein
			Fungi	Intracellular bacteria and protozoa	Virus			
P1	2007	8	—	<i>M tuberculosis</i>	—	Pneumonia, otitis,	c.475 G>A	p. W140X
P2	2005	10	<i>Pneumocystis jirovecii</i>	—	HPV, herpes simplex	Otitis, sinusitis, pneumonia	c.213_216delATAG	p.I53fsX65
P3	2007	8	<i>P jirovecii</i> , <i>C albicans</i>	<i>Cryptosporidium parvum</i>	—	Otitis, sinusitis, pneumonia	c.213_216delATAG	p.I53fsX65
P4†	1993	22	<i>P brasiliensis</i> , <i>P jirovecii</i>	<i>M tuberculosis</i>	—	Pneumonia, otitis, sinusitis	c.345_402del	Exon 3 skipping
P5	2004	11	<i>Aspergillus</i> species, <i>P jirovecii</i>	<i>C parvum</i>	—	Diarrhea	170-bp Deletion in 5' UTR (promoter)	Absence of RNA and protein expression
P6	2006	9	—	<i>M tuberculosis</i>	—	Pneumonia, otitis urinary tract infection	c.633_634insAGCC	p.L193fsX201

JAK-STAT, Janus kinase–signal transducer and activator of transcription; *UTR*, untranslated region.

*The nomenclature for the description of mutations is in accordance with guidelines of Human Genome Variation Society.^{11,12}

†Patient P4 recently died in a cachectic state after recurrent diarrhea caused by *Cryptosporidium* species infection and concomitant severe mycobacterial tuberculosis infection. Therefore his macrophages were not analyzed for CD86, CD163, and CD206 or PRR expression, respectively, as shown in Fig E4 and Fig 6.

APÊNDICE H – Interferon-gamma reduces the proliferation of *M. tuberculosis* within macrophages from a patient with a novel hypomorphic NEMO mutation. **Pediatric Blood & Cancer. 2016**

BRIEF REPORT

Interferon-gamma reduces the proliferation of *M. tuberculosis* within macrophages from a patient with a novel hypomorphic NEMO mutation

Taj Ali Khan^{1,2} | Lena Friederike Schimke¹ | Eduardo Pinheiro Amaral¹ |
Muhammad Ishfaq³ | Caio César Barbosa Bonfim¹ | Hazir Rahman² | Asif Iqbal⁴ |
Maria Regina D'Império Lima¹ | Beatriz Tavares Costa Carvalho⁵ |
Otavio Cabral-Marques^{1,6} | Antonio Condino-Neto¹

¹Department of Immunology, Institute of Biomedical Sciences, University of São Paulo, São Paulo, SP, Brazil

²Department of Microbiology, Kohat University of Science and Technology, Kohat, Pakistan

³Basic Science Research Department, Shaukat Khanum Memorial Cancer Hospital & Research Centre, Lahore, Pakistan

⁴Laboratory of Biochemistry and Biophysics, Butantan Institute, Sao Paulo, Brazil

⁵Division of Allergy-Immunology and Rheumatology, Department of Pediatrics, Federal University of São Paulo, SP, Brazil

⁶Department of Rheumatology, University of Lübeck, Lübeck, Germany

Correspondence

Antonio Condino-Neto, MD, PhD, Department of Immunology, Institute of Biomedical Sciences, University of São Paulo, 1730 Lines Prestes Avenue, São Paulo, SP.05508-000, Brazil.
Email: condino@icb.usp.br

Otavio Cabral-Marques contributed equally to this work.

Grant sponsor: Fundação de Amparo a Pesquisa do Estado de São Paulo (FAPESP); Grant sponsor: Conselho Nacional de Desenvolvimento Científico e Tecnológico (CNPq).

Abstract

X-linked ectodermal dysplasia with immunodeficiency (XL-EDA-ID) is caused by mutations in the nuclear factor-kappa B essential modulator (NEMO) gene. Here, we report the clinical and genetic features of a XL-EDA-ID patient who developed bacillus Calmette–Guérin infection. Patient lymphocytes failed to degrade I κ B- α , and sequencing of NEMO identified the novel mutation c.1238A>C/p.H413P. Furthermore, patient monocyte-derived macrophages ingested *Mycobacterium tuberculosis* normally, but failed to control the intracellular proliferation of bacilli, a defect which was improved in the presence of interferon-gamma (IFN- γ). This work expands the genetic spectrum of XL-EDA-ID and demonstrates improvement in macrophage function in a NEMO-deficient patient by IFN- γ .

KEYWORDS

BCGitis, ectodermal dysplasia, NEMO

1 | INTRODUCTION

X-linked anhidrotic ectodermal dysplasia with immunodeficiency (XL-EDA-ID) is a primary immunodeficiency disorder (PID) characterized by the absence of sweat glands, sparse scalp hair, defective tooth formation, and susceptibility to infections. XL-EDA-ID is caused by hypomorphic mutations in the nuclear factor-kappa B (NF- κ B) essential modulator (NEMO) gene (also known as *IKK gamma* or *IKKG*). NEMO is the regulatory subunit of the inhibitor of the NF- κ B-I κ B kinase complex. In resting cells, dimers of the pleiotropic transcription

factor NF- κ B are retained in the cytoplasm in an inactive form by interaction with the inhibitory κ B (I κ B) proteins such as I κ B- α , I κ B- β , and I κ B- ϵ . Upon cell activation, NEMO promotes I κ B phosphorylation and its proteasomal degradation through polyubiquitination. This allows NF- κ B nuclear translocation and transcriptional activation of target genes.¹

Patients with XL-EDA-ID are susceptible to recurrent infections by opportunistic pathogens, including pyogenic bacteria and fungi. These patients are also susceptible to mycobacteria infections, including the weakly virulent bacillus Calmette–Guérin (BCG).² Both in vitro and in

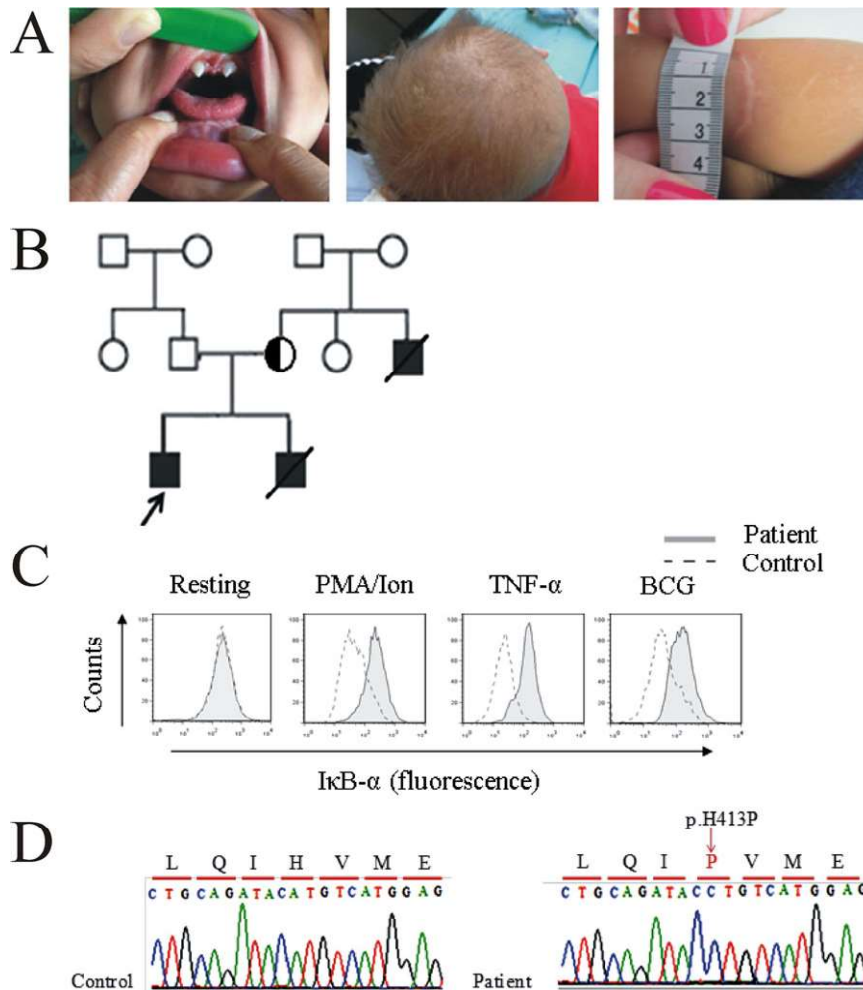


FIGURE 1 Pedigree, phenotype, and molecular analysis of NEMO from a Brazilian patient with XL-EDA-ID. (A) Conical teeth (left panel), sparse scalp hair (middle panel), and BCGitis scar on the right arm of the patient (right panel). (B) Family pedigree of our index patient, indicated by arrow. (C) Histograms showing defective $I\kappa B\alpha$ degradation in response to PMA/PHA, $TNF-\alpha$, and BCG. (D) Chromatogram of NEMO complementary DNA (cDNA) showing the novel missense mutation (c.1238A>C/p.H413P).

vivo studies demonstrated that $NF-\kappa B$ signaling plays an essential role in the regulation of the macrophage immune response.^{3,4} However, the control of *M. tuberculosis* proliferation in macrophages from NEMO-deficient patients remains to be investigated.

Here, we describe the occurrence of disseminated BCG disease (BCGitis) in a patient with XL-EDA-ID induced by a novel hypomorphic NEMO mutation. Moreover, we demonstrate the therapeutic effect of recombinant human interferon-gamma ($rhIFN-\gamma$), which effectively inhibits the proliferation of *M. tuberculosis* in the patient's monocyte-derived macrophages (MDMs).

2 | RESULTS

2.1 | Case report

A male child born to a nonconsanguineous Brazilian family with positive history of PID was selected. The patient's brother died of pneumonia followed by septic shock in the first year of life, and a maternal uncle died due to an unidentified infectious disease in child-

hood (Fig. 1B). The child was born with ectodermal dysplasia and in the first months of life developed BCGitis characterized by axillary adenopathy and a suppurative scar that evolved to necrotizing pneumonia (Fig. 1A), which required treatment with isoniazid, rifampicin, and ethambutol. The patient was admitted at 2 months of age with simultaneous occurrence of a popliteal abscess from *S. aureus*, *E. coli* infection of urinary tract, bacteremia caused by *K. pneumoniae*, and interstitial pneumonia. Later on, at 6 months of age, he developed *S. aureus* and *C. parapsilosis* suppurative acute otitis media with secondary facial palsy and bilateral pneumonia with lung abscess followed by septic shock caused by *S. aureus*. From 15 months onward, the patient lived with urinary tract infection, bacteremia, chronic diarrhea with blood, eczema, hypohydrosis, hyperthermia, and recurrent mucocutaneous candidiasis. Routine laboratory evaluation showed normal blood cell counts, hyper-IgM phenotype, and absence of antipneumococcal antibodies following vaccination. However, memory T- and B-cell subpopulations were not evaluated. The patient was treated with intravenous human immunoglobulin (800 mg/kg/month) and received trimethoprim-sulfamethoxazole for *P. jiroveci* prophylaxis. The patient received a matched unrelated donor

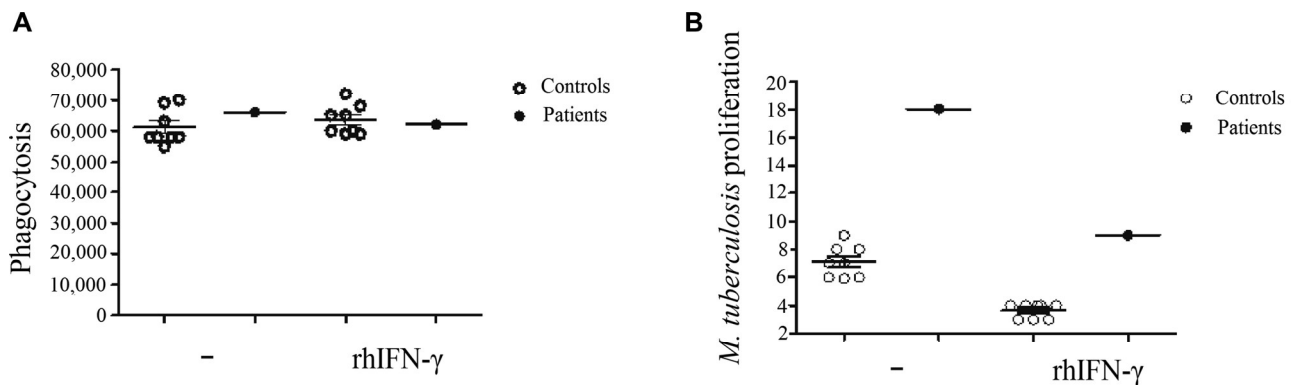


FIGURE 2 Defective control of *M. tuberculosis* proliferation by MDMs from the NEMO-deficient patient is improved by rhIFN- γ . (A) Phagocytosis of *M. tuberculosis* and (B) control of intracellular proliferation by MDMs were evaluated after 24 hr of culture in the presence of rhIFN- γ (100 IU/ml). The results are representative of two independent experiments performed in triplicate. Results from the patient were compared to seven healthy controls.

transplant at 27 months of age without relevant GVHD, and after 3 months, he had over 80% of engraftment. Immunosuppressive treatment was discontinued. However, his lymphocytes number dropped dramatically. He would have received a booster transplant, but he developed overwhelming sepsis by *S. aureus* 4 months after HSCT and died.

The study was approved by the Ethics Committee at the Institute of Biomedical Sciences, University of São Paulo, according to the Helsinki Convention and the Ministry of Health of Brazil. The patient presented a normal karyotype (46,XY) and based on the family history and clinical findings suggesting XL-EDA-ID, he was investigated for NEMO deficiency. Lymphocytes from the patient displayed normal NEMO expression by flow cytometry when compared to healthy controls (Fig. S1A in the Supporting Information). However, unlike healthy controls, the patient's lymphocytes failed to degrade I κ B- α in response to synergistic treatment with phorbol myristate acetate (300 ng/ml; Sigma Laboratories, St. Louis, MO) and ionomycin calcium ionophore (ionomycin, 1 μ g/ml; Sigma Laboratories), tumor necrosis factor alpha (TNF- α , 20 ng/ml; R&D Systems Europe), or BCG stimulation (1 lymphocyte:10 BCG) (Fig. 1C). Sequencing of the *NEMO* gene identified a novel missense mutation (c.1238A>C/p.H413P) (Fig. 1D) localized at the C-terminal region of the protein (Fig. S1B in the Supporting Information). In silico analysis demonstrated that the p.H413 amino acid is conserved among different species (Fig. S1C in the Supporting Information). Polyphen (<http://genetics.bwh.harvard.edu/pph2/>) and MutationTaster (www.mutationtaster.org) analysis indicated that the p.H413P substitution is likely pathogenic (Figs. S2A and S2B in the Supporting Information). In addition, the mutation was not found in 600 healthy Brazilian controls, suggesting that this missense mutation is not a single-nucleotide polymorphism.

NF- κ B activation has been shown to be important for the activation of macrophages, which are essential for the immune response against *Mycobacteria*.⁵ Considering the activating properties of rhIFN- γ on phagocytes and its beneficial therapeutic effect for patients with susceptibility to mycobacterial infections,⁶ we assessed the capacity of macrophages from our patient to phagocytose and control the proliferation of *M. tuberculosis* in response to rhIFN- γ (Imukin, Boehringer Ingelheim, Vienna, Austria) treatment in vitro, as previ-

ously described.⁷ MDMs from the patient displayed a normal capacity to phagocytose *M. tuberculosis* in comparison to healthy controls (Fig. 2A), which was not significantly increased by rhIFN- γ . However, MDMs from the patient failed to inhibit the proliferation of *M. tuberculosis*, a functional defect that was improved in the presence of rhIFN- γ (Fig. 2B).

3 | DISCUSSION

Here, we report a patient with XL-EDA-ID phenotype who developed infections early in life, including severe BCGitis. BCG complications, ranging from regional lesions to disseminated and life-threatening infections, can be developed by patients with XL-EDA-ID, or other PIDs, including severe combined immunodeficiency, chronic granulomatous disease, CD40L deficiency, and defects of the IL-12/IFN- γ axis.⁸ The incidence of mycobacterial infections in NEMO deficiency, usually by atypical mycobacteria, has been reported in 39% of patients with hypomorphic mutations.⁹ However, the actual incidence of BCG complications in NEMO deficiency in Latin America is unknown. For this propose, the expansion of specialized centers is required to enable NEMO sequence analysis in Brazil and other countries¹⁰ where BCG vaccine is routinely administered.

The clinical spectrum of patients with hypomorphic *NEMO* mutations is hugely diverse, hindering our ability to determine a precise genotype-phenotype correlation. Approximately 80 different phenotypes with 32 different *NEMO* mutations have been described so far, of which only 77% developed EDA-ID while others developed EDA-independent immunodeficiency. The former is the case of our patient whose XL-EDA-ID phenotype was associated with defective I κ B- α degradation due to a novel missense mutation. The p.H413P substitution is located within the zinc finger domain of NEMO, a hotspot mutation region.¹¹

Because of the pleiotropic role of NF- κ B in the immune system, patients with NEMO deficiency develop multiple immunopathological defects.¹² The impaired ability to control the proliferation of *M. tuberculosis* by patient-derived MDMs suggests a novel mechanism

that induces increased susceptibility to mycobacterial infections in XL-EDA-ID. The cytokine rhIFN- γ is able to activate phagocytes and has been used successfully to treat patients with chronic granulomatous disease. In accordance, rhIFN- γ improved the defective control of *M. tuberculosis* proliferation by MDMs from our NEMO-deficient patient. Taking together, our data suggest that rhIFN γ can be an adjunctive therapeutic option for NEMO-deficient patients. In contradiction, previous work with a single NEMO-deficient patient reported that the patient remained chronically ill despite adjuvant rhIFN- γ treatment.¹³ This fact indicates that in vivo rhIFN- γ is not able to compensate for the multiple immunological functions affected in NEMO deficiency. However, studies with a greater number of patients are required to demonstrate the clinical effect of rhIFN- γ in patients with different NEMO mutations.

In conclusion, our data expand the genetic spectrum of NEMO deficiency and highlight the important role of NF- κ B signaling in the immune response of macrophages against *M. tuberculosis*.

ACKNOWLEDGMENTS

This study was supported by Fundação de Amparo a Pesquisa do Estado de São Paulo (FAPESP) and the Conselho Nacional de Desenvolvimento Científico e Tecnológico (CNPq). We thank Dr. Jing Sun from the Institute for Systemic Inflammation Research, University of Lübeck for proofreading.

CONFLICT OF INTEREST

The authors declare that there is no conflict of interest.

ABBREVIATIONS

BCG	bacillus Calmette–Guérin
IFN- γ	interferon-gamma
MDMs	monocyte-derived macrophages
XL-EDA-ID	X-linked ectodermal dysplasia with immunodeficiency

REFERENCES

- Hanson EP, Monaco-Shawver L, Solt LA, et al. Hypomorphic nuclear factor-kappaB essential modulator mutation database and reconstitution system identifies phenotypic and immunologic diversity. *J Allergy Clin Immunol*. 2008;122:1169–1177.e16.
- Picard, C., Casanova, J.L., Puel, A., Infectious diseases in patients with IRAK-4, MyD88, NEMO, or IkappaBalpha deficiency. *Clin Microbiol Rev*. 2011;24:490–497.
- Gutierrez, M.G., Mishra, B.B., Jordao, L., Elliott, E., Anes, E., Griffiths, G., NF-kappa B activation controls phagolysosome fusion-mediated killing of mycobacteria by macrophages. *J Immunol*. 2008;181:2651–2663.
- Yamada, H., Relative importance of mycobacterial infection, p50 in NF-B. *Infect Immun*. 2001;69:7100–7105.
- Caamaño, J., Hunter, C.A., NF-kappaB family of transcription factors: central regulators of innate and adaptive immune functions. *Clin Microbiol Rev*. 2002;15:414–429.
- Gao, X.F., Yang, Z.W., Li, J., Adjunctive therapy with interferon-gamma for the treatment of pulmonary tuberculosis: a systematic review. *Int J Infect Dis*. 2011;15:e594–e600.
- Esquivel-Solis, H., Quinones-Falconi, F., Zarain-Herzberg, A., Amieva-Fernandez, R.I., Lopez-Vidal, Y., Impaired activation of Stat1 and c-Jun as a possible defect in macrophages of patients with active tuberculosis. *Clin Exp Immunol*. 2009;158:45–54.
- Lammas, D.A., Casanova, J.L., Kumararatne, D.S., Clinical consequences of defects in the IL-12-dependent interferon-gamma (IFN-gamma) pathway. *Clin Exp Immunol*. 2000;121:417–425.
- Norouzi, S., Aghamohammadi, A., Mamishi, S., Rosenzweig, S.D., Rezaei, N., Bacillus Calmette–Guérin (BCG) complications associated with primary immunodeficiency diseases. *J Infect*. 2012;64:543–554.
- Cabral-Marques, O., Klaver, S., Schimke, L.F., et al., First report of the hyper-IgM syndrome registry of the Latin American Society for immunodeficiencies: novel mutations, unique infections, and outcomes. *J Clin Immunol*. 2014;34:146–156.
- Fusco, F., Pescatore, A., Bal, E., et al., Alterations of the IKBKG locus and diseases: an update and a report of 13 novel mutations. *Hum Mutat*. 2008;29:595–604.
- Niehues, T., Reichenbach, J., Neubert, J., et al., Nuclear factor kappaB essential modulator-deficient child with immunodeficiency yet without anhidrotic ectodermal dysplasia. *J Allergy Clin Immunol*. 2004;114:1456–1462.
- Errante, P.R., Frazao, J.B., Condino-Neto, A., The use of interferon-gamma therapy in chronic granulomatous disease. *Recent Pat Antiinfect Drug Discov*. 2008;3:225–230.

SUPPORTING INFORMATION

Additional Supporting Information may be found online in the supporting information tab for this article.

APÊNDICE I – Synthesis, cytotoxic activity on leukemia cell lines and quantitative structure-activity relationships (qsar) studies of morita-baylis-hillman adducts.
Medicinal Chemistry, 2016

RESEARCH ARTICLE

Synthesis, Cytotoxic Activity on Leukemia Cell Lines and Quantitative Structure-Activity Relationships (QSAR) Studies of Morita-Baylis-Hillman Adducts



Claudio G. Lima-Junior¹, Gláucia V. Faheina-Martins², Caio C. B. Bomfim², Bruna B. Dantas², Everton P. Silva¹, Demetrius A. M. de Araújo², Edilson B. A. Filho³ and Mário L. A. A. Vasconcellos^{1,*}

¹Laboratório de Síntese Orgânica Medicinal da Paraíba (LASOM-PB), Departamento de Química, Universidade Federal da Paraíba, Campus I, João Pessoa, PB 58059-900, Brazil; ²Laboratório de Biotecnologia Celular e Molecular, Departamento de Biotecnologia, Centro de Biotecnologia, Universidade Federal da Paraíba, Campus I, João Pessoa, PB 58059-900, Brazil; ³Colegiado Acadêmico do Curso de Ciências Farmacêuticas, Universidade Federal do Vale do São Francisco, Campus Petrolina-Centro, Petrolina, PE 56306-000

Abstract: Background: The Morita-Baylis-Hillman reaction is an organocatalyzed chemical transformation that allows access to small poly-functionalized molecules and has considerable synthetic potential and promising biological profiles. The Morita-Baylis-Hillman adducts (MBHA) are a new class of bioactive compounds and highlight its potentialities to the discovery of new cheaper and efficient drugs, e.g. as anti-*Leishmania chagasi* and *Leishmania amazonensis*, anti-*Trypanosoma cruzi*, anti-*Plasmodium falciparum* and *Plasmodium berghei*, lethal against *Biomphalaria glabrata*, antibacterial, antifungal, herbicide and others.

Methods: The goal of this work is to describe the primary cytotoxic activities against strains of human leukemia HL-60 cell line for thirty-four Morita-Baylis-Hillman adducts (MBHA), followed by a Quantitative Structure-Activity Relationships study (QSAR).

Results: The conventional or microwave-assisted syntheses of MBHA, derived from substituted aromatics or Isatin, were performed in good to excellent yields (70-100%) in short reaction times, using protocols recently developed by us. Isatin derivatives, MBHA 31 and 32, were the most active in this congener series of compounds, with IC₅₀ values of 10.8 μM and 7.8 μM, respectively. The primary cytotoxic activities against chronic leukemia cells (K562) were also evaluated to these two most active compounds (MBHA 31 and 32), presenting IC₅₀ values of 53 μM and 43 μM respectively. QSAR study was performed considering 3D, 2D and constitutional molecular descriptors. These were selected from Ordered Predictor Selection algorithm and submitted to Partial Least Squares Modeling.

Conclusion: We present an interesting investigation about cytotoxic activities on human leukemia cell line (HL-60) for 34 synthetic MBHA. In a good way we discovered that the most cytotoxic compounds (31-32, 10.8 μM and 7.8 μM respectively) were also prepared quantitatively (100% yields) in a short reaction time using microwave irradiation. We demonstrate that 31 and 32 induced apoptosis and not necrosis in HL-60 cells, observed by externalization of PS and increase Annexin-V positive cells. Quantitative Structure-Activity Relationships considering 3D, 2D and constitutional descriptors provided a robust and predictive PLS model, in accordance with SAR observations.



Mário L. A. A. Vasconcellos

ARTICLE HISTORY

Received: March 05, 2015
Revised: April 19, 2016
Accepted: May 05, 2016

DOI:
10.2174/1573406412666160506150
924

Keywords: Morita-Baylis-Hillman adducts, cytotoxic activities, leukemia, QSAR.

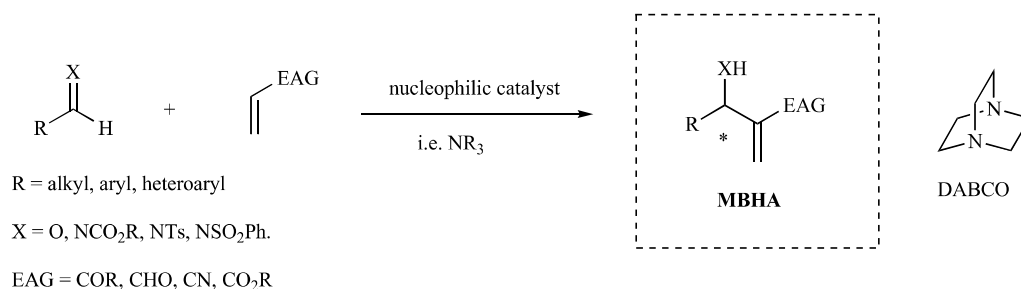
INTRODUCTION

The Morita-Baylis-Hillman reaction (MBHR) is one of the most synthetically valuable reactions for the construction

of densely functionalized products in a highly atom economic manner [1-3]. It involves alkenes coupling containing electron-withdrawing groups (EWG) using tertiary amines as nucleophilic catalysts, which of 1,4-diazabicyclo [2.2.2] octane (DABCO) is the most widely used (Scheme 1). The electrophiles used in the MBHR are mostly aldehydes and imines.

Over the past three decades, adducts obtained from the MBHR have served as handy synthons for the synthesis of

*Address correspondence to this author at the Laboratório de Síntese Orgânica Medicinal da Paraíba (LASOM-PB), Departamento de Química, Universidade Federal da Paraíba, Campus I, João Pessoa, PB 58059-900, Brazil; Tel: +55 83 3248 2352; Fax: +55 83 3216 7433; E-mail: mlaav@quimica.ufpb.br



Scheme 1. General Morita-Baylis-Hillman reaction.

various heterocycles and carbocycles [1]. Furthermore, Morita-Baylis-Hillman adducts (MBHA) also emerged as potential bioactive compounds by showing various biological activities [4].

Recently, MBHA have been described as anticancer compounds [5], and our research group published antimetabolic activity against sea urchin embryonic cells. Inhibition of cell division is a match point in cancer pharmacology [6].

Drug discovery is an area of research that demands high cost and comparatively long time to generate new chemicals entities. In the early stages of this process and to optimize the pharmacokinetic and/or pharmacodynamic profiles, Computer Assisted Drug Design (CADD) has shown a promising strategy, whether in structure or ligand-based drug design (molecular docking, virtual screening, Quantitative Structure-Activity Relationship - QSAR, among others) [7-9].

In connection with our continuing interest in organic synthesis of biological active MBHA [4], we prepared thirty-four aromatic MBHA using the same protocol described recently by us [10] (Fig. 1) in very good yields, and short reaction times. After this, we present *in vitro* cytotoxicity evaluations of all thirty-four MBHA (Figs. 2 and 3) against HL-60 human leukemia lines [11]. The more active compounds (**31** and **32**) were also tested against chronic leukemia cells (K562). Moreover, a Quantitative Structure-Activity Relationship (QSAR) model is presented to verify the influence of some molecular descriptors in MBHA cytotoxic activity, directing future synthesis of potentially most active analogues.

MATERIAL AND METHODS

Chemistry

General

All commercially available reagents and solvent were obtained from commercial providers and used without further purification. Reactions were monitored by TLC using Silica gel 60 UV254 Macherey-Nagel pre-coated silica gel plates and detection was made using an UV lamp. Flash column chromatography was performed on 300-400 mesh silica gel. Organic layers were dried over anhydrous MgSO₄ or Na₂SO₄ prior to evaporation on a rotary evaporator. Reactions requiring microwave irradiation were performed in a microwave reactor CEM[®] model system Discover benchmate with temperature monitored by built-in infrared sensor. ¹H NMR and

¹³C NMR spectra were recorded using Varian Mercury Spectra AC 20 spectrometer (200 MHz for ¹H, 50 MHz for ¹³C). Chemical shifts were reported relative to internal tetramethylsilane (δ0.00 ppm) for ¹H, using CD₃OD or DMSO-*d*₆ as solvent. FTIR spectra were recorded on a Shimadzu spectrophotometer model IRPrestige-21 in KBr pellets.

General Procedure for Synthesis of 1 – 30

Reactions were carried out using the corresponding aldehydes (0.5 mmol), acrylonitrile (0.2 mL, 3.1 mmol) or methyl acrylate (0.5 mL, 5.3 mmol) and DABCO (56 mg, 0.5 mmol) at 0 °C. After that, the reaction media was directly filtered through silica gel, using hexane/ethyl acetate (7:3) as solvent and the reaction products were concentrated under reduced pressure [10]. Molecules were obtained as racemic mixture.

General Procedure for Synthesis of 31 – 34 (Method A)

Isatin (73.5 mg, 0.5 mmol) or *N*-methylisatin (80.5 mg, 0.5 mmol), acrylonitrile or methyl acrylate, THF (1 mL) and DABCO (56 mg, 0.5 mmol) were placed in a 10 mL glass microwave tube with magnetic stirrer at 80 °C for the time indicated in Table 1. After completion, the mixture was concentrated under reduced pressure and the product was isolated from the crude reaction by column chromatography through silica gel, using EtOAc:hexane as solvent.

General Procedure for Synthesis of 31 - 34 (Method B)

To a stirred solution of isatin (73.5 mg, 0.5 mmol) or *N*-methylisatin (80.5 mg, 0.5 mmol) and acrylates **3a-3e** in THF (1 mL) was added DABCO (56 mg, 0.5 mmol) and stirred at room temperature for the time indicated in Table 1. After completion, the mixture was concentrated under reduced pressure and the product was isolated from the crude reaction by column chromatography through silica gel, using EtOAc:hexane as solvent.

General Procedure for Synthesis of 31 - 34 (Method C)

To a stirred solution of isatin (73.5 mg, 0.5 mmol) or *N*-methylisatin (80.5 mg, 0.5 mmol) and acrylates in THF (1 mL) was added DABCO (56 mg, 0.5 mmol) and stirred at 0 °C for the time indicated in Table 1. After completion, the mixture was concentrated under reduced pressure and the product was isolated from the crude reaction by column chromatography through silica gel, using EtOAc:hexane as solvent.

2-(3-hydroxy-2-oxindolin-3-yl)acrylonitrile (**31**): IR (KBr): 3348, 3264, 2226, 1708, 1620, 1474 cm⁻¹; ¹H NMR

(200 MHz, DMSO-*d*₆): δ 10.67 (s, 1H); 6.86-7.32 (m, 4H); 6.32 (s, 1H); 6.21 (s, 1H). ¹³C NMR (50 MHz, DMSO-*d*₆): δ 175.2, 142.0, 132.1, 130.4, 129.0, 124.5, 122.8, 122.4, 116.3, 110.3, 76.1.

2-(3-hydroxy-1-methyl-2-oxoindolin-3-yl)acrylonitrile (32): IR (KBr): 3306, 2229, 1713, 1620 cm⁻¹; ¹H NMR (200 MHz, DMSO-*d*₆): δ 7.09-7.47 (m, 4H); 6.36 (d, *J* 3.2 Hz, 1H); 6.23 (d, *J* 3.4 Hz, 1H); 3.17 (s, 3H). ¹³C NMR (50 MHz, DMSO-*d*₆): δ 173.5, 143.3, 132.5, 130.7, 128.4, 124.3, 123.2, 122.6, 116.3, 109.4, 75.8, 26.2.

Methyl 2-(3-hydroxy-2-oxoindolin-3-yl)acrylate (33): IR (KBr): 3421, 3232, 1717, 1697, 1620, 1470 cm⁻¹; ¹H NMR (200 MHz, CD₃OD): δ 6.88-7.28 (m, 4H); 6.57 (s, 1H); 6.53 (s, 1H); 3.54 (s, 3H). ¹³C NMR (50 MHz, CD₃OD): δ 180.5, 166.4, 144.2, 141.1, 132.7, 130.9, 128.1, 124.6, 123.4, 111.3, 77.3, 52.2.

Methyl 2-(3-hydroxy-1-methyl-2-oxoindolin-3-yl)acrylate (34): IR (KBr): 3225, 1716, 1697, 1616, 1496 cm⁻¹; ¹H NMR (200 MHz, DMSO-*d*₆): δ 7.26-7.35 (m, 1H); 6.93-7.04 (m, 3H); 6.46 (d, *J* 1.2 Hz, 1H); 6.44 (d, *J* 1.2 Hz, 1H); 3.48 (s, 3H), 3.13 (s, 3H). ¹³C NMR (50 MHz, DMSO-*d*₆): δ 180.6, 169.6, 149.7, 144.9, 136.0, 134.7, 132.5, 128.1, 127.2, 113.7, 80.1, 56.9, 31.2.

Pharmacology

Cell Culture

Human promyelocytic leukemia (HL-60) cell line was acquired from Rio de Janeiro Cell Bank (Federal University of Rio de Janeiro, RJ, Brazil). Leukemia cells were maintained in RPMI 1640 medium supplemented with 10% FBS, 2 mM glutamine, 100 U/ml penicillin, and 100 µg/ml streptomycin at 37°C with 5% CO₂.

MTT Assay

The cytotoxicity of compounds to leukemic cells was evaluated using the original enzymatic reduction of 3-(4,5-dimethylthiazol-2-yl)-2,5-diphenyltetrazolium bromide (MTT) assay to produce formazan crystals [12]. The MTT viability assay is a widely used method to evaluate cancer cells chemosensitivity and antiproliferative capacity. Cells were seeded at 5 × 10⁴ cells/well in 96-well tissue culture plates and were exposed to different concentrations (from 3 to 100 µM), which were dissolved in the RPMI medium (three wells per concentration) with 10% FBS. After 24 hours of incubation, plates were centrifuged (500 × *g*, 5 min) and the supernatant was removed, followed by the addition of MTT solution (0.5 mg/mL in PBS) and incubation at 37°C. After 3 hours, the MTT formazan product was dissolved in SDS/HCl 0.01N and absorbance was measured at 570 nm in reader plate ELISA (Biotek ELx800, USA).

QSAR Studies

A Quantitative Structure–Activity Relationship (QSAR) approach was performed. The objective was to find out a model to relate some molecular descriptors to the cytotoxic activity of MBHA, and guide future syntheses seeking more promising optimized compounds [13]. Molecular descriptors

are numerical values that describe structure or shape of molecules, some of which can be directly related to activity of analogous series [14, 15]. For our QSAR studies, about 1,666 descriptors were generated using E-Dragon online platform [13]. The E-Dragon descriptors are subdivided into 20 logical blocks, representing constitutional, topological, 2D autocorrelations, 3D descriptors among others [16].

Preparation of Data Set

For holding QSAR approach, initially 3D geometries of the compounds were constructed using GaussView5[®] [17] and submitted to a Relaxed Potential Energy Surface Scan (RPESS) using Gaussian09W[®] software [18] at AM1 semiempirical level [19]. The RPESS procedure consists to select rotational degrees of freedom (sigma bonds), which are submitted to variations on dihedral angles (10° to 360°). At each step of 10° the angle is fixed and the remained portion of molecule is optimized. The objective of RPESS approach is to generate curves of energy to find out the most stable geometries on conformational equilibrium. After this step, the most stable conformational minima for each MBHA was selected and completely optimized on *ab initio* Hartree-Fock 6-31+(d) level of calculation. 3D geometries were then converted to .sdf format and used on E-Dragon platform to calculate molecular descriptors.

After E-Dragon calculations, a matrix with 34 compounds and about 1,666 descriptors was generated. The values of IC₅₀ obtained for HL-60 were converted to –LogIC₅₀ (pIC₅₀) to reduce the standard deviation and conveniently the highest values correspond to the most active compounds [13]. These large numbers of generated data were reduced using a selection variable method. In this step, the Ordered Predictor Selector (OPS) algorithm was applied using QSAR modeling program [20]. The essence of OPS consists in sorting the most important variables for an initial informative vector (correlogram, regression coefficients, etc.) and to investigate these ordered variables from the most relevant [21]. Thus, Partial Least Squares (PLS) regression models [22] are systematically constructed from an initial window of most relevant variables and incremented by others less relevant. At each step, quality parameters are evaluated (Standard Deviation of Prediction Error Sum of Squares – SPRESS, Coefficient of Determination for Cross-Validation Q², etc.) [21] and finally, models are presented in order of the best parameters. Our research group has successfully used the OPS-PLS methodology in the development of QSAR models [13, 23].

PLS analysis is a regression method which allows working with large number of variables, including correlated. The initial matrix is reduced to a fewest factors (latent variables) similar to Principal Component Analysis (PCA) scheme, but during this construction the best correlations between dependent and independent variables are searched [22]. An important step on PLS method applied to QSAR is the pre-treatment of variables, where the autoscaling is commonly applied [24].

After a general OPS procedure, 17 variables were selected as the most relevant to activity of MBHA. The 34 compounds were then subdivided in training and test sets, being 27 corresponding to training and 7 to test (20%). The

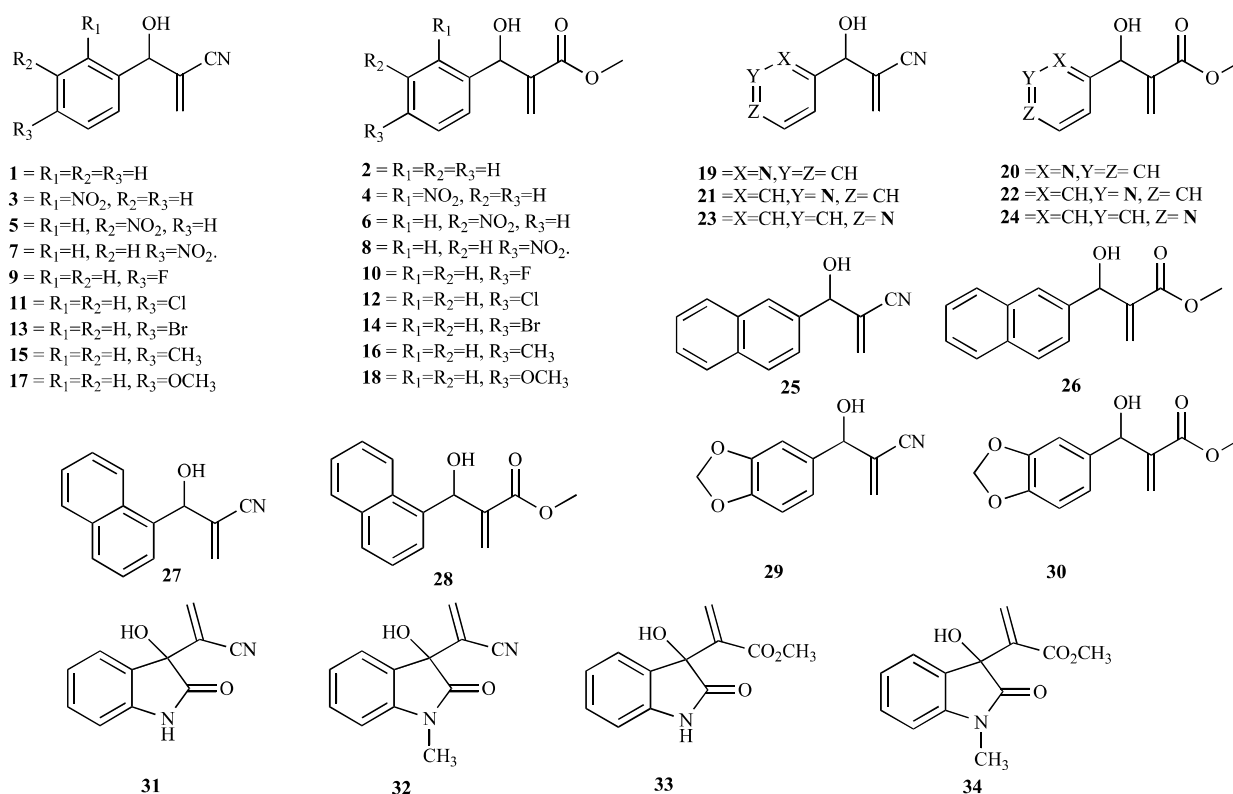


Fig. (1). Structures of thirty-four AMBH studied in this work.

test set was chosen to represent the variability of structural and activity of different analogues and corresponds to **7**, **12**, **18**, **22**, **23**, **27**, and **28**. These compounds were used in external validation step. Considering observations about the importance of presence of nitrile and nitro group on MBHA analogues (results and discussion about cytotoxicity), the fragment based descriptors to CN and NO₂ (where 1 means presence and 0 absence of these groups) were included, totalizing 19 descriptors. The training set was submitted to a new OPS variable selection and the matrix were reduced to 7 descriptors, representing tridimensional aspects, 2D autocorrelations and constitutional characteristics.

Calculation of Validation Parameters

A QSAR study needs parameters certifying the quality of the model. The Validation parameters used are: Root Mean Square Error for Cross Validation (RMSECV), Coefficient of determination for calibration (R^2), for leave-one-out cross validation (Q^2_{loo}) and leave-n-out cross validation (Q^2_{lno}), Y-scrambling [24, 25].

The RMSECV values were used to choose the number of Latent Variables (LV) of final PLS modeling. This parameter is calculated from the following equation:

$$RMSECV = \sqrt{\frac{\sum (y_i^{prev} - y_i^{exp})^2}{n}}$$

where y_i^{prev} is the activity forecast for the sample "i" with the built model without this sample, and y_i^{exp} matches the experimental value (true) activity.

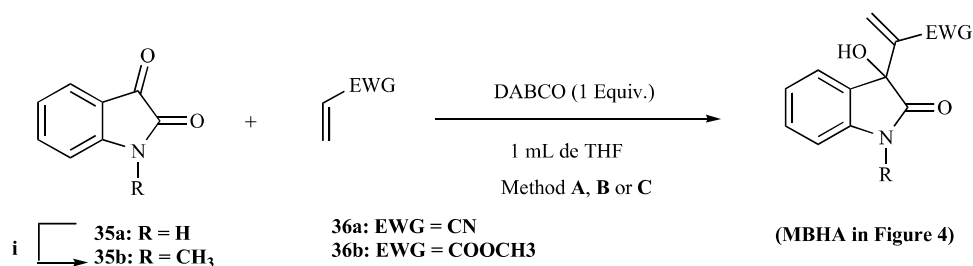
The R^2 and generic Q^2 parameters are calculated from the expression:

$$R^2 \text{ or } Q^2 = 1 - \frac{\sum (y_i^{exp} - y_i^{prev})^2}{\sum (y_i^{exp} - y_i^{mean})^2}$$

where y_i^{mean} is the mean of the experimental data. The difference is that in R^2 all samples used in the model building are used in the forecasts. In Q^2_{loo} , a sample is taken every construction stage model and forecast the value of this sample. Q^2_{lno} , in turn, is calculated by taking "n" samples of each construction, calculating its value.

For leave-n-out internal validation, after choosing the optimal number of LV, QSAR modeling program allows to generate different M/n block of test samples for each "n" (where M is a total number of compounds in training set), initialing with n = 2 until a specified number (in general 30% of compounds) [26]. Thus, in this procedure, we generated ten values of Q_{lno}^2 (with different compounds in each M/n blocks) to each eight values of "n" (2-9, max. 30%). The mean for ten values to each "n" may be close to the value of Q_{loo}^2 and not present a deviation greater than 0.1 [26].

Y-scrambling was performed to test the possibility of chance correlations between the dependent variable and selected descriptors. This procedure consists in developing parallel models with the values of descriptors maintained and the values of dependent variable exchanged. If a true correlation exists, the value of R^2 and Q^2_{loo} must be higher than values of parallel models. In general, models with exchanged Y should have R^2 and Q_{loo}^2 values less than 0.4 [26].



Scheme 2. i- (a) NaH, DMF (b) CH₃I (100%); MBHR between Isatin (**35a**) or *N*-Methylisatin (**35b**) and Michael acceptors **36a–b** under **A**, **B** or **C** methods; method **A**: Mw irradiation, 80 °C; method **B**: conventional room temperature; method **C**: conventional 0 °C, as described on Table 1.

Table 1. Preparation of MBHA from isatin (35a) or *N*-Methylisatin (35b) under microwave irradiation or conventional condition.

Entry	MBHA	Time/ Isolated Yields (%)		
		Microwave Reaction Method A ^a	Room Temperature Method B ^b	0 °C Method C ^c
1	31 ^d	20 min. / 100	150min. / 100	300min. / 100
2	32 ^d	45 min. / 100	90 min. / 95	90min. / 96
3	33 ^e	60 min. / 78	18 h / 93	18 h / 62
4	34 ^e	120 min. / 24 (73) ^f	5 days / 93	6 days / 85

^aThe reactions were carried out at 80 °C under microwave irradiation; ^bThe reactions were carried out at conventional room temperature; ^cThe reactions were carried out at conventional 0°C; ^dExcess of Michael acceptors were used as reagent and solvent (0.2 mL, 3.1 mmol); ^eExcess of Michael acceptors were used as reagent and solvent (0.5 mL, 5.3 mmol); ^fYield obtained by microwave irradiated at 120 °C, using 1 mL of dioxane;

RESULTS AND DISCUSSION

Chemistry

Initially, thirty aromatics MBHA **1–30** (Fig. 1) were prepared using the same procedures recently described by us [10].

In sequence, *N*-Methylisatin was prepared by reacting Isatin (**35a**) with NaH in dry DMF as solvent followed by addition of methyl iodide, producing **35b** in quantitative yield (Scheme 2). Thereafter, three different methods (A, B or C) were investigated to prepare the four MBHA shown in Fig. 1 (see Scheme 2 and Table 1).

Some aspects of reactions shown in Table 1 deserve comments. Initially, we noticed that the MBH reactions with isatin (**35a**) or with *N*-Methylisatin (**35b**) are faster and occurs in quantitative yield when acrylonitrile is the Michael acceptor (Entry 1 and 2 versus 3 and 4). Another point to emphasize is that use of microwave irradiation was effective for all reactions. These reactions were also successfully performed at low temperature (0°C). In accordance with the unified mechanism presented by Cantilo and Kappe [27] and supported by our research group results [10], the reversibility on the MBH reaction is temperature dependent. We believe that in these cases, lowering temperature prevents reaction reversibility, leading efficiently to products. Another relevant point to notice is that in all cases shown in Table 1, the reactions with isatin (**35a**) are faster than reactions with *N*-Methylisatin (**35b**) (see Table 1). Cantilo & Kappe also emphasized in their unified mechanism article [27] that when

phenol (pKa=10) is present as additive on reaction, there is a significant acceleration on the MBH reaction. They proposed that phenol makes the hydrogen transfer to be a fast-step in the mechanistic cycle of reaction. In this case, the aldol addition becomes a slow-step reaction in this mechanism [27]. Considering that the acidic hydrogen of isatin (pKa=10.34) is as acid as the acidic hydrogen of phenol (**35a**), we propose that it may also serve as a hydrogen donor, accelerating reactions.

Cytotoxic Activity

The cytotoxic activities of all MBHA were first evaluated on human promyelocytic leukemia (HL-60) cell line using the original enzymatic reduction of 3-(4,5-dimethylthiazol-2-yl)-2,5-diphenyltetrazolium bromide (MTT) assay to produce formazan crystals [28]. The results are shown in Table 2.

It is observed that most MBHA presenting the nitrile group (CN) are more active than the analogous carboxymethylester. In addition, MBHA showing the nitro substituent on the aromatic ring are significantly more active (**3–8**). Adducts presenting α -naphthyl, β -naphthyl substituents also show a low IC₅₀ (**25–28**). Adducts where the aromatic rings are unsubstituted (**1–2**), presenting CH₃ (**16–17**) and oxygen substituents (**29–30**) have higher IC₅₀ values. In general the trend of structure–activity relationships obtained in this work is in accordance with what was reported by Kohn *et al.* [5].

Continuing the analysis of table data, we can also observe that the compounds **31**, **32**, **33** and **34**, which are the

Table 2. Cytotoxic effects of aromatics MBHA on HL-60 cells.

MBHA	IC ₅₀ (μM)	MBHA	IC ₅₀ (μM)
1	103.5	18	106.2
2	158.3	19	250.3
3	24.3	20	131.8
4	45.7	21	88.10
5	17.3	22	159.1
6	39.4	23	73.7
7	22.4	24	63.4
8	29.1	25	16.4
9	74.1	26	30.6
10	105.9	27	25.4
11	213.8	28	30.3
12	40.3	29	103.9
13	27.2	30	125.2
14	73.8	31	10.8
15	104.9	32	7.8
16	120.9	33	69.6
17	143.1	34	69.0

Table 3. Effect of compounds 31 and 32 on the growth of cell lines by 24 hours.^a

Cell Line	31	SI	32	SI
HL-60	10.8	12.3	7.8	14.4
K562	53	2.5	43	2.6
MCF-7	65.7	2.0	61.1	1.8
HT-29	199	0.7	133	0.8
L-929 ^b	133	-	112	-

^aResults are reported as IC₅₀ values (concentration required to inhibit cell growth by 50%) values in micromolar. Data represent the means of three independent experiments, with each concentration tested in triplicate. ^bNon tumorigenic cell line. SI = selective index.

only ones with a 3-hydroxy-oxindole scaffold, proved to be cytotoxic on the tumoral cell line. In this sense, this study highlights the largest activity of **31** and **32**, which the nitrile group is present in contrast of carboxymethylester. The importance of the 3-hydroxy-oxindole architecture has been demonstrated in the recent literature [29, 30], displaying diverse activities such as potent antioxidant, anticancer, anti-HIV, and neuroprotective properties. Thus, the novel activities shown by MBHA based on 3-hydroxy-oxindoles privileged scaffold represent promising results. Additionally there is a wide variety of literature describing the bioactivities of isatin derivatives [31, 32].

The most bioactive compounds under HL-60 cell line (MBHA **31** and **32**) were also evaluated other Multidrug-resistant Cell Line. The results are present in Table 3. Although the compounds were not as effective as expected in this point, the rationalization of presented activities, especially data set of thirty-four compounds in HL-60, may lead to the design and synthesis of more promising future analogues.

Induction of Apoptosis

This method is used as a good anti-cancer strategy. It is well known that the externalization of phosphatidylserine (PS) is early events leading to apoptosis. Then, it was investigated whether compounds incubated with HL-60 cells for 24 h were able to induce apoptosis. We demonstrate that the most active compounds **31** and **32** induced apoptosis and not necrosis in HL-60 cells, observed by externalization of PS and increase Annexin-V positive cells (Fig. 2).

QSAR Studies

The selected descriptors by OPS method and values of pIC₅₀ for all 34 compounds are shown in Table 4.

The best number of LV for PLS modelling was 3, based on RMSECV, R² and Q²₁₀₀ values (Table 5). These last two validation parameters fulfill what is expected of a good QSAR model. The regression vector to selected PLS model, considering original non scaling variables [33], can be visualized in equation (1).

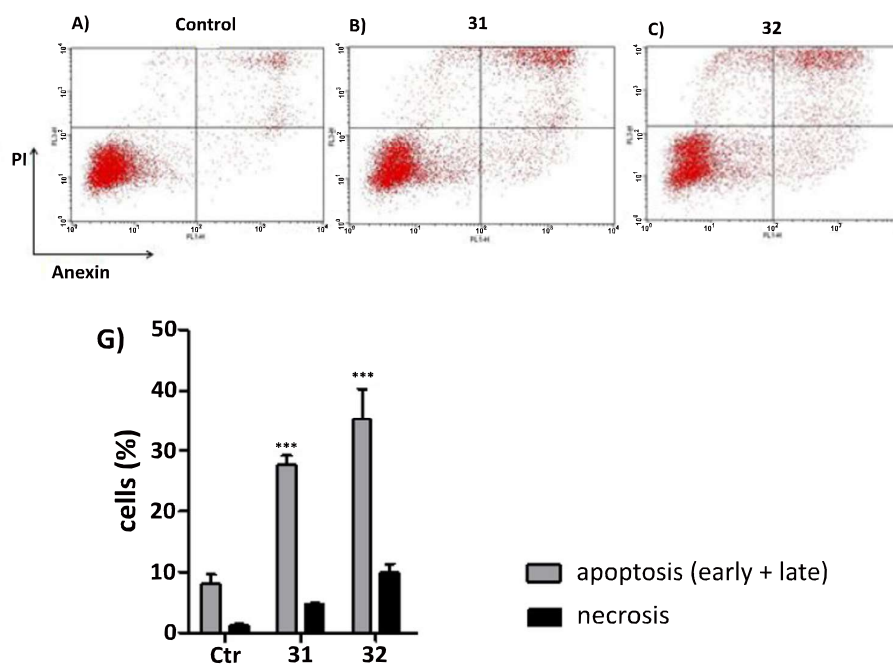


Fig. (2). AMBH molecules (31-32) inducing apoptosis in HL-60 cells after 24 hours. Representative dotplots of cells double stained with annexin V-FITC/PI double. Cells (5×10^5 per well) were treated with respective IC_{50} for 24 h washed with PBS and stained with annexin V-FITC/PI for flow cytometry analysis. In the control cells without any treatment (A). Treatment with adducts **31** 10 μ M (B), **32** 8 μ M (C). In graph (G) data shown represent means \pm SEM of three different experiments done in duplicate. The dates were analyzed by ANOVA followed posttest Newman Keuls. ** $p < 0.01$, *** $p < 0.001$ versus the control.

Table 4. pIC_{50} values and molecular descriptors selected after OPS algorithm.

MBHA	pIC_{50}	RDF065u	RDF025v	NO2	E2m	R4p	nN	R6u+
1	3.99	1.418	9.007	0	0.389	0.491	1	0.062
2	3.80	5.911	9.51	0	0.273	0.476	0	0.044
3	4.61	1.151	9.802	1	0.493	0.55	2	0.082
4	4.34	6.888	10.305	1	0.32	0.529	1	0.06
5	4.76	3.641	9.865	1	0.311	0.49	2	0.052
6	4.40	7.101	10.489	1	0.206	0.498	1	0.041
7	4.65	2.544	10.003	1	0.374	0.534	2	0.058
8	4.53	3.123	8.532	1	0.196	0.508	1	0.043
9	4.13	1.126	8.846	0	0.321	0.486	1	0.062
10	3.97	4.656	11.057	0	0.246	0.468	0	0.043
11	3.67	2.534	8.694	0	0.268	0.515	1	0.062
12	4.39	3.791	10.845	0	0.191	0.498	0	0.043
13	4.57	1.25	8.669	0	0.175	0.533	1	0.063
14	4.13	4.427	9.281	0	0.11	0.519	0	0.043
15	3.98	3.003	10.864	0	0.37	0.53	1	0.06
16	3.92	7.901	11.401	0	0.263	0.515	0	0.042
17	3.84	4.487	9.776	0	0.318	0.533	1	0.057
18	3.97	9.792	10.263	0	0.217	0.517	0	0.04

Table 4. contd...

MBHA	pIC ₅₀	RDF065u	RDF025v	NO2	E2m	R4p	nN	R6u+
19	3.60	3.56	6.515	0	0.365	0.464	2	0.069
20	3.88	3.994	7.212	0	0.245	0.452	1	0.049
21	4.05	0.656	7.498	0	0.387	0.484	2	0.069
22	3.79	4.736	8.865	0	0.287	0.464	1	0.051
23	4.13	0.668	8.133	0	0.357	0.5	2	0.06
24	4.19	5.19	8.163	0	0.266	0.481	1	0.046
25	4.78	6.273	15.05	0	0.293	0.516	1	0.048
26	4.51	7.373	15.76	0	0.249	0.54	0	0.041
27	4.59	4.647	15.222	0	0.199	0.533	1	0.05
28	4.52	11.271	15.653	0	0.184	0.589	0	0.038
29	3.98	6.607	9.561	0	0.328	0.525	1	0.056
30	3.90	9.444	9.999	0	0.248	0.492	0	0.044
31	4.97	1.285	9.705	0	0.277	0.635	2	0.059
32	5.11	2.1	12.282	0	0.176	0.626	2	0.041
33	4.16	4.727	10.387	0	0.327	0.574	1	0.049
34	4.16	7.074	12.552	0	0.257	0.596	1	0.045

Table 5. Some validation parameters of PLS modeling.

N° LV	RMSECV	R ²	Q ₁₀₀ ²
1	0.2603	0.73	0.55
2	0.2213	0.78	0.67
3	0.2287	0.80	0.65
4	0.2306	0.81	0.64
5	0.2355	0.81	0.63
6	0.2377	0.81	0.62
7	0.2384	0.81	0.62

$$pIC_{50} = -0.052(RDF065u) + 0.078(RDF025v) + 0.423(NO2) - 1.497(E2m) + 2.269(R4p) + 0.219(nN) - 5.806(R6u+) + 2.918 \quad (1)$$

The leave-n-out cross validation results are present in (Fig. 3). As can be observed, the graphic profile satisfies the acceptance criteria for this evaluation parameter.

The Y-scrambling for the best OPS-PLS model shows that the model presents tolerable chance correlation (Fig. 4). The graph was construct considering 50 randomizations.

External validation considering test set showed a $Q_{ext}^2 = 0.88$ (coefficient of determination for external validation) which indicates, together with other internal validation procedures, that a robust and predictive QSAR model was obtained.

The main goal of QSAR modeling is to rationalize the structure-activity relationships, providing a mathematical model which allows predicting the trend of activity for a compound not tested, knowing only the molecular descriptors, as well as to visualize the general influence of each descriptor on activity. However, interpreting a QSAR model in terms of the specific contribution of substituents and other molecular features is always a difficult work [34]. The 7 descriptors selected in this work, which proved to be important for the cytotoxic activity, are described below.

RDF065u: Radial Distribution Function unweighted, a 3D descriptor. The Radial Distribution Function (RDF) of an ensemble of A atoms can be interpreted as the probability distribution of finding an atom in a spherical volume of radius r , weighted or not by an atomic property [35, 36]. The equation that represents the Radial Distribution Function is:

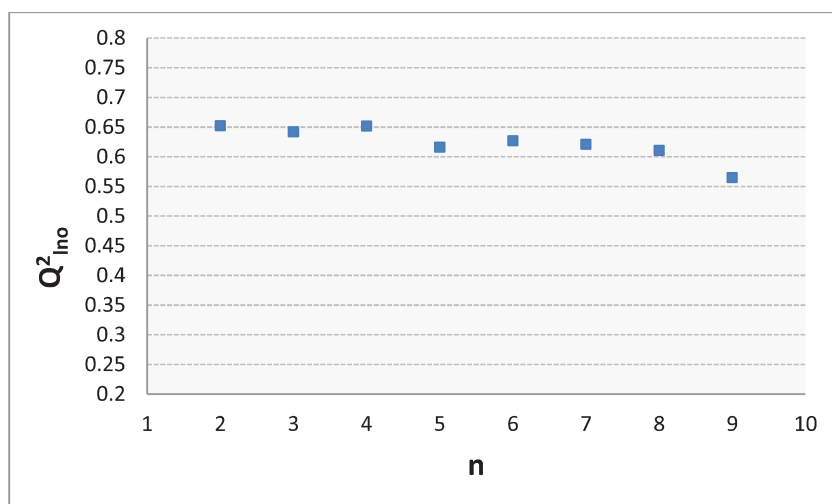


Fig. (3). Results of Leave-n-out cross validation.

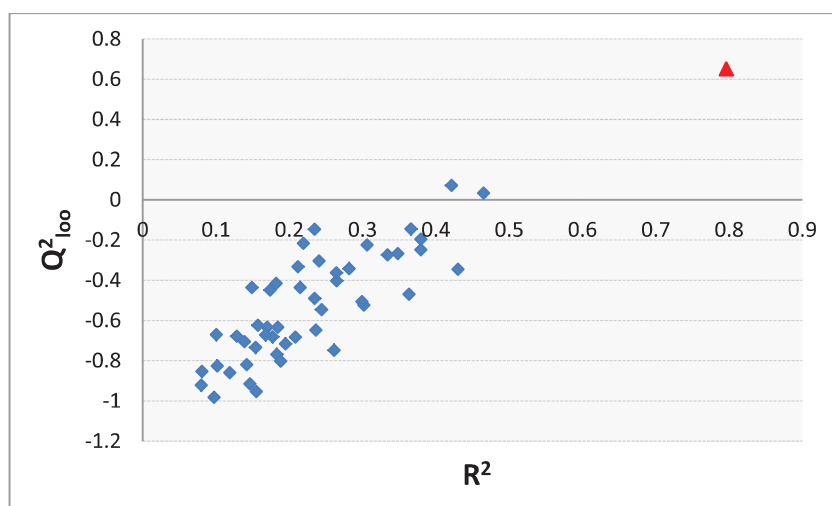


Fig. (4). Results of Y-scrambling (Red triangle corresponds to values of original model).

$$RDF(rw) = f \sum_{i=1}^{A-1} \sum_{j=1}^A w_i w_j e^{-B(r-r_{ij})^2} \quad (2)$$

where f is a scaling factor and A is the number of atoms. By including characteristic atomic properties w of the atoms i and j , the RDF codes can be used in different tasks to fit the requirements of the information to be represented. The exponential term contains the distance r_{ij} between the atoms i and j and the smoothing parameter B , which defines the probability distribution of the individual distances [34]. A typical RDF descriptor is denoted by $RDFrw$, where r take the values $1.0 \leq r \leq 15.5$ in units of 0.5 \AA and w denotes an atomic property as mass (m), van der waals volume (v), polarizability (p) or unweighted (u). As can be seen in Table 4 and molecular representations, MBHA with CO_2CH_3 moiety have highest values of $RDF065u$. This descriptor contributes negatively to pIC_{50} value. Since no property of atoms is considered (unweighted), in general we can interpret that this property is related directly with presence of CO_2CH_3 group impairing the activity, in accordance with previous SAR observations.

RDF025v: Radial Distribution Function weighted by van der Waals volume. This differs from previous about the sphere radius (2.5) and weighting (v). In general higher values enhance the activity. Thus, specific contribution of this descriptor can be interpreted as atoms near with highest van der waals volumes to enhance the cytotoxic activity (**3**, **4**, **31**, and **32**).

E2m: 2nd component accessibility directional WHIM index / weighted by mass. WHIM descriptors are based on the statistical indices calculated on the projections of atoms along principal axes [37, 38]. They are built in such a way as to capture relevant molecular 3D information regarding the molecular size, shape, symmetry, and atom distribution. The algorithm consists of performing a Principal Components Analysis on the centered Cartesian coordinates of a molecule by using a weighted covariance matrix obtained from different weighting schemes for the atoms (mass, van der Waals volumes, etc.) [37]. Mathematically WHIM accessibility descriptors calculated as $Emw = 1/km$, where m is principle axes ($m = 1, 2, 3$), w is weighting scheme and k is Kurtosis value. Kurtosis values are related to the atom distribution

and density around the origin and along the principal axes. [39]. Thus E2m related to the quantity of unfilled space in atomic masses term per projected atom in 2nd principle axes. In general, a highest value of E2m decrease pIC50 and reveals that branched and dense substitution at 2nd principle axes favor for the activity.

R4p: R autocorrelation of lag 4 / weighted by polarizability. Is a GETAWAY descriptor (GEometry, Topology, and Atom-Weights Assembly) [40]. These descriptors seek to combine three-dimensional molecular geometry (provided by the molecular influence matrix H) with chemical information by using different atomic weighting schemes w (mass, polarizability, electronegativity) [37]. The matrix of molecular influence H is calculated from the coordinate matrix M (consisting of three columns representing the coordinates x, y, z of all atoms):

$$H = M(M^T \cdot M)^{-1} M^T \quad (3)$$

The diagonal elements h_{ii} represents the leverage of each atom in determining the shape of the molecule. The off-diagonal elements, h_{ij} represents the degree of accessibility to interactions between the atoms j and i separated by a lag k (number of bonds between i and j). For Rkw descriptor, an additional matrix R_{ij} is defined by diagonal elements: $\sqrt{h_{ii} \cdot h_{jj}} / r_{ij}$ where r_{ij} is the geometric distance between the atoms i and j . The general way to calculate this descriptor, submitted to a weighting function w , is:

$$Rkw = \sum_{i=1}^{n-1} \sum_{j>i}^n \left(\frac{\sqrt{h_{ii} \cdot h_{jj}} / r_{ij}}{r_{ij}} \right) \cdot w_i \cdot w_j \cdot \delta(k; d_{ij}) \quad (4)$$

where, $\delta(k; d_{ij}) = 1$ if $d_{ij} = k$ (in the Topological Level Matrix), and zero otherwise. In general, isatin moiety and nitrile provide highest value of this descriptor, weighted by polarizability. This groups provides interactions between relatively polarizable atoms (nitrogen-oxygen) at a lag of 4 bonds. Considering Eq. 1, **R4p** contributes positively to the activity.

R6u+: R maximal autocorrelation of lag 6 / unweighted. [38] The $Rkw+$ descriptor represents the highest value of $((\sqrt{h_{ii} \cdot h_{jj}} / r_{ij}) \cdot w_i \cdot w_j \cdot \delta(k; d_{ij}))$ for any particular lag k and w . This descriptor contributes negatively to the activity.

NO2: Fragment based descriptor. This descriptor was chosen *a priori* from SAR observations and denotes presence (1) or absence (0) of nitro group in MBHA structure. The regression coefficient in Eq. 1 show that the presence of this group increases the activity, as previously discussed.

nN: Number of nitrogen atoms. Regression coefficient indicates that the greater number of hydrogens presents, the better activity. These constitutional indices may be related to the presence of CN, NO₂ and isatin groups, which proved to be important on SAR discussion.

CONCLUSION

We present an interesting investigation about cytotoxic activities on human leukemia cell line (HL-60) for 34 syn-

thetic MBHA. In a good way we discovered that the most cytotoxic compounds (**31-32**, 10.8 μ M and 7.8 μ M respectively) were also prepared quantitatively (100% yields) in a short reaction time using microwave irradiation. We demonstrate that **31** and **32** induced apoptosis and not necrosis in HL-60 cells, observed by externalization of PS and increase Annexin-V positive cells. Quantitative Structure-Activity Relationships considering 3D, 2D and constitutional descriptors provided a robust and predictive PLS model, in accordance with SAR observations. Evaluations of other cancer cell lines and further studies on the biological mechanism of action of **31** and **32** are now under investigation.

CONFLICT OF INTEREST

The authors confirm that this article content has no conflict of interest.

ACKNOWLEDGEMENTS

The authors gratefully acknowledge CNPq and CAPES for financial support. Vasconcellos, M.L.A.A. and Araújo, D.A.M., are CNPq fellows.

REFERENCES

- Basavaiah, D.; Reddy, B. S.; Badsara, S. S. Recent Contributions from the Baylis-Hillman Reaction to Organic Chemistry. *Chem. Rev.*, **2010**, *110*, 5447-74.
- Wei, Y.; Shi, M. Recent advances in organocatalytic asymmetric Morita-Baylis-Hillman/aza-Morita-Baylis-Hillman reaction. *Chem. Rev.*, **2013**, *113*, 6659-6690.
- Ma, G.-N.; Jiang, J.-J.; Shi, M.; Wei, Y. Recent extensions of the Morita-Baylis-Hillman reaction. *Chem. Commun.*, **2009**, *37*, 5459-5514.
- Lima-Junior, C. G.; Vasconcellos, M. L. A. A. Morita-Baylis-Hillman adducts: Biological activities and potentialities to the discovery of new cheaper drugs. *Bioorg. Med. Chem.*, **2012**, *20*, 3954-71.
- Kohn, L. K.; Pavam, C. H.; Veronese, D.; Coelho, F.; Carvalho, J. E.; Almeida W. P. Antiproliferative effect of baylis-Hillman adducts and a new phthalide derivative on human tumor cell lines. *Eur. J. Med. Chem.*, **2006**, *41*, 738-44.
- Leite, J. C.; Junior, C. G. L.; Silva, F. P. L.; Sousa, S. C.; Vasconcellos, M. L. A. A.; Marques-Santos, L. F. Antimitotic activity on sea urchin embryonic cells of seven antiparasitic Morita-Baylis-Hillman adducts: A potential new class of anticancer drugs. *Med. Chem.*, **2012**, *8*, 1003-11.
- Ma, D. L.; Chana, D. S. H.; Leung, C. H. Molecular docking for virtual screening of natural product databases. *Chem. Sci.*, **2011**, *2*, 1656-1665.
- Ma, D. L.; Chana, D. S. H.; Leung, C. H. Drug repositioning by structure-based virtual screening. *Chem. Soc. Rev.*, **2013**, *42*, 2130-2141.
- Leung, C. H.; Chan, D. S. H.; Yang, H.; Abagyan, R.; Lee, S. M. Y.; Zhu, G. Y.; Fonga, W. F.; Ma, D. L. A natural product-like inhibitor of NEDD8-activating enzyme. *Chem. Commun.*, **2011**, *47*, 2511-2513.
- Junior, C. G. L.; Silva, F. P. L.; Oliveira, R. G.; Subrinho, F. L.; Andrade, N. G.; Vasconcellos, M. L. A. A. Microwave irradiation or low temperature improved synthesis of antiparasitic Morita-Baylis-Hillman adducts. *J. Braz. Chem. Soc.*, **2011**, *22*, 2220-24.
- Fabeina-Martins, G. V.; Silveira, A. L.; Cavalcanti, B. C.; Ramos, M. V.; Moraes, M. O.; Pessoa, C. O.; Araujo, D. A. M. Antiproliferative effects of lectins from *Canavalia ensiformis* and *Canavalia brasiliensis* in human leukemia cell lines. *Toxicol. in Vitro*, **2012**, *26*, 1161-69.
- Mosman, T. Rapid colorimetric assay for cellular growth and survival: application to proliferation and cytotoxicity assays. *J. Immunol. Methods*, **1983**, *65*, 55-63.

- [13] Alencar Filho, E. B.; Weber, K. C.; Vasconcellos, M. L. A. A. Selection of 2D/3D molecular descriptors and QSAR modeling of aromatic Morita-Baylis-Hillman adducts with leishmanicidal activities. *Med. Chem. Res.*, **2014**, *23*, 5328-35.
- [14] Judge1, V.; Narasimhan, B.; Ahujal, M.; Sriram, D.; Yogeewari, P.; De Clercq, E.; Pannecouque, C.; Balzarini, J. Synthesis, Antimycobacterial, Antiviral, Antimicrobial Activity and QSAR Studies of N2-acyl isonicotinic Acid Hydrazone Derivatives. *Med. Chem.*, **2013**, *9*, 53-76.
- [15] Tetko, I. V.; Gasteiger, J.; Todeschini, R.; Mauri, A.; Livingstone, D.; Ertl, P.; Palyulin, V. A.; Radchenko, E. V.; Zefirov, N. S.; Makarenko, A. S.; Tanchuk, V. Y.; Prokopenko, V. V. Virtual computational chemistry laboratory - design and description. *J. Comput. Aid. Mol. Des.*, **2005**, *19*, 453-463.
- [16] Vcclab, Virtual Computational Chemistry Laboratory. 2005. Available in <http://www.vcclab.org>.
- [17] Dennington, R.; Keith, T.; Millam, J.; GaussView Version 5, Semicem Inc., Shawnee Mission KS, **2009**.
- [18] Frisch, M. J.; Trucks, G. W.; Schlegel, H. B.; Scuseria, G. E.; Robb, M. A.; Cheeseman, J. R.; Scalmani, G.; Barone, V.; Mennucci, B.; Petersson, G. A.; Nakatsuji, H.; Caricato, M.; Li, X.; Hratchian, H. P.; Izmaylov, A. F.; Bloino, J.; Zheng, G.; Sonnenberg, J. L.; Hada, M.; Ehara, M.; Toyota, K.; Fukuda, R.; Hasegawa, Y.; Ishida, M.; Nakajima, T.; Honda, Y.; Kitao, O.; Nakai, H.; Vreven T.; Montgomery Jr., J. A.; Peralta, J. E.; Ogliaro, F.; Bearpark, M.; Heyd, J. J.; Brothers, E.; Kudin, K. N.; Staroverov, V. N.; Kobayashi, R.; Normand, J.; Raghavachari, K.; Rendell, A.; Burant, J. C.; Iyengar, S. S.; Tomasi, J.; Cossi, M.; Rega, N.; Millam, J. M.; Klene, M.; Knox, J. E.; Cross, J. B.; Bakken, V.; Adamo, C.; Jaramillo, J.; Gomperts, R.; Stratmann, R. E.; Yazyev, O.; Austin, A. J.; Cammi, R.; Pomelli, C.; Ochterski, J. W.; Martin, R. L.; Morokuma, K.; Zakrzewski, V. G.; Voth, G. A.; Salvador, P.; Dannenberg, J. J.; Dapprich, S.; Daniels, A. D.; Farkas, Ö.; Foresman, J. B.; Ortiz, J. V.; Cioslowski, J.; Fox, D. J. Gaussian 09, Revision A.1, Gaussian, Inc., Wallingford CT, **2009**.
- [19] Dewar, M. J. S.; Zebisch, E. G.; Healy, E. F.; Stewart, J. J. P. Development and use of quantum mechanical molecular models. 76. AM1: a new general purpose quantum mechanical molecular model. *J. Am. Chem. Soc.*, **1985**, *107*, 3902-3909.
- [20] Martins, J. A. M.; Ferreira, M. M. C. QSAR modeling: um novo pacote computacional open source para gerar e validar modelos QSAR. *Quim. Nova*, **2013**, *36*, 554-560.
- [21] Teófilo, R. F.; Martins, J. P.; Ferreira, M. M. C. Sorting variables by using informative vectors as a strategy for feature selection in multivariate regression. *J. Chemom.*, **2009**, *23*, 32-48.
- [22] Wold, S.; Sjöström, M.; Eriksson, L.; PLS-regression: a basic tool of chemometrics. *Chemom. Intel. Lab. Sys.*, **2001**, *58*, 109-130.
- [23] Filho, E. B. A.; Moraes, I. A.; Weber, K. C.; Rocha, G. B.; Vasconcellos, M.L.A.A. DFT/PCM, QTAIM, 1H NMR conformational studies and QSAR modeling of thirty-two anti-Leishmania amazonensis Morita Baylis Hillman Adducts. *J. Mol. Struct.*, **2012**, *1022*, 72-80.
- [24] Ferreira, M. M. C. Multivariate QSAR. *J. Braz. Chem. Soc.*, **2002**, *13*, 742-53.
- [25] Kononov, D. A.; Llewellyn, L. E.; Heyden, Y. V.; Coomans, D.; Robust Cross-Validation of Linear Regression QSAR Models. *J. Chem. Inf. Model*, **2008**, *48*, 2081-2094.
- [26] Kiralj, R.; Ferreira, M. M. C. Basic Validation Procedures for Regression Models in QSAR and QSPR Studies: Theory and Application. *J. Braz. Chem. Soc.*, **2009**, *20*, 770-787.
- [27] Cantillo, D.; Kappe, C. O. A Unified Mechanistic View on the Morita-Baylis-Hillman Reaction: Computational and Experimental Investigations. *J. Org. Chem.*, **2010**, *75*, 8615-8626.
- [28] Faheina-Martins, G. V.; Silveira, A. L.; Ramos, M. V.; Marques-Santos, L. F.; Araujo, D. A. M. Influence of fetal bovine serum on cytotoxic and genotoxic effects of lectins in MCF-7 cells. *J. Biochem Mol. Toxicol.*, **2011**, *25*, 290-296.
- [29] Peddibhotla, S. 3-Substituted-3-hydroxy-2-oxindole, an Emerging New Scaffold for Drug Discovery with Potential Anti-Cancer and other Biological Activities. *Curr. Bioact. Compounds*, **2009**, *5*, 20-38.
- [30] Yan, T.; Wang, X.; Liu, H. S. J.; Xie, Y. Facile Creation of 3-Substituted-3-Hydroxy-2-Oxindoles by Arginine-Catalyzed Aldol Reactions of α,β -Unsaturated Ketones with Isatins. *Molecules*, **2013**, *18*, 14505-18.
- [31] Vine, K. L.; Matesic, L.; Locke, J. M.; Ranson, M.; Skropeta, D. Cytotoxic and anticancer activities of isatin and its derivatives: a comprehensive review from 2000-2008. *Anti-Cancer Agents Med. Chem.*, **2009**, *9*, 397-414.
- [32] Pakravan, P.; Kashanian, S.; Khodaei, M. M.; Harding, F. J. Biochemical and pharmacological characterization of isatin and its derivatives: from structure to activity. *Pharmacol. Rep.*, **2013**, *65*, 313-35.
- [33] Bastien, P.; Vinzi, V. E.; Tenenhaus, M. PLS generalized linear regression. *Comp. Stat. & Data Anal.*, **2005**, *48*, 17-46.
- [34] González, M.P.; Gándara, Z.; Fall, Y.; Gómez, G. Radial Distribution Function descriptors for predicting affinity for vitamin D receptor. *Eur. J. Med. Chem.*, **2008**, *43*, 1360-1365.
- [35] Hemmer, M. C.; Steinhauer, V.; Gasteiger, J. Deriving the 3D structure of organic molecules from their infrared spectra. *Vibrat. Spect.*, **1999**, *19*, 151-164.
- [36] Todeschini, R.; Consonni, V. Molecular Descriptors for Chemoinformatics. *Wiley-VCH*, **2009**, *41*.
- [37] Strand life science p. Ltda. Theory Descriptors. **2007**. Available in http://www.strandls.com/sarchitect/documents/manual_html/desctheory.html.
- [38] Todeschini, R.; Gramatica, P. SD-modelling and Prediction by WHIM Descriptors. Part 5. Theory Development and Chemical Meaning of WHIM Descriptors. *Quant. Struc.-Act. Relat.*, **1997**, *16*, 113-119.
- [39] Gupta, A.K.; Jain, A.; Mishra, S.; Jiaswal, A. Design and Synthesis of Substituted Imidazole Derivatives as Antifungal Agents. *Int. J. Drug Design Discov.*, **2012**, *3*, 943-954.
- [40] Consonni, V.; Todeschini, R.; Pavan, M. Structure/Response Correlations and Similarity/Diversity Analysis by GETAWAY Descriptors. 1. Theory of the Novel 3D Molecular Descriptors. *J. Chem. Inf. Comp. Sci.*, **2002**, *42*, 682-692.

APÊNDICE J – Effects of curine in HL-60 leukemic cells: cell cycle arrest and apoptosis induction. **Journal of Natural Medicines, 2015**



Effects of curine in HL-60 leukemic cells: cell cycle arrest and apoptosis induction

Bruna Braga Dantas · Gláucia Veríssimo Faheina-Martins · Tangbadioa Hervé Couliadiati · Caio César Barbosa Bomfim · Celidarque da Silva Dias · José Maria Barbosa-Filho · Demetrius Antônio Machado Araújo

Received: 25 August 2014 / Accepted: 7 December 2014 / Published online: 24 January 2015
© The Japanese Society of Pharmacognosy and Springer Japan 2015

Abstract Curine is a natural alkaloid isolated from *Chondrodendron platyphyllum* and it has been reported that this alkaloid has vasodilatory and anti-inflammatory effects. The aim of this study is to analyze the cytotoxic effects of curine in cancer cell lines HL-60, K562, and HT-29, and in primary cultures of peripheral blood mononuclear cells (PBMC). Cells were treated with curine (from 3 to 15 μM) for 24 and 48 h. Cell viability was analyzed by the 3-(4,5-dimethylthiazole-2-yl)-2,5-diphenyltetrazolium bromide (MTT) test and flow cytometry with propidium iodide (PI) assay. To assess the type of cell death induced in HL-60, the cell cycle, morphological, and biochemical alterations were analyzed, which were determined by differential staining with acridine orange/ethidium bromide, and annexin V/PI double-labeling and change in mitochondrial membrane potential assays. Curine demonstrated a potent cytotoxic effect on leukemic cell lines (HL-60 and K562). Its cytotoxic effects in HL-60 cells was related to plasma membrane damage and cell cycle arrest at the G1 phase from 43.4 ± 1.0 to 56.7 ± 1.4 % ($p < 0.05$). Curine (15 μM) also increased the apoptotic cells number by around 60 % in HL-60 cells and caused phosphatidylserine

externalization, inducing about 57 % of apoptosis. Moreover, this alkaloid provoked 20 % of mitochondrial membrane depolarization. We conclude that curine presented a cytotoxic effect and induced apoptosis in HL-60 cells. Thus, it can be considered a promising pharmacological drug.

Keywords Apoptosis · Curine · Cytotoxicity · Cytometry · HL-60 cells

Introduction

Cancer is a high-mortality disease caused mainly by environmental factors that mutate genes or induce epigenetic alterations causing critical change in important cell-regulatory proteins. The resultant aberrant cell behavior leads to uncontrolled growth and spread of abnormal cells that destroy surrounding normal tissue and can spread to vital organs, generating metastase [1, 2]. The search for new anticancer therapies has increased and natural products or their structural derivatives have always been an important source due to their diverse pharmacological properties [3].

The bisbenzylisoquinoline alkaloid (BBA) curine is a natural product isolated from *Chondrodendron platyphyllum* plant [4, 5]. The chemical structure of curine is shown in Fig. 1. Recent studies demonstrated that curine did not demonstrate toxicity in mice. Its alkaloid showed a vasodilator effect associated with the inhibition of calcium influx and an anti-inflammatory effect related with alteration in eosinophil functions [6–8].

The aim of the present study was to determine the antiproliferative activity of curine on cancer cell lines, such as human leukemia cells, HL-60 and K562, and human

Electronic supplementary material The online version of this article (doi:10.1007/s11418-014-0881-5) contains supplementary material, which is available to authorized users.

B. B. Dantas · G. V. Faheina-Martins · T. H. Couliadiati · C. C. B. Bomfim · D. A. M. Araújo (✉)
Department of Biotechnology, Center of Biotechnology, Federal University of Paraíba, Cidade Universitária, Campus I, 58051-900 João Pessoa, PB, Brazil
e-mail: demetrius@cbiotec.ufpb.br

C. da Silva Dias · J. M. Barbosa-Filho
Health Sciences Center, Federal University of Paraíba, 58051-900 João Pessoa, Brazil

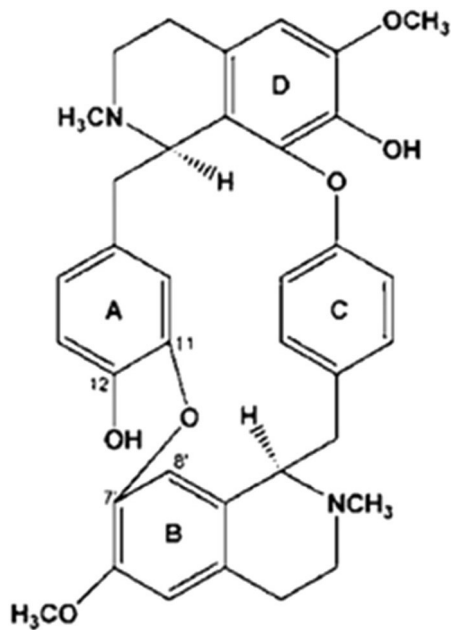


Fig. 1 Chemical structure of curine

colon adenocarcinoma cells, HT-29, as well as the human peripheral blood mononuclear cells (PBMC).

Materials and methods

Chemicals and reagents

3-(4,5-dimethylthiazole-2-yl)-2,5-diphenyltetrazolium bromide (MTT) (Amresco, USA), annexin V-Alexa Fluor (Invitrogen, USA), carbonyl cyanide 3-chlorophenylhydrazide (CCCP; Sigma-Aldrich, USA), RPMI-1640, DMEM (Himedia, USA), L-glutamine (Amresco, USA), penicillin/streptomycin (Sigma-Aldrich, USA), HEPES (Amresco, USA), DNase-free RNase (Amresco, USA), fetal bovine serum (FBS) (Cultilab, Brazil), propidium iodide (PI) (Sigma-Aldrich, USA), tetramethylrhodamine (Invitrogen, Sigma-Aldrich, USA), 3-methyladenine (Sigma-Aldrich, USA), Ficoll-Paque (GE Healthcare, Sweden), ethidium bromide (10 mg/ml), and trypan blue (Sigma-Aldrich, USA).

Drug preparation

Spectroscopically pure curine was isolated from the root barks of *Chondrodendron platyphyllum*, as described previously [8]. The curine was dissolved in DMSO at a concentration of 30 mM for stock solution and dilutions were made to adjust the appropriate concentrations for the experiments. The highest DMSO concentration used

was 0.5 % and we did not observe any effect of this dispersant.

Cell culture

Human acute promyelocytic leukemia cells (HL-60), human chronic promyelocytic leukemia cells (K562), and colon adenocarcinoma cells (HT-29) were obtained from the Cell Bank Rio de Janeiro (Brazil). HL-60 and K562 cells and PBMC were grown in RPMI-1640 medium and HT-29 cells were grown in DMEM medium. Both media were supplemented with 10 % FBS, L-glutamine (300 mg/l), 100 IU/ml penicillin, and 100 µg/ml streptomycin, and placed in humidified air at 37 °C with 5 % CO₂ atmosphere.

Human PBMC isolation

Blood samples were obtained from healthy donors. PBMC were isolated with Ficoll-Hypaque as described by the manufacturer. Collected cells were washed twice in PBS and were kept in culture medium consisting of RPMI-1640 medium and 10 % FBS. All procedures were in agreement with the Committee of Ethics in Research with Humans from the Federal University of Paraíba (CEP/HULW/UFPB), protocol #655/10-318119.

Cytotoxic assays

MTT reduction

Curine cytotoxicity was determined by MTT [9]. HL-60 and K562 (5×10^5 cells/well), HT-29 (3×10^5 cells/well), and PBMC (1×10^6 cells/well) were seeded on 96-well plates and incubated for 24 and 48 h at 37 °C in 5 % CO₂ with different concentrations of curine. Afterwards, the medium was replaced with free medium containing 5 mg/ml of MTT for 4 h. The supernatant was aspirated and formazan crystals were dissolved in 100 µl SDS/HCl solution. Absorbance was measured at 570 nm. Cell growth was calculated by comparing the absorbance of treated and untreated cells.

Analysis of membrane integrity: flow cytometry

Cells (5×10^5 cells/ml) were incubated in 24-well plates with different concentrations of curine during a period of 48 h. Subsequently, the cells were transferred to tubes, centrifuged at a speed of 450g for 5 min at room temperature, the supernatant was then discarded, and the cells were resuspended in a PI solution, diluted in PBS, and then assayed in a flow cytometer (Becton-Dickinson, USA) using ten thousand events by analysis.

Cell cycle phase distribution

HL-60 cells (5×10^5 cells/ml) were seeded in 24-well plates and incubated with different concentrations of curine during a period of 48 h. Subsequently, the cells were collected in tubes and centrifuged at a speed of 450g for 5 min at room temperature. The supernatant was then discarded and cells were incubated with 1 U/ml RNase A (DNase-free) and PI solution (0.1 % sodium citrate, 0.1 % triton X-100, and 50 mg/l PI) for 30 min at room temperature in the dark. After that, samples were analyzed in a flow cytometer (Becton-Dickinson, USA). Sample acquisition was performed using the CellQuest software, and ten thousand events were acquired for each sample.

Ethidium bromide/acridine orange staining

HL-60 (2×10^5 cells/ml) cells were grown in 24-well plates and treated with different concentrations of curine during a period of 48 h. After incubation, cells treated with fluorescent dyes, ethidium bromide (50 μ g/ml) and acridine orange (10 mg/ml). Cells were observed in the dark in an inverted fluorescence microscope using UV excitation.

Evaluation of apoptosis

The apoptotic cells were quantified using annexin V/PI dual staining. HL-60 cells (5×10^5 cells/ml) were exposed to curine (3, 7, or 15 μ M) or etoposide (2.5 μ M). After 48 h of incubation, the cells were centrifuged (450g, 5 min) and stained with 1 μ l of annexin V-Alexa Fluor 488 and 2 μ l of 50 μ g/ml PI in 100 μ l binding buffer (10 mM HEPES, 140 mM NaOH, and 2.5 mM CaCl_2 , pH adjusted to 7.4) for 15 min at room temperature in the dark. The analysis was performed in a flow cytometer (Becton-Dickinson, USA). Sample acquisition was performed using the CellQuest software, and ten thousand events were acquired for each sample.

Analysis of mitochondrial membrane potential

HL-60 cells (5×10^5 cells/ml) were seeded in 24-well plates and incubated with different concentrations of curine during a period of 48 h. Subsequently, the cells were collected in tubes and centrifuged at a speed of 450g for 5 min at room temperature. The supernatant was then discarded and the cells incubated with tetramethylrhodamine, at a concentration of 10 μ M at 37 °C for 30 min in the dark, and then washed with PBS and resuspended in PBS and fluorescence was also measured by flow cytometry. Ten thousand events were evaluated for each sample. CCCP was used as a positive control for inducing mitochondrial depolarization.

Results

Cytotoxic effects of curine

In order to determine the anticancer effect of curine *in vitro*, it was tested for cell growth inhibition in different cancer cell lines at various concentrations for 24 and 48 h. As shown in Table 1, curine exhibited low cytotoxicity towards PBMC. However, curine showed a strong inhibitory effect against HL-60 cells with a IC_{50} values of 9.7 μ M and 8.9 μ M for 24 and 48 h of incubation, respectively. K562 cells were more sensitive to curine after 48 h of exposure, with an IC_{50} of 3.8 μ M. HT-29 cells were shown to be more resistant to curine cytotoxic effect. Therefore, HL-60 cells were used for the next investigations.

Analysis of membrane integrity

The PI penetrates cells with damaged membranes and it was excluded in normal membrane. To discover if the

Table 1 Cytotoxic effects of curine in HL-60, K562, and HT-29 cancer cell lines and in PBMC using the MTT assay

Cells	Curine		Etoposide	
	24 h	48 h	24 h	48 h
HL-60	9.7 \pm 5.1	8.9 \pm 6.4	6.5 \pm 5.6	2.3 \pm 5.4
K562	17.8 \pm 5.2	3.8 \pm 6.9	>100	44.5 \pm 4.8
HT-29	51.73 \pm 6.7	32.4 \pm 5.3	>100	ND
PBMC	53.2 \pm 5.1	56.2 \pm 5.6	>100	ND

The IC_{50} values are expressed as mean \pm standard deviation, in μ M, and were obtained by nonlinear regression using the GraphPad software package (Intuitive Software for Science, San Diego, USA)

ND not determined

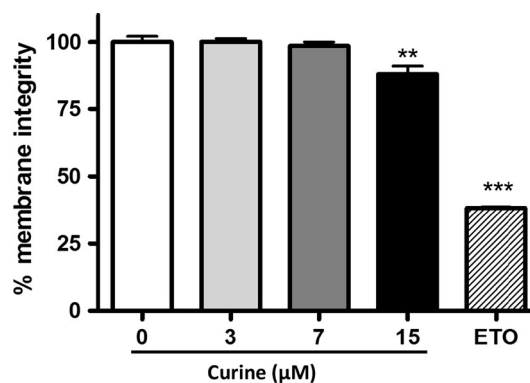


Fig. 2 Effect of curine on membrane integrity in HL-60 cells after 48 h of incubation. Data, expressed as mean \pm standard error, are the average of three independent experiments performed in duplicate. ** $p < 0.01$, *** $p < 0.001$ compared with control by ANOVA followed by the Newman–Keuls post-test. ETO etoposide (5 μ M)

Table 2 Curine effect on cell cycle phases in HL-60 cells

Cell phase	Control	3 μ M	7 μ M	15 μ M	ETO
Sub-G1	1.6 \pm 0.9	1.1 \pm 0.6	1.0 \pm 0.6	1.5 \pm 0.9	63.8 \pm 1.1***
G1	43.4 \pm 1.0	45.0 \pm 2.2	46.9 \pm 1.7	56.7 \pm 1.4*	4.6 \pm 0.9***
S	22.09 \pm 1.3	21.43 \pm 1.1	21.51 \pm 1.2	22.7 \pm 1.9	9.7 \pm 0.7***
G2/M	25.01 \pm 1.5	24.7 \pm 0.9	22.4 \pm 1.1	19.6 \pm 1.5**	11.5 \pm 1.2***

Data, expressed as mean \pm standard error, show perceptual values of three independent experiments. The results were obtained during 48 h of incubation

* $p < 0.05$, ** $p < 0.01$, *** $p < 0.001$ compared with control by ANOVA followed by the Newman–Keuls post-test

ETO etoposide (2.5 μ M)

cytotoxic effect of curine is related to cell membrane damage, the PI assay was performed using flow cytometry. Figure 2 shows that curine had little effect on the HL-60 cell membrane, which was shown only after 48 h of exposition.

Effect of curine on the HL-60 cell cycle distribution

To verify an inhibitory effect of curine on the growth of HL-60 cells being related to its effect on the cell cycle, these cells were treated with curine and assessed by flow cytometry. After 48 h of incubation, 15 μ M of curine induced cell cycle arrest in the G1 phase with a concomitant decrease of G2/M. However, even at high concentrations used, curine failed to increase the sub-G1 population (Table 2; Fig. S1).

Morphological analysis by fluorescence microscopy

To discover whether curine induced apoptosis or necrosis, double-staining using acridine orange/ethidium bromide (AO/EB) was performed. After 48 h, HL-60 cells treated with different concentrations of curine showed an increase in the acridine orange cell population in a concentration-dependent manner (Fig. 3), suggesting that curine can be a potent inducer of apoptosis in HL-60 cells.

Annexin V/PI double-labeling

This double-labeled test allowed viable cells, apoptotic cells, and necrotic cells to be distinguished. When phosphatidylserine is externalized during apoptosis, it interacts with annexin V, while the PI fluoresces when interacting with DNA, which happens only in cells with cell membrane damage. We showed that curine reduced cellular viability, inducing cell death mainly by an apoptosis effect. At 15 μ M, curine shows an induction of around 57 % of apoptotic cells, compared to 51 % of apoptosis induction caused by 2.5 μ M ETO (Table 3; Fig. S2).

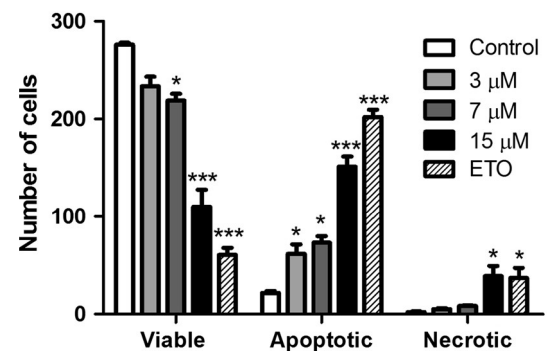


Fig. 3 Effect of curine in apoptosis induction in HL-60 cells after 48 h of incubation. The results were obtained using the AO/EB staining assay. Data, expressed as mean \pm standard error, are the average of three experiments. * $p < 0.05$, *** $p < 0.001$ compared to control. ETO etoposide (2.5 μ M)

Analysis of mitochondrial membrane potential

Mitochondrial remodeling and release of apoptotic factors are characteristics for the activation of pathway intrinsic apoptosis [10]. To determine whether the mitochondrial pathway was involved in the curine inhibitory effect, we examined the effect of curine on mitochondrial membrane depolarization. HL-60 treated cells showed mitochondrial membrane depolarization at high concentrations of curine after 48 h of incubation (Fig. 4).

Discussion

Various patients with cancer conditions fail to respond to chemotherapy because of the resistance mechanism of cancer cells and also due to cytotoxicity of drugs on normal cells [11, 12]. Therefore, it has been an important task to find new compounds with antineoplastic activity and more selectivity to cancer cells. In recent years, significant attention has been focused on identifying natural products that can retard or reverse the process of multistage carcinogenesis [13]. In the present study, we showed that curine

Table 3 Curine induces externalization of phosphatidylserine in HL-60 cells

Cell	Control	3 μ M	7 μ M	15 μ M	ETO
Viable (%)	94.8 \pm 0.6	95.2 \pm 0.6	86.4 \pm 0.4	28.3 \pm 4.4***	11.5 \pm 0.7*
Apoptosis (%)	4.5 \pm 0.5	3.0 \pm 0.6	11.7 \pm 0.5	56.9 \pm 8.4***	51.3 \pm 0.6***
Necrosis (%)	0.4 \pm 0.1	1.8 \pm 0.2	1.9 \pm 0.3	14.5 \pm 5.1*	33.8 \pm 1.6***

Data, expressed as mean \pm standard error, show perceptual values of three independent experiments. The incubation time was 48 h

* $p < 0.05$, *** $p < 0.001$ compared with control by ANOVA followed by the Newman–Keuls post-test

ETO etoposide (2.5 μ M)

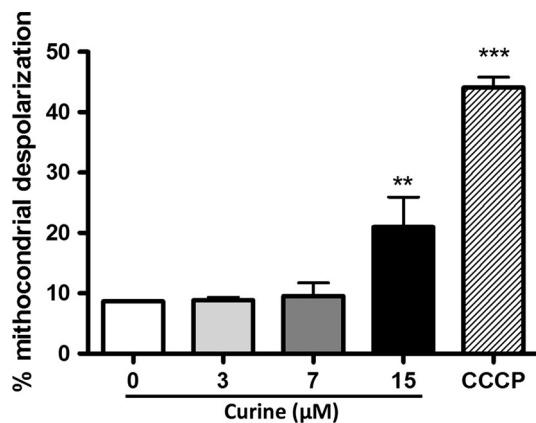


Fig. 4 Assessment of mitochondrial depolarization in HL-60 cells treated with curine for 48 h of incubation. Data, expressed as mean \pm standard error, were the average of two experiments in duplicate. ** $p < 0.01$; *** $p < 0.001$ compared with control by ANOVA followed by the Newman–Keuls post-test. CCCP carbonyl cyanide 3-chlorophenylhydrazone (15 μ M)

induced inhibition of cancer cells and had little effect on normal PBMC (Table 1). Medeiros and colleagues demonstrated that 300 μ M curine produced a vasorelaxant effect without damage in endothelial cells [8]. The balance between the therapeutic and toxicological effects of a substance is an important parameter for drug discovery. Many cytotoxic drugs tend not to be selective in their actions, acting and damaging noncancerous cells [3].

The plasma membrane integrity is a characteristic of cell death. The loss of membrane integrity occurs in the late stages of apoptosis or necrosis [14, 15] and we verified that curine caused slight damage to the plasma membrane (Fig. 2).

Cell cycle arrest has been shown to increase the sensitivity of cancer cells to different cytotoxic drugs, which can lead to an important factor for inhibiting cellular multiplication [16]. Our results showed that curine induced cell cycle arrest at the G1 phase in HL-60 cells. Furthermore, subsequent decrease of cell numbers in the S phase and the G2/M phase were detected, as expected (Table 2). That way, the growth inhibitory effect of curine in HL-60 cells was associated with the G1 phase cell cycle arrest. This

effect was consistent with the results of other investigators, showing that antiproliferative effects of alkaloids were linked to G1 phase cell cycle arrest [17, 18]. It was also noted that BBA inhibited growth and induced G1 arrest in cancer cells [19]. Cell cycle progression is tightly regulated by the cyclin/CDK complex and curine possibly interfered with the expression of cyclins involved in the regulation of the G1 phase of the cell cycle. Subsequent studies can confirm this possibility.

Apoptosis was confirmed as the main mechanism of cell death induced in cancer cells. The clinical applicability of chemotherapeutic drugs is dependent on their ability to trigger cancer cell death, and activation of apoptosis is one of the well-studied mechanisms involved in this process [4]. Therefore, analysis of apoptotic cells was carried out by differential staining with ethidium bromide and acridine orange to elucidate the type of cell death induced by curine in HL-60 cells. Figure 3 showed that curine increased the apoptotic cells number in a concentration-dependent manner after 48 h of treatment in HL-60 cells. Actually, the data showed in Table 3 corroborate the idea that curine is inducing cell death mainly by apoptosis.

It has been reported that activation of the apoptotic pathway is a key mechanism by which cytotoxic drugs kill cancer cells. The advantage of apoptosis induction by anticancer drugs is that the formation of apoptotic bodies could be eliminated by the immune system without inducing inflammation [20]. Many studies have reported the ability of BBA to induce apoptosis in tumor cells [4, 16, 21] and it is known that apoptosis is induced mainly by triggering the death receptor and/or mitochondrial, leading to the activation of caspases [20]. This study demonstrated that curine induced depolarization of the mitochondrial potential at a concentration of 15 μ M after 48 h of exposition (Fig. 4). This result suggests that curine triggered apoptosis in HL-60 cells through the intrinsic pathway.

In conclusion, curine inhibited HL-60 cells proliferation that was mediated by cell cycle arrest and apoptosis, and this alkaloid also showed a cytotoxic effect on K562 and HT-29 cells, with less cytotoxicity on PBMC. Thus, curine can represent a potential drug candidate for acute myeloid leukemia treatment. Obviously, it is necessary to conduct

further experiments to better elucidate this mechanism of cell death.

Acknowledgments This research was supported by grants from CNPq (Conselho Nacional de Desenvolvimento Científico e Tecnológico) and CAPES (Coordenação de Aperfeiçoamento de Pessoal de Nível Superior).

Conflict of interest The authors declare no conflict of interest.

References

- Hanahan D, Weinberg RA (2011) Hallmarks of cancer: the next generation. *Cell* 144:646–674
- Alison MR (2001) Cancer. Encyclopedia of life sciences. Nature Publishing Group, London
- Mishra T, Khullar M, Bhatia A (2011) Anticancer potential of aqueous ethanol seed extract of *Ziziphus mauritiana* against cancer cell lines and Ehrlich ascites carcinoma. *Evid Based Complement Alternat Med*. pii: 765029. doi:10.1155/2011/765029
- Wang L, Liu L, Shi Y, Cao H, Chaturvedi R, Calcutt MW, Hu T, Ren X, Wilson KT, Polk DB, Yan F (2012) Berberine induces caspase-independent cell death in colon tumor cells through activation of apoptosis-inducing factor. *PLoS One* 7(5):e36418. doi:10.1371/journal.pone.0036418
- Barbosa-Filho JM, da-Cunha EVL, Gray AI (2000) Alkaloids of the menispermaceae. *Alkaloids Chem Biol* 54:1–190
- Ribeiro-Filho J, Leite FC, Costa HF, Calheiros AS, Torres RC, de Azevedo CT, Martins MA, da Silva Dias C, Bozza PT, Piuvezam MR (2014) Curine inhibits mast cell-dependent responses in mice. *J Ethnopharmacol* 155:1118–1124
- Ribeiro-Filho J, Calheiros AS, Vieira-de-Abreu A, de Carvalho KI, da Silva Mendes D, Melo CB, Martins MA, da Silva Dias C, Piuvezam MR, Bozza PT (2013) Curine inhibits eosinophil activation and airway hyper-responsiveness in a mouse model of allergic asthma. *Toxicol Appl Pharmacol* 273(1):19–26
- Medeiros MA, Pinho JF, De-Lira DP, Barbosa-Filho JM, Araújo DA, Cortes SF, Lemos VS, Cruz JS (2011) Curine, a bisbenzylisoquinoline alkaloid, blocks L-type Ca^{2+} channels and decreases intracellular Ca^{2+} transients in A7r5 cells. *Eur J Pharmacol* 669:100–107
- Mosmann T (1983) Rapid colorimetric assay for cellular growth and survival: application to proliferation and cytotoxicity assays. *J Immunol Methods* 65:55–63
- Tanner EA, Blute TA, Brachmann CB, McCall K (2011) Bcl-2 proteins and autophagy regulate mitochondrial dynamics during programmed cell death in the *Drosophila* ovary. *Development* 138:327–338
- Al-tel TH (2010) Design and synthesis of novel tetrahydro-2H-Pyran[3,2-c]Pyridazin-3(6H)-one derivatives as potential anticancer agents. *Eur J Med Chem* 45:5724–5731
- Pedram B, Van oeveren A, Mais DE, Marschke KB, Verboost PM, Groen MB, Zhi L (2008) A tissue-selective nonsteroidal progesterone receptor modulator: 7,9-difluoro-5-(3-methylcyclohex-2-enyl)-2,2,4-trimethyl-1,2-dihydrochromeno[3,4-f]quinoline. *J Med Chem* 51:3696–3699
- Sharma M, Agrawal SK, Sharma PR, Chadha BS, Khosla MK, Saxena AK (2010) Cytotoxic and apoptotic activity of essential oil from *Ocimum viride* towards COLO 205 cells. *Food Chem Toxicol* 48:336–344
- Kroemer G, Galluzzi L, Vandenabeele P, Abrams J, Alnemri ES, Baehrecke EH, Blagosklonny MV, El-deiry WS, Golstein P, Green DR, Hengartner M, Knight RA, Kumar S, Lipton SA, Malorni W, Nuñez G, Peter ME, Tschopp J, Yuan J, Piacentini M, Zhivotovsky B, Melino G; Nomenclature Committee on Cell Death 2009 (2009) Classification of cell death: recommendations of the Nomenclature Committee on Cell Death 2009. *Cell Death Differ* 16:3–11
- Andrade R, Crisol L, Prado R, Boyano MD, Arluzea J, Aréchaga J (2009) Plasma membrane and nuclear envelope integrity during the blebbing stage of apoptosis: a time-lapse study. *Biol Cell* 102:25–35
- Chidambara Murthy KN, Jayaprakasha GK, Patil BS (2012) The natural alkaloid berberine targets multiple pathways to induce cell death in cultured human colon cancer cells. *Eur J Pharmacol* 688:14–21
- Ding YF, Bao YM, An LJ (2005) Progress research of antitumor agents vinblastine analogues. *Chin J Pharm* 36:424–428
- Lu JJ, Bao JL, Chen XP, Huang M, Wang YT (2012) Alkaloids isolated from natural herbs as the anticancer agents. *Evid Based Complement Alternat Med* 2012:485042. doi:10.1155/2012/485042
- Ehrhardt H, Wachter F, Grunert M, Jeremias I (2013) Cell cycle-arrested tumor cells exhibit increased sensitivity towards TRAIL-induced apoptosis. *Cell Death Dis* 4:e661. doi:10.1038/cddis.2013.179
- Liu JJ, Lin M, Yu JY, Liu B, Bao JK (2011) Targeting apoptotic and autophagic pathways for cancer therapeutics. *Cancer Lett* 300:105–114
- Elumalai P, Gunadharini DN, Senthilkumar K, Banudevi S, Arunkumar R, Benson CS, Sharmila G, Arunakaran J (2012) Induction of apoptosis in human breast cancer cells by nimbolide through extrinsic and intrinsic pathway. *Toxicol Lett* 215:131–142